GEOCHEMICAL SIGNATURE OF ROCKS AND WEATHERING PRODUCTS IN LUXEMBOURG

SABINE ROTH

GRAND-DUCHÉ DE LUXEMBOURG

MINISTÈRE DES TRAVAUX PUBLICS

ADMINISTRATION DES PONTS ET CHAUSSÉES

PUBLICATIONS DU SERVICE GÉOLOGIQUE DU LUXEMBOURG

VERÖFFENTLICHUNGEN DES LUXEMBURGER GEOLOGISCHEN DIENSTES

VOLUME XXXI

GEOCHEMICAL SIGNATURE
OF ROCKS AND WEATHERING PRODUCTS
IN LUXEMBOURG

SABINE ROTH

fonds national de la
recherche

LUXEMBOURG 2007

SERVICE GÉOLOGIQUE DU LUXEMBOURG

MINISTÈRE DES TRAVAUX PUBLICS
Administration des ponts et chaussées

Service géologique du Luxembourg

Geochemical signature of rocks and weathering products in Luxembourg

Dissertation

zur

Erlangung des Doktorgrades (Dr. rer. nat.)

der

Mathematisch-Naturwissenschaftlichen Fakultät

der

Rheinischen Friedrich-Wilhelms-Universität Bonn (D)

vorgelegt von

Sabine Roth

aus

Bergisch-Gladbach (D)

Bonn 2005

Angefertigt mit Genehmigung der Mathematisch-Naturwissenschaftlichen Fakultät der

Rheinischen Friedrich-Wilhelms-Universität Bonn

1. Referent: Prof. Dr. Agemar Siehl

2. Referent: Prof. Dr. Jean Thein

Tag der Promotion: 27.01.2006

Table of Contents

List of Figures

List of Tables

Abstract

Indoor radon concentrations in Luxembourg are strongly correlated with the geological age of the bedrock. Houses in the Eisléck, the northern part of the country, with a basement of Palaeozoic rocks, were found to have a median indoor radon activity of 128 Bq/m³, while for houses built on Mesozoic rocks in the south (Gutland) the median was 75 Bq/m³. The objective of this study was to investigate the distribution and bondings of natural radionuclides in rocks and soils and to determine the parameters influencing the observed differences in indoor radon concentrations.

Representative rock samples were collected, together with their accompanying weathering products, from representative geological units throughout the country. The samples were analysed for their content of natural radionuclides (^{232}Th, ^{238}U, ^{230}Th, and ^{226}Ra) by γ-spectrometry and for their radon emanation by a newly developed method. Additionally, a series of Gedinnian samples from Hatrival (Belgium) with increased radionuclide activities were selected to determine the speciation of ^{232}Th, ^{238}U, and ^{226}Ra in rocks and their weathering products by sequential extraction.

The activities of Th, U, and Ra are higher in Palaeozoic rocks (medians: ^{232}Th: 47 Bq/kg, ^{238}U: 32 Bq/kg, ^{226}Ra: 32 Bq/kg) than in Mesozoic rocks (medians: ^{232}Th: 25 Bq/kg, ^{238}U: 25 Bq/kg, ^{226}Ra: 22 Bq/kg). In weathering products, all radionuclides are enriched compared to the parent rocks, especially in Palaeozoic samples (medians: ^{232}Th: 55 Bq/kg, ^{238}U: 44 Bq/kg, ^{226}Ra: 44 Bq/kg). The Gedinnian samples from Belgium exhibit especially high radionuclide activities in their weathering products (medians: ^{232}Th: 83 Bq/kg, ^{238}U: 223 Bq/kg, ^{226}Ra: 425 Bq/kg), where ^{226}Ra is always in secular equilibrium with ^{230}Th.

The emanation coefficients of weathering products are usually higher than those of rocks. They are especially high for weathered materials with more than 10% Fe_2O_3. There is a significant positive correlation of indoor radon concentrations to emanation coefficients of weathering products, but not to rocks of the geological units on which the houses were built.

Thorium is distributed relatively uniformly in the fractions of the sequential extraction of rocks and weathering products. Uranium in rocks is most abundant in the extraction residual, followed by the iron oxide fractions. In weathering products, the most uranium is found in the iron oxide fractions and less than 10 % in the extraction residual. Radium compounds differ considerably from those of uranium. In rocks and weathering products, most radium appears in the extraction residual, followed by the mobile exchangeable fraction or the fraction of the crystalline iron oxides, and for weathering products also in the Mn oxide fraction.

The high indoor radon activities in the Eisléck can be explained by an enrichment of radium in crystalline iron oxides, located as weathering products in fissures and fractures of

the Palaeozoic bedrock, which provide many pathways for passive advective and thermodiffusive upward radon transport.

Kurzfassung

In Luxemburg korreliert die Radonkonzentration in der Raumluft von Gebäuden stark mit dem geologischen Alter des Untergrundes. Der Norden des Landes (Eisléck) besteht aus variskisch gefalteten Unterdevonschichten und weisst in der Raumluft einen Median-Wert von 128 Bq/m³ auf. Die Radonkonzentrationen in den Häusern, die auf mesozoischem Untergrund im südlichen Gutland gebaut wurden, sind mit einem Median-Wert von 75 Bq/m³ signifikant geringer.

In dieser Studie werden die Ursachen für die Unterschiede der Raumluft-Belastungen durch die Bestimmung der Konzentration, Verteilung und Bindungsformen der Mutternuklide des ^{222}Rn (^{238}U, ^{230}Th und ^{226}Ra) und des ^{232}Th in Gesteinen und Böden untersucht.

Von repräsentativen geologischen Einheiten Luxemburgs wurden Gesteinsproben zusammen mit deren Verwitterungsprodukten genommen. Die Aktivitätskonzentrationen der natürlichen Radionuklide ^{232}Th, ^{238}U, ^{230}Th und ^{226}Ra wurden mit einem γ-Spektrometer gemessen. Zur Bestimmung der Radonemanation wurde eine neue Methode entwickelt.

Zusätzlich wurden in Belgien (Hatrival), in einem Gebiet mit erhöhter Radon-Belastung in Innenräumen, Gesteinsproben und deren Verwitterungsprodukte (Gedinne) genommen. Diese Proben mit erhöhter Radionuklidaktivität wurden ausgewählt, um durch sequentielle Extraktion die Bindungsformen von ^{232}Th, ^{238}U und ^{226}Ra zu bestimmen.

Die Aktivitäten von Th, U und Ra sind in paläozoischen Gesteinen (Median-Werte: ^{232}Th: 47 Bq/kg, ^{238}U: 32 Bq/kg, ^{226}Ra: 32 Bq/kg) höher, als in mesozoischen Gesteinen (Median-Werte: ^{232}Th: 25 Bq/kg, ^{238}U: 25 Bq/kg, ^{226}Ra: 22 Bq/kg). Die natürlichen Radionulkide sind in den Verwitterungsprodukten im Vergleich zu den Ausgangsgesteinen angereichert; dies gilt insbesondere für die Proben des Paläozoikums (Median-Werte: ^{232}Th: 55 Bq/kg, ^{238}U: 44 Bq/kg, ^{226}Ra: 44 Bq/kg). Die Verwitterungsprodukte des belgischen Gedinne zeigen besonders hohe Aktivitäten (Median-Werte: ^{232}Th: 83 Bq/kg, ^{238}U: 223 Bq/kg, ^{226}Ra: 425 Bq/kg). ^{226}Ra ist immer in säkularem Gleichgewicht mit ^{230}Th.

Die Emanationkoeffizienten der Verwitterungprodukte sind höher als die der Gesteine, insbesondere bei Proben mit mehr als 10% Fe_2O_3. Die Radonaktivitätskonzentrationen der Häuser korrelieren signifikant mit den Emanationskoeffizienten der Verwitterungsprodukte, aber nicht mit denen der Gesteine.

Thorium ist für Gesteine und Verwitterungsprodukte relativ gleichmässig in den Fraktionen der sequentiellen Extraktion verteilt. Uran in Gesteinen verbleibt zum grössten Teil im Residuat und erscheint am zweithäufigsten in den Fraktionen der Eisenoxide. In den Verwitterungsprodukten tritt Uran dagegen in der höchsten Konzentration in den Eisenoxid-Fraktionen auf und weniger als 10% des gesamten Urans im Residuat. Die Bindungsformen des Radium weichen stark von denen des Uran ab. Sowohl in den Gesteinen, als auch in den Verwitterungsprodukten findet sich das meiste Radium im Residuat, gefolgt von den

Anteilen in der mobilen, austauschbaren Fraktion bzw. der Fraktion der gut kristallinen Eisenoxide. In den Verwitterungsprodukten ist ausserdem eine hohe Konzentration in der Fraktion der Manganoxide zu finden.

Die hohen Radon-Belastungen im Eisléck sind bedingt durch die Anreicherung von Radium in gut kristallinen Eisenoxiden, welche in den zahlreichen Klüften, Verwerfungen und Spalten des Unterdevons als Verwitterunsprodukte vorkommen, in Verbindung mit den guten Wegsamkeiten für passive Advektion und thermodiffusen Transport von Radon an die Oberfläche.

1   Introduction

Significant differences between indoor radon concentrations in the northern Eisléck and the southern Gutland have been reported by KIES et al. (1994). The regional distribution has been proven beyond doubt to be correlated with the geological age of the bedrock (KIES et al. 1996a, KIES & FEIDER 1996), but the reasons were not quite clear, as no evident relation could be established between radium activities of rocks, soil gas radon concentrations, and indoor radon concentrations (KIES & FEIDER 1996).

More than 40% of the dwellings in the north exceed the action level of Luxembourg (150 Bq/m^3), therefore it was essential to find an explanation for the high indoor radon concentrations and, furthermore, to provide a more detailed basis for assessing the geogenic radon exposure of the population in Luxembourg.

Since TANNER (1980) many efforts have been made to understand and quantify the influence of radon in soil gas on radon in dwellings. Most previous work has focussed on radon activity concentrations in soil gas in relation to the geological bedrock and the impact of the permeability of soils on the transfer of radon into dwellings (e.g. DUVAL & OTTON 1990; KEMSKI et al. 1992; GUNBY et al. 1993; KIES et al. 1994; KIES & FEIDER 1996; VON GUNTEN et al. 1996; KEMSKI et al. 1998, 1999, 2001, 2002). Many studies have dealt with special parameters affecting the migration of radon from soil into a dwelling, especially the physical soil parameters (e.g. MEGUMI & MAMURO 1974; BARRETTO et al. 1975; STRANDEN et al. 1984a; STRANDEN et al. 1984b; LINDMARK & ROSEN 1985; BARTON & ZIEMER 1986; KELLER & SCHÜTZ 1988; STRONG & LEWINS 1991; HOWARD et al. 1995). So far, there has been a lack of detailed investigations into the geochemistry of the parent radionuclides of radon and the influence of their speciation on radon emanation. Only two substantial surveys have been published, focusing on the geochemistry of natural radionuclides and the radon emanation in selected soil profiles (VON GUNTEN et al. 1996; EDSFELDT 2001).

An area-wide analysis of rocks with their accompanying weathering products was chosen for this survey, in preference to the analysis of few selected soil profiles, to achieve meaningful results for the distribution of natural radionuclides and radon emanation in different stratigraphic units and distinct lithologies throughout the country. Detailed geochemical analysis of selected samples was performed to reveal the differences in speciation of radionuclides of rocks and weathering products and to test, whether there is a connection between the speciation of radionuclides - especially radium - and radon emanation.

This study attempts to disclose the relations between geology, lithology, activities, and speciation of Th, U and Ra and radon emanation in order to understand the determining factors for radon transport into dwellings.

1.1 Radon risk in dwellings

In the past thirty years, radon has been recognised as a health hazard. Radon is considered to be the major source of natural radiation, together with its daughters (Table 1). The WHO (World Health Organisation) has therefore recommended that surveys of radon in buildings should be conducted (WHO 1987).

Two different radon isotopes are significant: ^{222}Rn, a decay product of the ^{238}U decay series, with a half-life of 3.8 days, and ^{220}Rn, a decay product of the ^{232}Th decay series, with a half-life of 56 s. Due to the short half-life of ^{220}Rn, the radiation exposure to this radon isotope is usually much lower than is the case for ^{222}Rn (0.07 vs. 1.2 mSv a^{-1}, UNSCEAR 1993). ^{220}Rn is only of importance under special conditions, e.g. when people are sleeping close to the soil surface, especially in the case of Th-rich bedrock (WIEGAND & FEIGE 2002).

In this study, only ^{222}Rn is analysed. The use of the term radon, unless otherwise indicated, always refers to ^{222}Rn.

Table 1: Average natural radiation exposure in Germany and worldwide

Source	Average annual effective dose (mSv)	
	Germany*	Worldwide**
Cosmic/ Cosmogenic	0.3	0.4
Terrestrial		
External	0.4	0.5
Internal		
Inhaled (mainly radon)	1.1	1.2
Ingestion	0.3	0.3
Total	2.1	2.4

* Bundesministerium für Umwelt, Naturschutz und Reaktorsicherheit 2002
** UNSCEAR Report 2000

Based on numerous studies of lung cancer in radon-exposed underground miners (IARC 1988), radon was classified as a human carcinogen. Many epidemiological studies have been carried out with the aim of quantifying the risk of lung cancer due to increased radon levels in dwellings, (WICHMANN et al.1998; WICHMANN et al.1999; FIELD et al. 2000; GERKEN et al. 2000 cum lit). An overview of the earlier studies including documentation of the regions investigated, the design of the studies and their main findings, is given in WICHMANN (1996).

Only a few of these studies have proven a significant lung cancer risk as a result of exposure to residential radon, notably the Swedish case-control study of PERSHAGEN et al. (1994) and the German (East and West) case-control study of WICHMANN et al. (2002). For the latter, a significant influence of exposure to radon on the lung cancer risk was only observed for so-called "radon-prone areas" (Table 2). It is anticipated that the significance of the entire German study will rise when the German data (6,500 cases) is pooled with the data of the Eifel-Ardennes study (3,000 cases) (KREIENBROCK et al. 1993).

The Swedish case-control study documents a significant relationship between residential radon and lung cancer risk for the whole region covered by the study: $OR^1 = 1.3$ for 140-400 Bq/m^3 and 1.8 for > 400 Bq/m^3 vs. < 50 Bq/m^3. In Sweden, radon is considered the second largest cause of lung cancer after smoking. Of the total of about 3,000 cases of lung cancer in 1994, the annual incidence due to radon was estimated to be of the order of 400 to 900 (Ministry of Health and Social Affairs, Sweden 1996; National Board of Health and Welfare, Sweden 1997). It is estimated that 7% of all lung cancer deaths in Germany are caused by indoor radon (STEINDORF et al. 1995).

Table 2: Lung cancer risk due to radon in present dwellings in East and West Germany (after WICHMANN et al. 2002, KREIENBROCK et al. 2001)

Radon [Bq/m^3]	Adjusted odds ratio (OR)			
	East Germany		West Germany	
	Entire study area	Radon-prone area	Entire study area	Radon-prone area
0 – 49	1.00	1.00	1.00	1.00
50 – 79	0.97	1.07	0.98	1.57
80 – 139	1.05	1.07	1.09	1.93
> 140	1.37	1.62	0.99	1.93

The inconsistencies of the results of epidemiological studies have many causes. LUBIN et al. (1995) and MUIRHEAD (2002) discussed the uncertainties and sources of error that can arise for such studies. GERKEN et al. (2000) developed an improved method of assessing individual radon exposure histories, which is one of the major elements of uncertainty.

Due to the latent radon risk, many countries started indoor radon survey programmes with the aim of reducing the exposure of the population to radon.

---

[1] OR = odds ratio

1.2 Indoor radon measurements

Luxembourg, just as many other countries, has a national radon programme. Indoor radon concentrations are monitored in order to obtain information about the regional variation of radon in dwellings and at workplaces. Indoor radon measurements, which are free of charge, were started in Luxembourg with etch track detectors of the original Karlsruhe design with Makrofol film in 1989 by the Ministry of Health (Radiation Protection Department) and are still being conducted (KIES & FEIDER 1996). The detectors were placed in dwellings, schools and at workplaces.

Measurements were conducted over a three-month period, generally starting in the autumn or late winter. The detectors were distributed randomly throughout the country with the help of local fire brigades. A small percentage (< 5%) of houses investigated in the national survey were measured on request of the house owners. The building characteristics of each house were recorded by questionnaire during the survey (KIES et al. 1994).

The distribution of indoor radon activities in Luxembourg, including unpublished data provided by the Ministry of Health (Radiation Protection Department), is presented in Figure 1. In contrast to data published previously by KIES & FEIDER (1996) and KIES et al. (1996 a, b), only data from the ground floor are shown.
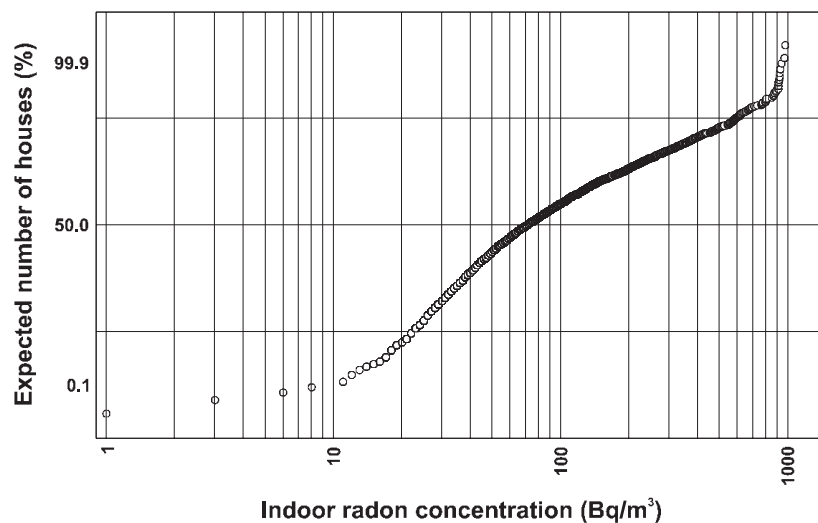
Figure 1: Normal probability distribution of indoor radon activities on the ground floor (living room, bedroom and kitchen) in about 3000 houses in Luxembourg (median: 71 Bq/m^3). Measurements conducted between 1989 and June 1998; data provided by the Ministry of Health (Radiation Protection Department).

While the median indoor radon activity in Luxembourg is 71 Bq/m^3, a clear distinction between radon levels of the northern Eisléck (median: 128 Bq/m^3) and the southern Gutland (median: 75.4 Bq/m^3) is evident (KIES & FEIDER 1996; KIES et al. 1996 a, b; unpublished

data, Radiation Protection Department of Luxembourg). About 11% of the houses in the Eisléck have radon concentrations exceeding 400 Bq/m^3 (proposed European action level), but less than 1% of the houses measured in the Gutland are affected. Only 6.3% of the dwellings in the south, but more than 40% of the dwellings in the north were found to have indoor radon concentrations exceeding the action level of Luxembourg of 150 Bq/m^3, with maximum values up to 2000 Bq/m^3 (FEIDER & KIES 1996). The north of the country can be considered to be a radon prone area in accordance with the recommendations of the ICRP65 (ICRP 1993), because radon concentrations in more than 1% of the dwellings exceed ten times the national average value (KIES et al. 1994).

Apparently, indoor radon concentrations increase with the geological age of underlying bedrock (Figure 2) as well as with the age of houses. This effect is most relevant for houses that are older than 70 years (KIES & FEIDER 1996). While houses that were built after 1945 show a median radon level of 56 Bq/m^3, the median radon activity for houses built between 1900 and 1945 is 71 Bq/m^3 and for houses built before 1900 it is 109 Bq/m^3 (unpublished data, Radiation Protection Department of Luxembourg).
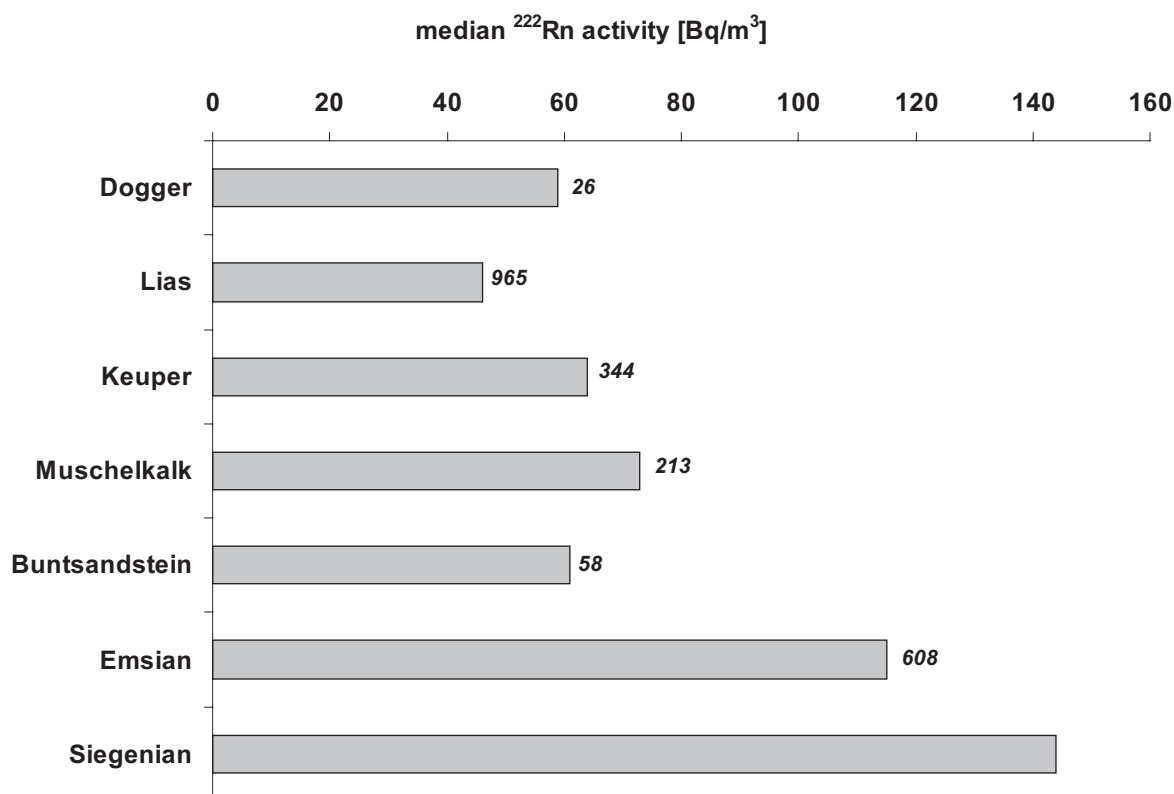
Figure 2: Median radon activities on the ground floor (living room, bedroom and kitchen) in about 2,700 houses in Luxembourg in relation to geological age of bedrock. Measurements conducted between 1989 and June 1998. The number of houses investigated is stated for each geological age. Data provided by the Ministry of Health of Luxembourg (Radiation Protection Department).

1.3 Source of radon

The main sources of radon in dwellings are the bedrock and soil. Many attempts have been made to predict the radon risk for certain areas by measuring the activity of naturally occurring ^{238}U and ^{226}Ra - as the parent radionuclides - in rocks and soils, the radon activity concentrations in soil gas, the permeability of soils as well as the emanation and exhalation rates of soils (KELLER & SCHÜTZ 1988; DUVAL & OTTON 1990; KEMSKI et al. 1992, 1996 c, 1998; ZHU et al. 1998; KEMSKI et al. 1999; STEGEMANN et al. 1999; KEMSKI et al. 2001, 2002, 2003). The parameters affecting indoor radon concentrations are very complex. Many factors influence the migration of a radon atom from its place of origin into a dwelling. The knowledge of the bulk activity of ^{238}U and ^{226}Ra in rocks and soils alone is not sufficient for indoor radon prediction, since the spatial distribution of the radionuclides in minerals and soil particles is one of the most important factors for the release of radon (radon emanation). Emanation is defined as the fraction of total radon, formed in a solid by radium decay, that escapes e.g. from a soil particle into the pore or fracture space. Besides the distribution of the parent isotopes, the internal structure of a material, the particle size distribution within a material, the moisture content, and the temperature have an influence (BARRETTO et al. 1975; BARTON & ZIEMER 1986; BOSSUS 1984; FLEXSER et al. 1993; HEINRICH 1994; HOWARD et al. 1995; MEGUMI & MAMURO 1974; MORAWSKA & PHILLIPS 1993; SEMKOW & PAREKH 1990; STRONG & LEWINS 1991).

Once radon gas is released into the pore space, it migrates by diffusion in inter-granular spaces and soil pores in response to a gradient of radon concentration and/or by advection, carried by soil gas or water. The rate of diffusion (effective diffusion coefficient) depends primarily on the degree of liquid saturation of the soil and secondly on the porosity, pore sizes, adsorptive properties of the soil grains and of the liquid phase (TANNER 1991). The transport of radon by advection is dependent on the presence and nature of carrier media such as circulating sub-surface waters and soil gas. Increased radon activities are usually caused by advection along faults, shear zones, caverns, or fractures (HAKL et al. 1992), which may transport radon over a distance of more than a hundred metres (KEMSKI et al. 1992; VON GUNTEN et al. 1996).

The structurally controlled advective flow of radon is strongly influenced by the weathering history of an area. Highly weathered areas usually show higher permeabilities and may provide more pathways at discontinuities (APPLETON & BALL 1995). Besides, highly weathered soils often contain higher radionuclide activities, as uranium, radium and thorium can be retained in soils (LATHAM & SCHWARCZ 1987, IVANOVICH et al. 1992, VON GUNTEN 1996). The enrichment of radionuclides in soils and weathering products is dependent on the type of bedrock, because the various types of rocks differ in their content of radionuclides, and on the intensity of the weathering. While granites and pegmatites

contain high uranium and radium activities, sediments usually have low activities, except phosphates, black shales, and bauxites (KEMSKI et al. 1996 a cum lit). In most cases, rocks with high uranium and radium concentrations develop soils with high radionuclide activities, whereas rocks with low uranium and radium concentrations lead to soils with low radionuclide activities. Exceptions are described by SURBECK (1991), SCHUMANN & GUNDERSEN (1996) and KEMSKI et al. (1996 a).

The formation of distinct types of rocks during the history of the Earth tends to be typical for geological ages. Considering sediments, which are the only rock types in Luxembourg, the variety of deposited rocks reflects the palaeogeographical and environmental changes of sedimentary conditions over time. A connection between geological age and indoor radon levels is reported not only for Luxembourg but also for other countries e.g. the United Kingdom (GUNBY et al. 1993, APPLETON & BALL 1995), Germany (e.g. KREIENBROCK & SIEHL 1996, KEMSKI et al. 1999), Belgium (TONDEUR et al. 1996), and Switzerland (BÖHM 2003).

The distinct difference in indoor radon concentrations between the northern Eisléck and the southern Gutland can be explained by the different nature of outcropping rocks. The Eisléck consists of strongly faulted and folded Palaeozoic siliciclastic rocks, while the Mesozoic rocks of the Gutland are generally flat-lying and often carbonatic. Not only does the type of the rock have an effect, but also different structural environments. The Palaeozoic rocks of the Eisléck, as part of the Ardennes, have been strongly deformed during the variscian orogenesis, resulting in intense folding, faulting, and fracturing. In contrast, the Mesozoic deposits of the Gutland were affected only by the uplifting of the southern Eifel during the Tertiary and Quaternary, leading to block faulting with displacements up to some tens of metres (LUCIUS 1948, BERG 1965, DITTRICH 1989). An important factor is also the weathering grade, which is much higher for Palaeozoic rocks, because two phases of intense weathering had affected the Ardennes. The first one during Permotriassic times under arid climate conditions and the second phase during Late Cenozoic to Early Tertiary under tropical to subtropical conditions (MEYER 1998). The weathering of the Ardennes is assumed to be as intense as for the *Rheinisches Schiefergebirge*, leading to deep weathering zones of several hundred metres (MÜCKENHAUSEN 1958, KNAPP 1978, FELIX-HENNINGSEN 1990 cum lit, MEYER 1998).

1.4   Results of previous research in Luxembourg

Investigations of the origin of different indoor radon levels in the northern and southern part of Luxembourg (KIES et al. 1994) started in 1994. Rock and soil samples were taken mainly from excavated building sites, usually at a depth of one meter to determine

radium activity concentrations. In addition, samples were taken outside villages with a soil auger at a depth of one meter (ROWLINSON 1998). At the same sites, radon soil gas measurements with "Czech rods" (NEZNAL et al. 1991) and soil permeability measurements with a special device called a "Radon JOK"[2] were undertaken, to estimate the radon availability (ROWLINSON 1998). Both parameters were measured because the radon availability is dependent on radon activity concentration in soil gas (production) and permeability of soils (migration) (TANNER 1988).

The **radium activity** measurements reveal a range of 4.2 to 116 Bq/kg and did not show distinct differences either between Palaeozoic and Mesozoic samples, or between rock and soil samples (KIES et al. 1996a). If soil samples included rock particles, they were not removed and weathered materials were not cleaned off the rock samples (KIES, ROWLINSON, ROBINET oral communications). Differences between rock and soil samples were therefore most probably blurred.

The **soil gas radon** measurements showed higher radon activities for the Eisléck (10 - 200 kBq/m^3) than for the Gutland (10 - 120 kBq/m^3) (ROWLINSON 1998). Nevertheless, the median soil gas radon activities are about equal (Eisléck: 35.5 kBq/m^3; Gutland: 34.5 kBq/m^3) and a correlation of radon activities in soil gas to geological age could not be established because of the small number of measurements (KIES & FEIDER 1996). Even soil gas radon measurements near houses in selected villages of the Eisléck (Asselborn, Bigonville), where extensive indoor radon measurements had also been conducted, did not show a significant positive correlation between radon levels in soil gas and in dwellings (ROWLINSON 1998).

The **permeability of soils** in the Eisléck varies between 2 x 10^{-11} m^2 and 6 x 10^{-14} m^2, but is sometimes even lower than the detection limit of 10^{-14} m^2. The permeability of soils in the Gutland is variable for the stratigraphic units of the substratum, but dependent on their lithology. Several siliciclastic stratigraphic units have elevated median or third quartile permeability values. Soils with marl or argillitic lithology show characteristic low permeability. Considering the third quartile of the measurements, the values for the Eisléck are consistently higher when compared to those of the Gutland (ROWLINSON 1998).

---

[2] Radon V.O.S., Praha
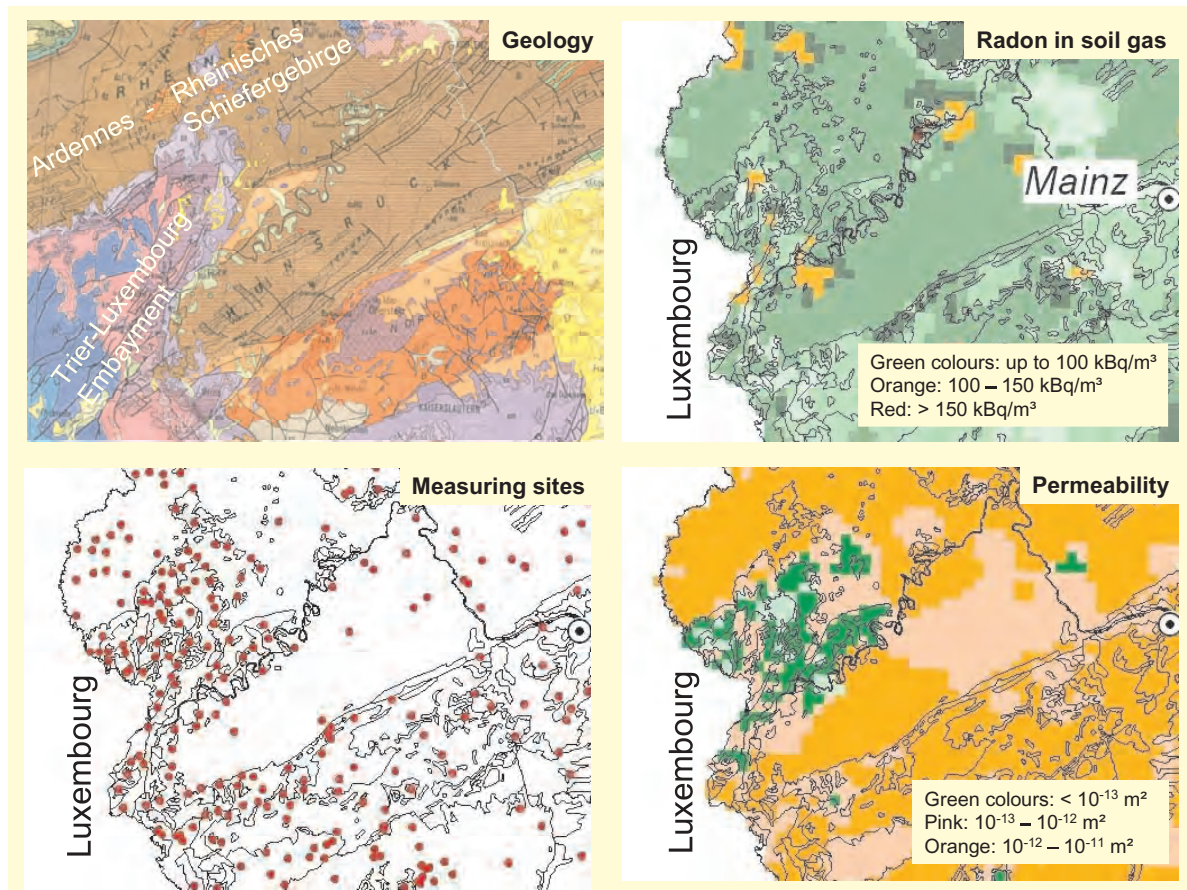
Figure 3: Results from radon in soil gas and permeability measurements in Germany on the border to Luxembourg (redrawn after SIEHL 2004)

Measurements of radon in soil gas and permeability of soils in Germany on the border to Luxembourg showed no general differences of radon activities in soil gas between the Devonian of the Eifel, which corresponds to the Devonian of the Ardennes and the Mesozoic of the Trier-Luxembourg Embayment. The permeability of the soils above Devonian rocks is clearly elevated (SIEHL 2004). Although variations of permeability of soils for this region occur, KEMSKI et al. (2001, 2003) regard the radon activity concentration in soil gas as the determining factor for the radon potential in Germany. Because more than 95% of all soils in Germany have revealed highest permeability (> 10^{-11} m²), they take highest soil permeability for the whole country as a "worst case assumption".

In 1994, an **airborne gamma-ray survey** was conducted in Luxembourg. The data of the flight lines of a south-north traverse with a spacing of only 0.5 km were analysed (ROBINET 1996, KIES et al. 1996b). Aerial radiometric data, without radon correction, were discussed in relation with radionuclide concentrations in upper soil layers (ROBINET 1996, KIES et al. 1996b). Soil samples for the ground check were taken with a soil auger from three different depths down to 40 cm from grass covered, relatively flat-lying fields

(ROBINET 1996) but the radionuclide activities did not show any noticeable depth-induced difference. Though the airborne gamma-ray survey yielded higher equivalent uranium (eU) counting rates for the Eisléck, the soil samples did not show any significant difference between the Gutland and the Eisléck.

Radon measurements in soil gas and permeability measurements using the same methods are still in progress in Luxembourg (KIES & FEIDER 1996; KIES, oral communication). In 1996, radon measurements in ground and drinking water were started (SCHMITZ 1997, KLOSEN 1998). A strong positive correlation between radon concentrations in groundwater and geology, as observed in southern Belgium (CHARLET et al. 1995), is expected.

1.5   Aim of this study

One of the main objectives of the current study is to draw attention to the relevance of weathering products of different bedrocks for the prediction of the radon potential. The radon potential is defined as the radon activity concentration in soil gas independent of the permeability of soils, following the argumentation of KEMSKI et al. (2001). Nevertheless, the results of this study will be discussed with regard to the permeability of soils, because soil permeability measurements in Germany (Figure 3) and Luxembourg showed clear variations between the Mesozoic and the Devonian.

Representative rock samples are collected together with their accompanying weathering products from representative geological units. After carefully separation of the weathering products from the rocks, the samples are analysed for their content of natural radionuclides (U, Ra, and Th) by γ-spectrometry, and for their radon emanation. It is expected that strong differences in radium activities and radon emanation occur not only between rock samples and their weathering products, but also between weathering products of rocks of different geological age. Thorium and uranium activities are measured for completeness. It may be shown that uranium cannot be used as an analogue for radium, as some authors do (e.g. FLEXSER et al. 1993), because the geochemical behaviour of radium and uranium diverges considerably. Furthermore, it is assumed that emanation is not only dependent on the emanation coefficient and the total radium activity concentration, but also on specific speciations of radium.

A newly developed method for measuring radon emanation allows the comparison of samples with different grain size and varying initial water contents. Not only emanation coefficients are discussed, but also radon activity concentrations, which refer to the released radon in sample pore gas related to the weight of the emanating material under equilibrium conditions. Elevated radon activity concentrations are expected for the weathering products.

Some attempts have been made to determine the distribution of radium in rocks and soils over the past thirty years (e.g. DUVAL & OTTO 1990, GREEMAN 1992, FLEXSER et al. 1993, VON GUNTEN 1996, ROTH 1997, EDSFELDT & FERNLUND 1998, EDSFELDT 2001). One method to determine radium distribution is to analyse the bonding of radium by sequential extraction, but many contradictory results are documented in the literature, mainly because of the use of insufficiently selective extraction methods (GREEMAN 1992, ROTH 1997, EDSFELDT & FERNLUND 1998).

For the current work, an appropriate sequential extraction scheme (ZEIEN 1995) with good selectivity was used. Due to the lack of samples with elevated radionuclide activities in Luxembourg, samples of similar rock types, geological age, comparable structural environment and the same weathering grade as the Palaeozoic rocks in the Eisléck were taken from the Gedinnian in the Belgian part of the Ardennes.

2   The Geology of Luxembourg

Luxembourg can be divided into two main geological and morphological areas. The Eisléck in the north, belonging to the Ardennes, consists of highly deformed schists and quartzites of Lower Devonian age.

The Mesozoic sediments of southern Luxembourg, mainly of Triassic and Jurassic age, overlay unconformably the Palaeozoic basement and are part of the north-eastern Paris Basin (Figure 4 and Map A6 (Appendix 6)).

2.1   Devonian Basement

The Devonian stratigraphy in Luxembourg was established by LUCIUS (1950 a) and is based mainly on lithological characteristics of the rock sequence (MAQUIL, MOSAR & THEIN 1984, KONRAD & WACHSMUT 1973). Exceptions are the Schist of Wiltz and the Quartzite of Berlé, which are rich in fauna and can be correlated with the corresponding strata of the *Rheinisches Schiefergebirge*. The Lower Devonian sequence in Luxembourg includes Early Siegenian (*Sg1*) up to earlier Upper Emsian (*E3*) (Figure 5).

During Early Devonian times the Ardennes were affected by the subsidence of the Rhenohercynian Basin under an extensional regime. Marine transgressions commenced in the Gedinnian (ZIEGLER 1988), but the oldest outcropping sediments in Luxembourg are of Early Siegenian (*Sg1*) age, corresponding in general to the *Tonschiefergruppe* in the *Rheinisches Schiefergebirge* after MITTMEYER (1974). The eroded landmass of the Old Red Continent was situated only 50 km further north, so that intertidal shallow sea sediments, predominantly dark schists, siltstones and sandstones, were deposited. In the West of the Eisléck (Schimpach), the *Sg1* occurs in roof slate (*Dachschiefer*) facies (LUCIUS 1937).

The ongoing subsidence during Middle Siegenian (*Sg2*) led to the deposition of coarser clastic sediments, such as sandstones and sandy schists, in a shallow sea environment, which corresponds to the *Rauhflaserschichten* in the Eifel (ASSELBERGHS 1926). Occasional fossil-bearing horizons in the *Sg2* give evidence of marine conditions (LUCIUS 1950 a).

The top layers of the Middle Siegenian are slates, while the sediments of the Upper Siegenian (*Sg3*) consist mainly of sandy schists partly including quartzitic sandstone layers several meters thick. Sedimentary characteristics such as megaripples, groove marks, flute marks and load casts are abundant.

Legend
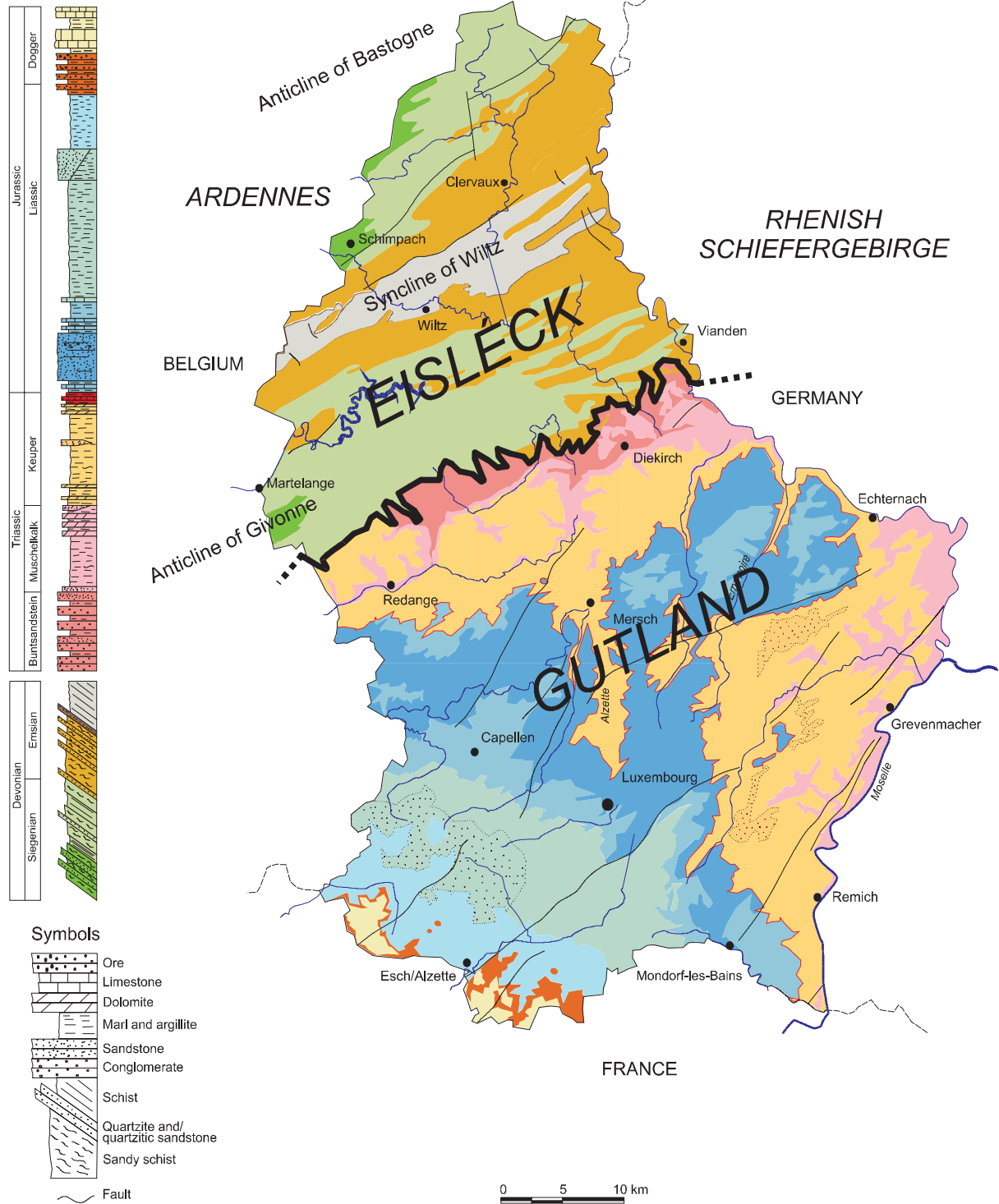
Figure 4: Geological map of Luxembourg, redrawn after "Carte Géologique Générale 1:100 000"

Sediments of Upper Siegenian age are found north and south of the Syncline of Wiltz (Figure 4). The northern facies is sandier than the southern one. The latter can be divided into the basal *Dachschiefer* (grey schists that are poor in fossils) and the *Grobschiefer* (sandy schists) at the top. Basal schists, which locally occur in roof slate facies, are similar to

the *Hunsrückschiefer* Facies of the eastern Mosel Syncline (ASSELBERGHS 1926, MITTMEYER 1974). The upper part of the *Grobschiefer* belongs to the Emsian, comparable to the Ulmen Group of the *Hunsrückschiefer* (LUCIUS 1950 a).

The lowest Lower Emsian (*E1a*) is characterised by slightly sandy, mainly green, or green-grey schists including some quartzite layers. In the upper Lower Emsian (*E1b*), the schists become sandier, documenting a continental influence. Quartzitic schists and quartzitic sandstones are common.
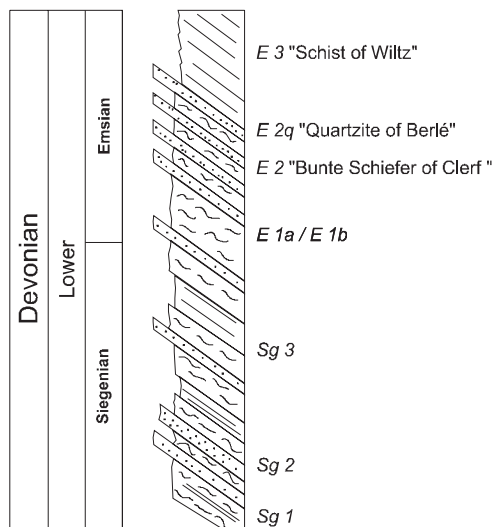
Figure 5: Stratigraphic section of the Devonian. Redrawn after Geological Map of Luxembourg 1 : 100000 (Service Géologique 1996)

The *Bunte Schiefer of Clerf* were deposited during the Middle Emsian (*E2*). They correspond to the *Klerfschichten* in the Eifel. The continental influence becomes even more distinct. Red and green schist and sandstone interlayers often show mud cracks. In the upper part of the Middle Emsian, lenticular quartzites mark the beginning of the *Quartzite of Berlé* (*E2q*), which is a white or reddish quartzite only 2-15 m thick. This layer marks the boundary to the Upper Emsian (*E3*) and may be correlated with the Emsian-Quartzite of the *Rheinisches Schiefergebirge*.

The Upper Emsian (*E3*) sediments include mainly schists, which may locally be sandy. The youngest Devonian sediments in the core of the Syncline of Wiltz are rich in fossils.

After the Late Palaeozoic Variscian Orogeny, the Devonian basement was eroded and peneplained during Permian times. The tectonic depression in the area of the *Eifel Nord-Süd-Zone* and the Mosel-Syncline was an area of sedimentation in the Early Triassic.

2.2 Mesozoic Cover

The Mesozoic cover of the north-eastern part of the Paris Basin, which is called the Trier-Luxembourg Embayment, is build up by Triassic and Jurassic sediments from Middle Buntsandstein to Middle Jurassic (Dogger). The embayment is a conjunction between the Lothringian Depression and the *Eifel Nord-Süd-Zone*.

The oldest Triassic deposits are coarse-grained fluvial sediments, lying unconformably on the Devonian basement. The sediments have been transported from South to North through the *Eifel Nord-Süd-Zone* into the northern part of the German Basin. Previously they were considered to be of Middle Buntsandstein age, but recent investigations point to Lower Buntsandstein (*su*) age (DITTRICH 1999).

The marine transgression during Middle and Upper Buntsandstein (*sm - so*) results in the marginal marine Voltziensandstein (Figure 6). The Saargemünd-Zweibrücker depression linked the Trier-Luxembourg Embayment with the basin of south-western Germany. A connection to the North existed through the *Eifel Nord-Süd-Zone*. The shoreline ran in a north-south direction along the Ardennes in the west and the Eifel in the east.
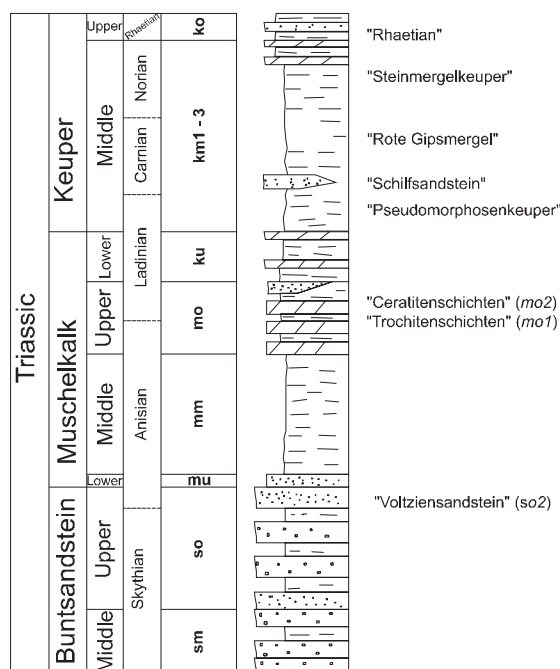
Figure 6: Stratigraphic section of the Triassic. Redrawn after Geological Map of Luxembourg 1 : 100 000 (Service Géologique 1996)

The basin broadened up to the west and to the east. The rocks of the Lower Muschelkalk (*mu*) consist of marine sediments, which can be seen as a marginal facies of the Wellenkalk in the German Basin. In contrast to the limestones and marls of the

Wellenkalk, sandstones, clayey marls and dolomites were deposited in the Trier-Luxembourg Embayment.

During the Middle Muschelkalk (*mm*), the sea was regressing. The connection to the German Basin through the *Eifel Nord-Süd-Zone* was closed. A sequence of lagoonal-evaporitic sediments is followed by a marine-lagoonal and fluviomarine phase, both of them poor in fossils.

From Upper Muschelkalk (*mo*) times on, shallow sea sediments were deposited with dolomitic marls and dolomites (Figure 6). The latter are partly rich in crinoids ("trochites") and oolites, which mainly originated at the Sierck Swell and drifted towards the *Eifel Nord-Süd-Zone*. The Sierck Swell obstructed the bay to the South. While the northern Eifel region could be considered a swell, subsidence was strongest in the southern Eifel (SCHRADER 1983).

Lower and Middle Keuper (*ku - km*) rocks are characterised by frequent changes from marine-fluviomarine and lagoonal to hypersaline sediments on a shore platform with poor relief. The junction to the northern German Basin opened again through the *Eifel Nord-Süd-Zone*. The interlayer of the Schilfsandstein (*km2s*) gives evidence of a high-energy, partly fluvial, environment during the middle of the Middle Keuper (DITTRICH 1989). The series of the "*Rote Gipsmergel*" were traditionally assigned to the *km2* (LUCIUS 1949, DITTRICH 1984). Since a revision of the Upper Triassic stratigraphy by DITTRICH (1989), this series is considered to belong to the *km3.*

During Rhaetian (*ko*) times, starting with a basal terrestrial conglomerate, marine conditions prevailed again. The Triassic seas reached their greatest extent in Upper Rhaetian, after some changes from intertidal and subtidal cycles of sedimentation in the Middle Rhaetian (DITTRICH 1989).

The transgression went on until the Jurassic. The Liassic Sea was not only connected to the Nordic Sea but also to the Tethys. Intercalated into pelitic and carbonatic sediments of the central basin, the offshore sand dunes of the Luxembourg Sandstone (*li2*) were deposited at the southern border of the Ardennes and the *Eifel Nord-Süd-Zone* (BERNERS 1983). The sandstone interfingers to the Northwest with marls and limestones of the Hettangian and Sinemurian (*li3*) (Figure 7).

Since Upper Lias (*lo*) times the connection to the Nordic Sea has been closed. Until the end of Lias, ferruginous calcitic and silty sandstone sequences intercalate the marly-calcitic Lothringian facies. Upper Toarcian (lo_6-lo_7) and Aalenian (*dou*) sediments are characterised by the oolithic ironstones of the Minette, which were deposited in a near-shore shallow marine environment (LUCIUS 1945; THEIN 1975; SIEHL & THEIN 1978; TEYSSEN 1984; SIEHL & THEIN 1989).

The Mesozoic sequence in the Luxembourg area ends with coral limestones of Bajocian age (Figure 7). The course of the eastern shore line of the Paris basin during

Middle and Upper Jurassic is not evident, as is also the case for the coastline of the Cretaceous sea. Remnants of Cretaceous cherts in quaternary fluvial terraces of the Luxembourg Ardennes and in the southern Eifel indicate a flooding of the Trier-Luxembourg Embayment in Upper Cretaceous (MAQUIL & LÖHNERTZ 1984).

	Dogger	Middle	Bajocian	dom 1 - 3	"Limestone of Haut-Pont"
		Lower	Aalenian	dou	
				lo 6 - 7	"Minette"
		Upper	Toarcian	lo 1 - 5	
Jurassic				lm3b	"Upper Spianatus"
				lm3a	"Lower Spianatus"
	Lias	Middle	Pliensbachian	lm 1 - 2	
		Lower	Sinemurian	li 3	"Marl and Limestone of Strassen"
			Hettangian	li 2	"Luxembourg Sandstone"
				li 1	
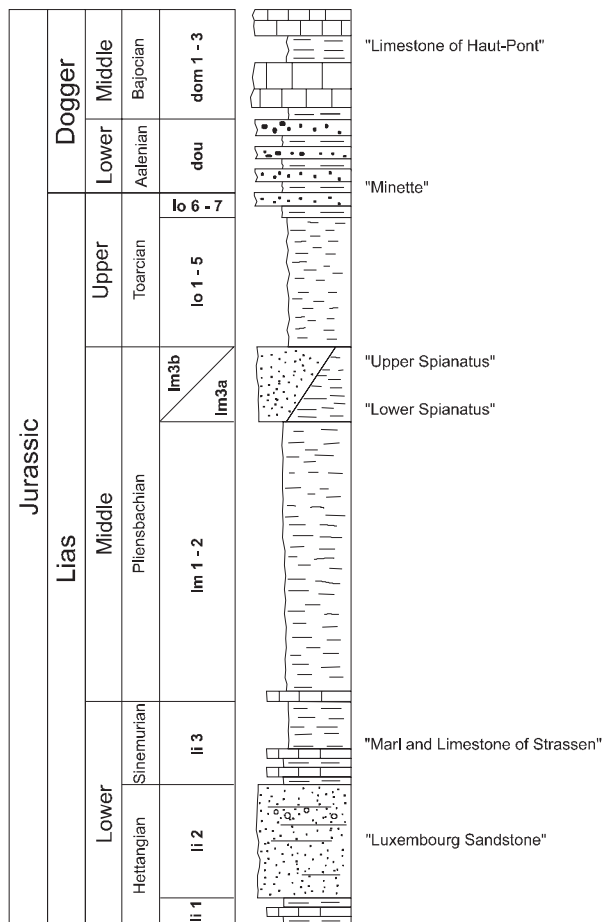
Figure 7: Stratigraphic section of the Jurassic. Redrawn after Geological Map of Luxembourg 1:100 000 (Service Géologique 1996)

The Trier-Luxembourg Embayment was disconnected from the Paris Basin during Tertiary. The southern Eifel was part of the uplifting Rhenish and Ardennish Massive.

Intense tropical weathering and erosion took place in Palaeocene/Eocene times; derivates are the lateritic ores in the karst of the Triassic dolomites and Jurassic limestones.

During the Oligocene, limnic sediments such as bog iron ores were deposited.

In Pliocene and Pleistocene times, the uplift of the Gutland was not as strong as of the Eisléck. Vertical movements along faults controlled the development of the present cuesta landscape. Apart from that, the erosion and sedimentation of the rivers in the Pleistocene, forming valley cuts down to a depth of 300 m, was most important for the development of the geomorphological relief (BERNERS & MULLER 1984, BINTZ 1984).

17

3   Materials and Preparation

3.1 Sampling

A total of 266 samples of rocks and their weathering products were collected from 26 stratigraphic units all over Luxembourg with an emphasis on the Eisléck. All sampling sites are located in Luxembourg except one, which was about 1 km Northwest of Hatrival, in Belgium (x [6]66 020 / y [55]42 050), where there are not only high indoor radon concentrations, but also very high radon concentrations in the spring, ground and drinking water (DOREMUS et al. 1992; TONDEUR 1996; ZHU et al. 1995). Sampling sites were mainly outcrops along roads and old quarries. If no outcrops were accessible, samples from excavations were taken and, in individual cases, fragments of bedrock from fields. A list of sample sites can be found in Appendix 1, Table A1 and are shown on the General geological map, Appendix 6.

At most of the 90 sites both types of sample were taken, with 50 pairs or multiples. The weathering products were separated in two size classes: > 2 mm (skeletal soil) and < 2 mm (fine soil). The terms "rock samples", "weathering products > 2 mm" and "weathering products < 2 mm" will be used to distinguish between the different types of sample.

3.2 Sample Preparation

The weathering products were removed from the rock samples with distilled water. The weathering products were collected and sieved in the wet state with distilled water to separate the < 2 mm fraction. The organic matter (mainly roots) was removed manually. All samples were dried at 40°C. The weathered material > 2 mm fraction was sieved again after drying, to ensure that no aggregates of finer grains were left in this fraction.

The rock samples and the samples of the weathered material > 2 mm were crushed to a diameter of about 2 mm. Approximately 50 g of the crushed material were used for γ-spectrometry analysis after drying at 105°C. 200 - 300 g of the samples were milled to a grain size < 200 µm and dried at 105°C for XRF analysis, emanation measurements and chemical sequential extractions.

Samples of lower weight were first crushed and measured by γ-spectrometry, before being milled for XRF analysis. Very few samples of less than 30 g were milled directly and the γ-spectrometric measurements were done with the same pill that was prepared for the XRF.

4 Methods

4.1 Determination of radionuclides

The activities of ^{238}U, ^{226}Ra, ^{210}Pb, ^{232}Th and ^{40}K were determined by γ-spectrometry.

Initially measurements were carried out at the Geologisches Institut der Universität Bonn using a semi-planar Ge-detector (EURISYS) with a resolution of 0.57 keV at 122 keV and 1.8 keV at 1322 keV. The relative efficiency of the detector is 8.4% and the Peak-Compton ratio 37. The INTERGAMMA (EURISYS) software was used for analysing the spectra.

50 g of each broken sample were put into 300 ml cylindrical polyethylene beakers, which were sealed with silicone paste. The measurements were carried out after 30 days, by which time equilibrium between radium, radon, and its decay products was reached. The measuring time was usually 172,800 sec. Samples of less than 50 g were measured using pressed pills prepared for XRF analysis.

Subsequently, the measurements were mainly performed at the Laboratoire Physique des Radiations of the Centre Universitaire in Luxembourg using a semi-planar Ge detector (EURISYS) with a resolution of 1.0 keV at 122 keV and 2.3 at 1322 keV. The relative efficiency of the detector is 44% and the Peak-Compton ratio 67. The analytical software was INTERWINNER (EURISYS). The sample preparation method used was the same, but the samples were put into 50 ml polystyrene beakers and vacuum-packed in aluminium-plastic sandwich foil. The measuring time was reduced to 86,400 sec.

The activity of ^{226}Ra was determined based on the decay products ^{214}Pb and ^{214}Bi (arithmetic mean). For the calculation of equivalent activity of ^{232}Th, the activities of the decay products ^{208}Tl, ^{212}Pb and ^{228}Ac were used (arithmetic mean). The standard deviations of ^{226}Ra and ^{232}Th were calculated as follows:

$$SD_{Ra-226} = \sqrt{\left(\frac{1}{2}SD_{Pb-214}\right)^2 + \left(\frac{1}{2}SD_{Bi-214}\right)^2} \qquad \textbf{(Equation 1)}$$

$$SD_{Th-232} = \sqrt{\left(\frac{1}{3}SD_{Tl-208}\right)^2 + \left(\frac{1}{3}SD_{Pb-212}\right)^2 + \left(\frac{1}{3}SD_{Ac-228}\right)^2} \qquad \textbf{(Equation 2)}$$

As the equivalent activity of ^{238}U (eU), which cannot be measured directly by γ-spectrometry, the activity of ^{234}Th was taken. The SD of ^{238}U is the same as for ^{234}Th.

To ensure that the measurements of both detectors are comparable, some of the samples measured in Bonn were also measured in Luxembourg. The difference between the results is generally lower than 5%. The same applies for the pressed pills, except for the determination of ^{234}Th and ^{210}Pb. If the activities are very low, results may vary by up to 15%.

For some interpretations, the activities of Uranium and Thorium are given in ppm:

1 ppm ^{238}U $\cong$ 12.42 Bq kg^{-1}

1 ppm ^{232}Th $\cong$ 4.061 Bq kg^{-1}

The concentration of ^{238}U (eU) is directly equivalent to chemical uranium, proven by a significant correlation of the γ-spectrometric results with those of the XRF (r = 0.97 at 95%, n = 177) (Figure 8). The results for ^{238}U will therefore not be called eU, but are taken as true values. The correlation of ^{232}Th to chemical thorium is significant, too (r = 0.93 at 95%, n = 127). However, the results of the XRF measurements were not used, as the detection limit of the XRF is higher and the SD of the results is much higher than for the γ-spectrometry, especially at low concentrations.
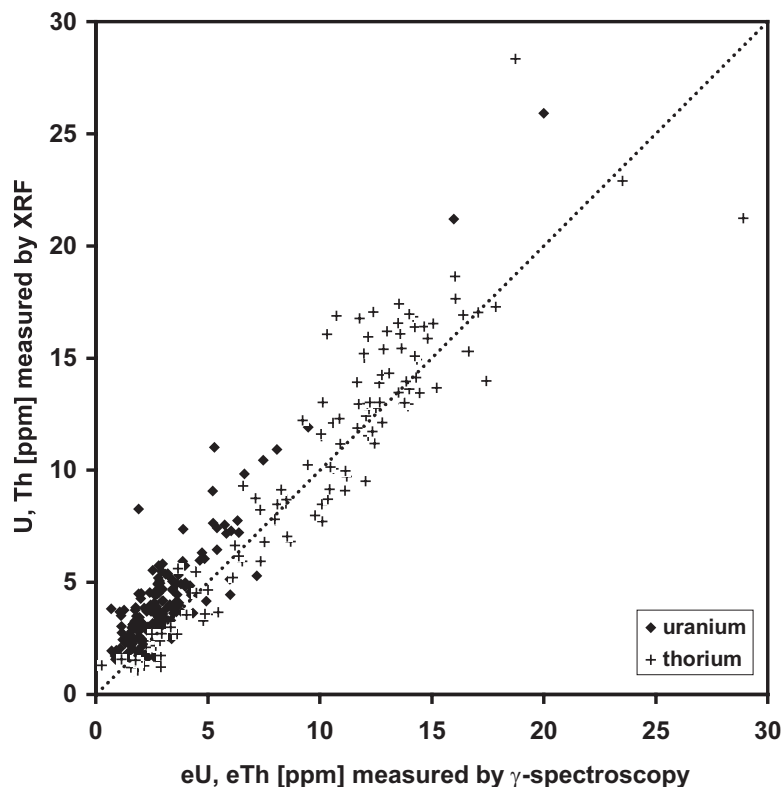
Figure 8: Correlation of ^{238}U (eU) and ^{232}Th (eTh) determined by γ-spectrometry and their counterparts measured by XRF.

The ^{40}K activity was partly measured using an n-type detector and partly using a p-type detector at the Laboratoire Physique des Radiations in Luxembourg. Measurements of the same samples on both detectors showed good agreement. A few samples were

measured for K_{nat} by XRF. Due to the proportionality of activity and mass of a substance, the following conversion applies: 1% $K_{nat} \cong 311.7$ Bq kg^{-1} ^{40}K.

4.2 Determination of geochemical composition

The chemical composition of the samples was analysed by XRF. Four grams of each ground sample were homogenised with 0.6 g of wax, for stabilisation, and pressed to a pill in an aluminium plate with a force of 32 t/cm^2. The analysis was performed with a computer-controlled SIEMENS SRS 303 X-Ray fluorescence spectrometer. The standard deviations were calculated from 10-fold measurements of one pill. The SD of the oxides is usually lower than 1%, exceptionally up to 5%. The SD of the trace elements could rise up to about 10%, especially close to the detection limit. The measuring range of each element is given in Table 3.

Table 3: Measuring range of the x-ray analyses (XRF). The indicated values correspond to the reproducible limit of determination.

Oxides	Measuring Range	Element	Measuring Range	Element	Measuring Range
SiO$_2$	8 – 90%	As	4 - 330 ppm	Ni	5 - 2300 ppm
Al$_2$O$_3$	0.1 – 50%	Ba	30 - 8000 ppm	Pb	4 - 240 ppm
Fe$_2$O$_3$	0.05 - 50%	Ce	20 - 150 ppm	Rb	15 - 3500 ppm
MgO	0.1 – 50%	Cr	5 - 300 ppm	Sr	10 - 1400 ppm
CaO	0.1 – 50%	Cs	3 - 180 ppm	V	5 - 1000 ppm
Na$_2$O	0.05 – 10%	Cu	4 - 450 ppm	Y	10 - 700 ppm
K$_2$O	0.01 – 5%	Ga	2 - 100 ppm	Zn	8 - 1300 ppm
MnO	0.03 - 0.8%	La	4 - 80 ppm	Zr	10 - 1300 ppm
TiO$_2$	0.01 – 3%	Mo	4 - 300 ppm	U*	> 1.5 ppm
P$_2$O$_5$	0.01 – 2%	Nd	20 - 150 ppm	Th*	> 1 ppm

* XRF results were not used for the interpretation of data

The quantity of organic carbon (C_{org}) was measured using a carbon analyser (LECO EC-123).

4.3 Determination of mineral composition

The mineral phases were analysed for selected samples, namely those, which were extracted sequentially (see Chapter 7). The samples were carefully ground to a grain size of 5 – 10 µm. Mineral grains were separated by gravity and determined by XRD. In addition, some extraction residuals of sequential extractions and samples of iron and manganese oxide/hydroxide coatings were analysed by XRD.

---

3 LECO Corporation, 3000 Lakeview Avenue, St. Josep, MI 49085, USA

Gravity separation was performed after removing iron and manganese oxides with citrate-bicarbonate dithionite. 6 – 8 g of sample were immersed in 70 ml of bromoform (density 2.89 g/cm^3) and centrifuged 3 times for 10 minutes at 3,000 rpm. Samples were stirred between the centrifugation steps. The light minerals were sucked off with a pipette. After removing any remaining light minerals from the tube wall, the heavy minerals could be poured out with the remaining bromoform. Light and heavy minerals were sampled separately in filter paper, washed with ethanol, and dried.

The method of mineral separation by centrifugation is described by BOENIGK (1983), because this method is especially applicable for samples with a grain size < 200 µm, as in this case for the ground material.

5 Distribution and geochemistry of natural radionuclides in Luxembourg

5.1 Natural radiation environment

The radionuclides of the decay series of uranium and thorium - together with ^{40}K - cause most of the natural environmental radiation. The distribution of ^{238}U and especially ^{226}Ra, the direct mother nuclide of ^{222}Rn, is of fundamental importance for the assessment of the geogenic radon potential of a specific area.

The distribution of radionuclides is primarily governed by the regional distribution of the various rock types, which contain varying radionuclide concentrations. Distinct types of rocks tend to be typical for certain geological ages, reflecting the palaeogeographical and environmental changes of sedimentary conditions as well as the variation of tectonic and magmatic activities of the lithosphere in the course of the Earth's history. This may result in significant variations of radionuclide concentrations of different stratigraphic units.

Weathering processes could cause enrichment and/or depletion of certain radionuclides in soils and in weathering products located in joints and fissures of the bedrock. The possible enrichment of ^{238}U, or of the decay products in weathered materials and on rock surfaces respectively, are of great importance for the highly folded Devonian area, where not only the enrichment of uranium and radium near the surface may be a source of radon, but where many fracture zones serve as pathways for ascending radon with circulating water and soil gas.

5.2 Uranium

Only three of the 24 known radioactive isotopes of uranium are of importance in nature: ^{234}U (0.0054%), ^{235}U (0.720%) and ^{238}U (99.267%). ^{238}U has a half life of 4.47 x 10^9 years and is the parent isotope of the ^{238}U-decay series. ^{234}U is the 3rd member of this series and has a half life of 2.45 x 10^5 years. ^{235}U (half life: 7.04 x 10^8) is the parent isotope of the ^{234}U decay series.

Due to its relatively large ionic radius, uranium does not fit very well into the crystal lattice of common rock-forming minerals. During the cooling of magma, uranium is enriched in the fluid phase and concentrates mainly in accessory minerals, formed at a late stage of magma differentiation, with concentrations as high as 35,000 ppm. Furthermore, it also concentrates during later stages in secondary minerals at grain boundaries and along microcracks of the rock-forming minerals, from where it can easily be leached. Even if no

magmatic rocks occur in Luxembourg, their erosion products are the primary source of uranium.

Only the U^{4+} and U^{6+} oxidation states are of interest in geochemistry. U^{5+} is formed as a metastable ion during the oxidation from U^{4+} to U^{6+} but it is only stable in environments with low oxidation potentials and may be present in some natural waters as $(UO_2)^+$. U^{4+} (ionic radius: 1.05 Å), which is stable under reducing conditions and nearly immobile because of its low solubility, occurs predominantly in primary minerals of igneous rocks. Under natural oxidising conditions U^{4+} oxidises to U^{6+} (ionic radius: 0.80 Å). The redox potential of a solution controls the concentration of the uranium ions in the tetravalent and hexavalent state:

$$U^{4+} + 2H_2O \leftrightarrow UO_2^{2+} + 4H^+ + 2e^-$$

The solubility of uranium in the hexavalent state is much higher than in the tetravalent state.

Of further importance for the release of uranium from the crystal lattice is a nuclear process, called the Szilard-Chalmers effect, in which uranium isotopes and their daughters are fractionated because atomic bonds are broken during alpha decay and crystal lattices are damaged by recoil of the daughter nuclei. Fluids may then leach the damaged crystal lattice and release the daughter nuclide into the aqueous phase. Daughter isotopes of the same element are therefore considered to have higher mobility in rocks, soils, and ground water (TITAYEVA & VEKSLER 1977; FLEISCHER & RAABE 1978; FLEISCHER 1988).

In most sedimentary rocks, uranium concentrations vary between 0.2 - 11 ppm, increasing with content of phosphorous, clay, iron oxides/hydroxides, and organic matter. Organic-rich black shales and marine phosphates can contain up to 1,200 ppm uranium. The uranium concentration of psammitic rocks increases with the content of weathering-resistant minerals such as monazite and zircon. Carbonate rocks only contain a little uranium due to the good solubility of carbonate complexes in water and the usually low content of primary uranium-bearing or absorbing detritus in the carbonates. During weathering, the carbonate content is leached and insoluble residues of clay minerals and iron hydroxides remain as coatings on corroded rock surfaces. The clayey residue adsorbs uranium, thorium, and radium from circulating fluids and provides great surface areas for the emanation of radon, so that regions dominated by carbonate rocks very often have a high radon potential, especially in karst regions (VON GUNTEN et al. 1996).

Uranium in sediments and soils occurs mainly as oxide, hydroxide, uranate, carbonate, silicate, sulphate, phosphate, arsenate, molybdate, selenite, tellurite and

vanadate. The most common secondary minerals are autunite, carnotite, schroeckingerite, torbernite, uranophane, zeunerite and zippeite.

Both U^{4+} and $(UO_2)^{2+}$ form several complexes with carbonates, halides, hydroxyl, nitrates, phosphates, silicates and sulphates. In geochemistry the various U^{4+} complexes of the type $[UCl]^{3+}$, $[UF_6]^{2-}$, $[UF_8]^{4-}$, $[U(SO)_4(H_2O)_4]^o$, $[U(SO_4)(H_2O)_6]^{2+}$and $[UO(SO_4)_2]^{2-}$ are of interest as well as the complexes of $(UO_2)^{2+}$, namely $[UO_2F]^+$, $[UO_2Cl]^+$, $[UO_2NO_3]^+$, $[UO_2SO_4]^o$, $[UO_2(SO_4)_2]^{2-}$, $[UO_2H_2PO_4]^+$, $[UO_2H_3PO_3]^{2+}$, $[UO_2(HPO_4)_2]^{2-}$, $[UO_2(CO_3)_2]^{2-}$and $[UO_2(CO_3)_3]^{4-}$. Especially $(UO_2)^{2+}$ also tends to form organic complexes, such as soluble uranium chelates and uranium-organic complexes e.g. with citrate, tartrate and humic materials (BOYLE 1982). Uranium is extensively mobilised as an anion by aerobically decomposing plant matter, which is an important process not only in the upper horizons of soil profiles but also for saprolite, where plant roots often grow in fissures.

Table 4: Uranium activities of rocks.

^{238}U [Bq/kg]		Luxembourg*			Literature**		
		Min	Mean	Max	Min	Mean	Max
Sandstones					10	26	40
	Palaeozoic sandstones	26	33	37	21[‡]		32[‡]
	Mesozoic sandstones	3	20	118			
	Siltstones	19	28	40			
	Quartzites	6	7	7		6	
Schists		16	35	89	17[‡]	40	70
Carbonates					1	27	224
	Limestones	7	13	17		27[#]	109
	Dolomites	9	25	79	0.5[†]		25[†]
	Marls	19	38	75			

* Data for Luxembourg from this survey
** Data after: DYBEK (1962), [#] DURRANCE (1986) after KLEMENT (1982),
[†] IVANOVITCH & HARMON (1992), [‡] KEMSKI (1993)

Uranium concentrations in sediments in Luxembourg are mainly in the range of published data, which of course reflect a mixture of rocks of different ages, various regional distribution, and sediment composition. The variance of activities of rocks of different ages is reflected by the data measured in this survey, where Palaeozoic sandstones exceed the uranium activity of Mesozoic sandstones with one exception.

For further analysis, the uranium activities of rocks and weathering products of Luxembourg are grouped by stratigraphy. Results are plotted in Figure 9; the complete dataset with standard deviations is detailed in Appendix 2, Table A2.

rocks

weathering products
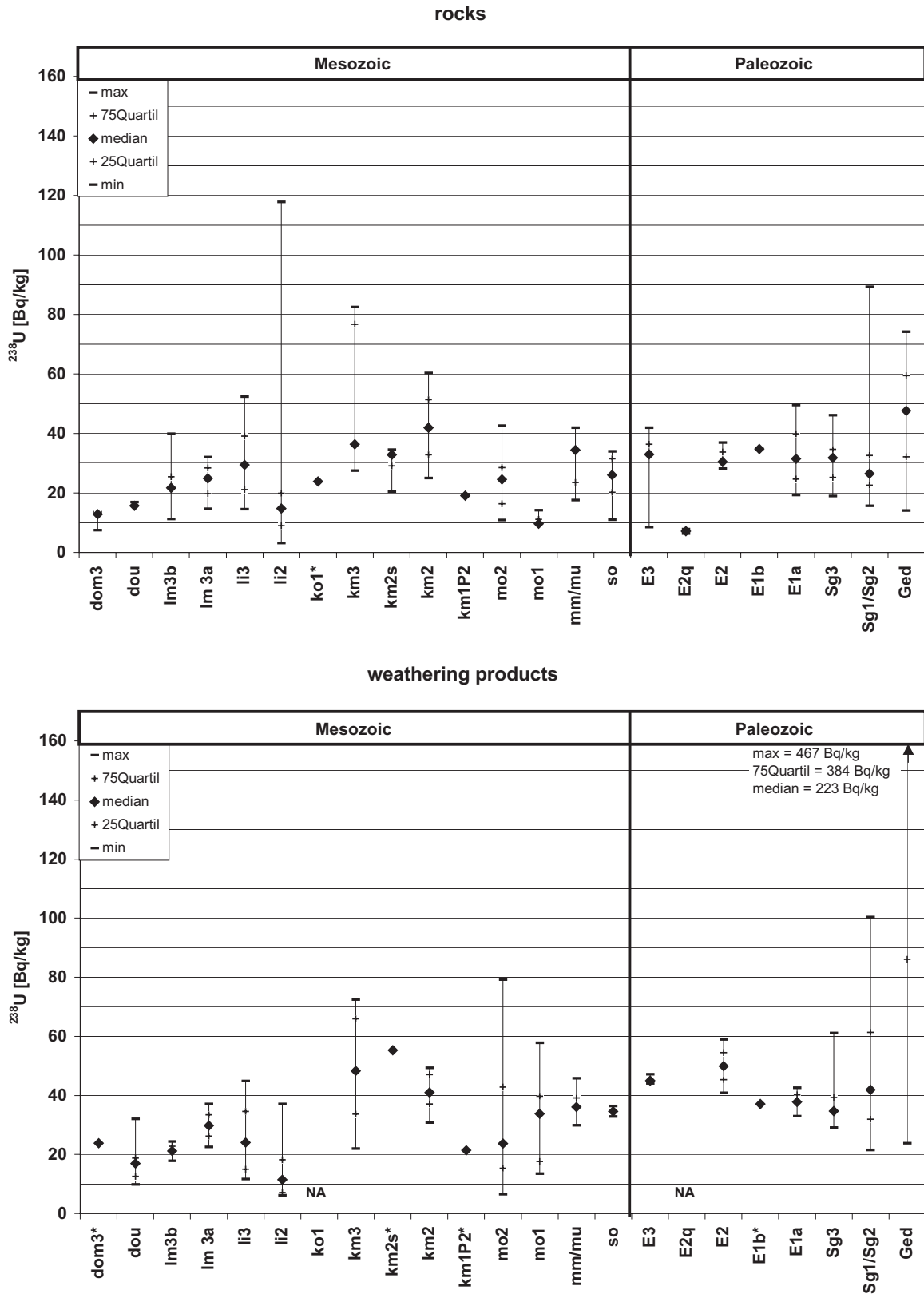
Figure 9: Uranium activities of rocks and their weathering products of Luxembourg grouped by stratigraphy.

Uranium activities of sediments in Luxembourg range between 3 and 118 Bq/kg. The activities of Palaeozoic rocks are usually higher when median values are taken into consideration. Whereas most median values of Devonian units are higher than 30 Bq/kg, only four median values of Mesozoic strata exceed this activity (Figure 9).

Nevertheless, the highest uranium activity, of 118 Bq/kg, occurs in phosphate and iron rich Liassic sandstone (*li2*). The sample was taken from a top layer of the Luxembourg Sandstone (*li2*) south of Aspelt (x 85 100/ y 64 440). At this site, the boundary *li2/li3* was exposed during the construction of a road. The sandstone layer is only a few centimetres thick, nearly black, and coarse grained. The activities of all radionuclides of the uranium series in this layer are about five times higher than that of unweathered sandstones of the *li2* from the same place. Even iron coatings on weathered samples of the *li2* show much lower activities (about 40 Bq/kg). This sample originates from a pyritic or limonitic sandstone layer, which is often described (DITTRICH 1993) for the top of the *li2* as *"surface taraudée"*, a phosphate-rich hard ground generated during low sedimentation rates. Uranium was probably co-precipitated with phosphate during carbonate sedimentation.
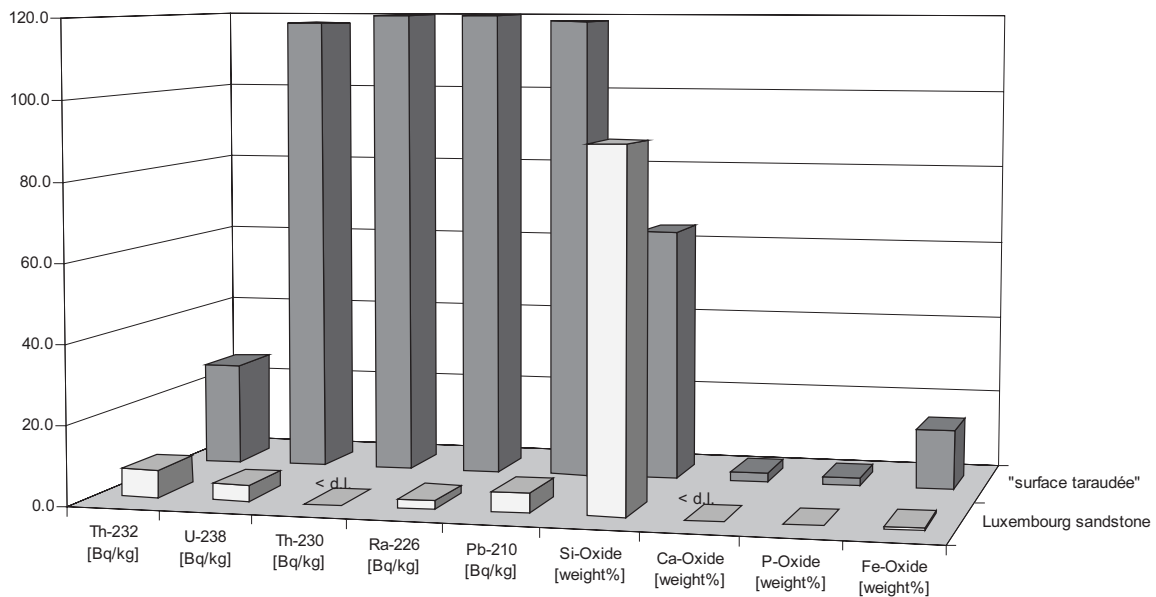
Figure 10: Radionuclide activities and selected oxide percentages of the Luxembourg Sandstone (li2) and the "surface taraudée" layer at the top of the li2 (see Appendix 3, Table A3).

The elevated radionuclide activities of the *"surface taraudée"* do not give rise to a greater radon potential of the Luxembourg sandstone, because the layer is only a few centimetres thick. Additionally, it is covered by several meters of impermeable clay- and marl-layers of the Upper Luxembourg Sandstone (*li2*) and the Sinemurian (*li3*).

Gedinnian near Hatrival (Belgium)
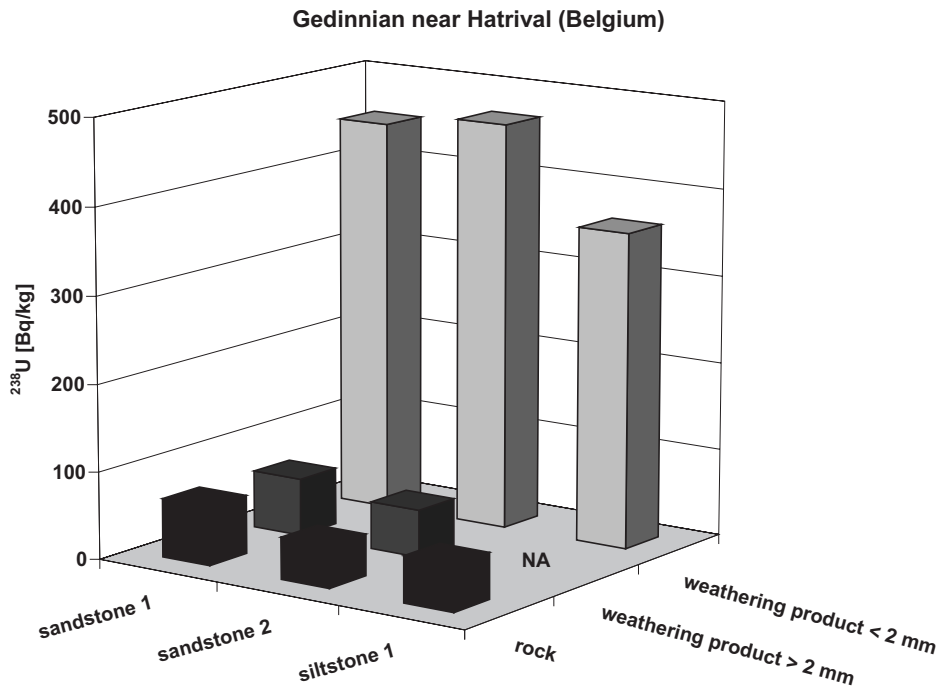
Figure 11: Uranium activities of different Gedinnian rocks and their weathering products.

Gedinnian near Hatrival (Belgium)
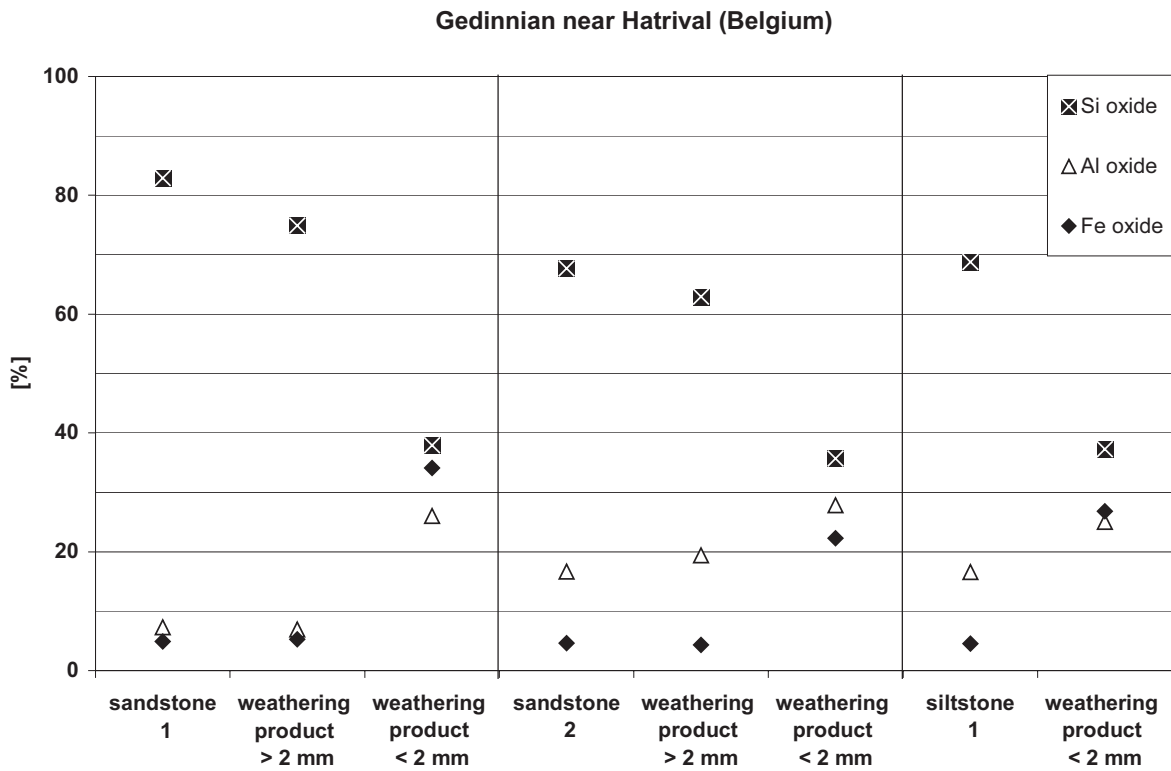
Figure 12: Concentrations of Si, Al and Fe of different Gedinnian rocks and their weathering products.

The weathering products show mainly higher uranium activities than the parent rocks, up to 467 Bq/kg (Figure 9). The median uranium concentrations are highest for the samples of the Devonian ($\geq$ 35 Bq/kg) and lowest for those of the Jurassic ($\leq$ 30 Bq/kg).

Variations in uranium activities of rocks and weathering products are very low for Jurassic samples. They are largest for samples of the Upper Muschelkalk and the Devonian, especially the Gedinnian (Figure 9).

The Gedinnian samples could be taken as examples for the behaviour of uranium during weathering of siliciclastic sediments (Figure 11), where uranium is mobilised as a complex ion. It may be transported over long distances and precipitated under appropriate conditions e.g. with the oxidation from Fe^{2+} to Fe^{3+}. It may also be adsorbed by previously generated oxides or hydroxides of iron, manganese, aluminium, and titanium as well as by silicate gels, clay minerals or phosphates.

In Figure 11 and Figure 12, uranium activities and some selected oxide percentages are plotted for Gedinnian sand- siltstone, and their weathering products. Uranium is enriched in weathering products, especially in the < 2 mm fraction (Figure 11). It is positively correlated with Al, Mn, P and Fe, while correlation to Si is negative.
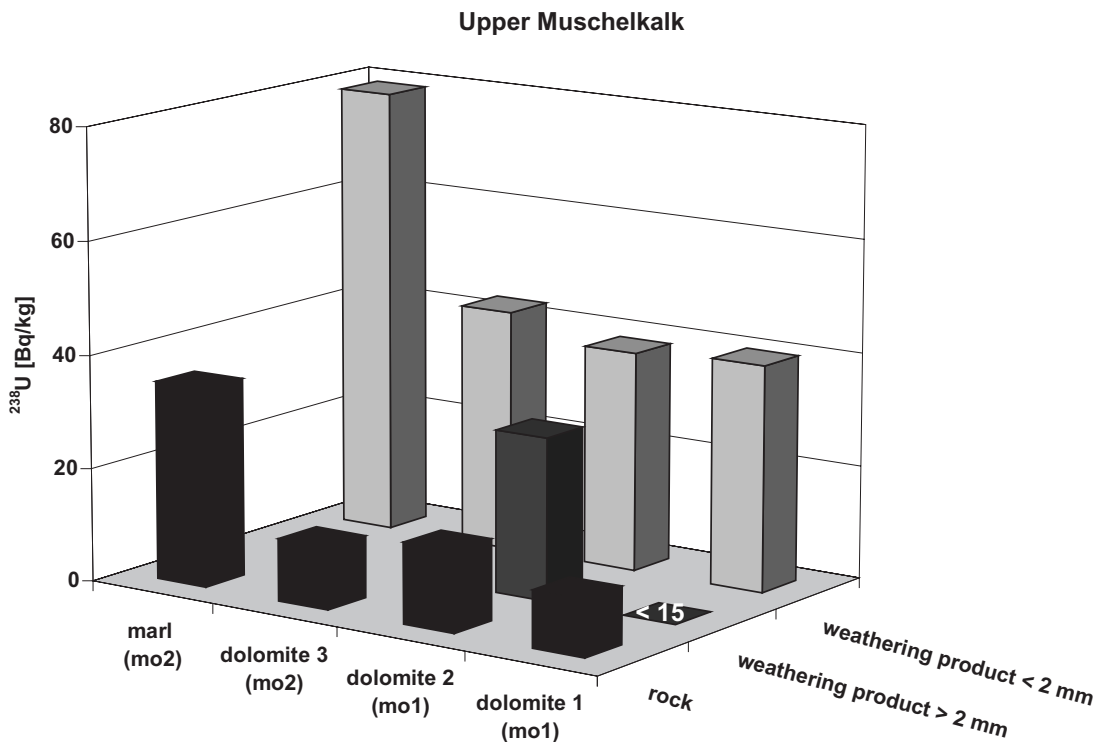
Upper Muschelkalk

Figure 13: Uranium activities of different rocks of the Upper Muschelkalk and their weathering products.

While silica is relatively depleted in the weathering products, concentrations of aluminium and iron are increased in the < 2 mm fraction (Figure 12). Enrichment of uranium

in weathering products is accompanied by enrichment of clay minerals and iron oxides/hydroxides (goethite, hematite, ferrihydrite).

The weathering products of dolomites and marls of the Upper Muschelkalk also show increased uranium activities (Figure 13). The carbonates are dissolved during weathering, resulting in depletion of Ca and Mg in the weathering products (Figure 14). Uranium may be partly mobilised as a carbonate complex, but the correlation with Ca and Mg is negative. The dominating processes - as for the Gedinnian samples - are precipitation with oxides and hydroxides or adsorption onto clay minerals, indicated by significantly positive correlations with Al, K, Ti, P and Fe.
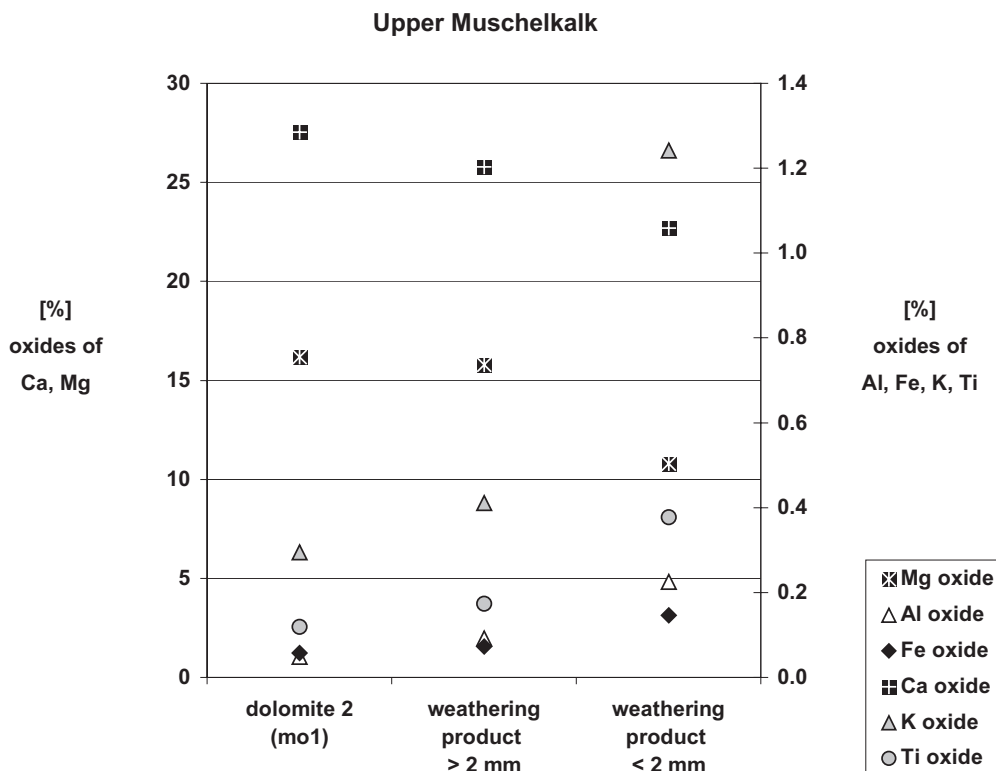
Figure 14: Concentrations of oxides of Mg, K, Ti, Al and Fe of a dolomite (*mo1*) and the accompanying weathering products.

5.3 Radium

Thirty isotopes of radium are reported, ranging from ^{206}Ra to ^{230}Ra. All isotopes are radioactive and decay via alpha emission except ^{228}Ra, which decays via beta emission. Naturally occurring isotopes are ^{228}Ra and ^{224}Ra, which belong to the thorium series, ^{223}Ra in the ^{235}U series and ^{226}Ra in the ^{238}U series. The latter is the most important radium isotope occurring in nature, due to its long half-life (1,622 years) and to the natural abundance of its parent ^{230}Th (MOLINARI & SNODGRASS 1990). In this study, only ^{226}Ra will be examined,

since it is the immediate parent isotope of [222]Rn. The use of the term radium, unless otherwise indicated, always refers to [226]Ra.

The chemical behaviour of the lithophile, alkaline earth element radium during weathering processes differs significantly from that of uranium. Individual samples of rocks and especially weathering products may show clear departures from equilibrium in the [238]U series. The long half-lives up to 2.5×10^5 years ([234]U) of intermediate isotopes between [238]U and [226]Ra provide enough time for chemical changes and redistribution of elements. Radioactive disequilibrium may be caused by the oxidation of immobile U^{4+} to mobile U^{6+}, relative enrichment of [230]Th in insoluble weathering residues or preferential adsorption of [230]Th and [226]Ra onto clay minerals. Natural water shows higher radium activities because of the better solubility compared to parent isotopes. In addition, disequilibrium conditions could be caused by the radioactive decay itself, through hits of α-particles disturbing the mineral lattice or through alpha recoil pushing newly generated atoms out of the mineral. The influence of the radioactive decay is indicated by the increased mobility of [226]Ra (3 alpha emissions) compared to [228]Ra (1 alpha emission) (WIEGAND & KUSCHKOWITZ 1998).

If no separation took place for the last 10 000 years, [226]Ra is present in rocks and minerals in secular equilibrium with [238]U. Radium does not form minerals of its own. It substitutes other elements in newly generated minerals (MOLINARI & SNODGRASS 1990). Ra^{2+} may displace Ba^{2+} in barite as well as Mn^{2+} in kryptomelane ($K_2Mn_8O_{16}$) and Ca^{2+} in apatite.

Results of radium analysis of rocks and weathering products of Luxembourg are plotted in Figure 15; the complete dataset with standard deviations is detailed in Appendix 2, Table A2.

The Ra/U activity ratio of analysed sediments from Luxembourg usually approaches the condition of secular equilibrium. Enrichment of radium was found only for Gedinnian sandstone due to exceptionally thick encrustations of iron and manganese oxides/hydroxides and for iron-rich sandstone from the *lm3b*.

During weathering, radium may be absorbed by organic substances, clay minerals, and iron and manganese oxides. Co-precipitation with calcium and barium salts is also common. Like Ba, Sr and Ca, radium forms very insoluble sulphate, carbonate, phosphate and chromate salts. Water-soluble compounds are the chloride, bromide, nitrate and hydroxide salts. Ra^{2+} dominates in the pH range 4-8.

As well as the other alkaline earth cations (except beryllium), radium shows no tendency to hydrolyse. The chemical properties of radium are similar to barium although it has a larger ion radius. Radium salts have a lower solubility than the corresponding barium salts. The tendency of radium to build complexes is less pronounced than of the other

alkaline earth metals. Complexes with oxalic, citric, tartaric, succinic and some other acids are documented for pH 7.2 to 7.4 (AMES & RAI 1978).
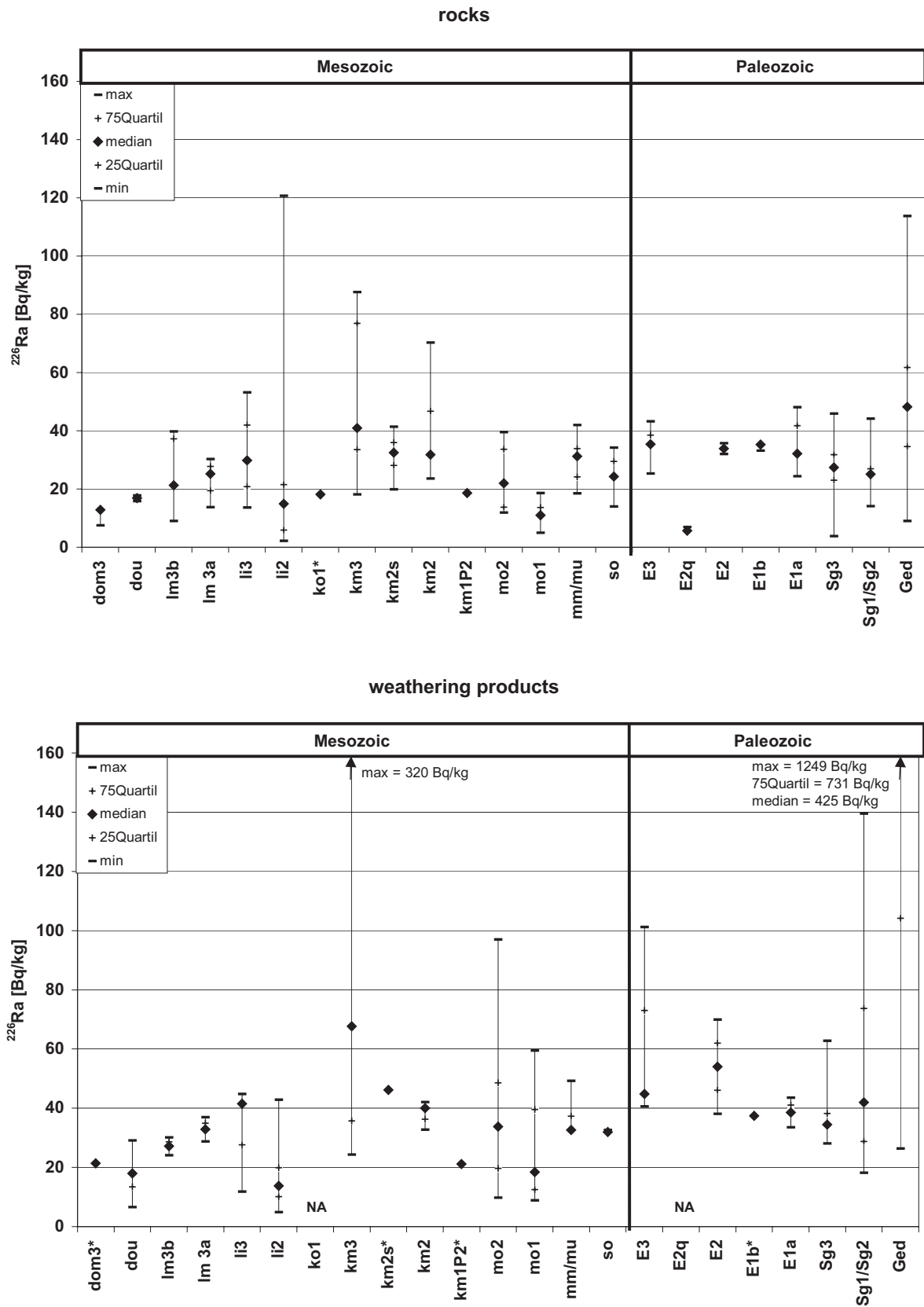
Figure 15: Radium activities of rocks and their weathering products of Luxembourg grouped by stratigraphy.

In Luxembourg, radium activities of weathering products up to 1,249 Bq/kg are higher than those of rocks (max. 302 Bq/kg, usually lower than 100 Bq/kg). Enrichment of radium is - as for uranium - highest for the Devonian samples and the weathering products of the Upper Muschelkalk. In addition, radium activities are much higher for the weathering products of the Middle Keuper (*km3*) in comparison to the accompanying rocks (Figure 15).

Radium is in secular equilibrium with uranium in the weathering products of the *mo2*, but not in those of the *km3*. The latter are fissure-filling secondary carbonate precipitations of dolomites and dolomitic marls with very high radium activities of up to 320 Bq/kg, located east of Graulinster (x 88 680 / y 89 550). The dolomite and marl layers of this outcrop are disturbed by small faults, which displace the layers up to some tens of centimetres. They might be connected to the fault zone of Audun-le-Tiche, which is close to the outcrop (BINTZ et al. 1973).
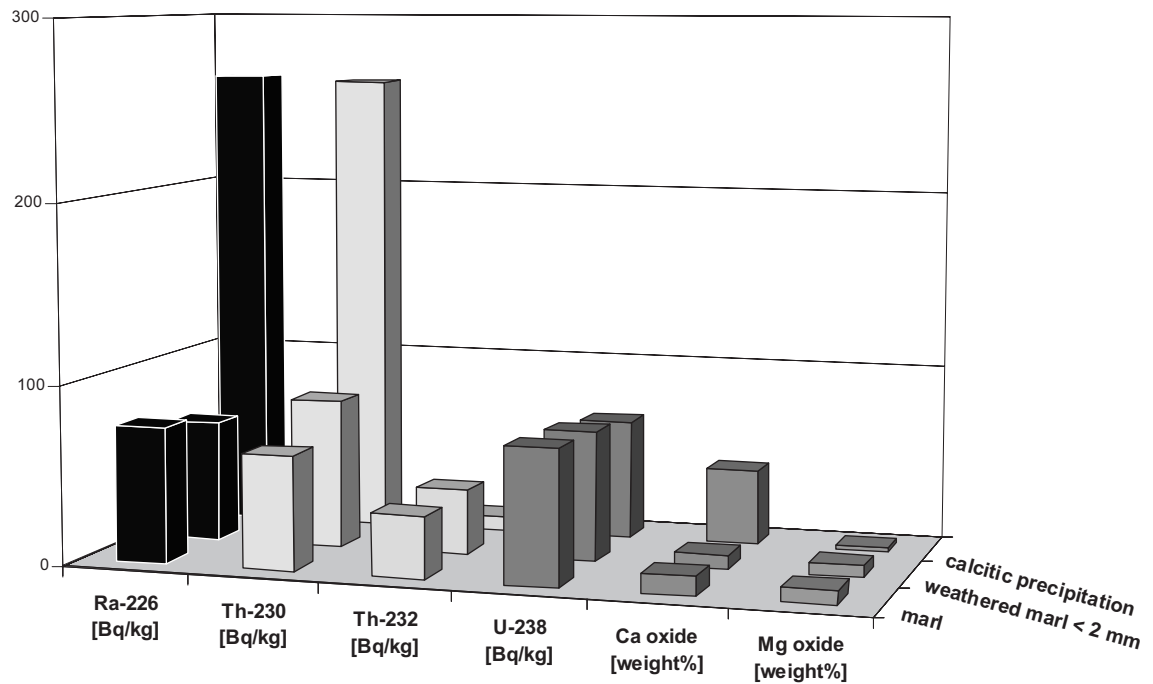
Figure 16: Example of radionuclide activities and concentrations of Ca and Mg in fissure-filling secondary carbonate precipitations of dolomites and dolomitic marls of the *km3*, east of Graulinster.

Radium enrichment is attributed to enrichment of [230]Th in the weathering product, as carbonatic precipitations appear to have a Ra/U activity ratio of 4 – 5, while radium is in secular equilibrium with [230]Th (Figure 16). VON GUNTEN, SURBECK & RÖSSLER (1996) found the same for Karst soils of the Jura Mountains in Switzerland. While uranium is

released during weathering and migrates as a stable uranyl carbonate complex, [230]Th hydrolyses and is strongly absorbed to soil particles and/or forms insoluble compounds.

By far the highest [226]Ra activities, of up to 1,249 Bq/kg, were found for Gedinnian weathering products, nearly all of them showing radium enrichment. Radium is precipitated as oxide or hydroxide together with iron or manganese. It may also be absorbed onto clay minerals, which are enriched in the weathering products as well, indicated by high concentrations of Al, K, Ti and P (Figure 17).
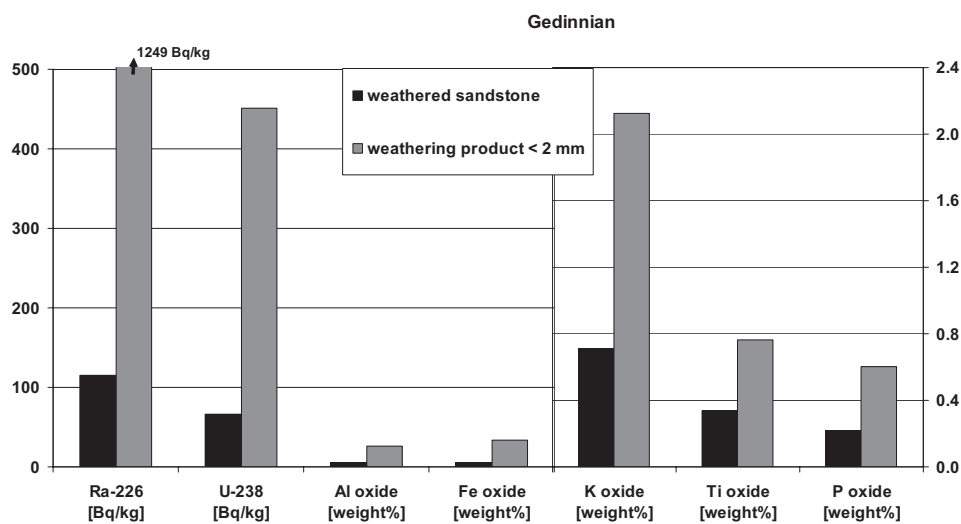
Figure 17: Example of a weathered sandstone (Gedinnian) and the accompanying weathering product < 2 mm. Radium and uranium activities are plotted together with the concentrations of the oxides of Al, Fe, K, Ti, and P.

Radioactive equilibrium is disturbed for 26% of the samples, all of them showing radium enrichment. Radium and thorium appear with similar activities in only 4% of the cases.

The differences in the distribution of uranium and radium among rocks and their accompanying weathering products show that the prediction of radon potentials for certain areas cannot be based on the knowledge of the uranium activities of rocks alone. The assessment of the radon potential of a specific area, especially if the rocks were fractured by tectonic deformation, has to be based on the investigation of radium activities, in particular those of the weathering products.

5.4 Thorium

Twenty-five isotopes are known, ranging from [216]Th to [236]Th, but only six isotopes occur in nature. The longest-lived isotope is [232]Th, the parent isotope of the thorium series, with a half-life of 1.4×10^{10} years. In the decay series one other thorium isotope originates, [228]Th, with a half-life of 1.9 years. Because of the usually short-lived nuclides in the [232]Th

chain, the whole series is expected to be in secular equilibrium. The four other natural thorium isotopes originate in the uranium series ([234]Th and [230]Th) and in the actinium series ([231]Th and [227]Th).

Thorium has - as does uranium - a relatively large ionic radius (Th[4+]: 1.10 Å). Rock-forming minerals therefore only contain low concentrations of thorium, and there is commonly extensive reciprocal replacement of uranium and thorium.

The thorium content of igneous rocks tends to increase with increasing silica. Like uranium, thorium mainly occurs in accessory minerals. The remainder is present as an absorbed phase or in tiny mineral grains (e.g. thorite) along grain boundaries and microfractures. In sediments, the location of thorium is similar to those described for igneous rocks. In some sediment, thorium may be abundant in chemically resistant detritic mineral grains such as monazite, sphene and zircon. A considerable amount of thorium may be bound in clay mineral complexes and in limonite, wad, and other colloidal materials. Shales and other argillaceous rocks with high alumina content usually show elevated thorium activities (BOYLE 1982).

During weathering processes, only tetravalent thorium is of importance. Th[3+] is rare and not stable in aqueous media. Thorium chemically resembles titanium, zirconium, and hafnium. Of importance are hydrolytic, colloidal and adsorption reactions. At the pH of most soils (pH 5-8) part of the soluble thorium salts (nitrate, sulphate and chloride) may undergo hydrolysis, leading to the formation of the positive hydroxide colloid or gel, from which water is removed to form ThO_2. On the other hand, thorium in the ionic and colloidal hydroxide and silicate form may be absorbed onto or co-precipitated with clay minerals, silica-alumina gels, hydrous ferric oxide, hydrous manganese oxide, hydrous titanium oxide, hydrous zirconium oxide, vanadium oxide and the humic matter of soils, for example as a thoriferous humate. Thorium tends to substitute potassium in clay minerals. Beyond pH 7, clay minerals and organic matter absorb most thorium. Nevertheless, much of the thorium in soils occurs in resistant minerals such as zircon, monazite, allanite, sphene, thorianite and thorite. Besides, thorium is present in minerals generated during weathering processes such as baddeleyite and thorogummite (BOYLE 1982).

Like uranium, thorium has a strong tendency to form complexes due to its high charge. Besides organic complexes with acids such as gallic, tannic, oxalic and aspartic, inorganic complexes with chlorides, fluorides, nitrates, sulphates, carbonates, hydroxides, silicates and phosphates occur. The occurrence and stability of these complexes is not completely known, but in general, thorium complexes are more stable than uranium complexes, except for the carbonate complexes. Many colloidal forms of thorium compounds are known, e.g. the generally positively charged hydroxide, which may be negative under certain conditions, and the negative silicate (BOYLE 1982).

During weathering, the Th/U ratio tends to increase because of the differing mobility of the two elements. Uranium is more easily dissolved from rocks by weathering processes than thorium. Additionally, the complexes of U^{6+} are several orders of magnitude more stable in solution than tetravalent Th and uranium can therefore migrate over large distances until it is fixed by reduction and/or adsorption. Hexavalent U can occur in the mg/L range in near-neutral solution, while tetravalent Th amounts to only << 0.1 µg/L in such solutions (DYCK 1978).

Thorium activities of the analysed sediments of Luxembourg do not correspond very well to the - rather sparse and unspecific - literature data (Table 3). In particular thorium activities of limestones and sandstones are higher, the latter showing a clear difference between Palaeozoic and Mesozoic sandstones (factor 1.7) in Luxembourg.

Table 5: Thorium activities in rocks.

Rock types		^{232}Th [Bq/kg]					
		Luxembourg*			Literature**		
		Min	Mean	Max	Min	Mean	Max
Sandstones					4	7[#]	37
	Palaeozoic sandstones	43	48	55	28[‡]		43[‡]
	Mesozoic sandstones	5	28	61			
Siltstones		30	45	62		48	
Quartzites		< 1	6	12			
Schists		27	54	69	24[‡]	41	77[†]
Carbonates						12°	
	Limestones	15	35	56	< 1[†]	7[#]	10[†]
	Dolomites	6	11	18			
	Marls	7	31	62		28^	

* excluding data from Belgium
** Data after: BOYLE, R.W. (1982), [#] DURRANCE (1986), after KLEMENT (1982),
[†] IVANOVITCH & HARMON (1992), [‡] KEMSKI (1993), ° BOYLE, M. (1988), ^ HINDEL (1991)

Results of thorium analysis are plotted in Figure 9; the complete dataset, with standard deviations, is detailed in Appendix 2, Table A2.
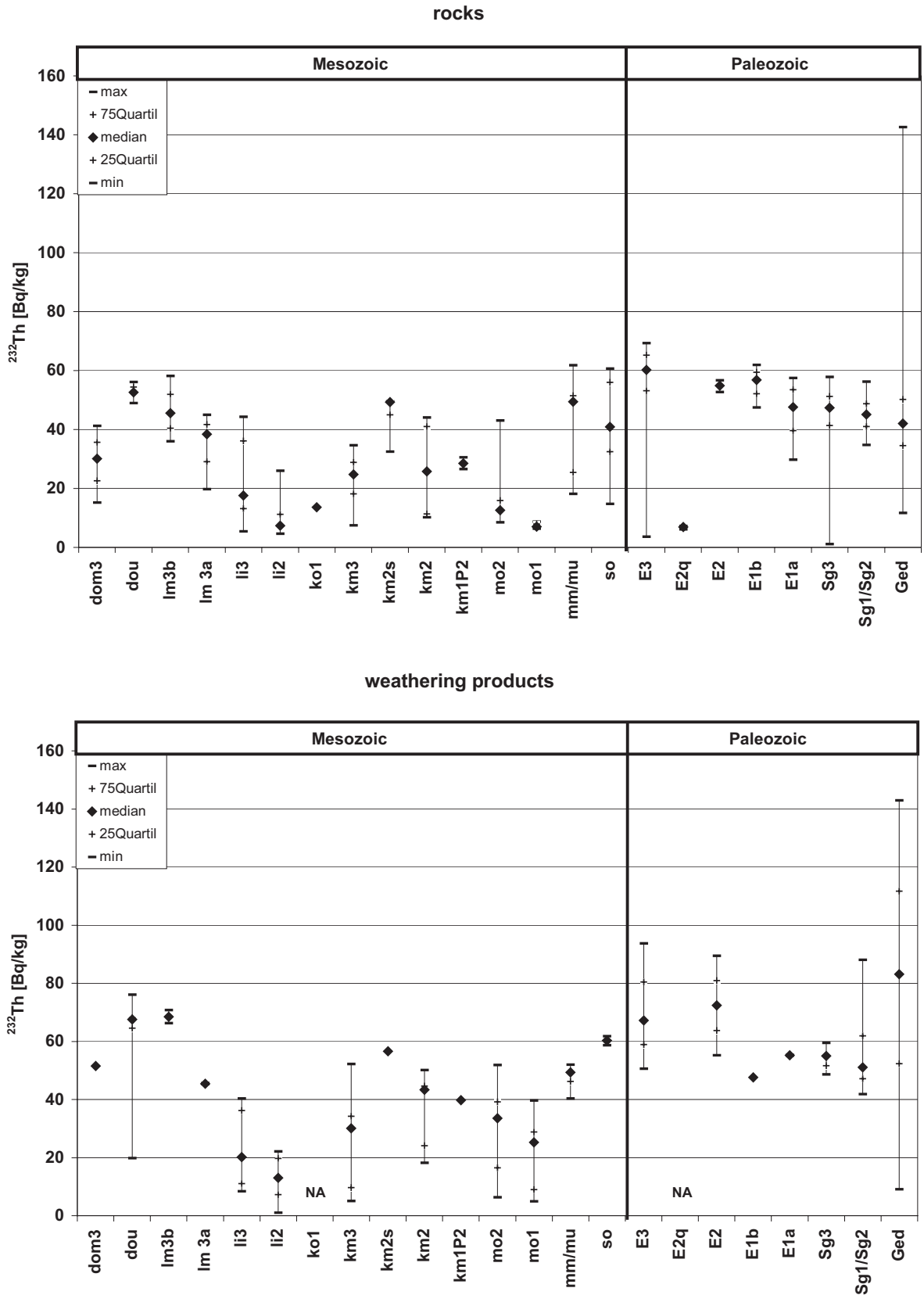
Figure 18: Thorium activities of rocks and their weathering products of Luxembourg grouped by stratigraphy.

Thorium activities of the sedimentary rocks in Luxembourg range between 1 and 142 Bq/kg, Palaeozoic rocks showing generally higher thorium activities than Mesozoic rocks, when considering the median values (Figure 18). Except for the quartzites of the *E2q*, all median values of the Devonian exceed 40 Bq/kg. Only a few Mesozoic sediment types, namely the sandstones and marls of the *mm*/*mu*, the sandstones of the *so*, *km2s* and *lm3b* and the limestones of the *dou*, exceed this value. Most Mesozoic stratigraphic units do not even reach a maximum value of 45 Bq/kg. The highest thorium activities were found for the Gedinnian samples.

The Liassic *(li2)* sample from the "*surface taraudée*", which is enriched in uranium and radium, shows only low ^{232}Th activities, but high ^{230}Th activities. The uranium decay chain is in secular equilibrium.

Only a few rock samples show similar activities for thorium as for uranium and radium. About half of the rock samples (51%) show excess thorium, 27% equal activities and 18% lower thorium activities. Most samples with enhanced thorium activities belong to Devonian and Jurassic strata.

Compared to the activities of uranium and radium, thorium activities of the weathering products are only slightly elevated in relation to the parent rocks. Median values of the Devonian weathering products are higher than 50 Bq/kg, except for the stratigraphic unit *E1b*. Only a few Mesozoic weathering products exceed this value (*so*, *km2s*, *lm3b, dou* and *dom3*).

Thorium, uranium, and radium are separated during weathering in most cases. Only 24% of the weathering products have similar activities of all three radionuclides, 34% have higher and 16% have lower thorium activities. The latter are weathering products of Mesozoic marls and dolomites (*mo1*, *mo2*, *li3*, *km2* and *km3*) and two iron coatings from surfaces of Luxembourg Sandstone (*li2*). Almost all parent rocks of these samples show lower thorium activities than uranium and radium activities, too. Enrichment factors for thorium in weathering products are nevertheless in the same range for all samples (1 - 4.5). Enrichment of thorium is highest in weathering products < 2 mm.

6   Emanation

6.1   The process of emanation

Emanation is defined as the release of radon from the solid phase of rocks and soils into pores, microfissures or fracture systems.

^{222}Rn and ^{220}Rn occur in all rocks and soils as decay products of the radium isotopes ^{226}Ra and ^{224}Ra. During the α-decay of radium, an α-particle and a radon atom are formed, which move by recoil in opposite directions. Because of ejection, Radon atoms may enter the space between rock grains.
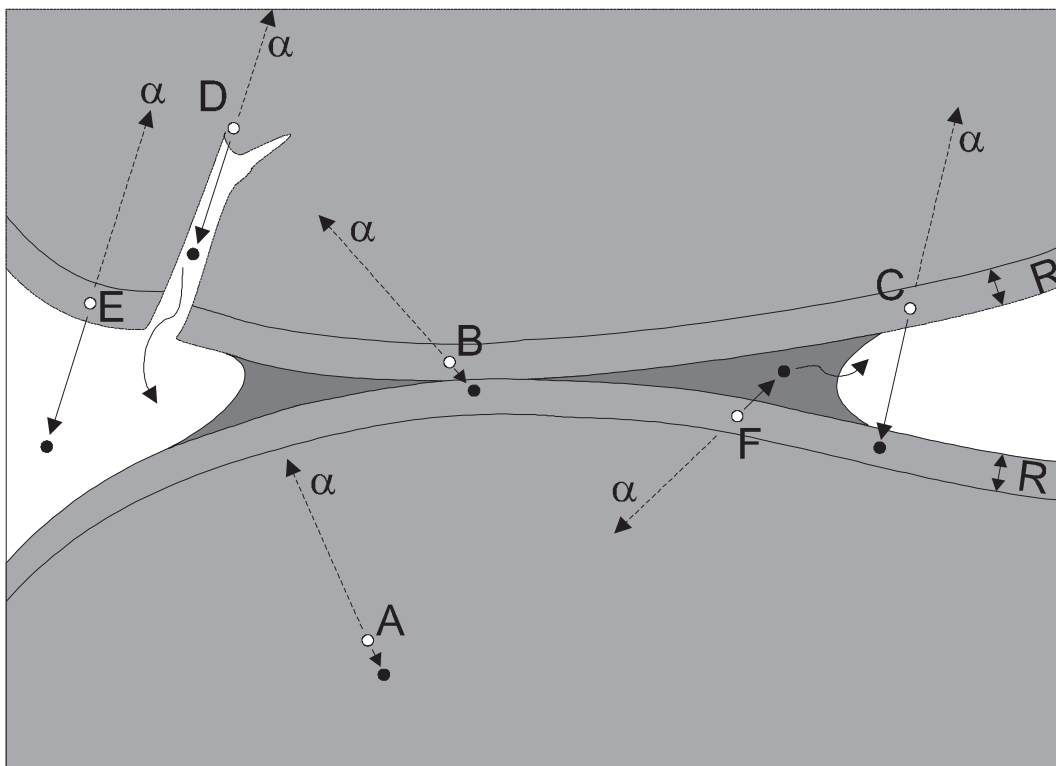
Figure 19: Possible scenarios for the α-decay of radium (°) to radon (•) in soil (after TANNER 1980 and KEMSKI et al. 1996 b). Explanation see text.

The maximum recoil distance (R) for a radon atom in a specific material is marked in Figure 19 for two rock particles. If a radon atom is formed within this region, its kinetic energy will be high enough to leave the particle. Depending on whether the pores are filled only with air or also with water, different processes are possible. As long as the radon atom enters the pore space, but does not loose all of its recoil energy, it may lodge in the opposite wall of the pore (C). If it loses all of its recoil energy in the pore space, the radon atom will diffuse in the pore network (E). The radon atom may also reach the pore space if the radium atom is located close to a crack in the mineral from where the radon atom can diffuse into the pore

space (D). Radon atoms entering water-filled pores may be stopped due to the decrease of the recoil energy and diffuse from there into the air filled pore space (F). In cases where the radium atom is located somewhere in the particle (A) or too close to another grain (B), the radon atom cannot reach the pore space.

Radon emanation is usually given as the emanation coefficient. It is calculated as the quotient of released radon activity (A_{Rn-222}) in a sample gas at secular equilibrium and total radium activity (A_{Ra-226}) of a sample. The emanation coefficient is usually given as a percentage:

$$E = \left[\frac{A_{Rn222}}{A_{Ra226}} \right] 100\%$$ (**Equation 3**)

The most important factors affecting radon emanation are

- distribution of parent isotopes in rock and soil
- internal structure of a material
- particle size distribution within a material
- moisture content
- temperature
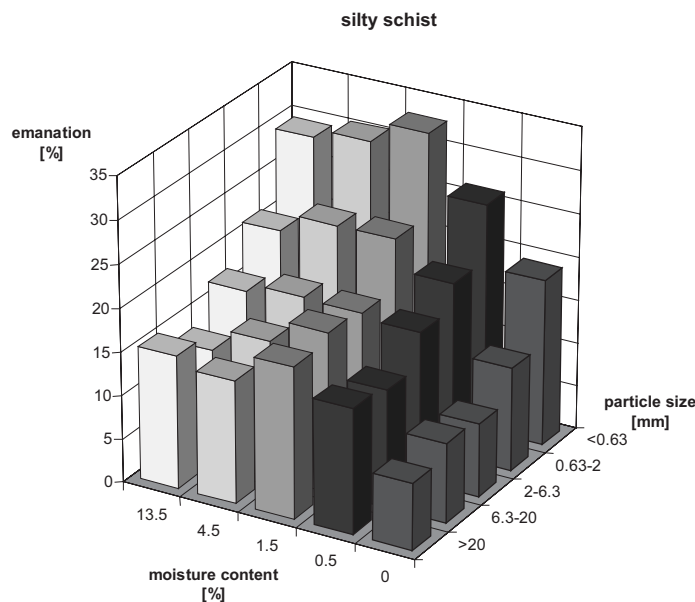
Figure 20: Emanation coefficients of a silty schist (Devonian; *Rheinisches Schiefergebirge, near Dreckenach*) in dependence on particle size and water content (after HEINRICH 1994).

40

Figure 20 shows the dependence of the emanation coefficient on particle size and water content. The differing emanation coefficients of this sample (silty schist of Lower Emsian age; HEINRICH 1994) give an example of the general tendency of materials to vary in emanation.

The radium activity of this partly weathered silty schist is 29 Bq/kg. While the emanation coefficient of the dry and crushed original sample (not sieved and separated) is about 13%, the emanation coefficients of the sieved samples measured at different moisture contents vary between 5% (> 20 mm fraction, 0% moisture) and 33% fraction (< 0.63 mm; 1.5% moisture fraction). The maximum emanation of all particle size classes is at 1.5% moisture by weight.

The wide range of emanation coefficients is in line with results of other investigators, documenting factors of up to 20 - 30 between the minimum and the maximum emanation (STRANDEN, KOLSTAD & LIND 1984 a, b; LINDMARK & ROSEN 1985).

The effect of particle size has been investigated many times (e.g. BARTON & ZIEMER 1986; EDSFELDT & FERNLUND 1998; FLÜGGE & ZIMENS 1939; HEINRICH 1994; MARKKANEN & ARVELA 1992; MEGUMI & MAMURO 1974; MORASWKA & JEFFRIES 1994; RUTHERFORD, DUDAS & AROCENA 1995). By way of example, the results of HEINRICH (1994) are quoted here.

Table 6: Emanation coefficients in relation to particle size (after HEINRICH 1994)

Dry samples	Emanation coefficients [%]				
	<0.63 [mm]	0.63-2 [mm]	2-6.3 [mm]	6.3-20 [mm]	>20 [mm]
Schist (Devonian)	19.2	11.9	8.4	9.2	7.7
Volcanic tuff 1 (Quaternary)	4.3	2.0	1.2	1.2	1.4

Table 6 shows that emanation coefficients of the particle size fractions > 20 mm, 20 - 6.3 mm and 6.3 - 2 mm do not differ very much for most samples, whereas emanation coefficients of the fractions 2 - 0.63 mm and < 0.63 mm differ widely.

The influence of temperature on the emanation factor has been demonstrated (e.g. BARRETTO et al. 1975, PELLEGRINI 1997), but was not further investigated in this thesis because the range of temperature variability of surface soils is only of minor importance (NAZAROFF et al. 1989).

6.2   Standardisation of sample preparation

If radon emanation from materials with different particle size, water content, internal structure and radium distribution is to be compared, it is necessary to standardise sample preparation.

The samples used for this study were generally divided into rock samples, weathering products > 2 mm (skeletal soil) and weathering products < 2 mm (fine soil). They were not separated into more fractions, since the effect of particle size is well known.

The influence of water content on radon emanation was not investigated during preliminary tests, since it is well known that radon emanation of any material increases with increasing moisture to an optimum, and decreases again beyond that point (PRUTKINA & SHASKIN 1967; STRONG & LEVINS 1982; STRANDEN, KOLSTAD & LIND 1984 a, b; DAMKJÆR & KORSBECH 1985; GREINER 1985; LINDMARK & ROSEN 1985; BROOKINS 1991; HEINRICH 1994). Determining the optimum point of emanation for each individual sample seemed to require an unrealistic effort, when analysing hundreds of samples. The more convenient method for comparison of materials is to measure at the minimum of emanation, which is achieved after drying the samples at 105°C.

The influence of the grain size of samples was investigated in early tests (ROTH 1998, ROTH & FEIGE 1998), because crushing of material and grinding to a very fine particle size not only changes the particle size itself, but also the internal radium distribution. It was expected that differences in emanation between crushed and milled material would be found as BOSSUS (1984) presented a linear relation between specific surface area and emanation coefficient. He used a brick sample with a homogenous radium concentration, which was ground and sieved into five fractions. However, one of his conclusions was that this relationship might not be obtained for heterogeneous samples.

Preliminary studies performed for this thesis showed no difference in emanation between crushed materials with a maximum particle size of 2 mm and milled material of < 200 µm (ROTH 1998). The cause of this result is the heterogeneous distribution of active sites of radon emanation. Highly active sites, such as coatings of Fe hydroxides or displaced clay minerals, are located on the surface of a rock. Inside a rock comparatively low radium activities occur. By crushing a rock, the surface area is enlarged, but this effect is compensated by the mixing of high activity and low activity materials. Investigations by INGLES et al. (1977) give further support for this result, as no differences in emanation for ground or raw materials were found, either.

The preliminary tests, published elsewhere (ROTH 1998, ROTH & FEIGE 1988), showed that the optimum of comparability was given when grinding samples to a particle size of < 200 µm and drying at 105°. This kind of preparation was used for all of the samples in this study.

This standardised preparation method allows comparison of emanation rates of rocks and their weathering products. It is important to note that the emanation values produced give the minimum possible differences between the emanation of rocks and weathering products. The emanation of rocks is overestimated because of the enlargement of the

surface area, while the emanation of weathering products is underestimated, since the initial moisture content is reduced.

6.3 Measuring device and procedure

Each milled and dried sample was sealed for at least 30 days in a 1-liter radon-tight polypropylene-box (PP box) (Figure 21). In most cases, 200 g of sample were filled into a PP boxes to a filling height of approximately 2 cm. To ensure that the total amount of radon produced in pore space was measured, comparative studies were performed in which the samples were either shaken, or not shaken, during the measurements. No differences occurred between these methods of handling (ROTH 1998, ROTH & FEIGE 1998).
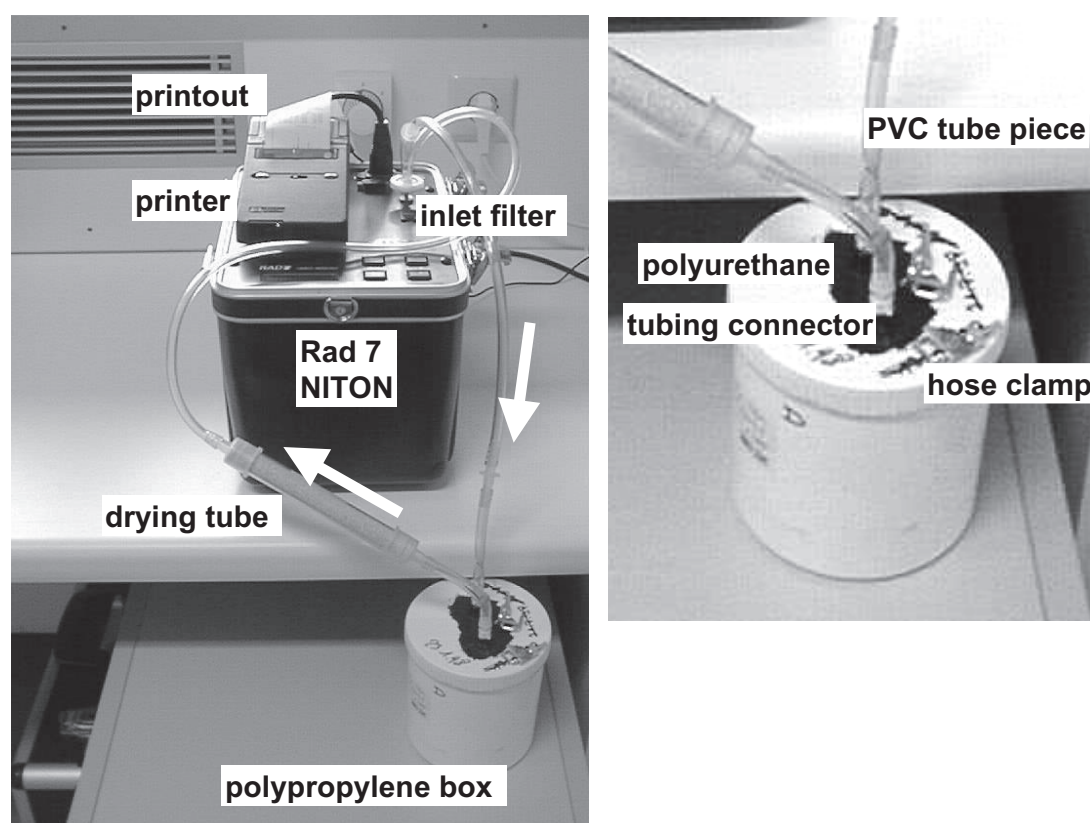
Figure 21: Measuring arrangement and sample box

It was necessary to modify the original PP box for the radon measurements. Two polypropylene tubing connectors were welded into the cover of the box, on to which two short pieces of tube were attached, which were locked with hose clamps. Additionally, the welding seams were covered with a polyurethane paste (Figure 18). The screw-type cap was sealed with stopcock grease, which does not absorb radon. The gas-tightness of this construction was examined by putting a piece of uranium ore into a PP-box and placing it into a radon-tight glass container together with a radon monitor (ALPHAGUARD; GENITRON[4]). This

---

[4] GENITRON INSTRUMENTS GmbH, Heerstraße 149, D-60488 Frankfurt a.M., Germany

examination was carried out twice and, in both cases, the radon concentrations in the container did not exceed the background radon level (Table 7).

Table 7: Radon activities measured in radon-tight glass container with radon monitor

	Measuring time [hours]	Radon activity [Bq/m^3]
Background level in glass container	24	32±18
Uranium ore without PP box	1	> 30,000
Uranium ore in closed PP box (1)	48	23±18
Uranium ore in closed PP box (2)	336	33±32

The radon measurements were carried out with a solid-state alpha monitor (RAD7; NITON[5]). The RAD7 has 200 channels in the range from 0 MeV to 10 MeV, covering the energy range of the alpha particles of the radon daughters of interest, from 6 MeV to 9 MeV (NITON ELECTRONICS 1992).
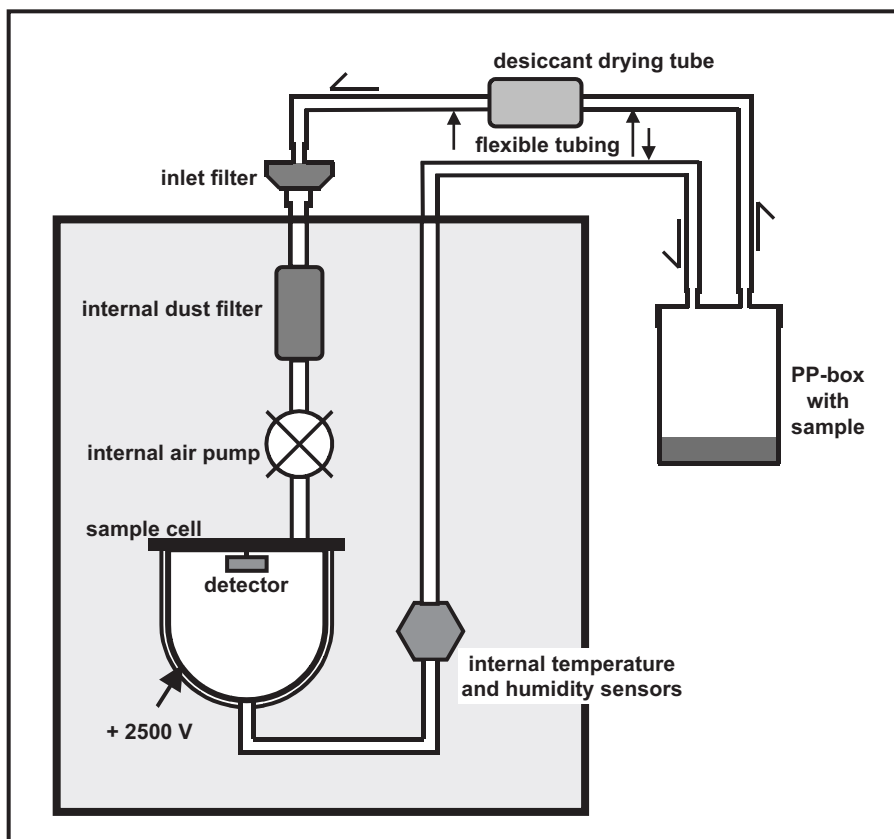
Figure 22: Air flow diagram of the RAD7

---

[5] The RAD7 was originally developed by NITON, but is now distributed by PerkinElmer ORTEC under the name "Durridge RAD7". ORTEC, 801 South Illinois Avenue, Oak Ridge, Tennessee 37831-0895 U.S.A.

To measure the radon concentration of a sample, air is pumped through the tube system with an internal pump. A fine inlet filter absorbs the radon decay products. Radon is analysed in the sample cell according to a preset measuring cycle (Figure 22).

The internal sample cell consists of a 700-ml hemisphere, coated on the inside with an electrical conductor, which has a potential of 2,000 to 2,500 V against the detector and thus creates an electric field in the cell. The electric field drives the positively charged decay products towards the detector located in the centre of the hemisphere.

Operating the RAD7, one can choose between several pre-programmed standard protocol settings such as radon-in-water measurements, sniff-tests or long-time measurements (from 1day to several weeks), but it is also possible to set an individual program. The most important settings for an individual adjustment are the cycle time (measuring time for one analysis), the number of cycles (number of measurements), the setting of the measuring mode (measuring only ^{218}Po ("Sniff") or also ^{214}Po ("Normal")) and the pump mode (set the pump on, off or alternating on/off ("Auto")).

As it was not possible to use any of the pre-programmed procedures, an individual program was used. In order to assure a homogeneous mixing of the air contained in the RAD7 sample cell, the box and the tubing, the cycle time was set to 60 minutes and the pump to "Auto" mode, where the pump does not run continuously, but instead runs for 1 minute every 5 minutes. The number of cycles was set to 13. As it takes three hours to reach secular equilibrium of ^{218}Po and ^{214}Po, the first three measurements were disregarded for the calculation of the result. Each sample was measured at least twice. The calibration of the RAD7 has been described previously (ROTH 2001).

The samples were measured after at least 30 days, when secular equilibrium between radium and radon in the PP boxes had been reached. The boxes were connected to the RAD7 using sections of tube to obtain a closed air cycle (Figure 18) and radon concentrations were measured as described.

The arithmetic mean of all cycles (10 for each measurement) is given as the result. Samples were measured at least twice. The result had to be corrected for the volume and the weight of each sample in order to obtain the radon activity concentration in Bq per kg solid sample, which is needed for the calculation of the emanation coefficient. To avoid confusion with the specific activity, this dimension is marked with an asterisk. The radon activity concentration refers to the released radon in sample pore gas relative to the weight of the emanating material at secular equilibrium:

$$A_{Rn-222}[Bq/kg*] = \left[A_{Rn-222} \cdot \frac{(V_{tot} - V_s)}{(V_{box} - V_s)}\right] \frac{1}{W_s} \qquad \textbf{(Equation 4)}$$

$A_{Rn\text{-}222}$ = radon activity concentration relative to sample weight
$A_{Rn\text{-}222'}$ = radon activity given by the RAD7
V_{tot} = total volume of box, sample cell and tubes with filters
V_{box} = volume of PP box
V_s = volume of sample
W_s = weight of sample

The emanation coefficients (E) were calculated according to Equation 3:

$A_{Rn\text{-}222}$ = radon activity concentration according to Equation 4
$A_{Ra\text{-}226}$ = radium activity concentration measured by $\gamma-$spectrometry

The standard deviation (SD) of the emanation coefficients were calculated according to Equation 5:

$$ SD = \frac{1}{A_{Ra-226}{}^2} \sqrt{A_{Rn-222}{}^2 SD_{Ra-226}{}^2 + A_{Ra-226}{}^2 SD_{Rn-222}{}^2} \qquad \textbf{(Equation 5)} $$

$A_{Rn\text{-}222}$ = radon activity concentration according to Equation 4
$A_{Ra\text{-}226}$ = radium activity concentration measured by γ-spectrometry
$SD_{Rn\text{-}222}$ = standard deviation of the radon activity concentration
$SD_{Ra\text{-}226}$ = standard deviation of the radium activity concentration

6.4 Results of emanation measurements

One hundred and eleven samples were measured in total, including 70 rock samples and 41 samples of weathering products. The samples cover 22 different stratigraphic units and in some cases different lithologies within one stratigraphic unit.

The results are given as emanation coefficients and as radon activity concentrations (see Equation 4). The latter is used to express the quantity of radon produced in the sample pore gas at secular equilibrium, independent of the radium activity concentration of a sample.

6.4.1 Emanation coefficients grouped by stratigraphy

The emanation coefficients, grouped by stratigraphy, are given in Figure 23 and Figure 25. The complete dataset with standard deviations is given in Appendix 4, Table A4-1 – A4-4.
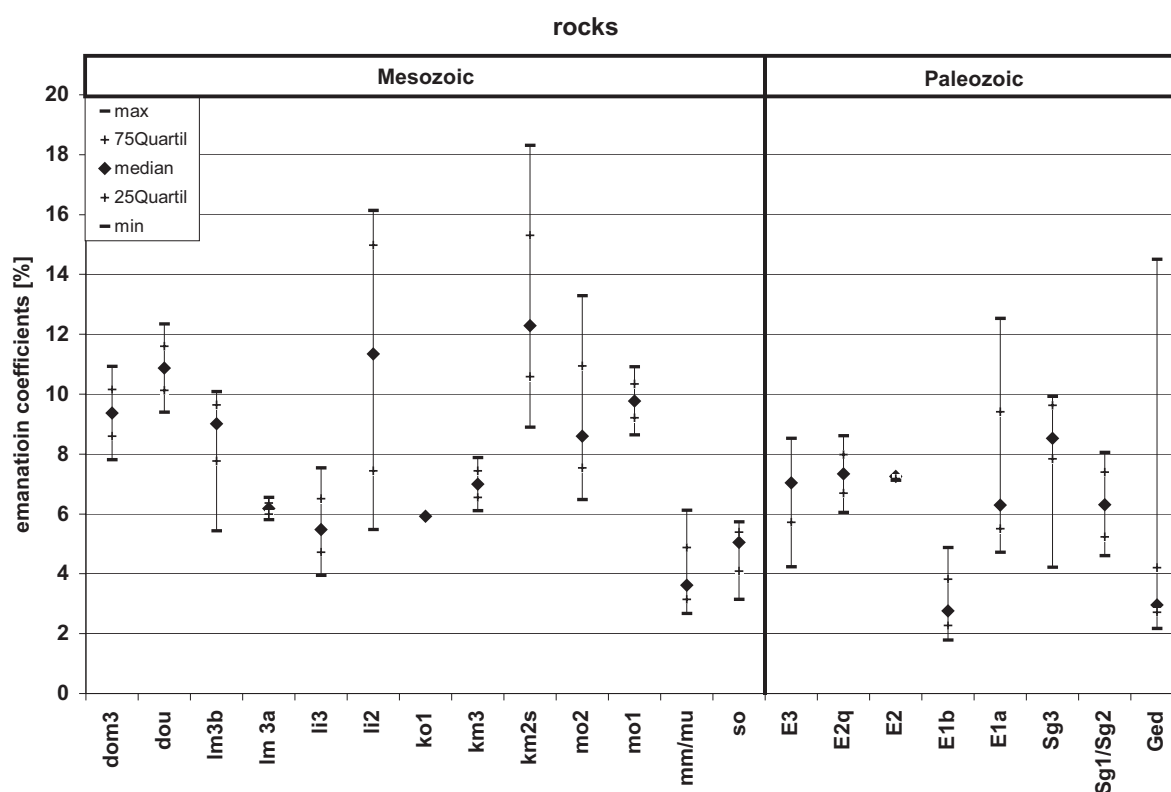
Figure 23: Emanation coefficients of rocks (see Appendix 4, Table A4-2).

The emanation coefficients range between 3 - 18% for the Mesozoic rock samples and between 2 - 15% for the Palaeozoic rocks (Figure 23). Looking at the median values, the emanation coefficients of the Mesozoic rocks exceed those of the Devonian (Figure 23). The highest emanation coefficients occur for the samples of the Luxembourg Sandstone (*li2*) and

the Schilfsandstein (*km2s*). The lowest emanation coefficients occur for the *E1b*, independent of the different rock types (schist, siltstone, sandstone).

When comparing the emanation coefficients of the rocks with their radium activities, there is no significant correlation (Figure 24). Samples with high radium activities (e.g. *Ged*) do not necessarily have high emanation coefficients and vice versa (e.g. *E2q*).
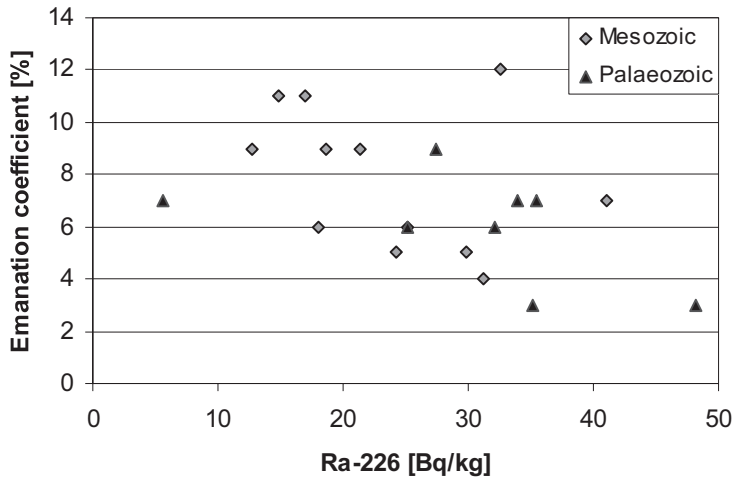
Figure 24: [226]Ra versus emanation coefficients of rock samples.
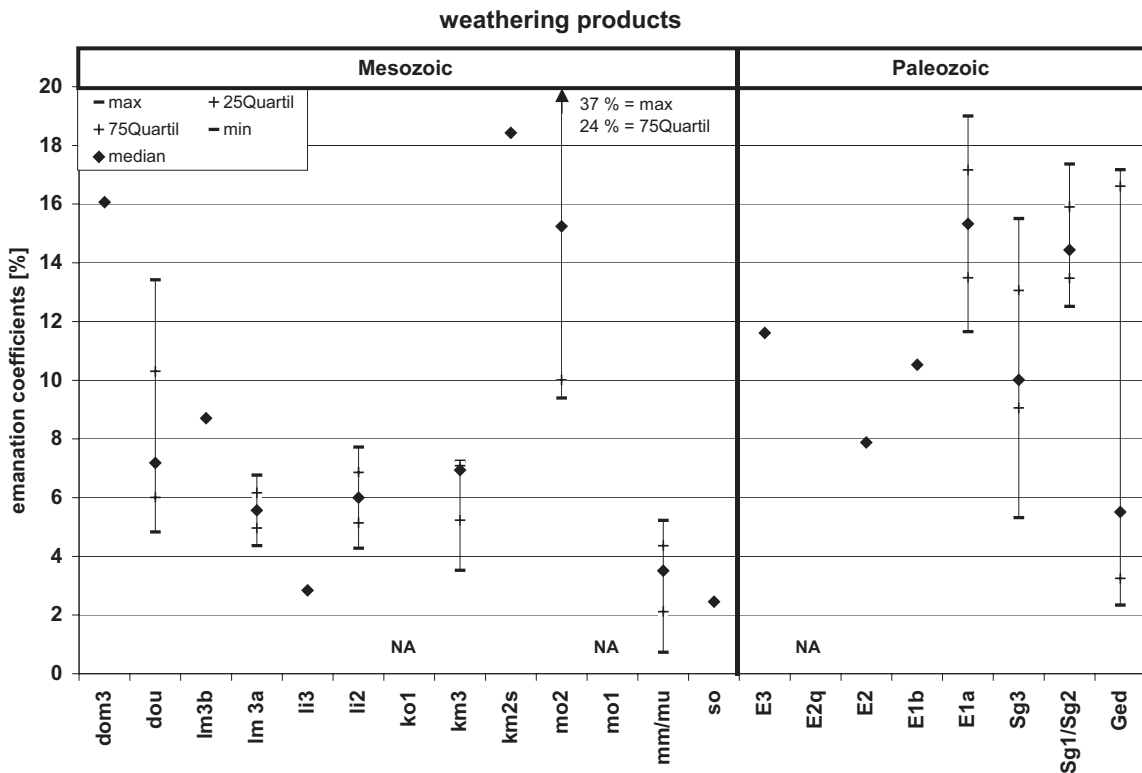
Figure 25: Emanation coefficients of weathering products (see Appendix 4, Table A4-3).

The emanation coefficients of the weathering products range between 1 – 37% for the Mesozoic samples and between 2-19% for the Palaeozoic samples (Figure 25). The highest emanation coefficients occur for the samples of the Schilfsandstein (_km2s_), the _dom3_ and the Upper Muschelkalk (_mo_).

Comparing the emanation coefficients of the rocks with those of their weathering products, noticeably higher emanation coefficients occur for weathering products of all Devonian units (by a factor of 2-4). This also applies to the Mesozoic units _dom3, km2s_ and the _mo_ (all by a factor of 2), which show the highest emanation coefficients of the Mesozoic weathering products. All other units show equal or lower emanation coefficients than their parent rocks.

These results show that high indoor radon concentrations observed at many sites in the Eisléck (KIES & FEIDER 1996) and the very high indoor radon concentrations occurring in Belgium (TONDEUR et al. 1996) can only be explained by high emanation coefficients of weathering products. An increase of emanation coefficients is only associated with an increase of ^{226}Ra activities for the Devonian units, _mo2_ and _km2s_ weathering products, leading to a higher geogenic radon potential of these stratigraphic units.

The investigations of KIES et al. (1996 a) provided no evidence for any correlation of ^{226}Ra activities of bedrocks with indoor radon concentrations. This may be explained by the choice of samples that were analysed for ^{226}Ra activities. Samples were usually taken as composite samples, including both rocks and weathering products (KIES, ROBINET, ROWLINSON, oral communication). As was demonstrated, it is essential to separate weathering products from rocks, because there is a great difference in ^{226}Ra activities and emanation coefficients between rocks and weathering products.

6.4.2 Radon activity concentrations grouped by stratigraphy

The importance of the weathering products for the radon potential of an area becomes even more distinct when considering the radon activity concentration, which is independent of the radium activity concentration (see Equation 4).

The radon activity concentrations of the rocks investigated range between 0.3 and 6.1 Bq/kg* with no overall difference between Palaeozoic and Mesozoic samples (Figure 26). The lowest radon activity concentrations were measured for the quartzites of the _E2q_, as anticipated from their low ^{226}Ra activity concentration.
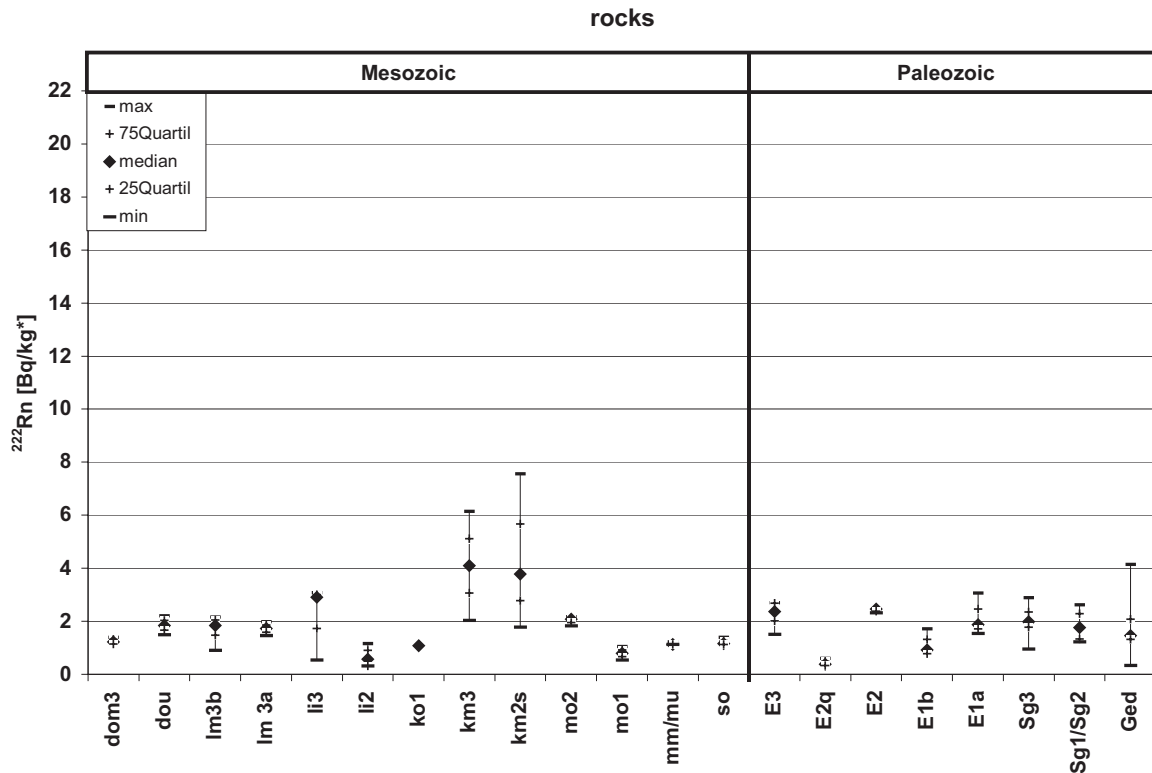
Figure 26: Radon activity concentrations of rock samples, referring to the released radon in sample pore gas related to the weight of the emanating material at secular equilibrium (see Equation 4) (see Appendix 4, Table A4-4).

Low radon activity concentrations, of less than 1.5 Bq/kg*, were measured for the sandstones of the *so*, the *li2* and the *ko*, as well as for iron rich limestones of the *dom3* and the various rock types of the *mm/mu* (Figure 26) such as dolomites, marl and sandstones. For the Palaeozoic rocks, only the samples of the *E2q* and the samples of the *E1b* show such low radon activity concentrations. The latter is unexpected, since the radium activity concentrations are in the same order of magnitude as those of the other Devonian units (Figure 23).

The highest radon activity concentrations were measured for the sandstones of the *km2s* and the dolomites and marls of the *km3*. Marls of the *li3* show high concentrations as well. Significant differences occur between the dolomites of the Upper Muschelkalk (*mo1, mo2*). The dolomites of the *mo2* release more than twice as much radon as the dolomites of the *mo1* (Figure 26), reflecting the radium activity concentrations of the samples. The emanation coefficients are therefore in the same range (Figure 23).

weathering products
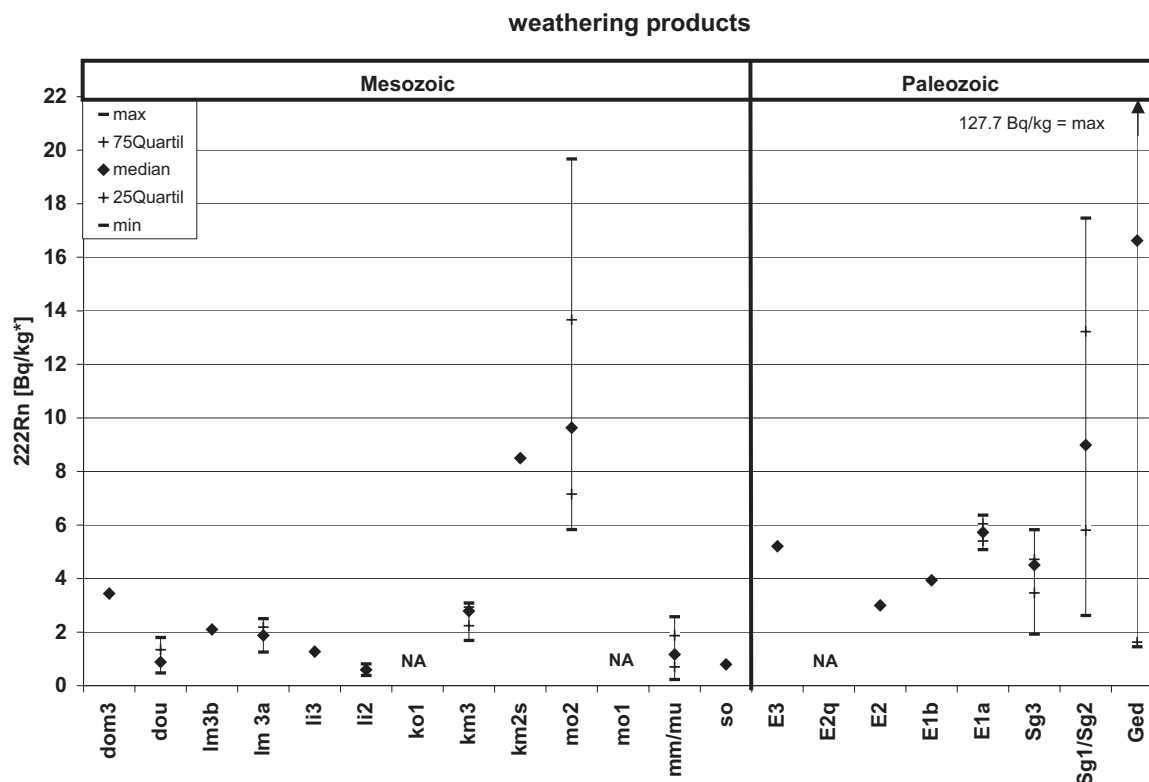
Figure 27: Radon activity concentrations of the weathering products (see Equation 4) (see Appendix 4, Table A4-4).

There is a general difference in radon release between Palaeozoic and Mesozoic weathering products, in contrast to the rocks. High radon concentrations of the Mesozoic occur only for the weathered, highly porous sandstones of the *km2s*, with a higher content of C_{org} from fossil plant remains, and especially for the weathered marls of the Upper Muschelkalk.

For most of the Mesozoic weathering products the median values of radon activity concentrations of less than 3 Bq/kg* are lower than the median radon concentrations for Palaeozoic samples (maxima generally > 5 Bq/kg*). This corresponds to higher emanation coefficients and higher ^{226}Ra activities found for Palaeozoic weathering products.

Focussing on the Palaeozoic weathering products, those from the Gedinnian have highest radon concentrations with a wide range between 1.7 and 128 Bq/kg*. The values of the Gedinnian are much higher than those of the Siegenian and the Emsian, which range between 2 and 18 Bq/kg*.

Comparison of radon activity concentrations in the pore gas of rocks and their accompanying weathering products (Figure 26) produces similar results to those found for the emanation coefficients. Noticeably higher radon activity concentrations occur for the weathering products of all Devonian units and the *mo*. Not only are the emanation

coefficients of the weathering products of most Mesozoic units lower than the accompanying rocks, but also the radon activity concentrations (Figure 27).

Considering radon activity concentrations instead of emanation coefficients clearly reveals how much more radon is released from Devonian weathering products than from their accompanying rocks. High geogenic radon potentials can be deduced not only for the Devonian, but also for the Schilfsandstein (*km2s*) and the Upper Muschelkalk (*mo*).

For the Schilfsandstein no indoor radon data are available, as they were grouped together with the other data of the Middle Keuper units. The high radon emanation of the weathering products of the Upper Muschelkalk is not matched by indoor radon measurements in Luxembourg (median: $67kBq/m^3$; 90%percentile: $153kBq/m^3$). This may be due to varying lithologies of the Upper Muschelkalk from the east of Luxembourg (dolomites and marls) to the west of Luxembourg (sandstones). While indoor radon measurements were performed throughout the area, the samples for the emanation measurements were mainly taken in the east.

Since the composition of the Upper Muschelkalk in eastern Luxembourg corresponds to the Upper Muschelkalk in the Eifel region of Germany, indoor radon values from this region can be used for comparison. The indoor radon measurements confirm a high geogenic radon potential of the Upper Muschelkalk with $950 Bq/m^3$ at the 90% percentile as well as soil gas measurements. Especially at the top of the Upper Muschelkalk, radon activity concentrations of more than $100 kBq/m^3$ were measured locally in soil gas (KEMSKI et al. 1999).

Table 8: Correlation coefficients of indoor radon measurements with radon activity concentrations and emanation coefficients of rocks and weathering products. The correlations were calculated with the median values of the stratigraphic units. Correlations in bold are significant at p < 0.05.

	Radon activity concentrations		Emanation coefficients	
	Rocks	**Weathering products**	**Rocks**	**Weathering products**
Indoor radon	-0.30	**0.52**	-0.17	**0.59**

Table 8 shows that neither radon activity concentrations, nor emanation coefficients of rocks, correlate significantly with indoor radon concentrations. However, there is a positive correlation of indoor radon concentrations with radon activity concentrations and with emanation coefficients of the weathering products. This underlines once again the assumption that high emanation coefficients of the weathering products are the reason for observed higher indoor radon values.

6.4.3 Emanation coefficients and radon activity concentrations of rock types

In the previous chapters, samples were grouped by stratigraphic units, meaning geological age irrespective of rock types. In fact, emanation is different for certain rock types, e.g. the lowest radon activity concentrations generally occur for quartzites. For this reason, samples are now additionally grouped by lithology. For comparison, only the results of undifferentiated weathered materials were plotted against rocks, subdivided by particle size but not by rock type origin (Figure 28 and Figure 29).
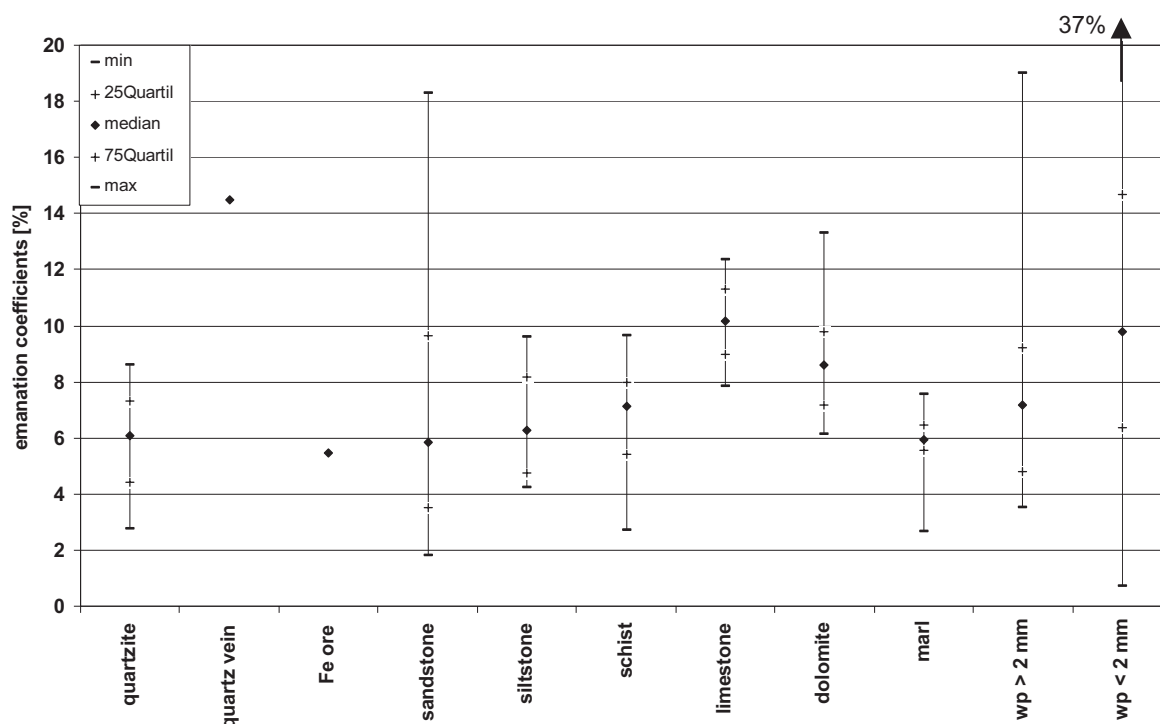
Figure 28: Emanation of different rock types and of undifferentiated weathering products (wp).

The highest radon emanation coefficients occur, as expected, for weathering products with a particle size < 2 mm, while emanation coefficients of weathering products > 2 mm do not differ significantly from those of rock samples (Figure 28). The median values of emanation coefficients of different rock types rise in the order: sandstone ≤ marl ≤ quartzite ≤ siltstone < schist < dolomite < limestone.

Table 9: Emanation and radon activity concentration of Mesozoic and Palaeozoic sandstones.

	Emanation coefficient [%]			^{222}Rn [Bq/kg]*		
	Min	Median	Max	Min	Median	Max
Mesozoic sandstone	3	8	18	0,3	1,1	7,6
Palaeozoic sandstones	2	3	13	0,7	1,5	3,4

The highest emanation coefficients (median > 8%) occur for limestones, dolomites and for the quartz vein sample. The widest range of emanation coefficients occurs for the sandstones. Mesozoic sandstones show higher emanation coefficients than Palaeozoic sandstones, but the release of radon is slightly higher for Palaeozoic sandstones (Table 9). Nevertheless, the highest emanation coefficient (18%) and a high radon activity concentration (7.8 Bq/kg*) occur for a Mesozoic sandstone of Schilfsandstein (*km2s*) age. This sandstone is special in that it has a high porosity and contains fossil plants, resulting in a lamellar structure, providing a high internal surface area. Radon was easily released from this sandstone, which is underlined by a loss of ^{210}Pb in this sample (25% lower activity concentration of ^{210}Pb compared to ^{226}Ra).
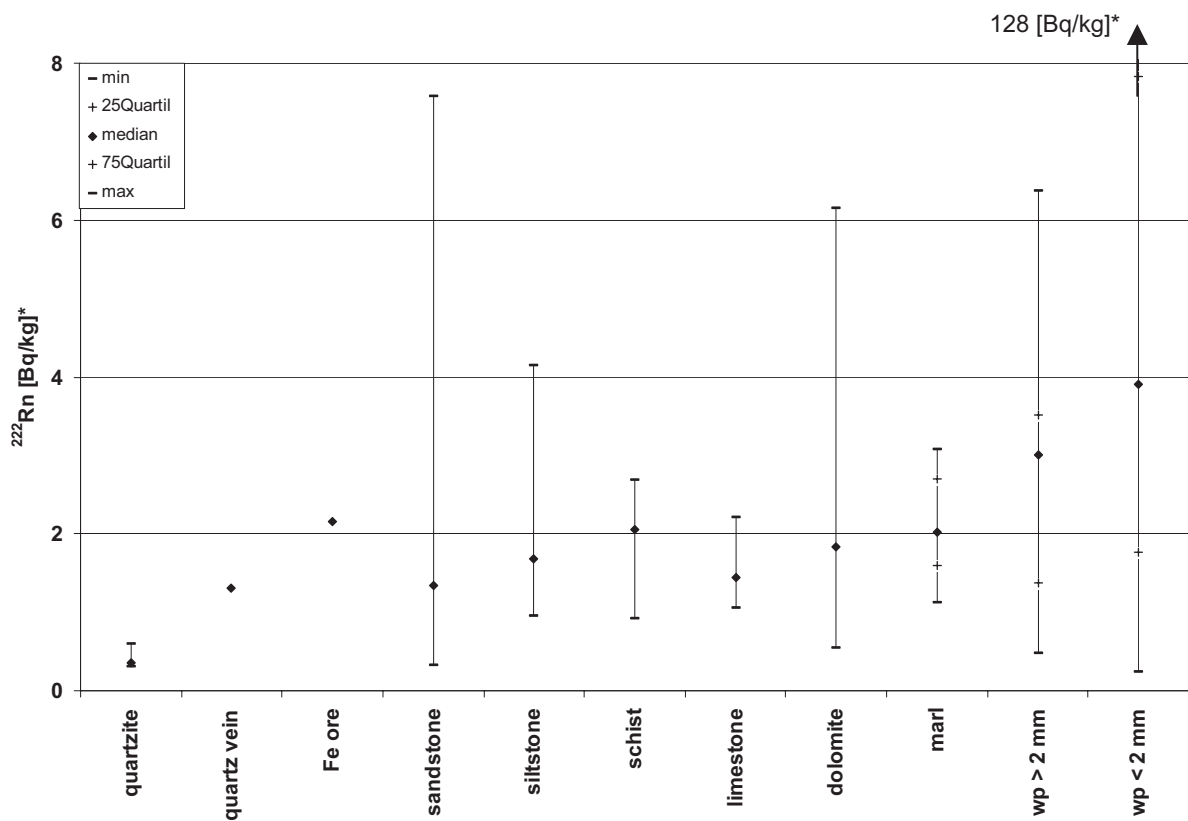
Figure 29: Radon activity concentrations of different rock types and undifferentiated weathering products (wp).

The radon activity concentrations are highest for the weathering products < 2 mm, too. Especially iron rich samples with an iron content of more than 10% of Fe_2O_3, deriving mainly from Gedinnian, show high radon activity concentrations. The difference between rock samples and weathering products > 2 mm is somewhat greater than for the emanation coefficients considering the medians, but the range of radon activity concentrations is similar.
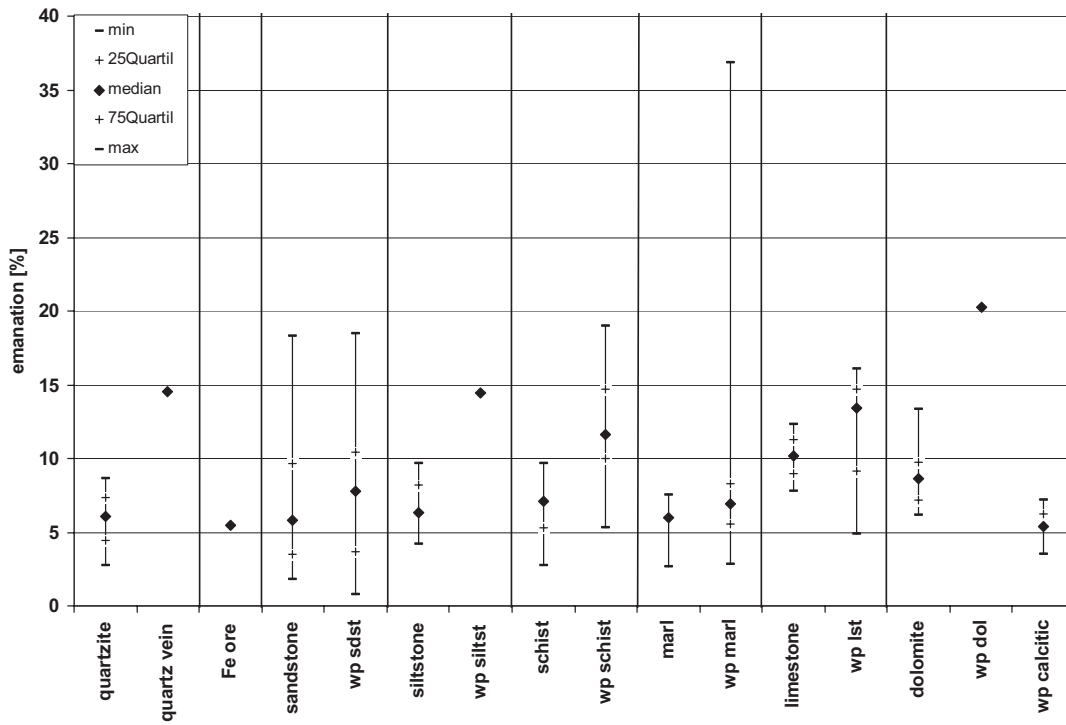
Figure 30: Emanation coefficients of the different rock types compared to their weathering products (wp).
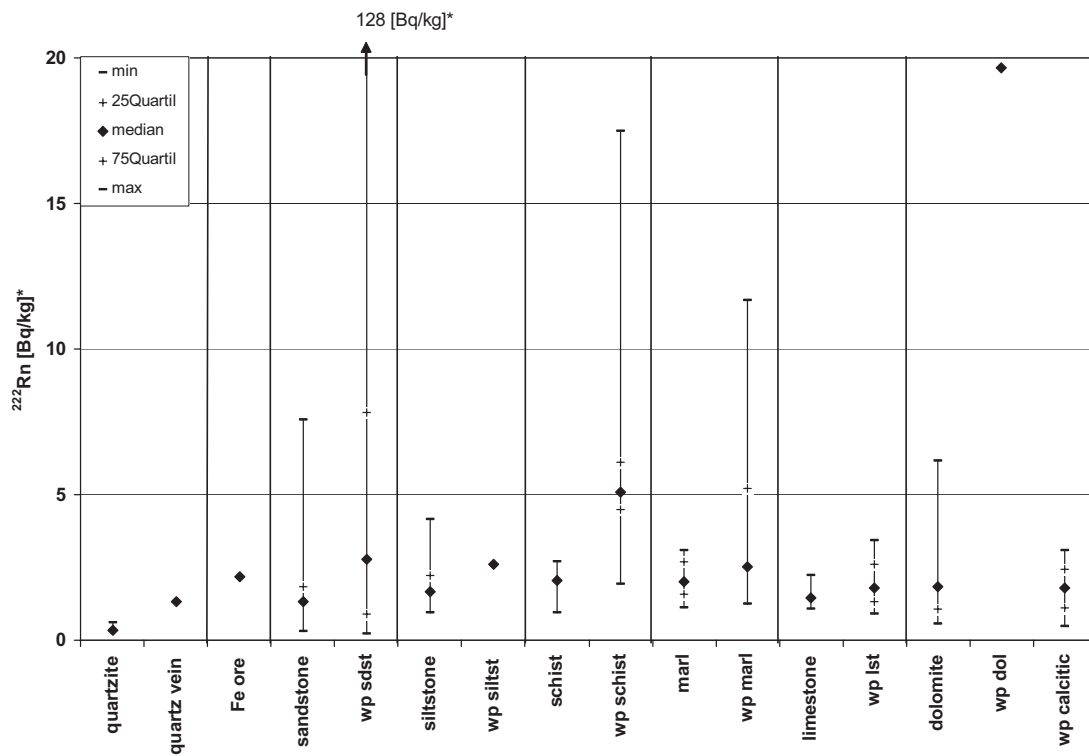
Figure 31: Radon activity concentrations of the different rock types compared to their weathering products (wp).

55

The lowest radon activity concentrations were measured for quartzites of Emsian and Gedinnian age (*E2q, Ged*) and a quartz vein sample from Gedinnian host rock. Though radium activities of the quartzites and the quartz vein sample are approximately equal, the latter releases much more radon (Figure 29), because radium in the quartz vein sample is located in iron oxide/hydroxide coatings on the surface of quartz grains and in fractures, resulting in a large internal active surface area to release radon.

A closer look at the weathering products, now in direct comparison to their parent rocks, shows that radon release and emanation coefficients are both higher for the weathering products. The largest differences between rocks and weathering products occur for dolomites, sandstones and schists, but there are only slight distinctions for limestones.

7   Speciation of Th, U, and Ra

7.1 Sequential extraction

Most procedures to determine the speciation of elements use sequential chemical extraction, which means that one sample is extracted with various chemical solutions in successive steps.

The selectivity of such a method is functionally defined by the chemical extractants used and the sequence of their application. It is difficult to find specific extractants exclusively effective on certain speciations of trace metals. During the extraction steps, not only desired, but also other compounds may be dissolved. The terms used for the different fractions (exchangeable, organic matter, etc.) are therefore not to be taken as a definite determination of specific compounds, but represent that part of a sample which was dissolved with a specific extraction agent.

7.1.1 Comparison of methods

Several procedures have been developed since the early nineteen seventies to determine compounds of heavy metals in sediments and soils. PICKERING (1981) and ZEIEN (1995) gave critical reviews of sequential extraction procedures. Only a few authors have analysed the mobility of radionuclides with sequential extraction. While an overview of the investigations up until the end of the 1980s was published by BENEŠ (1990), a discussion of some interesting studies since 1990 will be given in the following section.

GREEMAN (1992) examined the geochemistry of radionuclides in 12 well-developed soils from the eastern United States, chiefly in Pennsylvania. The distribution of thorium, uranium and radium was compared with soil properties. Three sequential extraction methods were used (ROSE et al. 1977; CIOLKOSZ et al. 1988; SHUMAN 1985), which differed mainly in the number of extraction steps, but not so much in the extractants used. The abundance and radiometric equilibrium conditions were first determined in the following successive extraction steps: exchangeable cations (MgCl), organic matter (NaOCl), Mn oxides (hydroxylamine hydrochloride), resistant organics (H_2O_2) and poorly crystalline iron oxides (Na-dithionite). Later the extraction steps for Mn oxides and resistant organics were omitted. Finally, only two extraction steps were performed on most samples, separating exchangeable cations together with organic matter from Fe oxides, the latter fraction also including oxides of Mn and Al. The extraction residuals left after sequential extraction were separated in to sand, silt and clay fractions. Additionally, the vegetation of the 12 sites was analysed for Th, U, and Ra.

The main results of the study showed that radium and uranium were nearly in equilibrium at all depths except the A horizons, where the Ra/U ratio ranged between 1.65 and 1.80. Radium occurred mainly in pedogenic phases. Whereas up to 24% of radium was bound to organic material, less than 1% of uranium occurred in this fraction. Radium greatly exceeded uranium in soil organic matter (Ra/U up to 30) and in vegetation (Ra/U up to 65). The enrichment of radium in A-horizons was explained by biogeochemical transfer of Ra to A-horizons from lower horizons by plants. In addition to this, excess radium was found in the fraction of poorly crystalline iron oxides (Ra/U up to 1.8) and in some C-horizons of deeply weathered soils (Ra/U up to 1.5).

VON GUNTEN, SURBECK & RÖSSLER (1996) analysed the behaviour of [234]U, [238]U, [230]Th and [232]Th in soils in Switzerland. They compared sixteen soil profiles located in the limestone Karst range of the Jura Mountains (Jurassic and partly Cretaceous formations) with profiles above limestone in the Central Alps (Gadmen) and in addition with two granite soils in the Central Alps (Handegg, Grimselpass), peat from Lake Burgäschi and Loess from Aargau (Möhlin). All soil samples were wet-sieved into different fractions in the range 100 - 1000 μm. Peat samples were ground to about 250 μm. The sequential extraction scheme separated humic fraction (NaOH), amorphous iron and Mn hydroxide phase (ammonium oxalate with oxalic acid), oxide mineral phase (ammonium oxalate, oxalic acid and ascorbic acid) and extraction residual (boiling conc. $HF/HNO_3/HClO_4$). Total uranium and thorium was calculated from the addition of all of the fractions.

They found activity ratios (ARs) of [234]U/[238]U slightly above unity for all of the soil samples and extracted fractions, reflecting the isotopic composition of uranium in soil solution. After IVANOVICH & HARMON (1992), soil solutions usually have [234]U/[238]U ARs of > 1, resulting from recoil processes in the solid phases related to α-decay (FLEISCHER 1982). The ARs of [230]Th/[234]U were much higher in the humic fraction, the amorphous and the oxidic phases of the limestone profiles (Jura and Gadmen), demonstrating the importance of thorium sorption to these phases. [230]Th is accumulated in Karst soils and [226]Ra grows until secular equilibrium is reached.

[230]Th/[234]U ARs of non-carbonatic soil samples were much smaller and sometimes even lower than 1 in all soil fractions, which suggests a relatively similar behaviour of uranium and thorium in these soils. It was assumed that, in contrast to carbonatic soils, where high CO_2 concentrations enhance the formation of stable, soluble and mobile uranium carbonate complexes, uranium forms more insoluble complexes in neutral or acidic soils, e.g. with humic substances.

Radium enrichment in soils above limestone is attributed to enrichment of [230]Th in the soil column. While uranium is released during weathering and migrates as a stable uranyl carbonate complex, [230]Th hydrolyses and is strongly absorbed to soil particles and/or forms

insoluble compounds. This process continues over time, [230]Th enriches more and more in soils and [226]Ra grows until secular equilibrium is approached.

Two studies were conducted with an extraction procedure developed by KLINGER (1993). The original work of TESSIER et al. (1979) was improved by CALMANO & FÖRSTNER (1982) and modified by KLINGER (1993), taking into account the results of CREMER (1986) and KLINGEL (1991). The extraction scheme separated the following fractions: mobile exchangeable (deionised water), exchangeable (ammonium acetate), carbonatic (sodium acetate), amorphous Fe/Mn oxyhydroxides (ammonium oxalate with oxalic acid), organic and sulfidic (boiling HNO_3 with H_2O_2).

KLINGEL et al. (1995) used this procedure to analyse stockpile material from uranium mines operated by the WISMUT GmbH near Trünzig/Culmitzsch (Gauernhalde and Waldhalde). The samples consisted primarily of quartz, as well as feldspar, dolomite, siderite and clay minerals. One sample was a sinter deposit from a location where drain water was seeping out of the stockpile. This sample had the highest concentrations of radium, uranium and some other heavy metals such as Zn, Ni and Co. The authors found that about 25% of the uranium (60% in the sinter sample) and about 45% of the radium (< 5% in the sinter sample) is potentially mobile in the spoil pile. In spite of the higher potential of radium to be mobile, much more uranium was actually found in the drain water. As a high percentage of the extracted radium was found in the exchangeable fraction, primarily dissolved radium may be adsorbed in the stockpile itself. The co-precipitation of radium with carbonate is documented by very high radium activities in the sinter sample.

ROTH (1997) used the same procedure as KLINGER (1993) to analyse the distribution of U, Ra and Th in three different soils (Upper Muschelkalk (*mo1*), Pseudomorphosenkeuper (*km1*), Luxembourg Sandstone (*li2*)). The soil profiles were located in the southwestern Eifel, close to the border between Germany and Luxembourg. The aim was to test alternative measurement methods for radionuclides in eluates of sequential extractions. Uranium was measured with a photometric method after KEIL (1979), which did not work very well for some reason (ROTH 1997). Radium and thorium in the eluates were measured by γ-spectrometry, but in most cases the activities were lower than the detection limit for both radionuclides.

Nevertheless, the study documented some problems with the selectivity of the extraction scheme after KLINGER (1993). The greatest drawbacks of the extraction scheme were dissolution of silicates in several extraction steps and the lack of an extraction step to dissolve crystalline Fe oxides. The fraction of the crystalline Fe oxides occurred in the extraction residual instead. Two problems occurred concerning the extraction step in which only amorphous Fe/Mn oxyhydroxides should have been dissolved. Firstly, part of the organic matter was dissolved in this fraction, leading to an underestimation of the following

organic fraction. Secondly, whewellite (Ca-oxalate) was precipitated during this extraction step, which was described earlier by CREMER (1986), who also found precipitation of Sr- and Ba-oxalate.

Especially for the carbonatic samples, the selectivity of the extraction scheme used was unsatisfactory because it was not possible to resolve total carbonate in the corresponding fraction (step III) for samples with a carbonate content > 4%, even though the extraction scheme was adjusted.

EDSFELDT (1998) used a four-step extraction scheme to analyse ^{226}Ra distribution in three Swedish soils (till, sand and clay). Samples were sieved in to four fractions (< 0.063 mm, 0.125-0.25 mm, 0.25-0.5 mm, 1-2 mm) prior to extraction, to determine the influence of grain-size on radium distribution. In addition, radon exhalation and emanation coefficients were determined on unleached samples.

The sequential extraction method separated four fractions: dissolved ions (deionised water), cation exchangeable (NH_4Cl), Fe/Mn oxyhydroxides (HCl) and extraction residuals (fused with $LiBO_3$, dissolved with HNO_3). The organic fraction was not separated, so organic-bound radionuclides occurred in step 2 as well as in step 3. The result of GREEMAN (1992), who found most radium correlated with the organic fraction, could therefore not be confirmed. EDSFELDT (1998) found most radium bound to Fe oxides, but assumed that some of the radium was primarily associated with Ca that had been co-precipitated with hydrous Fe oxides later, as the correlation of radium and calcium was better than the correlation of radium and iron in the iron oxide fraction. Emanation coefficients correlated best with the element concentrations in this fraction, indicating that radium bound to Fe oxyhydroxides was the primary source of radon emanated. Considering the grain-size separation, element concentrations increased with decreasing grain-size, as anticipated.

Subsequently, EDSFELDT (2001) changed to the extraction scheme after ZEIEN (1995), which will be described below. It was used to analyse radionuclide distribution in a Swedish spodosol, developed on till with underlying uranium-rich granite. As in previous studies, samples were separated in four grain-size fractions prior to sequential extraction. Exhalation and emanation coefficients were determined on unleached samples, as well as the specific surface area [m²/g] determined according to the BET(N_2) method.

Radium dominated in the exchangeable fraction or the extraction residuals, depending on the soil horizons. Ra in the extraction residual predominated in the upper layers, whereas exchangeable radium increased with depth and was enriched in the C-horizon. Little radium bound to organic matter was found in all samples, which was again inconsistent with GREEMAN (1992). Uranium was most abundant in the extraction residuals for most samples and oxide-bound uranium was only of secondary importance. Thorium prevailed only in the top soil horizon in the extraction residual. In the B-horizon and the C-

horizon, oxide-bound thorium dominated and only a small quantity of thorium remained in the extraction residual. The amorphous Fe oxide fraction was the most important fraction for both U and Th.

Emanation coefficients were similar for the fine sand fraction and the silt-clay fraction, but the amount of emanated radon increased with decreasing grain-size nevertheless. Emanated radon correlated well with oxide-bound radium. Total Ra, Th and Fe were significantly positively correlated with the specific surface area [m²/g]. A correlation between clay content and radionuclide concentration could not be determined.

A recent paper by MARTÍNEZ-AGUIRRE & PERIÁÑEZ (2001) deals with the distribution of uranium and thorium in different fractions of intertidal sediments in Spain, affected by the release of natural radionuclides from fertiliser industries. They found high radionuclide concentrations in all fractions. Uranium and thorium are positively correlated with amorphous Fe-/Mn oxides/hydroxides, but for thorium the contribution in the extraction residual fraction is higher than in the non-residual fractions.

7.1.2 Sequential extraction scheme used in this study

In all studies mentioned, the extraction methods used differed from each other to some extent, but were all based in general on the work of TESSIER et al. (1979). The work of ZEIEN & BRÜMMER in 1991, comparing four of the most common methods based on TESSIER et al. (1979), showed that they do not lead to similar results. A method was therefore developed (Table 10) that is suitable for rock and soil samples up to a carbonate content of 5%. A detailed description is given by ZEIEN (1995). The method of ZEIEN & BRÜMMER (1991) is recommended by the AD-HOC ARBEITSGRUPPE BODEN (1996).

For this study, sequential extraction was performed on 17 samples of sedimentary rocks (9 rock samples, 8 weathering products). Most samples originated from an old quarry about 1 km northwest of Hatrival in Belgium (see Chapter 3.1). These Lower Devonian (Gedinnian) samples were chosen because the radionuclide activities of the weathering products were exceptionally elevated and it was expected that clear differences in the geochemistry of rocks and weathering products would be found. For comparison, two Siegenian samples (*Sg2*) from Hautbellain (Luxembourg: x 65 495/ y 135 315) and two samples of Lower Triassic age (Buntsandstein, *so*) from Bornermillen (north of Born, Luxembourg: x 104 550/ y 93 750) were analysed.

2 g of each dried and milled sample (see Chapter 6.2) was used for sequential extraction. A brief overview of the extraction scheme is given in Table 10.

Prior to extraction, most samples were analysed for light minerals and heavy minerals by gravity separation and XRD (see chapter 4.3). The same applies to the extraction

residuals. In addition, separated iron and manganese oxide/hydroxide coatings were analysed by XRD, to determine their mineralogical composition.

Table 10: Sequential extraction procedure used in this study.

Step	Reagent	pH	Quantity [ml/2g]	Leaching procedure	Fraction
I	1M NH_4NO_3		50	agitate for 24 hours	Mobile exchangeable*
II	1M NH_4OAc and 1M NH_4NO_3	6.0	50 25	agitate for 24 hours agitate for 10 min	Exchangeable**
III	0.1M $NH_2OH*HCl$ and 1M NH_4OAc	6.0 5.5	50 2x25	agitate for 30 min agitate twice for 30 min	Mn oxides***
IV	0.025M NH_4-EDTA and 1M NH_4OAc	4.6	50 25	agitate for 90 min. agitate for 10 min	Organic matter***
V	0.2M NH_4-oxalate buffer	3.25	50 25	agitate in darkness for 4 hours agitate in darkness for 10 min	Amorphous Fe oxides[‡]
VI	0.1M ascorbic acid in 0.2M oxalate buffer and NH_4-oxalate buffer	3.25	50 25	boil for 30 min at 96°C agitate for 10 min	Crystalline Fe oxides

* water soluble and non-specifically adsorbed metals
** specifically adsorbed, occluded close to the particle surface, bound to carbonates and extracted from metal-organic complexes of low stability
***also a small part of clay minerals and other less stable silicates are dissolved
[‡]essentially ferrihydrite

7.2   Chemical analysis of eluates

The extraction solutions were analysed by ICP-MS (Elan 6000, PerkinElmer Sciex[6]) at Luxcontrol S.A. for U and Th, as well as for some trace elements and some REE (rare earth elements). Iron, aluminium, magnesium, and manganese were analysed by ICP-OES (SPECTRO[7]) at Luxcontrol S.A, when element concentrations were too high for a measurement with ICP-MS. Radium was determined by liquid scintillation counting (LSC) (Triathler™, HIDEX OY[8]).

7.2.1 ICP-MS

The technique of ICP-MS offers measurement of several elements as well as measurement of individual isotopes simultaneously, combined with very low detection limits, short analysis times, and minimal sample preparation. Samples are analysed as solutions, which are converted to an aerosol by means of a nebuliser. The aerosol is introduced into argon plasma and is ionised at about 7,000 °C. The ions are transferred into a vacuum chamber where they are focused by a row of ion lenses and separated according to their

---

[6] PerkinElmer Analytical Instruments, 710 Bridgeport Avenue, Shelton, CT06484-4794, USA
[7] SPECTRO Analytical Instruments GmbH & Co. KG, Boschstr. 10, 47533 Kleve, Germany
[8] Hidex Oy, Mustionkatu 2, 20750 Turku, Finland

mass/charge ratio by a mass spectrometer. The separated ions are quantified by means of a multistage semiconductor detector. Instead of detecting the light emitted by an analyte, the actual analyte ion itself is being detected.

7.2.1.1 Measuring device

The ICP-MS used in this study was an ELAN 6000 fitted with an AS-90/91 autosampler (PerkinElmer Corp.). The operating conditions for the ICP-MS were calibrated at least once a week according to the recommendations of the manufacturer. Performance tests were performed daily to ensure proper measuring conditions. If necessary, the operating parameters were adjusted (usually the nebuliser gas flow). The settings of the instrument can be found in Table 11.

Table 11: Operating parameters for the ELAN 6000

SWEEPS per reading	50
Readings per replicate	1
Replicates	3
DWELL time per AMU	20 ms
Integration time	1000 ms

7.2.1.2 Calibration

Preliminary investigations had shown that it was necessary to measure each sample with standard addition, because of the high matrix effects of the extractants. Calibration was carried out with a blank and five standards each. They were verified by analysing standards obtained from an independent source. Rh was used as the internal standard.

Between the measurements, the instrument was rinsed with 3% v/v HNO_3 for 450 s. This length of washing time was chosen to avoid summation effects for thorium (Figure 32).
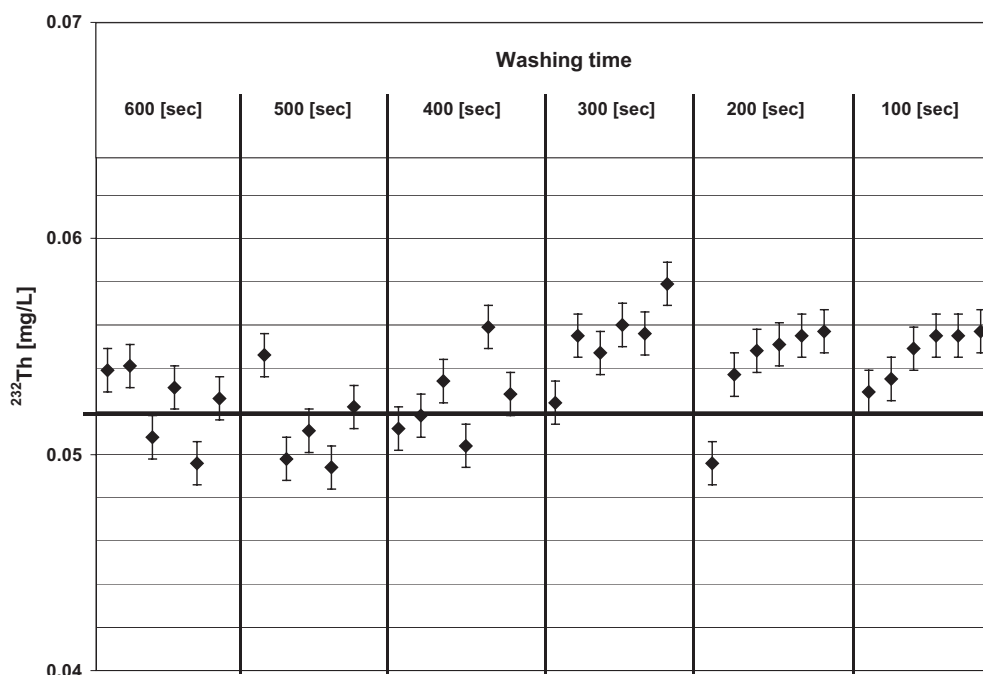
Figure 32: Stability test with a [232]Th standard (0.051 mg/l) and 3% v/v HNO$_3$ washing solution. Summation effects are detectable for washing times up to 400 sec. Washing times of 500 sec and 600 sec are sufficient for measuring thorium without summation effects.

7.2.1.3 Sample preparation and measurement

For ICP-MS measurements, the samples were generally diluted 1:20, except for step VI. Element concentrations in the phase of the crystalline Fe oxides were expected to be very high, so the eluates of step VI were diluted 1:100. Uranium was measured at mass 238 and thorium was measured at 232.

7.2.1.4 Accuracy of analytical results

Each sample was measured at least three times and the average of the measurements was taken as the result. The standard deviation was calculated from the three measurements. The detection limit was taken as three times the uncertainty of 10-fold measured blanks.

The measurements could not be normalised with a reference material, because no standard results for sequential extraction solutions exist. The reproducibility of the measurements was therefore tested by measurements of two samples (one sample with high thorium and uranium concentrations (136b: 37.5 ppm / 35.2 ppm), and one with low activities (136a: 4.3 ppm/ 10.4 ppm)). Measurements were repeated weekly. Both samples had been extracted in three parallel sessions, so that the measured reproducibility not only applies to the ICP-MS measurements but gives the reproducibility of the complete experimental procedure. The results generally vary within ± 1 - 20% depending on the element and the extractant (Appendix 5, Table A5).

7.2.2 Liquid Scintillation Counting

Radium in the eluates was measured by LSC. Liquid scintillation techniques allow counting of alpha and beta radiation in a more accurate and reproducible way than other methods, where pulse-shape discrimination is used to separate alpha from beta particles. Though alpha-particle energies cover the 4 - 8 MeV range, while beta-particle energies occur in the 0 - 2 MeV range, the produced scintillation effects are similar due to the different interactions of alpha- and beta-particles with scintillation cocktails (PRICHARD et al. 1992). By pulse-shape discrimination, alpha- and beta-pulses are separated on the basis of their different pulse lengths (MCDOWELL & MCDOWELL 1994).

There are two different ways of measuring radium with LSC. The first is to measure radium after extracting the radionuclide from a solution by chemical separation. For this, radium is co-precipitated from solution as barium sulphate and dissolved in EDTA. Radium can be extracted from EDTA solution with a toluene-based scintillant solution (SUOMELA 1993, MCDOWELL & MCDOWELL 1994). Samples can be counted immediately after preparation. The concentration of radium is determined by integrating the radium peak at 4.78 MeV (MCDOWELL & MCDOWELL 1994). Samples can also be determined after 30 days, when equilibrium between ^{226}Ra and ^{222}Rn is established, by the peaks of ^{226}Ra, ^{222}Rn (5.49 MeV), ^{218}Po (6.00 MeV) and ^{214}Po (7.69 MeV) (SUOMELA 1993).

An alternative method is to measure radium via radon. If a sample solution is stored long enough (30 days) to allow equilibrium between radium and radon to be reached, the measured radon concentrations are equivalent to those of radium. The measurements for this study were done in this way, as the accuracy of this method (< 0.03 Bq/L, according to PRICHARD & GESELL 1977) was assumed to be adequate.

7.2.2.1 Measuring device

The LSC measurements were carried out using a Triathler Multilabel Tester made by Hidex Oy. Not only liquid scintillation measurements are possible with this instrument, but also the detection of gamma radiation and high-energy beta emissions (^{32}P). The instrument is a portable stand-alone unit, but results can also be downloaded to a PC or a printer, either online during the measurements or after counting is completed. The instrument is capable of distinguishing between alpha and beta particles by pulse-shape discrimination. Avoiding interferences from beta-emitters and luminescence effects reduces natural background for the alpha-channel to less than 0.1 cpm. Low detection limits of 0.05 Bq/l Rn have been achieved at 100 minute counting periods (MÖBIUS et al. 1999).

Table 12: Operating parameters for the LSC (Triathler™, HIDEX OY)

Mode	Alpha
Bias Voltage	875 V
Scale	Log
PLI	Steps I, II, IV, V: 520 Steps III, VI: 540
Y gain	80
X pos	13
Counting time	180 min
Window A	152 - 1024
Window B	152 - 1024

7.2.2.2 Calibration

Calibration of the Triathler was done separately for the chemical solutions of each extraction step, as the different solutions may have different backgrounds and a different impact on the counting efficiency. Radium standards were prepared from a radium solution in 3% v/v HCl with an activity of 35.0 ± 0.35 Bq/l. Usually one blank and seven standards were prepared, ranging from 0.01 Bq/l to 1.05 Bq/l, except for the extractants of the mobile exchangeable fraction, for which the preparation of two more standards up to 5.25 Bq/l was necessary. Counting efficiencies for each extraction solution were determined during calibration measurements and ranged between 60% and 75%.

Each standard had to be prepared four times, as the different extraction steps provide unequal volumes of solution. Different standards were prepared with 40 ml and 90 ml extraction solution in 50 ml and 100 ml volumetric flasks. In addition, standards were prepared with variable volumes of extraction solution, adding deionised water up to 90 ml in 100 ml volumetric flasks, to test whether the use of different quantities of extraction solution has any influence on the measurements. The ratio of total solution to scintillation was kept constant. The efficiencies of the different prepared standards of one extraction step were in good agreement, being within ± 3%.

7.2.2.3 Sample preparation

Extraction solutions were stored together with a cocktail, which is immiscible with water (Betaplate Scint, Wallac HiSafe®, PerkinElmer Inc.), in volumetric flasks. The chosen cocktail is highly inflammable, biodegradable and offers excellent alpha-/beta-discrimination. Depending on the sample solution volume, different methods of sample preparation in 50 ml and 100 ml volumetric flasks were chosen (Table 13).

Table 13: Sample preparation for LSC.

Volumetric flask	Sample solution	Scintillant (Betaplate Scint)	Liquid scintillation vial	Transferred scintillant phase
50 ml	40 ml	4 ml	1.5 ml polyethylene vial (Type Eppendorf)	1.5 ml
100 ml	90 ml	9 ml	8 ml polyethylene vial	7 ml
100 ml	50 ml + 40 ml deionised water	9 ml	8 ml polyethylene vial	7 ml

As the scintillant is lighter than water, it covers the sample solution and seals it hermetically. Equilibrium is reached in the sample after about 30 days. The samples are than shaken for 15 min to extract radon into the organic cocktail phase. After the two phases have separated, part of the cocktail phase is transferred into a polyethylene LS vial (Table 13) and measured after three hours, when equilibrium between ^{222}Rn and its daughters ^{218}Po and ^{214}Po is reached. Radon concentration is determined by the peaks of the three alphas: ^{222}Rn (5.49 MeV), ^{218}Po (6.00 MeV) and ^{214}Po (7.69 MeV).

7.2.2.4 Accuracy of analytical results

Limits of detection and quantification were calculated according to DIN 32 645 (Table 14). Only the solution of extraction step V shows high limits of detection and quantification due to a high background and low accuracy in the lower measurement range.

Table 14: Efficiencies of radon measurements, limits of detection and limits of quantification for the extraction steps measured by LSC.

Extraction step	Efficiency	Limit of detection	Limit of quantification
	[%]	[Bq/l]	[Bq/l]
I	75	0.04	0.06
II	70	0.03	0.05
III	65	0.03	0.04
IV	70	0.02	0.03
V	60	0.10	0.14
VI	70	0.03	0.04

The reproducibility of results was additionally verified by 3-fold measurements of one sample. The reproducibility does not only refer to the radon measurements itself, but gives the reproducibility of the whole sample preparation, as the sample was extracted three times (Table 15).

Table 15: Results of a 3-fold preparation and measurement of one sample.

Extraction step	Meas. A	Meas. B	Meas. C
	[Bq/l]	[Bq/l]	[Bq/l]
I	0.29 ± 0.03	0.26 ± 0.02	0.27 ± 0.03
II	0.05 ± 0.01	0.05 ± 0.01	0.07 ± 0.01
III	0.03 ± 0.01	0.03 ± 0.00	0.05 ± 0.01
IV	0.02 ± 0.01	0.03 ± 0.00	0.03 ± 0.01
V	0.10 ± 0.02	0.06 ± 0.01	0.08 ± 0.01
VI	0.29 ± 0.03	0.29 ± 0.03	0.29 ± 0.05

7.3 Results of sequential extractions

7.3.1 Gedinnian samples

The Gedinnian samples derive from Hatrival in southern Belgium (see Chapter 3.1). In 1983, radiometric anomalies in rocks were detected in this region (CHARLET et al. 1983). Later studies found uraniferous mineralisations linked to fractures, which are filled with Fe oxyhydroxides (CHARLET et al. 1987, CHARLET et al. 1995). A detailed investigation by CHARLET et al. (1999) in a village 10 km south-west of Hatrival (Porcheresse) found very high indoor radon concentrations (> 4,000 Bq/m³) above hematite veins in the bedrock (St. Hubert Unit; Upper Gedinnian). These hematite veins have high uranium activities, but low thorium activities. CHARLET et al. (1999) analysed an iron ore sample from a stockpile and a sample from the surrounding rocks for U, Th, REE and trace elements by ICP-MS. The authors found high uranium activities in the hematite sample. Th is depleted in the hematite sample compared to the host rocks as well as Ba, Nb, La, Ce, Pr, Nd, Sr, Zr, Hf and La. It was concluded that uranium is concentrated in the iron phase, whereas Th and the REE are left in the extraction residual phase. Radium was not investigated.

In the present study, samples were taken from an old quarry near Hatrival. The samples belong to the Oignies Unit of the Upper Gedinnian. Most samples selected were fine-grained sandstones with their weathering products, but also siltstones, schists and quartzites were sampled. The rocks have been strongly deformed during the variscian orogenesis. Intense weathering during Permotriassic and Late Cenozoic to Early Tertiary times had lead to a precipitation of iron and manganese oxides/hydroxides in fractures, faults, on quartz veins and in weathered sandy rocks. The oxide accumulation for the quarry of Hatrival is not as extensive as it was described for Porcheresse, but the genesis of both is comparable to the genesis of the "*Hunsrückerze*" of the *Rheinisches Schiefergebirge* (FELIX-HENNINGSEN 1990 cum lit). The "*Hunsrückerze*" or "*Hunsrück iron-stones*" were developed under oxidising conditions in saprolites during phases of falling groundwater levels. The precipitation of oxides was restricted to the most permeable zones (e.g. joints, fractures and quartz veins), while adjacent domains of saprolite consisting of clay or silt slate were still saturated by ground water, leading to a continuation of reducing conditions. Diffusion of mobile elements therefore followed a redox and concentration gradient over a vertical distance of several meters. The "*Hunsrückerze*" consist in the deepest parts of the oxidation horizon of goethite, frequently accompanied by Mn concretions. Towards the upper zone of the saprolite, the content of hematite increases (FELIX-HENNINGSEN 2003).

The various rock types do not differ significantly in the activities of U, Ra and Th, except for the quartzites, which generally have lower activities for all radionuclides (Table

16). Most weathering products < 2 mm have elevated activities for all radionuclides, particularly for [226]Ra and [230]Th. Both radionuclides are in equilibrium, at least in samples with more than 120 Bq/kg of [230]Th. In samples with lower activity, a reliable determination of [230]Th by γ-spectrometry is not possible.

Table 16: Radionuclide distribution in the samples.

Sample	Description	[226]Ra [Bq/ kg]	[232]Th [Bq/ kg]	[238]U [Bq/ kg]	[210]Pb [Bq/ kg]	[230]Th [Bq/ kg]
Gedinnian						
133a	Quartzite	12.3	11.7	14.1	12.0	<
126	Quartz vein	9.1	20.3	18.9	11.3	<
124	Sandstone	64.6	34.5	67.1	82.7	<
135	Sandstone	34.8	35.3	32.2	27.5	<
136a	Sandstone	58.9	42.1	54.0	64.0	<
137	Sandstone	48.1	42.4	47.7	44.1	<
132a	Siltstone	53.1	42.5	52.4	61.3	<
131	Schist	76.5	143	74.2	65.3	<
127a	Weath. sandstone > 2 mm	26.4	45.2	23.8	27.9	<
127b	Weath. sandstone < 2 mm	69.5	54.7	92.8	82.5	<
132b	Weath. siltstone < 2 mm	718	110	362	403	709
134	Weath. sandstone < 2 mm	339	96	198	323	343
136b	Weath. sandstone < 2 mm	769	143	467	643	780
Siegenian 2						
77c	Schist	14.1	34.7	15.7	17.9	<
77a	Weath. schist < 2 mm	18.2	49.0	21.5	18.0	<
Buntsandstein						
98	Sandstone	23.0	41.0	20.2	20.1	<
102	Weath. sandstone < 2 mm	32.7	58.7	32.8	33.3	<

7.3.1.1 Gedinnian sand- and siltstones

Five samples of fine-grained sandstones (124, 127a, 135, 136a, 137) and one sandy siltstone (132a) from the quarry near Hatrival were selected for sequential extractions. The siltstone is similar in total activities of U, Ra and Th and distribution of radionuclides; the samples will therefore be discussed together.

The sand- and siltstones consist mainly of quartz, accompanied by muscovite, some feldspar and various amounts of ore mineral grains and heavy minerals (Table 17). Goethite and hematite are the most common ore mineral grains. Ilmenite, magnetite, and maghemite occur only in a few samples. Most common heavy minerals are rutile, zircon, anatase, chloritoid, ilmenorutile, monazite, pseudorutile, titanite and tourmaline (Table 17). Some thorium-bearing minerals were also detected by XRD, but their exact nature is uncertain.
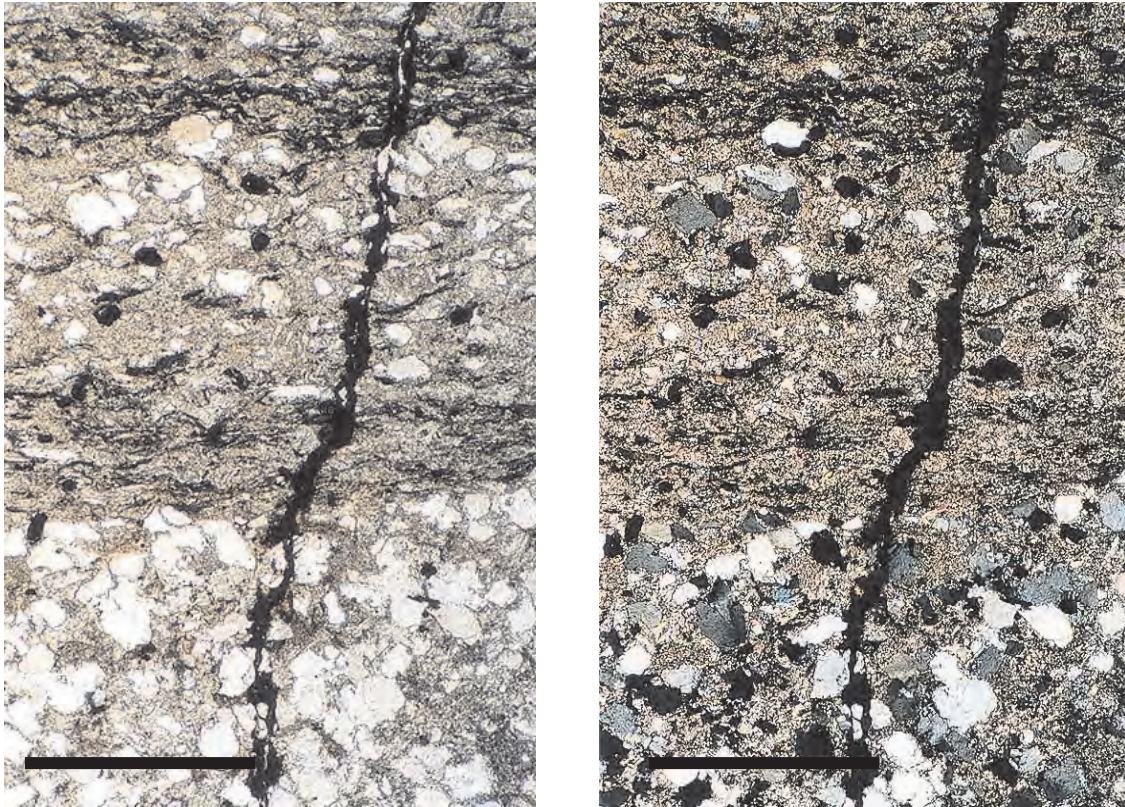
Figure 33: Silt- / clay intercalations in fine-grained Gedinnian sandstone (124). Mono- and polycrystalline quartz grains (mean ø 0.2 mm) are surrounded by an assemblage of clay minerals, goethite, hematite and authigenic quartz crystals. A distinction between detrital, replacement and pore-filling clay types is uncertain. The detrital quartz crystals of the fine-grained sandstone are partly corroded, have sutured contacts and show slightly undulose extinction. Opaque iron and manganese oxide/hydroxide precipitations (see text) can be found along bedding joints in the more clayey zones and fill the fracture transecting the sandstone. (Right figure: cross-polarised light; length of scale bar is 1 mm).

The cement, or matrix, of the rocks contains detrital and authigenic clay minerals (mica-, kaolinite- and smectite-group), chlorites (mainly chamosite and clinochlore), mica (muscovite and paragonite), quartz and Fe oxides/hydroxides such as hematite (Fe_2O_3) and goethite ($FeO(OH)$). The latter is generally more abundant. Oxides and hydroxides of manganese were also detected by XRD, but discrimination between specific minerals was not possible, therefore the general term Mn oxides/hydroxides will be used throughout the text.

Heavy minerals such as chloritoid and staurolite give evidence for rocks of metamorphic origin, at least of greenschist facies (Table 17). This assumption is underlined by the occurrence of muscovite (Figure 33; Figure 38) and of quartz with undulose extinction (Figure 33; Figure 38). Magmatic source rocks are indicated by heavy minerals such as zircon and monazite (Table 17), which, however, could also have been inherited from earlier sedimentary cycles.

Table 17: Heavy mineral composition of Gedinnian rock samples (x = abundant; x = less abundant; ? = uncertain; — = does not occur)

Sample		Anatase	Brookite	Chloritoid	Ilmenite	Ilmenorutile	Maghemite	Magnetite	Monazite	Pseudorutile	Rutile	Staurolite	Titanite	Tourmaline	Xenotime	Zircon
133a	Quartzite	x	—	x	?	x	—	—	x	?	x	?	?	x	x	x
124	Sandstone	x	x	x	—	x	—	x	x	x	x	?	x	x	?	x
135	Sandstone	?	—	x	x	x	?	?	x	x	x	—	x	x	—	x
136a	Sandstone	x	x	x	—	x	x	x	x	x	x	x	x	x	x	x
132a	Siltstone	x	x	x	?	x	—	—	—	?	x	—	x	?	x	x
127a	Weath. sandstone > 2 mm	?	x	?	—	x	x	x	x	x	x	—	x	x	x	x

An overview of the mineralogy and geochemistry of each sample will be given and the distribution of the radionuclides in the rocks will be discussed.

7.3.1.1.1 Quartzitic sandstones

Sample 124 is grey quartzitic sandstone with > 80% SiO_2. Joints and fissures in the rock are coated with goethite, hematite, and Mn oxides/hydroxides. The concentrations of Al, Na, K, Ba, V, Y and Th in the rock itself are relatively low, indicating low proportions of other terrigenous components such as feldspars, mica and clay minerals. The XRD analysis of the light minerals confirms this assumption, since only negligible amounts of feldspars occur and only a small amount of clinochlore. The latter occurs more frequently in the heavy mineral fraction, but in lower proportions compared to the other Gedinnian samples.

The sandstone is well sorted and no mica crystals occur between the quartz grains, except for the fine-grained intercalation in the top, which is not typical for this series (Figure 34). The iron content of this sandstone is, at 4.9% Fe_2O_3, in about the same range as for the other sand- and siltstones (Table 18). If not finely dispersed in inter-granular spaces, it is concentrated in heavy minerals and ore mineral grains. The heavy minerals in this sandstone are mainly ilmenorutile and rutile, other iron-bearing heavy minerals such as pseudorutile and magnetite occur as well. The latter is seldom found in the samples collected. It can therefore be deduced that iron is more concentrated in ore mineral grains than in coatings of goethite and hematite, as only few fractures transect the rock. The occurrence of goethite and hematite in the extraction residual is due to incomplete dissolution of ore mineral grains during sequential extraction, which might happen if they are too coarse.

Figure 34: Well sorted fine-grained quartzitic sandstone of Gedinnian age of sample 124 with silt- / clay intercalations in the upper part. Mean grain size of quartz is approx. 0.2 mm. Compared to the other sandstones, a relatively high percentage (about 3%) of fine grained (50-80 μ) transparent and opaque heavy minerals such as hematite, rutile, ilmenorutile, titanite occur. The heavy minerals were detected by X-ray diffraction. Length of scale bar is 1 mm.

U and Ra in sample 124 are in equilibrium (about 66 Bq/kg), whereas Th has half the activity (35 Bq/kg).

The bondings of the radionuclides differ. Thorium is dissolved at 42.3% (Figure 35). Most thorium is bound in the fraction of amorphous Fe oxides, followed by the fraction of crystalline Fe oxides (Table 18). Less than 0.1% is bound in the fractions I – III.

Table 18: Analytical results of sample 124[9].

124	original sample	SD	I mobile exchangeable	SD	II exchangeable	SD	III Mn-Oxides	SD	IV organic matter	SD	V amorphous Fe oxides	SD	VI crystalline Fe oxides	SD	residual***
Al [ppm]	38370	*	4	1	23	0.2	33	1	193	2	1395	25	2666	106.6	34060
Mg [ppm]	8850	*	121	1	43	2	36	3	47	1	393	6	1015	18.19	7196
Fe [ppm]	34390	*	2	0.3	4	0.2	90	1	393	29	3460	59	13189	23.9	17250
Zn [ppm]	166	**	0.5	0.1	1.4	0.1	7.3	2.3	NA²		24.2	0.5	74.5	2.0	< 58
Ba [ppm]	180	**	8.4	0.9	1.2	0.01	1.6	0.1	0.5	0.2	2.4	0.1	1.8	0.03	164
Mn [ppm]	389	*	40.7	1.7	22.3	0.3	46.5	0.3	27.0	2.5	69.8	2.6	41.7	1.3	141
Pb [ppm]	49	**	< 0.1		2.4	0.03	4.2	0.04	3.3	0.02	6.4	0.1	19.3	0.2	13
As [ppm]	71	*	< 0.1		0.1	0.004	0.2	0.01	1.0	0.03	14.6	0.2	52.8	0.4	< 4
Ti [ppm]	3340	**	0.1	0.01	0.1	0.01	0.2	0.01	0.6	0.04	4.6	0.1	6.9	0.1	3327
Ni [ppm]	100	**	1.5	0.02	1.0	0.01	2.2	0.2	3.1	0.1	16.0	0.3	40.6	0.7	36
V [ppm]	50	**	<		< 0.1		0.3	0.01	0.3	0.01	2.2	0.03	6.5	0.1	41
Cu [ppm]	81	**	0.2	0.01	1.1	0.02	1.6	0.1	2.0	0.1	13.9	0.2	49.3	0.3	13
Rb [ppm]	36	**	0.6	0.002	0.1	0.03	0.1	0.01	< 0.1		0.2	0.003	0.2	0.01	35
Sr [ppm]	32	**	2.0	0.02	1.0	0.1	1.0	0.1	0.9	0.1	0.7	0.01	0.8	0.01	26
Y [ppm]	24	**	< 0.1		0.5	0.01	0.2	0.001	0.2	0.01	1.5	0.02	1.8	0.01	20
Zr [ppm]	407	**	< 0.1		0.1	0.02	0.1	0.02	0.3	0.01	4.0	0.03	7.2	0.05	395
Cs [ppm]	4	**	0.04	0.001	< 0.01		0.01	0.001	< 0.01	0.001	0.03	0.001	0.04	0.001	4
La [ppm]	40	**	0.10	0.001	0.25	0.004	0.09	0.001	0.11	0.003	1.32	0.07	1.55	0.02	37
Ce [ppm]	93		0.13	0.001	0.63	0.01	0.26	0.002	0.34	0.01	3.72	0.20	4.06	0.05	84
Dy [ppm]	NA¹		< 0.01		0.10	0.001	0.04	0.001	0.06	0.002	0.50	0.02	0.56	0.01	ND
Er [ppm]	NA¹		< 0.01		0.04	0.001	0.02	0.001	0.03	0.001	0.22	0.01	0.27	0.003	ND
Yb [ppm]	NA¹		< 0.01		0.03	0.001	0.01	0.001	0.02	0.001	0.20	0.003	0.22	0.004	ND
Hf [ppm]	NA¹		NA		< 0.01		< 0.01		< 0.01		0.17	0.003	0.29	0.01	ND
Th [Bq/kg]	34.5		< 0.1		0.2	0.0	0.1	0.0	1.4	0.0	8.6	0.1	4.3	0.1	20
U [Bq/kg]	67.1		< 0.1		5.6	0.1	2.3	0.0	1.4	0.1	15.4	0.3	19.3	0.2	23
Ra [Bq/kg]	64.6		4.2	0.7	< 1.5		< 1.5		< 0.8		< 5.0		< 1.1		60

* standard deviation (SD) < 5 %; ** standard deviation (SD) < 10 %; *** standard deviation (SD) < 20 %
NA¹: element was not analysed; NA²: no calibration curve was obtained; ND = not detectable
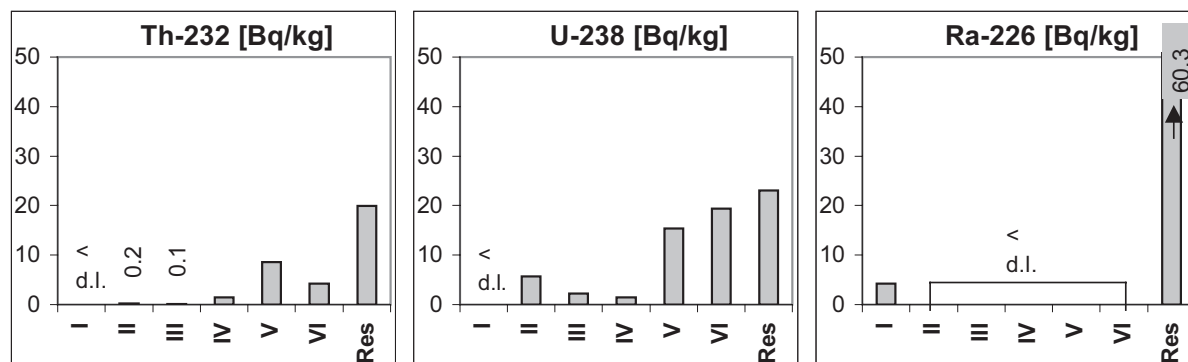
Figure 35: Radionuclide activities among extraction phases of sample 124 (Gedinnian quartzitic sandstone) (I = *mobile exchangeable*, II = *exchangeable*, III = *Mn oxides*, IV = *organic matter*, V = *amorphous Fe oxides*, VI = *crystalline Fe oxides*, Res = *extraction residual*)

Most uranium is found in both Fe oxide fractions, too. In contrast to thorium, about the same concentrations occur in the amorphous Fe oxide fraction and the crystalline Fe oxide fraction (Figure 35; Table 18).

---

[9] Element concentrations of total samples were measured by XRF and element concentrations of eluates of the sequential extraction fractures by ICP-MS/ICP-OES. Radionuclides were measured by γ-spectrometry (total samples), ICP-MS (U, Th in eluates) and LSC (Ra in eluates). Residuals were estimated by subtracting element concentrations/activities of eluates from total element concentrations / activities.

The proportion of uranium in fraction II, in which mainly specifically adsorbed and superficially occluded elements have been dissolved, is evidently higher than for thorium.

As no carbonate occurs in the sample, the possible bonding to carbonates in this extraction step could be neglected, as could the concurrently dissolved weakly bound metal-organic complexes, since C_{org} of the sample is less than 1% (Appendix 3; Table A3). Radionuclides occuring in the organic fraction are rather attributed to clay minerals and less stable silicates, which are dissolved in this fraction, too.

Relatively low concentrations of uranium - and especially thorium - were found in the Mn oxide fraction that matches with only a few Mn oxides in this sample. The lack of carbonates, a low content of C_{org} (< 1%) and few Mn oxides are actually typical for all Gedinnian sand- and siltstones. Due to the low content of C_{org}, the proportions of uranium and thorium found in the organic fraction (IV) are expected to be low as well. Indeed, U and Th occur with only 1.4 Bq/kg each in this fraction (Table 18).

Distribution of radium is completely unlike that of uranium and thorium. Radium is found only in the mobile exchangeable fraction (Table 18; Figure 35). For all other fractions, the radium concentration is below the detection limit. They are usually lower than 1.5 Bq/kg, except for the amorphous Fe oxide fraction (V), which has a very high detection limit of 5 Bq/kg. As the detection limit is higher than the activity measured in the mobile exchangeable fraction, this result will not be discussed further.

Table 19: Activity ratios ^{226}Ra/^{238}U in the fractions of the sequential extraction for the analysed Gedinnian sand- and siltstones (d. l. = detection limit).

^{226}Ra/^{238}U	Quartzitic sandstones		Sandstones			Siltstone
	124	135	137	136a	127a	132a
Total sample	1.0	1.1	1.0	1.1	1.1	1.0
Mobile exchangeable	U, Ra < d. l.	> 1	> 1	> 1	U, Ra < d. l.	> 1
Exchangeable	< 1	1.7	1.1	0.9	17.2	< 1
Mn oxides	< 1	6.1	2.4	1.6	30.4	Ra < d. l.
Organic	< 1	3.0	3.0	7.3	10.7	Ra < d. l.
Amorphous Fe oxides	< 1	1.7	< 1	< 1	Ra < d. l.	Ra < d. l.
Crystalline Fe oxides	< 1	0.5	0.5	1.2	1.3	< 1
Extraction residual	2.6	0.9	1.0	1.0	0.8	1.7

Nevertheless, it is remarkable that the distribution of radium differs from the distribution of uranium so strongly, though they are in equilibrium in the total sample (activity ratio (AR) ^{226}Ra/^{238}U: 1.0). Radium is, on the one hand, more soluble, as it occurs in the mobile exchangeable phase, in which unspecifically adsorbed elements are dissolved, while the uranium activity was not detectable in this fraction (Table 18). On the other hand, the AR ^{226}Ra/^{238}U of the extraction residual is 2.6, confirming a much higher concentration of radium in the extraction residual, which consists mainly of quartz, muscovite, clay minerals, chlorites

and heavy minerals. The heavy minerals that are dominant in the original rock sample are also dominant in the extraction residual (Table 20). The most abundant heavy minerals are ilmenorutile, rutile, titanite and zircon.

Table 20: Mineral groups of extraction residuals of selected samples (x = abundant; ? = uncertain; — = does not occur)

Sample	Quartz	Chamosite	Clinochlore	Kaolinite Group	Smectite Group	Illite	Mica Group	Plagioclase	Alkali feldspar Group	Anatase	Brookite	Chloritoid	Ilmenite	Ilmenorutile	Maghemite	Magnetite	Monazite	Pseudorutile	Rutile	Staurolite	Titanite	Tourmaline	Xenotime	Zircon
133a	x	x	x	x	x	x	x	x	x	?	?	x	—	—	—	—	x	—	—	?	—	x	x	x
124	x	x	x	x	x	x	x	x	x	x	?	x	x	x	—	?	x	—	x	x	x	x	—	x
135	x	x	x	x	x	x	x	x	x	x	—	x	—	—	—	?	x	x	x	—	x	x	—	x
132a	x	x	x	x	x	x	x	x	x	x	x	x	—	x	—	—	x	—	x	—	x	x	?	x
134	x	x	x	x	x	x	x	x	x	x	x	x	—	—	?	x	x	—	—	?	x	x	x	x
136a	x	x	x	x	x	x	x	x	x	x	x	x	—	?	—	x	x	—	x	?	x	x	?	x

Sample 135 is grey quartzitic sandstone (> 80% SiO_2) with coatings of goethite, hematite and Mn oxides/hydroxides (Figure 36). In-situ fragmentation of quartz grains, visible in the investigated sample, is characteristic for ferralitic soils and points to a descendent origin of the Fe-mineralisation (FELIX-HENNINGSEN 1990). Although the concentrations of Al, Na, K, Ti, Ba, V, Y and Th are as low as for the sandstone 124, much more mica (muscovite, paragonite), chlorite (chamosite, clinochlore, mixed layer chlorite) and clay minerals (smectite, kaolinite, halloysite and illite) were identified by XRD. The XRD analysis of the light minerals showed considerably higher proportions of feldspars compared to sample 124, plagioclase exceeding alkali feldspars.

The dominant heavy minerals are zircon, titanite, rutile, ilmenorutile, pseudorutile and tourmaline (Table 17). Although about 78% of total iron is left in the extraction residual, XRD analysis does not show any goethite or hematite. Uranium, radium and thorium occur in equal activities of about 35 Bq/kg.

The distribution of the radionuclides among the extraction phases is presented in Figure 37. The highest quantities of uranium and thorium were found in the extraction residual (65% of total sample) and bound to Fe oxides (30% of total sample). Whereas thorium dominates in the amorphous Fe oxide phase, uranium is slightly higher in the crystalline Fe oxide phase.

Radium occurs at 70% in the extraction residual (Figure 37). The activities in all other fractions are distributed relatively equally. The highest activities occur in the crystalline

fraction, the lowest in the organic fraction. Radium activity in the amorphous Fe oxide phase is below the detection limit of 5 Bq/kg and is not discussed.

Unless uranium and radium are in equilibrium (AR ^{226}Ra/^{238}U = 1.1; Table 19), their distribution in the sandstone appears to be different. The ARs of ^{226}Ra/^{238}U are higher than unity in the fractions I – V, but lower than unity in the crystalline Fe oxide fraction and the extraction residual (Table 19). This confirms that radium is more soluble than uranium in this sandstone. While the latter has to be attributed to the crystalline phase of the sandstone (well crystallised Fe oxides + extraction residual), radium is adsorbed on grain surfaces to a greater extent.
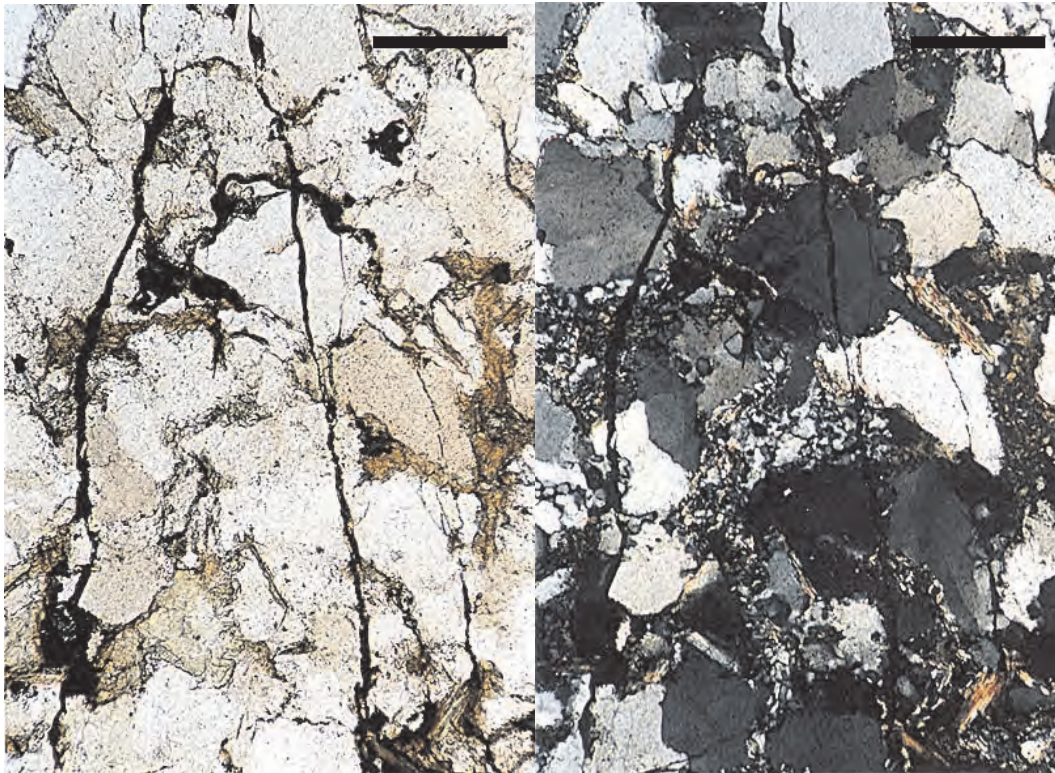
Figure 36: Strongly corroded and recrystallised mono- and polycrystalline quartz of fine-grained sandstone (135; Gedinnian). Fractures transect the sandstone, cutting the quartz grains and continuing from one grain to the next. The fractures are lined with iron and manganese oxides/hydroxides (see text). The quartz crystals show sutured contacts and undulose extinction. They are partly coated with clay films. The occurrence of clay minerals as oriented coatings indicates authigenic growth as a pore filling cement. Besides clay minerals, the cement consists of chlorite, muscovite, authigenic quartz crystals, goethite and hematite. (Right: crossed polarisers; length of scale bar is 200 μm)

The higher activities of radium in the exchangeable fractions (I + II) may be due to the differences in the atom radii of uranium and radium. Radium bondings are only metastable in uranium- bearing minerals, as the radium atom is much larger relative to the parent uranium atom. Radium may be lost from the mineral lattice of the host mineral by diffusion through

water layers adhered to grain surfaces. Radium in rocks is specifically concentrated in microfractures and along grain boundaries (MOLINARI & SNODGRASS 1990).
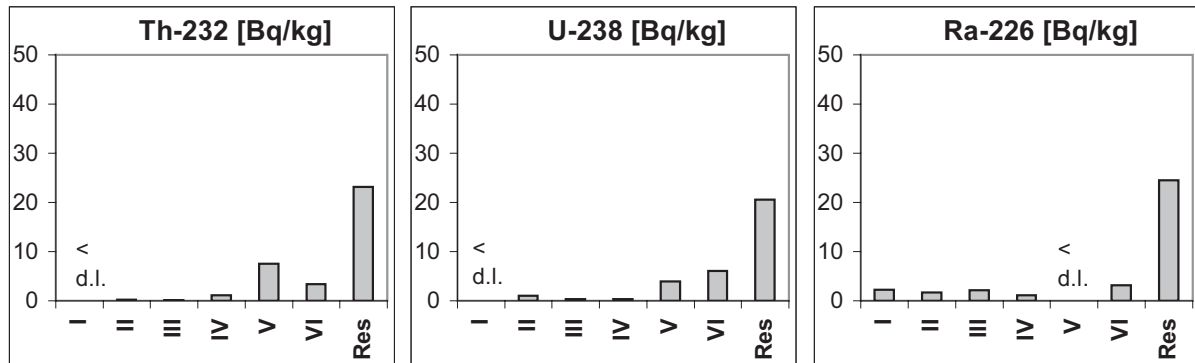
Figure 37: Radionuclide activities among extraction phases of sample 135 (Gedinnian quartzitic sandstone) (I = *mobile exchangeable*, II = *exchangeable*, III = *Mn oxides*, IV = *organic matter*, V = *amorphous Fe oxides*, VI = *crystalline Fe oxides, Res = extraction residual*)

Table 21: Analytical results of sample 135. For analytical methods see Table 18.

135	original sample		I mobile exchangeable		II exchangeable		III Mn-Oxides		IV organic matter		V amorphous Fe oxides		VI crystalline Fe oxides		residual***
		SD		SD		SD		SD		SD		SD		SD	
Al [ppm]	46102	*	5	1	46	1	55	1	181	1	1464	14	3071	20	41281
Mg [ppm]	9835	*	89	1	50	4	44	0.2	57	0.3	447	4	1389	10	7759
Fe [ppm]	30201	*	6	0.3	17	3	141	2	344	8	< 1		6000	67	23692
Zn [ppm]	83	**	< 0.1		1.4	0.2	3.1	0.4	2.0	0.1	9.5	0.1	21.0	0.4	46
Ba [ppm]	181	**	7.9	0.1	2.1	0.1	3.6	0.1	0.7	0.05	2.3	0.04	0.7	0.03	164
Mn [ppm]	525	*	13.9	0.2	33.0	1.6	65.7	0.6	19.7	0.1	61.4	0.4	46.4	0.4	285
Pb [ppm]	11	**	< 0.1		0.4	0.1	1.4	0.05	0.5	0.00	1.4	0.03	2.6	0.1	4
As [ppm]	18	*	< 0.1		0.1	0.01	0.1	0.02	0.4	0.01	5.2	0.1	8.7	0.1	4
Ti [ppm]	2943	**	0.1	0.00	0.1	0.01	0.3	0.003	0.7	0.01	<		4.8	0.1	2937
Ni [ppm]	60	**	0.4	0.01	0.9	0.1	1.4	0.03	1.2	0.002	7.5	0.05	11.1	0.02	38
V [ppm]	47	**	< 0.1		< 0.1		< 0.1		0.1	0.002	1.6	0.01	2.8	0.05	42
Cu [ppm]	9	**	0.1	0.01	0.6	0.1	0.8	0.04	0.7	0.003	3.2	0.03	NA²		< 4
Rb [ppm]	37	**	1.0	0.01	0.1	0.003	0.1	0.002	0.1	0.001	0.3	0.001	0.3	0.003	35
Sr [ppm]	55	**	3.2	0.1	1.1	0.1	1.1	0.02	1.0	0.003	1.0	0.002	0.7	0.01	47
Y [ppm]	25	**	0.2	0.004	0.4	0.02	0.1	0.002	0.2	0.001	0.8	0.003	0.9	0.01	22
Zr [ppm]	357	**	NA		< 0.1		0.2	0.002	0.5	0.01	3.3	0.04	NA²		< 353
Cs [ppm]	7	**	0.41	0.003	0.01	0.001	0.03	0.001	< 0.01		0.04	0.001	0.06	0.002	6
La [ppm]	36	**	0.14	0.003	0.13	0.01	0.05	0.001	0.07	0.001	0.55	0.004	0.79	0.01	34
Ce [ppm]	69		0.17	0.002	0.35	0.02	0.16	0.004	0.19	0.001	1.38	0.01	1.90	0.01	65
Dy [ppm]	NA¹		0.02	0.001	0.08	0.003	0.03	0.001	0.04	0.001	0.25	0.003	0.21	0.01	ND
Er [ppm]	NA¹		0.01	0.001	0.04	0.001	0.01	0.001	0.02	0.001	0.12	0.002	0.10	0.01	ND
Yb [ppm]	NA¹		< 0.01		0.03	0.001	0.01	0.001	0.02	0.001	0.12	0.001	0.09	0.001	ND
Hf [ppm]	NA¹		< 0.01		< 0.01		0.01	0.002	0.02	0.001	0.18	0.005	0.01	0.003	ND
Th [Bq/kg]	35.3		< 0.1		0.2	0.1	0.1	0.01	1.1	0.03	7.5	0.04	3.3	0.005	23
U [Bq/kg]	32.2		< 0.1		1.0	0.04	0.3	0.01	0.4	0.003	3.9	0.05	6.0	0.03	21
Ra [Bq/kg]	34.8		2.3	0.2	1.7	0.2	2.1	0.3	1.1	0.2	< 5.0		3.1	0.4	24

* standard deviation (SD) < 5 %; ** standard deviation (SD) < 10 %; *** standard deviation (SD) < 20 %
NA¹: element was not analysed; NA²: no calibration curve was obtained; ND = not detectable

Summarising the results from the first two quartzitic sandstone samples, thorium and uranium distribution in the rocks is about equal. Only small activities occur in the first four fractions, while 30 – 50% of total thorium and uranium is bound in the fractions of the Fe oxides.

Radium distribution appears to be different, not only in contrast to the other radionuclides, but also between the two sandstone samples. Radium occurs in high proportions in the mobile exchangeable fraction for both samples. The sample with the

higher content of terrigenous minerals (135), offering more adsorption places, also contains high proportions of radium in the easily soluble fractions II - V. The occurrence of 9% of total radium in the well crystallised Fe oxide fraction in sample 135, in contrast to activities below the detection limit in sample 124, are due to the differences in mineralogy, too. While sample 124 is a dense rock, consisting mainly of quartz minerals in quartz cement, the matrix of sample 135 contains much more iron oxide and the rock is transected by innumerable fractures lined with Fe oxides.

The highest activities are nevertheless found in the extraction residual, confirming that radium, if not adsorbed, has to be attributed to insoluble silicates and heavy minerals.

7.3.1.1.2 Fine-grained sandstones

At 63%, SiO_2 in **sample 136a** is less abundant than in the quartzitic sandstones. Considerably more Al_2O_3 (19%) occurs, together with some other typical terrigenous elements such as Na, K, Ti, Ba, Rb, Sr and V (Table 22). As for sample 124, the activities of U and Ra are elevated (up to 59 Bq/kg), while the activity of Th is low (42 Bq/kg).

A thin section of the sample is shown in Figure 38. The quartz grains and detrital muscovite crystals are floating in the cement/matrix of clay minerals, chlorites, mica, goethite, hematite, and Mn oxides/hydroxides. XRD analysis reveals high proportions of muscovite, chamosite, clinochlore, kaolinite, anatase, rutile, ilmenorutile, pseudorutile and titanite (Table 17). Goethite, hematite and Mn oxides/hydroxides are primarily precipitated along bedding joints and fill fractures transecting the rock. As in sample 135, the fractures are cutting quartz grains. Only few opaque mineral grains are apparent.
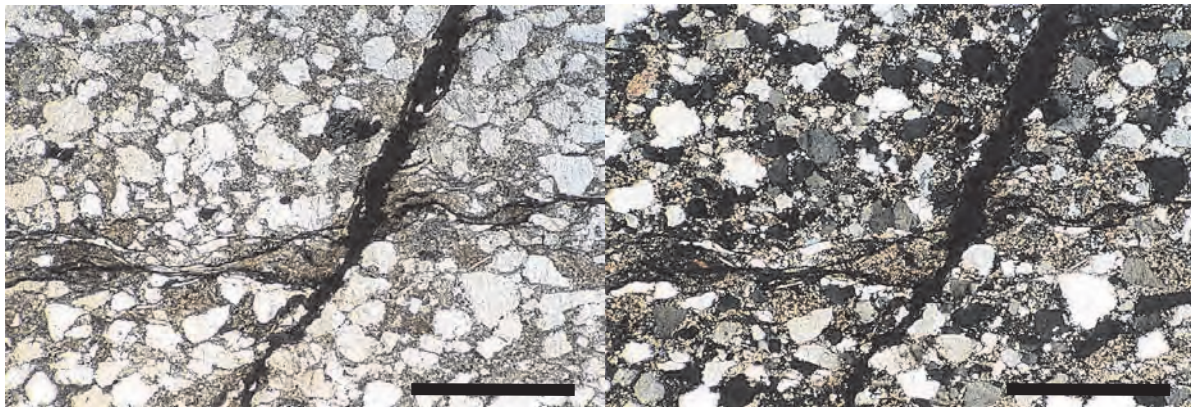
Figure 38: Gedinnian fine-grained sandstone (136a). Mono- and polycrystalline quartz crystals (mean ø 0.25 mm) and oriented muscovite crystals floating in a cement/matrix of authigenic quartz, clay minerals, chlorite, mica, goethite and hematite. The subrounded quartz grains are moderately sorted. Oriented muscovite crystals at the subhorizontal bedding joint served as a barrier for circulation of solutions, from which iron and manganese oxides/hydroxides were precipitated. Oxides and hydroxides of manganese and iron line the transecting fracture as well. In the upper left part some opaque mineral grains occur. (Right figure: crossed polarisers; length of scale bar is 1 mm)

The distribution of uranium is equivalent to that seen in sample 135, except that more uranium occurs in the exchangeable fraction (Figure 37, Figure 39). This is due to higher proportions of mica and clay minerals in the sample.

Thorium activities are again highest in the extraction residual and of secondary importance in the Fe oxide fractions. In contrast to samples 124 and 135, thorium activities in the crystalline Fe oxide fraction are higher than in the amorphous Fe oxide fraction (Figure 39).

Table 22: Analytical results of sample 136a. For analytical methods see Table 18.

136a	original sample		I mobile exchangeable		II exchangeable		III Mn-Oxides		IV organic matter		V amorphous Fe oxides		VI crystalline Fe oxides		residual***
		SD		SD		SD		SD		SD		SD		SD	
Al [ppm]	102700	*	8	2	91	16	44	6	147	49	1056	54	2236	357	99120
Mg [ppm]	7753	*	65	5	40	6	19	3	20	2	226	24	448	39	6936
Fe [ppm]	30020	*	4	1	47	10	58	8	145	11	2535	191	7808	1389	19420
Zn [ppm]	84	**	0.3	0.1	1.6	0.5	1.1	0.3	0.4	0.1	8.5	0.7	30.3	6.7	42
Ba [ppm]	524	**	7.3	0.1	1.6	0.2	2.2	0.1	0.3	0.1	3.2	0.6	2.7	0.5	507
Mn [ppm]	348	*	33.3	1.4	19.6	2.8	28.3	2.4	8.3	1.2	32.8	1.8	51.8	12.5	174
Pb [ppm]	29	**	< 0.1		3.2	0.4	2.4	0.2	1.0	0.2	3.1	0.2	7.5	0.3	12
As [ppm]	25	*	0.1	0.01	0.2	0.03	0.1	0.02	0.3	0.05	5.9	0.4	17.7	4.3	< 4
Ti [ppm]	4170	**	0.3	0.1	< 0.1		0.4	0.1	0.5	0.1	4.7	0.1	5.0	0.8	4159
Ni [ppm]	70	**	0.8	0.04	0.8	0.1	0.4	0.1	0.5	0.1	5.6	0.3	17.1	3.1	45
V [ppm]	114	**	< 0.1		0.1	0.01	0.3	0.03	0.1	0.01	1.8	0.1	4.4	0.8	107
Cu [ppm]	24	**	0.6	0.2	1.0	0.01	0.7	0.05	0.7	0.2	4.9	0.5	16.1	1.6	< 4
Rb [ppm]	114	**	1.2	0.02	0.2	0.02	0.3	0.01	< 0.1		0.4	0.1	0.5	0.1	112
Sr [ppm]	202	**	3.4	0.2	0.9	0.2	1.3	0.04	0.5	0.1	1.3	0.1	1.1	0.2	193
Y [ppm]	42	**	0.2	0.02	0.5	0.1	0.3	0.00	0.1	0.01	0.7	0.1	1.3	0.2	39
Zr [ppm]	322	**	< 0.1		0.1	0.01	0.2	0.03	0.5	0.03	< 0.1		NA²		< 321
Cs [ppm]	13	**	0.37	0.004	0.04	0.01	0.07	0.002	NA²		0.05	0.01	0.09	0.03	< 12
La [ppm]	41	**	0.16	0.01	0.16	0.04	0.10	0.004	0.03	0.002	0.45	0.01	0.69	0.10	39
Ce [ppm]	71		0.21	0.01	0.36	0.05	0.23	0.005	0.08	0.01	1.34	0.04	1.54	0.20	68
Dy [ppm]	NA¹		0.02	0.002	0.12	0.02	0.05	0.001	0.02	0.003	0.18	0.01	0.31	0.05	ND
Er [ppm]	NA¹		0.01	0.001	0.06	0.01	0.03	0.001	0.01	0.001	0.09	0.01	0.16	0.03	ND
Yb [ppm]	NA¹		< 0.01		0.05	0.01	0.02	0.001	< 0.01		0.08	0.01	0.15	0.02	ND
Hf [ppm]	NA¹		< 0.01		0.03	0.01	0.02	0.003	< 0.01		< 0.01		0.32	0.04	ND
Th [Bq/kg]	42.1		< 0.1		0.4	0.1	0.1	0.0	0.6	0.2	6.1	0.4	7.0	1.3	28
U [Bq/kg]	54.0		0.1	0.0	2.6	0.5	1.2	0.0	0.2	0.0	5.1	0.6	9.0	0.5	36
Ra [Bq/kg]	58.9		7.0	0.6	2.4	0.4	2.0	0.2	1.8	0.3	< 5.0		10.8	1.1	35

* standard deviation (SD) < 5 %; ** standard deviation (SD) < 10 %; *** standard deviation (SD) < 20 %

NA¹: element was not analysed; NA²: no calibration curve was obtained; ND = not detectable

Figure 39: Radionuclide activities among extraction phases of sample 136a (Gedinnian sandstone) (I = *mobile exchangeable*, II = *exchangeable*, III = *Mn oxides*, IV = *organic matter*, V = *amorphous Fe oxides*, VI = *crystalline Fe oxides, Res = extraction residual*)

The distribution of radium is again somewhat different, but the general trend is confirmed. Apart from highest activities in the extraction residual, high proportions of radium

occurs in the crystalline Fe oxide phase and in the mobile exchangeable phase (Figure 39). The detection limit of 5 Bq/kg for the amorphous Fe oxide fraction does not allow any prediction for this extraction phase.

   Sample 137 is also fine-grained sandstone, the grains of which are covered with coatings of goethite, hematite, and Mn oxides/hydroxides. Geochemical data do not show significant differences to sample 136a. Lower concentrations of terrigenous elements such as Na, Ba, Rb and Sr point to less clay minerals, but the overall mineral composition does not differ. Uranium, radium, and thorium occur in equal activities of about 45 Bq/kg (Table 23).
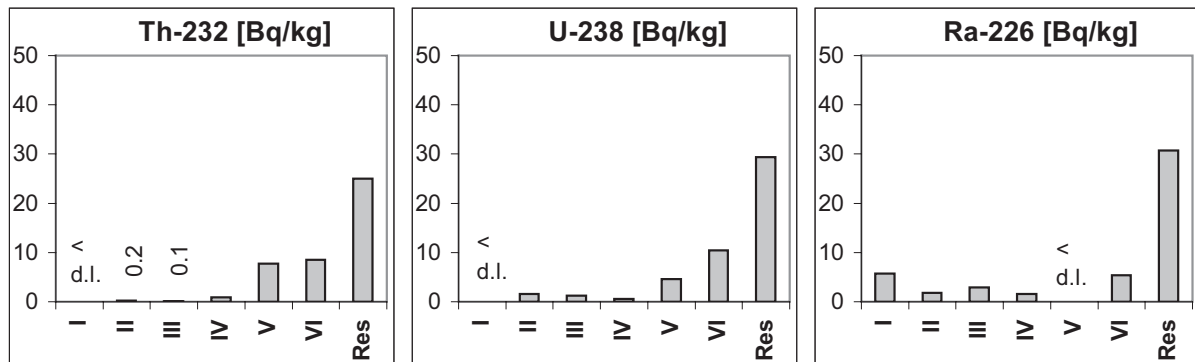
Figure 40: Radionuclide activities among extraction phases of sample 137 (Gedinnian sandstone) (I = *mobile exchangeable***, II =** *exchangeable***, III =** *Mn oxides***, IV =** *organic matter***, V = amorphous Fe oxides***, **VI =** *crystalline Fe oxides***, Res =** *extraction residual***)**

Table 23: Analytical results of sample 137. For analytical methods see Table 18.

137	original sample	SD*	I mobile exchangeable	SD	II exchangeable	SD	III Mn-Oxides	SD	IV organic matter	SD	V amorphous Fe oxides	SD	VI crystalline Fe oxides	SD	residual***
Al [ppm]	88030	*	3	0.1	< 1		NA³		157	2	1343	3	3021	8	< 83510
Mg [ppm]	8264	*	70	0.1	29	0.2	NA³		39	0.4	271	0.4	1041	11	< 6814
Fe [ppm]	32360	*	3	0.3	8	0.2	NA³		148	2	2203	14	7309	32	< 22690
Zn [ppm]	82	**	0.2	0.03	< 0.1		NA³		2.0	0.04	7.3	0.1	28.9	0.3	< 44
Ba [ppm]	442	**	7.8	0.02	2.0	0.2	NA³		0.7	0.01	2.7	0.004	1.3	0.01	< 428
Mn [ppm]	380	*	23.6	0.02	15.6	0.1	NA³		6.1	0.03	30.2	0.1	43.6	0.6	< 261
Pb [ppm]	17	**	< 0.1		1.1	0.01	NA³		0.7	0.005	2.1	0.001	5.0	0.04	< 8
As [ppm]	18	**	0.1	0.001	0.1	0.005	NA³		0.2	0.01	4.4	0.03	11.2	0.01	< 4
Ti [ppm]	4325	*	0.1	0.002	< 0.1		NA³		0.6	0.04	3.7	0.1	5.2	0.1	< 4316
Ni [ppm]	50	**	0.5	0.002	0.3	0.01	NA³		0.4	0.01	4.3	0.01	13.7	0.1	< 31
V [ppm]	88	**	< 0.1		< 0.1		NA³		< 0.1		1.5	0.01	3.7	0.03	83
Cu [ppm]	14	**	0.1	0.002	0.4	0.04	NA³		0.6	0.01	3.6	0.001	NA²		< 9
Rb [ppm]	92	**	0.9	0.002	0.1	0.001	NA³		0.1	0.001	0.3	0.001	0.4	0.005	< 90
Sr [ppm]	135	**	2.9	0.005	1.0	0.04	NA³		1.0	0.01	1.2	0.002	0.8	0.01	< 128
Y [ppm]	34	**	0.2	0.002	0.4	0.001	NA³		0.2	0.001	0.7	0.003	1.0	0.01	< 32
Zr [ppm]	300	**	NA²		NA²		NA³		0.7	0.01	4.5	0.02	NA²		< 295
Cs [ppm]	16	**	0.31	0.001	0.03	0.001	NA³		0.02	0.001	0.05	0.001	0.12	0.001	< 16
La [ppm]	39	**	0.15	0.001	0.10	0.001	NA³		0.07	0.001	0.56	0.004	0.64	0.001	< 37
Ce [ppm]	71	**	0.17	0.001	0.20	0.003	NA³		0.12	0.001	1.06	0.01	1.45	0.02	< 68
Dy [ppm]	NA¹		0.03	0.001	0.07	0.001	NA³		0.03	0.001	0.23	0.002	0.24	0.003	ND
Er [ppm]	NA¹		0.01	0.001	0.04	0.001	NA³		0.02	0.001	0.12	0.004	0.12	0.002	ND
Yb [ppm]	NA¹		< 0.01		0.03	0.001	NA³		0.02	0.001	0.12	0.003	0.12	0.003	ND
Hf [ppm]	NA¹		< 0.01		0.01	0.003	NA³		0.04	0.001	0.26	0.001	0.20	0.01	ND
Th [Bq/kg]	42.4		< 0.1		0.2	0.01	0.1	0.01	0.9	0.04	7.7	0.02	8.5	0.1	25
U [Bq/kg]	47.7		< 0.1		1.5	0.01	1.2	0.03	0.5	0.01	4.6	0.02	10.4	0.02	29
Ra [Bq/kg]	48.1		5.7	0.8	1.7	0.2	3.0	0.4	1.6	0.2	< 5.0		5.4	0.5	31

* standard deviation (SD) < 5 %; ** standard deviation (SD) < 10 %; *** standard deviation (SD) < 20 %
NA¹: element was not analysed; NA²: no calibration curve was obtained; NA³: loss of sample; ND = not detectable

Though the activities of uranium and radium are lower for sample 137, the distribution of all three radionuclides is equivalent to those described for sample 136a.

7.3.1.1.3 Sandy siltstone

Element concentrations in the sandy siltstone of **sample 132a** are in the same range as for samples 136a and 137 (Table 22, Table 23, Table 24). Uranium and radium are in equilibrium (53 Bq/kg). Thorium occurs with a lower activity (43 Bq/kg) than in the other two samples (Table 16).

The thin section of the sample in Figure 41 displays the structure of the siltstone. Siltstone layers are intercalated with sandstone and claystone layers. Goethite, hematite, and Mn oxides/hydroxides are concentrated along bedding joints, but the second thin section in Figure 42 shows that the cement of the rock is also rich in oxides and hydroxides of iron (mainly goethite).

Figure 41: Laminated fine sandstone and siltstone with intercalations of claystone (132a; Gedinnian). Mono- and polycrystalline quartz crystals accompanied by an assemblage of authigenic quartz, muscovite, clay minerals, goethite and hematite. Goethite and hematite are precipitated together with manganese oxides/hydroxides mainly along bedding joints. Length of scale bar is 1 mm.

Though only few opaque mineral grains occur in the thin section, they are confirmed by XRD. Besides ore mineral grains of goethite and hematite, heavy minerals like anatase,

brookite, ilmenorutile, rutile, and titanite are abundant (Table 17). Iron-bearing chlorites (chamosite, clinochlore) and kaolinite dominate illite and muscovite.

The distribution of numerous coated fractures within the rock is shown in Figure 43. Fractures transect the rock in many directions, lined with goethite, hematite, and Mn oxides/hydroxides. It is assumed that these oxides and hydroxides are of descendent origin and have a similar genesis to the *"Hunsrückerze"* (see Chapter 7.3.1). In contrast to the fine-grained sandstones (136a, 137), fractures transecting the rock do not cut quartz grains (Figure 43).
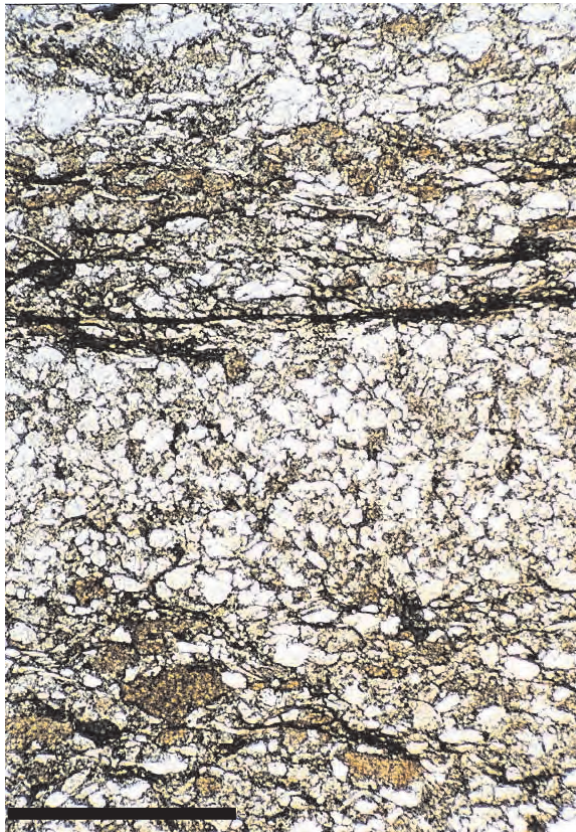
Figure 42: Laminated sandy siltstone (132a; Gedinnian). Mono- and polycrystalline quartz crystal grains coated by authigenic quartz in a cement of muscovite, clay minerals, chlorites, goethite and hematite. Iron and manganese oxides/hydroxides (see text) were precipitated especially parallel to bedding. The quartz grains are interlocked and show sutured contacts. Only few opaque ore mineral grains occur. Length of scale bar is 1 mm.
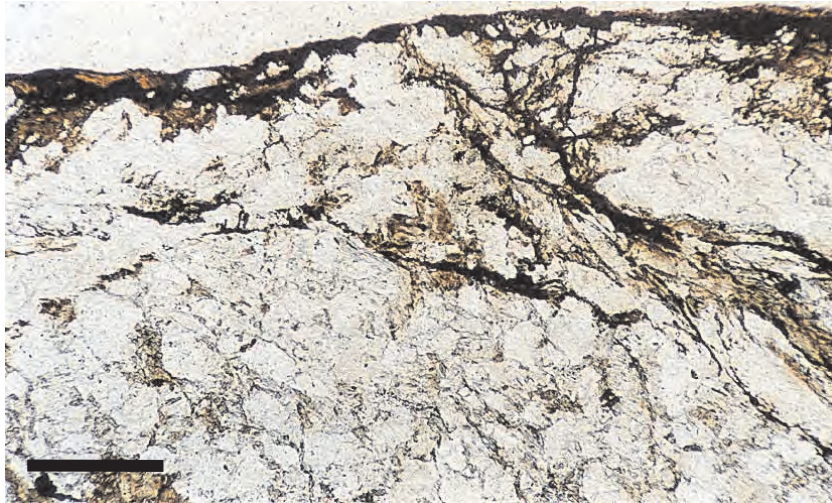
Figure 43: Gedinnian siltstone (132a). Massive coatings of iron and manganese oxides/hydroxides (see text) along fracture zones and internal joints, which were precipitated during intense weathering in Tertiary times. Length of scale bar is 200 μm.

Distribution of uranium is similar to that described for the other samples. As for sample 136a, uranium is found with 5.6% in the exchangeable fraction beside highest proportions in the extraction residual and the Fe oxide fractions (Figure 44).

Thorium does not differ in distribution, as already described for sample 136a.

Distribution of radium is again different compared to the other radionuclides. More than 90% of total radium occurs in the extraction residual and 7.8% is found in the mobile exchangeable fraction. The activities for all other fractions are below detection limits, as for sample 124. The results for the amorphous Fe oxide phase will be disregarded, as before (detection limit of 5 Bq/kg).
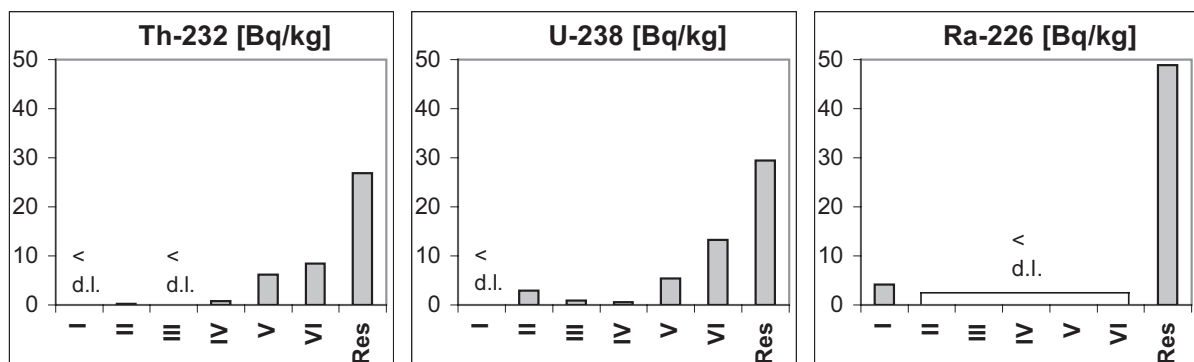
Figure 44: Radionuclide activities among extraction phases of sample 132a (Gedinnian siltstone) (I = *mobile exchangeable***, II =** *exchangeable***, III =** *Mn oxides***, IV =** *organic matter***, V =** *amorphous Fe oxides***, VI =** *crystalline Fe oxides***, Res =** *extraction residual***)**

84

Table 24: Analytical results of sample 132a. For analytical methods see Table 18.

132a	original sample	SD	I mobile exchangeable	SD	II exchangeable	SD	III Mn-Oxides	SD	IV organic matter	SD	V amorphous Fe oxides	SD	VI crystalline Fe oxides	SD	residual***
Al [ppm]	87810	*	8	2	37	1	33	0.4	193	7	1162	20	4569	79	81810
Mg [ppm]	6975	*	121	3	37	4	30	0.4	37	3	235	6	998	79	5516
Fe [ppm]	31510	*	11	2	5	1	60	3	212	4	3162	100	7762	722	20300
Zn [ppm]	87	**	0.9	0.3	0.8	0.2	1.2	0.2	NA		7.2	0.9	36.8	1.1	40
Ba [ppm]	445	**	7.0	0.2	1.3	0.1	1.4	0.1	0.5	0.1	2.1	0.02	2.0	0.1	431
Mn [ppm]	331	*	85.7	4.4	14.0	0.1	35.9	0.3	11.3	0.4	19.9	0.3	38.2	1.3	126
Pb [ppm]	28	**	< 0.1		1.8	0.1	5.2	0.03	1.5	0.02	2.2	0.1	9.4	0.5	7
As [ppm]	33	*	0.1	0.01	0.1	0.004	0.1	0.01	0.4	0.01	6.7	0.2	25.4	0.9	< 4
Ti [ppm]	4431	**	0.2	0.03	0.1	0.01	0.2	0.01	0.5	0.01	3.9	0.2	5.6	0.2	4420
Ni [ppm]	51	**	2.0	0.4	0.3	0.02	0.4	0.01	0.7	0.1	3.9	0.2	17.1	0.6	27
V [ppm]	92	**	< 0.1		< 0.1		< 0.1		0.3	0.03	1.4	0.03	5.2	0.2	85
Cu [ppm]	23	**	0.2	0.02	0.4	0.003	0.4	0.04	1.0	0.1	3.7	0.1	16.6	0.4	< 4
Rb [ppm]	97	**	0.6	0.01	0.1	0.002	0.2	0.002	0.1	0.004	0.3	0.01	0.3	0.02	95
Sr [ppm]	151	**	2.7	0.1	1.1	0.1	1.1	0.01	0.9	0.1	0.9	0.02	0.7	0.1	143
Y [ppm]	36	**	0.1	0.01	0.5	0.003	0.2	0.01	0.2	0.01	0.7	0.01	1.1	0.03	33
Zr [ppm]	312	**	NA		< 0.1		0.2	0.003	NA²		NA²		NA²		< 312
Cs [ppm]	9	**	0.15	0.002	0.03	0.001	0.07	0.001	0.01	0.001	0.05	0.001	0.08	0.003	9
La [ppm]	45	**	0.06	0.01	0.11	0.002	0.05	0.004	0.06	0.001	0.37	0.01	0.42	0.01	44
Ce [ppm]	79		0.07	0.02	0.27	0.003	0.19	0.01	0.17	0.01	0.92	0.03	1.01	0.02	76
Dy [ppm]	NA¹		< 0.01		0.09	0.001	0.03	0.002	0.04	0.003	0.16	0.002	0.27	0.01	ND
Er [ppm]	NA¹		< 0.01		0.05	0.001	0.02	0.001	0.02	0.001	0.08	0.002	0.14	0.004	ND
Yb [ppm]	NA¹		< 0.01		0.03	0.001	0.01	0.001	0.02	0.001	0.07	0.002	0.14	0.01	ND
Hf [ppm]	NA¹		NA		NA		0.01	0.002	< 0.01		0.09	0.003	0.35	0.02	ND
Th [Bq/kg]	42.5		< 0.1		0.2	0.003	0.1	0.01	0.8	0.03	6.1	0.1	8.5	0.3	27
U [Bq/kg]	52.5		< 0.1		2.9	0.04	0.9	0.1	0.6	0.1	5.4	0.1	13.3	0.5	29
Ra [Bq/kg]	53.1		4.2	0.4	< 1.5		< 1.5		< 0.8		< 5.0		< 1.1		49

* standard deviation (SD) < 5 %; ** standard deviation (SD) < 10 %; *** standard deviation (SD) < 20 %
NA¹: element was not analysed; NA²: no calibration curve was obtained; ND = not detectable

The high radium activity in the extraction residual of sample 124 was explained by high proportions of heavy minerals. This is also true for this sample. Heavy minerals, e.g. zircon, brookite, and anatase, are even more prominent in the extraction residual than for sample 124. In addition, much more residual feldspar, mica and clay minerals occur.

It is remarkable that no radium is detectable in the fractions of the Mn oxides and the crystalline Fe oxides. Radium was expected to occur in these fractions, because many fractures occur in this siltstone, which are all lined with oxides and hydroxides of iron and manganese.

7.3.1.1.4 *Weathered Gedinnian sandstones*

Sample 127a differs from the other sandstone samples, because this sandstone is highly weathered. The rocks are not as compact as the other samples partly due to disintegration by weathering. Nevertheless, the geochemistry is almost the same as for samples 136a and 137, except for lower concentrations of Na, K, Ba, Ga, Rb, Sr, U and Ra (Table 25). Uranium and radium are in equilibrium, but with 25 Bq/kg only half as abundant as for samples 136a and 137. Thorium occurs with equivalent activities (45 Bq/kg) to those of 136a and 137 (Table 25). In contrast to all other sand- and siltstone samples, thorium activities exceed the activities of uranium and radium (AR ^{232}Th/^{238}U: 1.9). Significantly higher concentrations of Zr are observed (805 ppm), being about twice as high as for the other sand- and siltstone samples. Furthermore, the concentration of Ti is higher.

Composition of the light minerals is different; besides quartz, clinochlore is abundant. Accompanying minerals of importance are illite, muscovite, kaolinite, and feldspars. While plagioclase dominates microcline in all other samples (except for sample 124), this is the other way round for sample 127a.

The dominant minerals in the spectrum of the heavy minerals are once again chlorites - clinochlore and chamosite. Abundant heavy minerals are anatase, brookite, tourmaline, and zircon (Table 17).

The speciations of all three radionuclides in sample 127a are unlike all other samples discussed so far. They have only few similarities: the highest percentage of radionuclides occurring in the extraction residual, U and Th activities < detection limit in the mobile exchangeable fraction (I) as well as low thorium activities in the exchangeable (II) and in the Mn oxide fraction (III).

Figure 45: Radionuclide activities among extraction phases of sample 127a (weathered Gedinnian sandstone) (I = _mobile exchangeable_**, II =** _exchangeable_**, III =** _Mn oxides_**, IV =** _organic matter_**, V =** _amorphous Fe oxides_**, VI =** _crystalline Fe oxides, Res = extraction residual_**)**

Table 25: Analytical results of sample 127a. For analytical methods see Table 18.

127a	original sample	SD*	I mobile exchangeable	SD	II exchangeable	SD	III Mn-Oxides	SD	IV organic matter	SD	V amorphous Fe oxides	SD	VI crystalline Fe oxides	SD	residual***
Al [ppm]	84670	*	13	1	3	0.2	6	1	258	3	1692	17	4329	26	78360
Mg [ppm]	7790	*	132	4	41	0.1	27	0.3	38	1	244	1	962	26	6345
Fe [ppm]	46420	*	19	1	< 1		23	1	361	4	4564	18	14990	95	26460
Zn [ppm]	124	**	< 0.1		< 0.1		1.0	0.1	2.5	0.2	10.9	0.1	33.7	0.2	75
Ba [ppm]	285	**	12.6	0.0	3.3	0.03	1.7	0.1	0.8	0.02	0.9	0.02	1.5	0.04	264
Mn [ppm]	686	*	3.0	0.0	8.0	0.03	151	0.3	34.6	0.1	40.2	0.2	50.2	0.4	399
Pb [ppm]	49	**	< 0.1		< 0.1		0.2	0.01	3.9	0.1	4.3	0.01	3.9	0.1	36
As [ppm]	81	**	< 0.1		0.1	0.004	< 0.1		0.4	0.005	2.4	0.02	6.9	0.1	71
Ti [ppm]	5312	*	3.4	0.1	0.7	0.005	0.3	0.05	2.1	0.1	5.9	0.1	17.5	0.1	5282
Ni [ppm]	102	**	0.1	0.0	0.2	0.02	1.4	0.02	0.9	0.02	3.6	0.03	9.1	0.1	87
V [ppm]	132	**	< 0.1		< 0.1		0.2	0.02	0.9	0.02	4.7	0.02	14.4	0.04	112
Cu [ppm]	64	**	0.1	0.0	7.4	0.04	0.2	0.002	NA²		2.3	0.01	NA²		54
Rb [ppm]	27	**	0.9	0.0	0.1	0.001	< 0.1		0.1	0.00	0.2	0.00	1.1	0.01	24
Sr [ppm]	25	**	15.6	0.1	4.9	0.003	1.4	0.003	5.5	0.01	1.1	0.00	1.3	0.01	< 10
Y [ppm]	35	**	< 0.1		0.6	0.004	0.5	0.002	8.1	0.03	1.2	0.00	0.8	0.00	24
Zr [ppm]	504	**	< 0.1		< 0.1		< 0.1		NA²		NA²		NA²		504
Cs [ppm]	5	**	0.09	0.001	0.02	0.001	< 0.01		< 0.01		0.02	0.001	0.12	0.002	5
La [ppm]	39	**	0.01	0.001	0.45	0.003	0.47	0.01	10.08	0.07	2.21	0.001	1.00	0.01	24
Ce [ppm]	73	**	0.03	0.001	0.97	0.01	1.29	0.01	30.42	0.18	5.54	0.017	2.73	0.01	32
Dy [ppm]	NA¹		< 0.01		0.12	0.002	0.12	0.004	2.06	0.02	0.29	0.001	0.19	0.003	ND
Er [ppm]	NA¹		< 0.01		0.05	0.001	0.05	0.002	0.84	0.01	0.15	0.001	0.11	0.004	ND
Yb [ppm]	NA¹		< 0.01		0.03	0.001	0.03	0.001	0.53	0.01	0.11	0.001	0.10	0.002	ND
Hf [ppm]	NA¹		< 0.01		< 0.01		< 0.01		< 0.01		< 0.01		< 0.01		ND
Th [Bq/kg]	45.2		< 0.1		< 0.1		0.1	0.01	15.1	0.1	7.7	0.1	2.6	0.2	20
U [Bq/kg]	23.8		< 0.1		0.1	0.002	0.1	0.002	0.1	0.004	0.5	0.001	1.2	0.01	22
Ra [Bq/kg]	26.4		1.5	0.3	1.8	0.3	2.6	0.4	1.4	0.2	< 8.4		1.4	0.3	18

* standard deviation (SD) < 5 %; ** standard deviation (SD) < 10 %; *** standard deviation (SD) < 20 %
NA¹: element was not analysed; NA²: no calibration curve was obtained; ND = not detectable

The main difference for thorium is the occurrence of the second highest activity in the so-called organic fraction, though the content of C_{org} (< 1%) is as low as for all sand- and siltstones (Appendix 3 – TableA3). Thorium activities in the Fe oxide fractions are only of tertiary importance, amorphous Fe oxides exceeding the crystalline Fe oxides (Figure 45), as in the quartzitic sandstones (124, 135), which have similar thorium activities in these fractions.

The differences in distribution of uranium are even more evident. More than 90% of total uranium is left in the extraction residual, in contrast to a maximum of 66% for the other sand- and siltstones. Uranium occurs with very low activities of less than 1.2 Bq/kg in all extraction phases, amounting up to only 2.0 Bq/kg. Uranium in the extraction residual can mainly be attributed to insoluble silicates, especially to chamosite and clinochlore and also to heavy minerals.

As mentioned above, radium occurs with highest activities in the extraction residual. The activities in the extraction phases are relatively low. Radium in the Mn oxide fraction exceeds that of the exchangeable fractions (I – II) and the crystalline Fe oxide fraction (VI). The low activity in the mobile exchangeable fraction may be due to a higher grade of weathering. Water-soluble elements had been removed earlier and may have reduced the amount of unspecifically adsorbed ions.

Radium activities in the amorphous crystalline Fe oxide fraction are again below the detection limit, which is especially high for this sample (8.4 Bq/kg).

7.3.1.1.5 *Some general trends for the distribution of uranium, radium and thorium*

Summing up the results for the Gedinnian sand- and siltstones, it can be concluded that thorium is most abundant in the extraction residual and of secondary importance in the Fe oxide fraction, with varying proportions in the amorphous and crystalline phase. The bondings in all other fractions are negligible.

Uranium is also found with the highest activities in the extraction residual, always followed by the crystalline Fe oxide fraction and the amorphous Fe oxide phase. The general sequence is: Res > VI > V > II > III > IV > I.

The highest proportions of radium occur in the extraction residual. Further important fractions are the mobile exchangeable and the crystalline Fe oxide fraction. Radium is therefore bound either in a very soluble form, or in the crystalline fraction (crystalline Fe oxides + extraction residual).

7.3.1.2 **Weathering products of Gedinnian sand- and siltstones**

Activities of all radionuclides are elevated in the weathering products. Usually, radium activities are highest and thorium activities are lowest (Table 16). The samples will be discussed in three groups, according to their geochemical composition and their activities of U, Ra and Th.

Samples 132b and 136b are weathering products of sandy siltstone 132a and of the sandstone 136a. They appear to have the highest radionuclide activities along with the highest total iron concentrations (> 20% Fe_2O_3, Table 26) and concentrations of Mn, P and most heavy metals (As, Cu, Ni, Pb, V, Zn). Si and Zr are lowest. As for all weathering products, the amount of organic matter is low (C_{org} < 1%; Appendix 3 – Table A3).

The mineralogical composition of the samples is similar. Besides quartz, clay minerals and chlorites (clinochlore and chamosite) are most abundant. Compared to the rock samples, fewer chlorites and more clay minerals occur. The nature of the clay minerals is different for the two samples. While illite dominates by a wide margin in the weathered sandstone, the weathered siltstone shows an assemblage of various clay minerals such as illite, kaolinite, and smectite. The most abundant iron oxides are goethite and hematite. As for the rock samples, a determination of specific Mn oxides and hydroxides with XRD was not possible. Besides ore mineral grains of iron and manganese oxides/hydroxides, the most abundant heavy minerals for both samples are anatase, rutile, ilmenorutile, pseudorutile, titanite and zircon. Considering the content of heavy minerals, it is about twice as high for the weathered sandstone. Though the elementary composition of both samples is similar, the mineralogy and the distribution of the radionuclides are not.

Thorium in both samples is about three times higher than in the rock samples (Table 16), leading to 110 Bq/kg for the weathered siltstone (132b) and to 143 Bq/kg for the weathered sandstone (136b). Compared to the rock samples, no substantial differences in

bondings of thorium occur, though the activities in most fractions are increased. Only negligible amounts of thorium were found in the first four fractions; while the most important fraction is the extraction residual, followed by the fractions of the Fe oxides (Figure 46). The percentage of dissolved thorium is somewhat higher for the weathered siltstone (55%) than for the weathered sandstone (40%), caused by a much higher proportion in the fraction of the crystalline Fe oxides, accompanied by high concentrations of Al, Fe, Pb, As, Ti, V, Y and REE (Table 26).

For the Fe oxide fractions, not only are the activities increased compared to the rock samples, but also the total percentages of thorium. This is in good agreement with other investigations (VON GUNTEN et al. 1996, GASCOYNE & CRAMER 1987, LONGWORTH et al. 1989, DEARLOVE et al. 1988, DEARLOVE et al. 1989). Thorium is accumulated in weathering products and soils as hydrolysed and insoluble compounds, which are preferentially fixed in thin grain surface layers consisting of oxides and hydroxides, mainly of iron, manganese, and aluminium.

This assumption is supported by the distribution of iron in the weathering products. About 38% of total iron was found in the oxide fractions: 30% in the crystalline Fe oxide fraction, 8% in the amorphous Fe oxide fraction and < 0.1% in the Mn oxide fraction. High Al concentrations in fraction VI (Table 26) may not only be due to the occurrence of Al oxides, but Al may also substitute iron in crystalline Fe oxides. Crystalline Fe oxides generally show aluminium substitution, in goethite up to 1/3 and in hematite up to 1/6 of the iron atoms (NORRISH & TAYLOR 1961, SCHWERTMANN 1984, TAYLOR 1987). Even substitution of iron by aluminium in ferrihydrite (amorphous Fe oxide) takes place. Experiments have shown that aluminium-substituted hematite readily forms from ferrihydrite synthesised in the presence of Al (SCHWERTMANN et al. 1979).

Only a few oxides other than SiO_2 in the weathering product are expected to be inherited from the parent rocks, most of them are of pedogenic origin, because typically oxidic-bound elements such as Fe, Al, Mn and Ti are greatly enriched in the weathering products.

Uranium is up to 9 times more prevalent in the weathering products. As for thorium, uranium activities are higher in the weathered sandstone (468 Bq/kg) than in the weathered siltstone (362 Bq/kg).
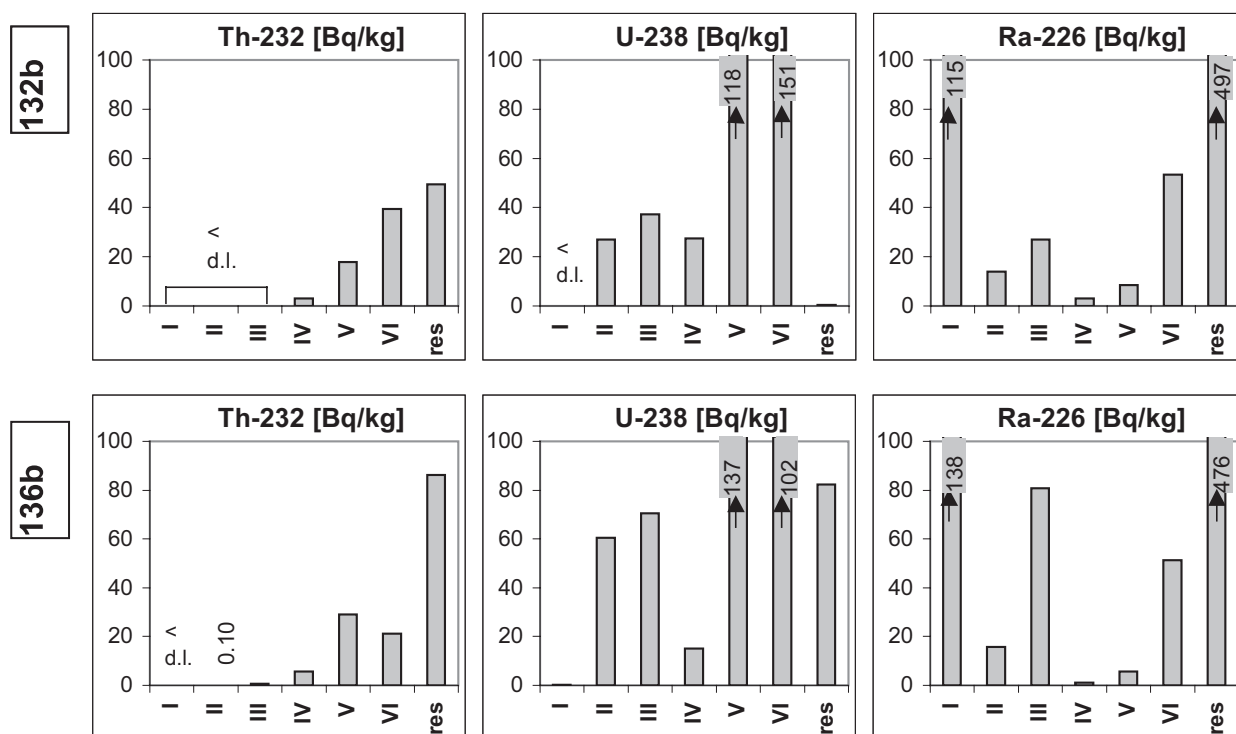
Figure 46: Radionuclide activities among extraction phases of samples 132b and 136b, weathering products of Gedinnian sandstone and a Gedinnian sandy siltstone. (I = *mobile exchangeable*, **II =** *exchangeable*, **III =** *Mn oxides*, **IV =** *organic matter*, **V =** *amorphous Fe oxides*, **VI =** *crystalline Fe oxides, res = extraction residual*)

Comparing both weathering products with each other, differences in the distribution of uranium are similar to those of thorium. Uranium is dissolved to a greater extent in the weathered siltstone than in the weathered sandstone. While uranium in the weathered siltstone is dissolved completely during sequential extraction, about 18% of uranium of the weathered sandstone is left in the extraction residual. In both samples uranium occurs primarily in one of the Fe oxide fractions (Figure 46), which is in good agreement with AMES et al. (1983 a, b).

Table 26: Analytical results of samples 132b and 136b. For analytical methods see Table 18.

132b	original sample	SD	I mobile exchangeable	SD	II exchangeable	SD	III Mn-Oxides	SD	IV organic matter	SD	V amorphous Fe oxides	SD	VI crystalline Fe oxides	SD	residual***
Al [ppm]	132300	*	10	0.4	< 1		14	0.3	662	8	2980	11	9162	65	119500
Mg [ppm]	5375	*	376	2	50	1	28	0.1	30	0.3	70	0.5	83	2	4738
Fe [ppm]	180000	*	10	1	4	0.2	77	1	782	3	13785	71	53696	337	111700
Zn [ppm]	508	**	2.0	0.02	< 0.1		14.8	0.1	23.5	0.3	34.8	0.2	43.1	0.9	390
Ba [ppm]	526	**	22.5	0.2	2.9	0.1	34.7	0.1	1.3	0.02	1.5	0.02	2.6	0.1	461
Mn [ppm]	> 6200	*	46.9	0.05	8.4	0.1	2936	26	249	1	543	1	76.6	0.9	ND
Pb [ppm]	> 240	**	0.1	0.01	1.0	0.02	198	2	233	3	59.1	0.03	116	1	ND
As [ppm]	> 330	*	< 0.1		0.1	0.001	< 0.1		0.9	0.02	68.9	0.3	334	6	ND
Ti [ppm]	6145	**	1.1	0.02	0.6	0.02	0.3	0.04	4.0	0.04	63.3	0.4	273	2	5803
Ni [ppm]	391	**	1.7	0.02	0.4	0.1	14.7	0.05	9.3	0.05	45.4	0.05	42.3	0.5	277
V [ppm]	230	**	< 0.1		<		1.6	0.01	2.4	0.01	9.2	0.01	53.0	0.5	164
Cu [ppm]	> 450	**	0.2	0.004	0.5	0.03	6.5	0.03	18.2	0.2	25.6	0.1	NA²		ND
Rb [ppm]	119	**	2.1	0.002	0.2	0.01	< 0.1		0.1	0.002	0.3	0.004	0.6	0.01	116
Sr [ppm]	131	**	6.9	0.1	1.4	0.02	1.0	0.01	0.9	0.01	0.8	0.003	1.1	0.03	119
Y [ppm]	69	**	1.1	0.01	1.2	0.01	3.1	0.03	6.0	0.1	6.3	0.01	8.2	0.1	43
Zr [ppm]	360	**	< 0.1		NA²		< 0.1		2.6	0.02	NA²		NA²		< 357
Cs [ppm]	35	**	3.90	0.03	0.67	0.003	0.05	0.001	0.15	0.003	0.28	0.003	0.25	0.003	30
La [ppm]	> 80	**	0.50	0.005	0.20	0.002	0.72	0.001	0.83	0.01	0.88	0.004	1.92	0.04	ND
Ce [ppm]	106		0.98	0.01	0.55	0.004	8.12	0.04	10.91	0.10	17.01	0.07	22.49	0.28	46
Dy [ppm]	NA¹		0.11	0.001	0.22	0.002	0.66	0.01	1.32	0.02	1.84	0.02	2.33	0.02	ND
Er [ppm]	NA¹		0.06	0.001	0.09	0.002	0.28	0.003	0.74	0.01	0.86	0.002	1.16	0.02	ND
Yb [ppm]	NA¹		0.03	0.001	0.05	0.001	0.17	0.001	0.69	0.01	0.76	0.005	1.17	0.02	ND
Hf [ppm]	NA¹		< 0.01		< 0.01		0.01	0.003	0.10	0.002	NA²		0.82	0.03	ND
Th [Bq/kg]	110		< 0.1		< 0.1		0.1	0.01	2.9	0.01	17.9	0.3	39.4	2.1	49
U [Bq/kg]	362		< 0.1		27.1	0.2	37.2	0.5	27.4	0.3	118	0.2	151	2	< 0.1
Ra [Bq/kg]	718		115	12	13.9	1.2	26.9	2.4	3.1	0.4	8.5	0.6	53.4	2.5	497

* standard deviation (SD) < 5 %; ** standard deviation (SD) < 10 %; *** standard deviation (SD) < 20 %
NA¹: element was not analysed; NA²: no calibration curve was obtained; ND = not detectable

136b	original sample	SD	I mobile exchangeable	SD	II exchangeable	SD	III Mn-Oxides	SD	IV organic matter	SD	V amorphous Fe oxides	SD	VI crystalline Fe oxides	SD	residual***
Al [ppm]	147300	*	52	2	27	4	52	7	795	106	4940	88	6332	393	135100
Mg [ppm]	5841	*	NA²		56	2	86	4	25	2	94	11	67	10	< 5513
Fe [ppm]	155500	*	7	2	24	4	189	25	870	42	12882	369	44012	2921	97520
Zn [ppm]	503	**	5.5	0.2	0.6	0.1	35.8	1.6	21.4	1.4	49.2	1.4	61.8	5.1	329
Ba [ppm]	592	**	46.4	1.1	4.7	0.3	69.8	2.8	0.7	0.1	1.7	0.4	3.0	0.7	465
Mn [ppm]	> 6200	*	129	2	15.8	0.3	3619	38	200	8	1280	36	208	9	ND
Pb [ppm]	>240	**	0.5	0.04	1.4	0.2	219	3	151	5	60.5	1.9	54.1	7.2	ND
As [ppm]	> 330	*	0.1	0.01	0.1	0.01	0.2	0.04	1.2	0.1	81.0	2.3	153	3	ND
Ti [ppm]	5907	**	1.2	0.1	1.0	0.1	1.4	0.04	6.3	0.3	NA²		213	2	< 5684
Ni [ppm]	403	**	3.5	0.1	1.1	0.1	34.9	0.4	10.0	0.5	111	3	42.9	1.9	200
V [ppm]	204	**	< 0.1		< 0.1		2.5	0.3	1.4	0.1	12.3	0.3	35.7	0.8	152
Cu [ppm]	> 450	**	0.6	0.1	1.0	0.1	18.8	0.1	24.0	0.7	37.5	1.0	0.8	0.05	ND
Rb [ppm]	149	**	5.1	0.1	0.5	0.01	1.0	0.05	< 0.1		0.5	0.1	0.6	0.03	141
Sr [ppm]	152	**	7.9	0.1	1.2	0.1	1.6	0.2	0.8	0.1	0.8	0.1	0.7	0.1	139
Y [ppm]	65	**	6.4	0.1	1.4	0.04	3.5	0.3	2.5	0.1	6.2	0.1	3.5	0.1	42
Zr [ppm]	340	**	0.2	0.04	NA²		0.2	0.05	NA²		NA²		21.3	0.4	< 318
Cs [ppm]	41	**	4.67	0.07	0.87	0.03	0.78	0.04	0.04	0.01	0.23	0.08	0.19	0.03	35
La [ppm]	75	**	2.03	0.03	0.22	0.01	0.90	0.10	0.47	0.04	1.12	0.09	0.72	0.22	69
Ce [ppm]	> 150		4.89	0.08	0.67	0.03	9.99	0.14	7.73	0.42	34.09	0.64	14.65	2.63	ND
Dy [ppm]	NA¹		0.74	0.02	0.29	0.01	0.83	0.07	0.60	0.03	1.67	0.03	0.95	0.07	ND
Er [ppm]	NA¹		0.39	0.01	0.13	0.004	0.39	0.03	0.36	0.01	0.87	0.02	0.54	0.03	ND
Yb [ppm]	NA¹		0.24	0.01	0.08	0.002	0.28	0.02	0.40	0.01	0.84	0.02	0.54	0.02	ND
Hf [ppm]	NA¹		NA²		NA²		0.06	0.01	< 0.01		NA²		0.61	0.08	ND
Th [Bq/kg]	143		0.1	0.02	0.1	0.02	0.7	0.1	5.7	0.8	29.1	0.8	21.1	1.7	86
U [Bq/kg]	468		0.3	0.02	60.4	0.6	70.4	11.8	15.1	1.8	137	2	102	6	82
Ra [Bq/kg]	769		138	10	15.6	2.0	80.7	9.2	1.1	0.2	5.6	0.6	51.2	4.1	476

* standard deviation (SD) < 5 %; ** standard deviation (SD) < 10 %; *** standard deviation (SD) < 20 %
NA¹: element was not analysed; NA²: no calibration curve was obtained; ND = not detectable

As for thorium, uranium in the silty weathering product is more abundant in the crystalline Fe oxide fraction, while the activity in the amorphous Fe oxide phase is higher for the weathered sandstone. This result can be explained by incomplete dissolution of crystalline Fe oxides during the last extraction step, because goethite, hematite, and magnetite were determined by XRD in the extraction residual of the weathered sandstone.

Iron and manganese oxide/hydroxide encrustations on the particles of the weathered sandstone are assumed to be thicker than the coatings on grains and fractures in the unweathered rock (Figure 38).

Considering the fractions I to IV, uranium occurs in much higher proportions in the exchangeable fraction (II), the Mn oxide phase (III) and the organic fraction (IV), in comparison to the rock samples. Not only is a higher mobility of uranium in weathering products documented by this result, but also a higher mobility of uranium in comparison to thorium. While thorium is fixed to more than 95% in the crystalline and the Fe oxide phase (V, VI + extraction residual), uranium activities amount to only 75% in these fractions. A much higher percentage of uranium is redistributed to more soluble pedogenic phases during weathering. Further evidence of the high mobility of uranium in the weathering products is the very low activity in the mobile exchangeable phase. Unspecific adsorption to negatively charged colloids is evidently of no importance for uranium. Uranium preferentially forms stable and mobile complexes rather than being adsorbed by negative charged soil surfaces (LIENERT, SHORT & VON GUNTEN 1994).

The low quantities of uranium in the extraction residual are not in accordance with values reported in literature. GREEMAN (1992) found a minimum of 62% U in the extraction residual and ROTH (1997) 65% U. However, neither of these results are comparable to the results of this study because of the different sequential extraction scheme used. Neither the methods of GREEMAN (1992) nor ROTH (1997) are capable of resolving crystalline Fe oxides, which are therefore left in the extraction residual. The only comparable study is the one by EDSFELDT (2001), who used the same extraction scheme as used in this study. The Swedish soil samples investigated, originate from a well-developed spodosol profile above till, with underlying granite. Uranium was found to dominate in most extraction residuals with 32 – 97% and was only of secondary importance in the oxide fraction (amorphous Fe oxides > crystalline Fe oxides > Mn oxides). Though no mineralogical investigations were carried out, the high activities of uranium in the extraction residuals can be attributed to a high content of primary, unweathered heavy minerals, because residual Zr concentrations, as an indicator for inherited rock minerals, show a significantly positive correlation to residual U.

In the present study, no significantly positive correlations of residual Zr to residual U occur for any sample and iron concentrations are ten times higher than those of the Swedish samples.

Radium in the weathering products is enriched about 13 times compared to the parent rocks, exceeding activities of 700 Bq/kg (Table 16). The activity in the weathered sandstone is higher; the AR ^{226}Ra/^{238}U is nevertheless a little lower: 1.6 instead of 2.0 for the weathered siltstone.

As was the case in the rock samples, radium is most abundant in the extraction residual. However, the proportion of radium in the crystalline phase (VI + extraction residual) is 9 – 16% lower.

The highest activities among the extraction phases are found in the mobile exchangeable fraction (I). The unspecific adsorption to clay minerals, organic matter, and oxides of Fe, Mn, Al and Si is of most importance for radium. Specific adsorption of radium, which is documented in the exchangeable fraction (II), amounts to only 2% for each weathering product.

Whereas radium in the Mn oxide phase is negligible for the weathered siltstone, the relatively high radium activity in this fraction for the weathered sandstone corresponds to a higher proportion of Mn oxides. Due to the high specific surface area of Mn oxides, which may amount several hundred m²/g (ANDERSON et al. 1973; LOGANATHAN & BURAU 1973) and the low isoelectric point, the adsorption or occlusion to Mn oxides is an important process in weathering products.

By far the lowest activities are found in the organic fraction (< 0.4%). This is contradictory to the findings presented by GREEMAN (1992), who attributed 24% of radium to organic matter. This discrepancy can be explained by the differences in the extraction schemes used. GREEMAN (1992) separated exchangeable from organically-bound elements for only half of the selected samples and did not present detailed results. The results of both fractions were pooled for all of the papers published. Apart from this simplification, the selectivity of the extractant used (5% NaOCl and saturated NaCl, pH 5) is not adequate. Besides organic matter, Mn oxides and inorganically-bound heavy metals are partly dissolved (SIMS & PATRICK 1978). The proportion of radionuclides associated with organic matter is therefore greatly overestimated (GREEMAN 1992).

The radium activities in the organic fraction found in this study are in the same range as the radium activities determined by EDSFELDT (2001).

Radium adsorbed to ferrihydrite is of only minor significance (1%). Activities in fraction V are just above the detection limits. This result allows the conclusion that radium in this fraction is not only of minor relevance in the weathering products, but is also of no importance for the rock samples. The results of the rock samples were not discussed in chapter 7.3.1.1 because the activities were below the relatively high detection limits (5 - 8 Bq/kg). Ferrihydrite is assumed to occur more frequently in weathered samples, and radium has thirteen times higher total activities there. The activities of radium in this fraction should thus be lower in the rock samples than for the weathering products. Though the detection limit is very high, one can estimate the maximum of the dissolved radium from the amount of radium of the weathering samples in this fraction. Only 1% of total Ra in the weathering

products is dissolved in this fraction, leading to assumed radium activities in the rock samples of between 0.3 and 0.7 Bq/kg.

The percentage of radium occurring in the fraction of the crystalline Fe oxides is about the same for both samples (7%; Figure 46,Table26). For the weathered sandstone, activities in this fraction are lower than for the parent rock, contrary to the weathered siltstone. The radium activities found in this fraction are low compared to uranium (ARs $^{226}Ra/^{238}U$: 0.5 and 0.4).

Radium in the extraction residuals is not supported by uranium (ARs $^{226}Ra/^{238}U \gg 1$).

Table 27: Activity ratios $^{226}Ra/^{238}U$ in the fractions of the sequential extraction for the analysed Gedinnian weathering products (d. l. = detection limit).

$^{226}Ra/^{238}U$	Weathered sandstones		Weathered siltstone	Weathered quartzitic sandstone
	127b	136b	132b	134
Total sample	0.7	1.6	2.0	1.7
Mobile exchangeable	> 1	453	> 1	> 1
Exchangeable	1.5	0.3	0.5	0.2
Mn oxides	8.0	1.1	0.7	1.6
Organic	2.2	0.1	0.1	0.4
Amorphous Fe oxides	Ra < d. l.	< 1	0.1	0.3
Crystalline Fe oxides	1.1	0.5	0.4	0.5
Extraction residual	0.7	5.8	1113	18

Sample 134 differs significantly from the first two weathering samples because of its lower iron and radionuclide concentrations. The weathering product of the quartzitic sandstone 135 shows highest concentrations of Ti, Na, K, Ba, Rb, Sr and Y. The high Ti concentrations are due to a high percentage of Ti-bearing heavy minerals such as anatase, brookite, titanite, ilmenorutile, pseudorutile and rutile. The relatively high concentrations of Na might be attributed to the high amount of tourmaline and mixed layer clay minerals. Compared to the other weathering products, high percentages of poorly crystalline clay minerals occur in this sample along with illite and kaolinite.

A much lower Fe concentration was determined for sample 134 (Table 28). It is about three times lower than for the samples of the first group of weathering products (Table26). Iron is most abundant in the fraction of the crystalline Fe oxides, as in the other samples. Although the total iron concentration is lower for sample 134, the percentage of iron in the crystalline Fe oxide fraction is much higher (68%). As the percentage of oxidic iron relative to total iron reflects the degree of weathering, this points to a much higher weathering intensity of the sample.

Thorium activity in the weathering product is three times higher than the activity in the rock sample and a little lower than for the other weathering products (95 Bq/kg). The distribution of thorium in this sample is similar to the other weathering products. About 50%

of the thorium remains in the extraction residual. Just as was the case for the sample of the weathered siltstone (132b), most of the dissolved fraction of thorium is found in the fraction of the crystalline Fe oxides (Table 28) and negligible activities occur in fractions I - IV (Figure 47).

Table 28: Analytical results of sample 134. For analytical methods see Table 18.

134	original sample		I mobile exchangeable	SD	II exchangeable	SD	III Mn-Oxides	SD	IV organic matter	SD	V amorphous Fe oxides	SD	VI crystalline Fe oxides	SD	residual***
Al [ppm]	156800	*	14	1	6	0.1	88	2	528	4	2028	3	4479	100	149700
Mg [ppm]	3542	*	213	2	37	0.3	43	0.3	27	0.2	51	0.3	60	1	3112
Fe [ppm]	59460	*	7	1	NA²		165	2	285	2	4241	18	36248	825	< 18510
Zn [ppm]	212	**	3.7	0.3	0.8	0.1	25.1	0.1	9.9	0.4	13.3	0.1	75.0	1.3	84
Ba [ppm]	977	**	25.7	0.2	3.2	0.04	121	1	1.2	0.02	1.6	0.00	2.1	0.1	823
Mn [ppm]	3087	*	72.0	1.1	11.7	0.04	2549	13	74.5	0.3	181	1	175	4	25
Pb [ppm]	241	**	< 0.1		0.8	0.01	136	0.23	33.8	0.2	17.5	0.1	37.0	0.7	15
As [ppm]	164	*	< 0.1		0.1	0.01	0.2	0.01	0.7	0.02	34.9	0.2	126	2	< 4
Ti [ppm]	7185	**	0.3	0.01	0.1	0.05	1.4	0.02	1.7	0.01	31.7	0.1	91.6	1.9	7059
Ni [ppm]	160	**	1.3	0.1	0.9	0.003	31.4	0.1	4.7	0.02	18.4	0.2	36.6	0.8	67
V [ppm]	174	**	< 0.1		< 0.1		1.1	0.01	0.7	0.004	4.1	0.01	24.5	0.5	144
Cu [ppm]	283	**	0.4	0.1	1.0	0.01	15.0	0.1	8.2	0.04	13.6	0.1	NA²		< 245
Rb [ppm]	178	**	2.4	0.03	0.2	0.004	0.5	0.005	0.2	0.002	0.3	0.003	0.6	0.01	174
Sr [ppm]	295	**	5.3	0.1	1.1	0.01	3.1	0.01	0.9	0.01	0.8	0.002	0.8	0.02	283
Y [ppm]	72	**	2.3	0.1	1.2	0.01	1.9	0.001	1.4	0.01	2.0	0.01	3.8	0.1	60
Zr [ppm]	463	**	< 0.1		< 0.1		0.8	0.02	4.3	0.02	14.3	0.004	NA²		< 443
Cs [ppm]	36	**	2.58	0.02	0.31	0.001	0.35	0.002	0.11	0.002	0.16	0.001	0.27	0.01	32
La [ppm]	80	**	0.88	0.02	0.20	0.01	0.62	0.002	0.24	0.002	0.90	0.003	1.06	0.02	76
Ce [ppm]	133		1.55	0.03	0.53	0.01	4.82	0.004	2.40	0.01	5.37	0.01	12.25	0.22	106
Dy [ppm]	NA¹		0.26	0.01	0.25	0.003	0.45	0.01	0.35	0.002	0.65	0.001	1.07	0.01	ND
Er [ppm]	NA¹		0.14	0.003	0.11	0.001	0.22	0.004	0.20	0.002	0.35	0.002	0.54	0.01	ND
Yb [ppm]	NA¹		0.08	0.002	0.07	0.001	0.17	0.001	0.21	0.002	0.35	0.002	0.51	0.01	ND
Hf [ppm]	NA¹		< 0.01		< 0.01		0.03	0.003	0.21	0.001	0.81	0.002	0.83	0.02	ND
Th [Bq/kg]	96		< 0.1		< 0.1		0.3	0.01	4.0	0.02	17.2	1.2	24.8	0.6	49
U [Bq/kg]	198		0.1	0.01	29.9	0.2	22.7	0.04	10.8	0.1	35.9	0.2	87.7	1.4	11
Ra [Bq/kg]	339		43.2	3.3	6.4	0.6	36.6	3.1	4.1	0.5	9.5	0.8	40.3	3.2	199

* standard deviation (SD) < 5 %; ** standard deviation (SD) < 10 %; *** standard deviation (SD) < 20 %
NA¹: element was not analysed; NA²: no calibration curve was obtained; ND = not detectable
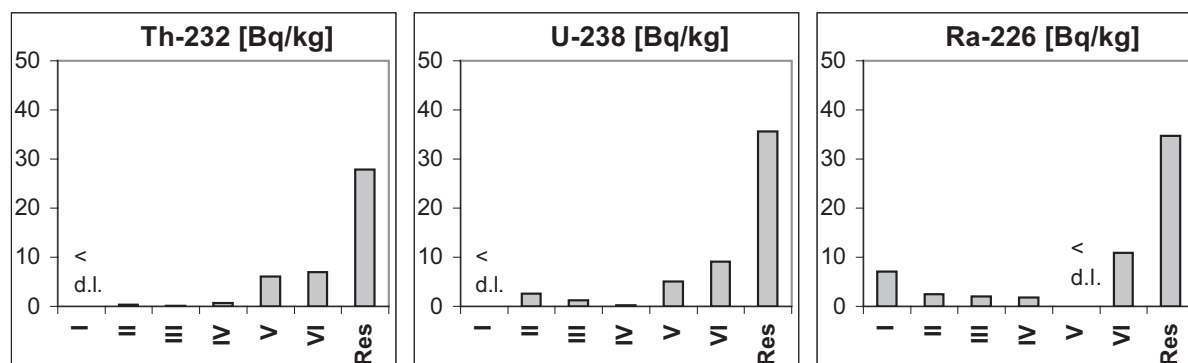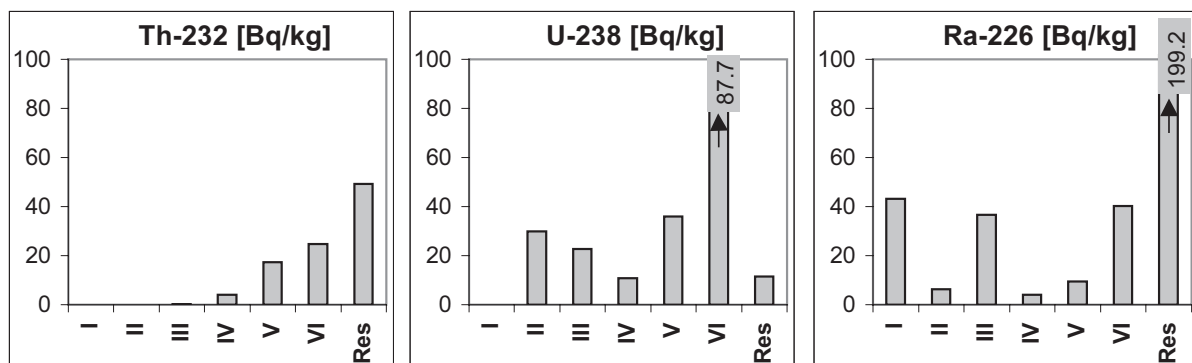

Figure 47: Radionuclide activities among extraction phases of sample 134, weathering product of Gedinnian quartzitic sandstone. (I = *mobile exchangeable***, II =** *exchangeable***, III =** *Mn oxides***, IV =** *organic matter***, V =** *amorphous Fe oxides***, VI =** *crystalline Fe oxides***, Res =** *extraction residual***)**

The uranium activity in sample 134 is much lower than for the other weathering products (199 Bq/kg), along with lower concentrations of P, Fe, As, Cu, Ni, V and Zn. By far the most uranium is bound to crystalline Fe oxides (44%). As mentioned above, total iron concentrations are only about one third of those in the other weathering products, but the concentration of iron in fraction VI is still in the same order of magnitude (Table 26 and

Table 28). This is not true for the fraction of the amorphous Fe oxides. The iron concentration is also about 3 times lower than in the other weathering products, which is reflected by a uranium activity that is 4 times lower (Figure 47).

The distribution of uranium among the other soil phases is similar to those of the weathered siltstone 132b. Only the uranium activities in the exchangeable fraction are higher. This is caused by a higher content of clay minerals, which offer more adsorption places.

Radium occurs primarily in the extraction residual, followed by about equal activities in the mobile exchangeable phase, the Mn oxide fraction, and the crystalline Fe oxide fraction, with about 12% each. Though the mineralogical composition of sample 134 is different, this does not influence the speciation of radium as much as that of uranium.

Sample 127b appears to have a different composition. Not only are the radionuclide activities much lower (Table 16), but also the concentrations of all measured elements except Si and Zr (Table 30), pointing to higher proportions of quartz and zircon in the sample. High zirconium concentrations had already been measured in the parent rock (127a).

For sample 127b, the XRD analysis shows by far the highest content of clinochlore, chamosite, muscovite/illite, kaolinite, and heavy minerals such as anatase, brookite, titanite and zircon of all weathering products (Table 29). Not only do the lower concentrations of typically oxide-bound elements such as Fe, Mn, Al, and Ti confirm a much lower percentage of oxides and hydroxides in this sample. XRD analysis also shows only weak peaks for goethite and potential Mn oxides/hydroxides. Hematite was not detected. The colour of this weathering product is yellow ochre, in contrast to more reddish brown of the other weathering products.

The thorium activity of this sample amounts to only half the activity of the other weathering products. The distribution among the soil phases is nevertheless similar to the other weathered samples. Most thorium occurs in the extraction residual, while bondings of the first four fractions are of no significance. The thorium proportions in the Fe oxide fractions are nearly equal.

Table 29: Mineralogical composition of extraction residuals of Gedinnian weathering products (x = abundant; ? = uncertain; — = does not occur)

Sample	Quartz	Chamosite	Clinochlore	Mixed layer	Kaolinite Group	Smectite group	Illite	Mica Group	Anatase	Brookite	Chloritoid	Ilmenite	Ilmenorutile	Maghemite	Magnetite	Monazite	Pseudorutile	Rutile	Staurolite	Titanite	Tourmaline	Xenotime	Zircon
132b	x	x	x	x	x	x	x	x	x	—	x	?	x	—	—	x	x	x	—	x	x	—	x
134	x	x	x	x	x	x	x	x	x	—	?	—	x	x	x	x	x	x	?	x	x	x	x
136b	x	x	x	x	?	x	x	x	x	—	x	x	x	—	x	x	x	x	?	x	x	—	x
127b	x	x	x	?	x	?	x	x	x	x	x	x	x	—	—	x	x	x	—	x	x	?	x

Uranium activities are three to five times lower than for the other weathering products. The distribution of uranium among the soil phases does not show any similarity to the other weathered samples. About 90% of total uranium is found in the extraction residual. In all other samples, uranium amounts to a maximum of only 18% in the extraction residual. About half of the dissolved uranium is found in the fractions of the Fe oxides (Table 30).

Table 30: Analytical results of sample 127b. For analytical methods see Table 18.

127b	original sample	*	I mobile exchangeable	SD	II exchangeable	SD	III Mn-Oxides	SD	IV organic matter	SD	V amorphous Fe oxides	SD	VI crystalline Fe oxides	SD	residual***
Al [ppm]	81700	*	13	0.1	2	0.2	11	0.2	84	1	412	3	1584	15	79590
Mg [ppm]	8776	*	50	1	23	0.1	24	0.4	23	0.04	81	1	435	3	8141
Fe [ppm]	36240	*	7	1	< 1		47	1	151	2	1549	8	8257	12	26230
Zn [ppm]	96	**	0.6	0.01	< 0.1		2.0	0.03	5.1	0.04	4.3	0.3	38.1	0.3	46
Ba [ppm]	230	**	2.2	0.01	0.5	0.02	0.8	0.01	0.5	0.04	0.6	0.1	< 0.1		225
Mn [ppm]	407	*	10.1	0.1	1.7	0.02	97.6	0.1	31.3	0.02	23.0	0.1	24.9	0.1	218
Pb [ppm]	17	**	< 0.1		0.2	0.004	1.5	0.01	1.2	0.01	1.1	0.01	9.1	0.1	4
As [ppm]	36	**	< 0.1		0.1	0.002	0.1	0.01	0.5	0.01	6.7	0.01	22.7	0.1	6
Ti [ppm]	6294	*	0.1	0.02	0.1	0.01	0.2	0.01	0.2	0.01	2.5	0.4	7.7	0.04	6283
Ni [ppm]	80	**	0.2	0.003	0.1	0.01	0.4	0.01	0.4	0.01	2.1	0.1	22.7	0.1	54
V [ppm]	137	**	< 0.1		< 0.1		< 0.1		0.2	0.01	1.2	0.01	5.5	0.03	130
Cu [ppm]	41	**	0.1	0.002	0.3	0.003	1.6	0.01	0.4	0.01	1.9	0.02	NA²		< 37
Rb [ppm]	28	**	0.1	0.001	< 0.1		< 0.1		< 0.1		< 0.1		0.1	0.002	28
Sr [ppm]	24	**	1.1	0.005	0.9	0.01	0.9	0.01	0.8	0.01	0.6	0.004	0.4	0.01	19
Y [ppm]	42	**	0.6	0.002	0.1	0.001	0.0	0.001	0.1	0.001	0.7	0.001	0.9	0.001	40
Zr [ppm]	805	**	< 0.1		NA²		< 0.1		NA²		NA²		NA²		< 805
Cs [ppm]	3	**	0.14	0.001	< 0.01		< 0.01		< 0.01		< 0.01		0.03	0.001	3
La [ppm]	50	**	0.11	0.001	0.01	0.001	< 0.01		0.02	0.001	1.25	0.02	1.00	0.004	48
Ce [ppm]	90	**	0.25	0.002	0.04	0.001	0.11	0.003	0.12	0.001	3.42	0.01	2.71	0.003	83
Dy [ppm]	NA¹		0.07	0.001	0.03	0.001	0.01	0.001	0.04	0.002	0.24	0.005	0.28	0.005	ND
Er [ppm]	NA¹		0.03	0.001	0.01	0.001	< 0.01		0.02	0.001	0.08	0.002	0.11	0.001	ND
Yb [ppm]	NA¹		0.02	0.001	< 0.01		< 0.01		0.02	0.001	0.06	0.001	0.09	0.002	ND
Hf [ppm]	NA¹		< 0.01		0.02	0.004	< 0.01		< 0.01		< 0.01		0.31	0.01	ND
Th [Bq/kg]	54.7		< 0.1		< 0.1		< 0.1	0.002	0.6	0.1	9.7	0.2	10.3	0.8	34
U [Bq/kg]	92.8		< 0.1		1.5	0.003	0.3	0.003	0.5	0.004	2.7	0.01	4.4	0.03	83
Ra [Bq/kg]	69.5		4.9	0.7	2.2	0.3	2.2	0.2	1.1	0.1	< 8.4		4.7	0.5	54

* standard deviation (SD) < 5 %; ** standard deviation (SD) < 10 %; *** standard deviation (SD) < 20 %
NA¹: element was not analysed; NA²: no calibration curve was obtained; ND = not detectable

Like uranium and thorium, radium shows much lower activities in sample 127b than in all other weathering products. The distribution of radium among the soil phases resembles much more the distribution of radium in the rock samples (Figure 48). Only 21% of radium is dissolved during sequential extraction. Most dissolved radium was found in the fraction of the crystalline Fe oxides and the mobile exchangeable phase.
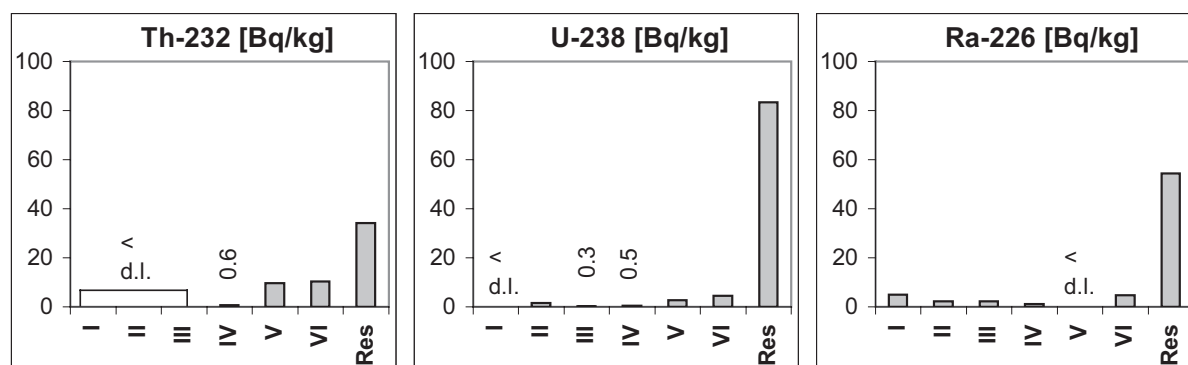
Figure 48: Radionuclide activities among extraction phases of sample 127b, weathering product of Gedinnian sandstone. (I = *mobile exchangeable***, II =** *exchangeable***, III =** *Mn oxides***, IV =** *organic matter***, V =** *amorphous Fe oxides***, VI =** *crystalline Fe oxides, Res = extraction residual***)**

This weathering product is special in that uranium activities exceed radium activities in the total sample (AR ^{226}Ra/^{238}U = 0.7), which is unique for the Gedinnian samples. Radium is depleted, rather than enriched. Due to the different potentials of uranium and radium to be leached from rocks, radium can be dissolved to a higher degree than uranium. Radium is mainly located in microfractures and along grain boundaries, while uranium occurs preferentially in mineral lattices. This leads finally to lower radium activities in the extraction residual, and - because of the better mobility of uranium in soils - to higher radium activities in the soil phases, which is documented by ARs ^{226}Ra/^{238}U > 1 (Table 27).

Apart from quartz, sample 127b consists of an assemblage of weathering-resistant minerals such as muscovite/illite, kaolinite, chlorites, and stable heavy minerals. It can be assumed that this sample was extensively leached and has to be considered as a weathering residue, in contrast to the other weathering products, which derive from enrichment zones with high contents of various oxides and hydroxides of Fe, Mn, Ti and Al besides clay minerals and chlorites.

7.3.1.3 Comparison of the distribution of uranium, radium and thorium in rocks and weathering products

The distribution of thorium is about equal for all weathering products and the parent rocks. Most thorium is bound in the extraction residual, followed by variable proportions in the Fe oxide fractions. Less than 5% of total thorium was determined in the fractions I – IV.

Uranium speciations in the weathering products differ from each other and differ very significantly from the speciations in the parent rocks. Whereas uranium in the rock samples was most abundant in the extraction residual and only of secondary importance in the Fe oxide phases, uranium in the weathering products from enrichment zones (132b, 134, 136b) occurs mostly in the fractions of the Fe oxide phases. Only small proportions of uranium are left in the extraction residual. Uranium is intensively leached during weathering and the weathering residue, presented by sample 127b, shows only low activity, pointing to low percentages of inherited rock minerals. The high mobility of uranium during weathering is also supported by less than 0.5% of total U occurring in the mobile exchangeable fraction.

While uranium in the samples of the enrichment zones is mainly associated with Fe oxides, radium is most abundant in the extraction residual, leading to disequilibrium in the uranium decay series. The weathering residue 127b, containing more primary uranium-bearing minerals, is the only sample with ARs $^{226}Ra/^{238}U < 1$ in the total sample and in the extraction residual. In contrast to uranium, radium in the weathering products is associated with minerals that remain in the extraction residual, consisting mainly of pedogenic clay minerals. Of secondary importance is the adsorption of radium onto the surfaces of various oxides/hydroxides of Si, Mn, Fe, Al, Zr and Ti, which provide the greatest proportion of unspecific adsorption sites or onto the surfaces of organic matter or clay minerals. Thirdly, radium is occluded in Mn oxides and crystalline Fe oxides.

A last point of note is the apparently different bonding of ^{226}Ra and ^{232}Th in the weathering products. In soil sample investigations it is often discussed, whether ^{232}Th can be used as an analogue for ^{230}Th, since ^{230}Th has a sufficiently long half-life in relation to soil forming processes (e.g. GREEMAN 1992, ROTH 1997, EDSFELDT 2001). For the weathering products investigated in the present study the occurrence of ^{232}Th seems to differ from that of ^{230}Th. Activities of ^{230}Th are about ten times greater than activities of ^{232}Th (Table 16). ^{230}Th and ^{226}Ra are in equilibrium and it has been stated that the geochemistry of ^{226}Ra is entirely governed by the geochemical behaviour of ^{230}Th, if they are in equilibrium (MOLINARI & SNODGRASS 1990). This would mean, conversely, that the speciations of ^{226}Ra would reflect the speciations of ^{230}Th, pointing to different geochemical behaviour of ^{230}Th and ^{232}Th in the weathering products, which is implausible. It is more likely that the different activities of ^{230}Th and ^{232}Th in the weathering products, since the activities of ^{238}U and ^{232}Th are equal in the sandstones, result from a separation of the more mobile ^{238}U from

^{232}Th at the beginning of weathering processes. A higher proportion of ^{232}Th was left to in the weathering residue since thorium complexes are less soluble than uranium complexes. This is confirmed by high ^{232}Th activities in the weathered sample 127b. ^{238}U was transported over longer distances, until it was partly precipitated with or adsorbed by oxyhydroxides. The intense weathering of the Gedinnian sandstones must have been completed more than 10 000 years ago, because ^{230}Th and ^{226}Ra are in secular equilibrium. Nevertheless, it can be assumed that some relocation of radium took place in the weathering products, as the distribution of radium and thorium differs.

The results of this study disprove the suggestion made by GREEMAN & ROSE (1996), that radium in Fe oxides is produced by ^{230}Th in thick pedogenetic coatings, buried deeper than the ^{222}Rn recoil length. It is shown that thorium and radium are in fact both attributed to Fe oxides/hydroxides, from where radon can escape easily.

7.3.1.4 Gedinnian quartzite and quartz vein

Both of these samples consist primarily of quartz, which is accompanied in the quartzite **sample 133a** by low proportions of muscovite, clay minerals, chlorites, goethite, and hematite in the cement/matrix. Some opaque minerals occur in the thin section (Figure 49), most probably ore mineral grains. The quartz vein **sample 126** contains, besides quartz, red to reddish brown coatings on fracture surfaces and encrustations of hematite and ferrihydrite.
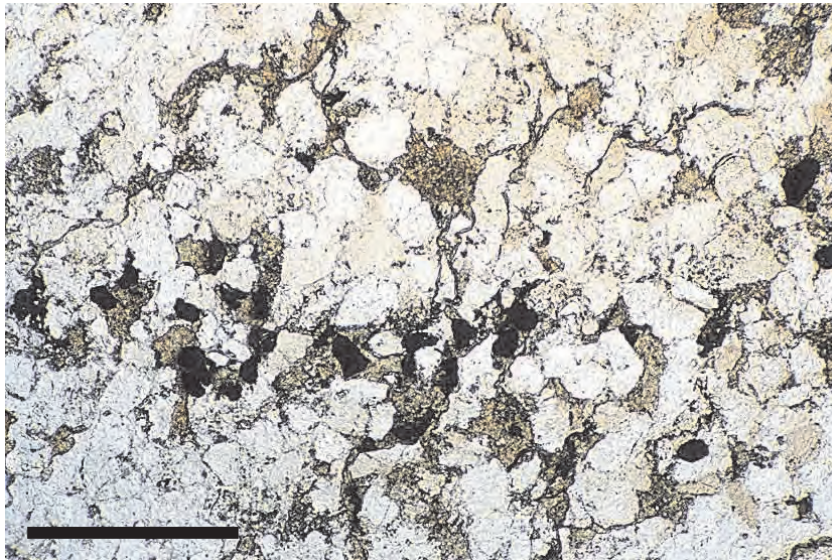
Figure 49: Fine-grained quartzite (133a) of Gedinnian age with strongly recrystallised, interlocked quartz crystals (mean ø 0.2 mm) coated by authigenic quartz in a cement/matrix of clay minerals, chlorite, some muscovite, goethite and hematite. The mono- and polycrystalline quartz crystals show sutured contacts and partly undulose extinction. In the lower part, a layer of opaque ore mineral grains occurs. Length of scale bar is 1 mm.

Table 31: Analytical results of the quartzite 133a. For analytical methods see Table 18.

133a	original sample	SD	I mobile exchangeable	SD	II exchangeable	SD	III Mn-Oxides	SD	IV organic matter	SD	V amorphous Fe oxides	SD	VI crystalline Fe oxides	SD	residual***
Al [ppm]	26880	*	NA²		31	0.3	39	6	166	8	1330	13	3071	65.6	< 22240
Mg [ppm]	9732	*	85	19	38	1	47	7	52	3	450	4	1272	21.80	7790
Fe [ppm]	32100	*	4	1	17	3	128	22	450	39	2577	96	5680	111.6	23240
Zn [ppm]	74	**	1.7	0.3	1.4	1	2.5	0.7	1.7	0.1	8.4	0.2	19.8	0.9	38
Ba [ppm]	64	**	7.3	0.6	1.3	0.04	3.2	0.5	0.5	0.02	1.5	0.04	0.9	0.02	49
Mn [ppm]	534	*	94.6	10.3	36.9	4.7	87.6	13.1	22.7	0.7	79.1	5.7	40.1	1.2	173
Pb [ppm]	18	**	< 0.1		1.7	0.1	4.3	0.7	1.7	0.1	3.1	0.2	2.4	0.2	4
As [ppm]	10	*	< 0.1		0.1	0.01	0.1	0.01	0.3	0.01	2.8	0.1	3.7	0.03	< 4
Ti [ppm]	1354	**	0.2	0.04	0.1	0.01	0.3	0.1	0.5	0.01	3.1	0.04	5.8	0.1	1344
Ni [ppm]	31	**	1.4	0.1	0.5	0.1	0.8	0.2	0.9	0.1	4.5	0.2	5.6	0.2	18
V [ppm]	21	**	< 0.1		< 0.1		0.1	0.02	0.1	0.01	1.3	0.03	2.8	0.1	17
Cu [ppm]	13	**	0.8	0.04	0.5	0.02	0.7	0.1	0.9	0.1	3.6	0.2	7.6	2.1	< 4
Rb [ppm]	6	**	0.2	0.01	< 0.1		0.1	0.01	< 0.1		0.1	0.002	0.1	0.005	< 15
Sr [ppm]	10	**	1.9	0.1	0.8	0.02	1.2	0.2	0.8	0.02	0.5	0.02	0.4	0.01	< 10
Y [ppm]	11	**	0.1	0.003	0.2	0.01	0.1	0.01	0.1	0.003	0.4	0.005	0.4	0.01	10
Zr [ppm]	102	**	0.1	0.01	< 0.1		0.1	0.02	0.1	0.01	1.8	0.03	2.5	0.02	97
Cs [ppm]	< 3	**	0.10	0.01	< 0.01		NA²		< 0.01		0.03	0.002	0.06	0.01	< 3
La [ppm]	22	**	0.08	0.002	0.09	0.003	0.05	0.01	0.04	0.002	0.27	0.01	0.48	0.01	21
Ce [ppm]	44		0.11	0.005	0.28	0.01	0.20	0.03	0.17	0.005	0.91	0.04	1.09	0.04	41
Dy [ppm]	NA¹		< 0.01		0.04	0.001	0.02	0.003	0.02	0.001	0.13	0.002	0.15	0.002	ND
Er [ppm]	NA¹		< 0.01		0.02	0.001	< 0.01		0.01	0.001	0.07	0.001	0.09	0.001	ND
Yb [ppm]	NA¹		< 0.01		0.01	0.001	< 0.01		< 0.01		0.08	0.001	0.08	0.001	ND
Hf [ppm]	NA¹		NA²		< 0.01		0.01	0.00	< 0.01		0.10	0.003	0.14	0.001	ND
Th [Bq/kg]	11.7		0.1	0.01	0.0	0.002	0.0	0.01	0.3	0.02	2.3	0.1	2.9	0.02	6
U [Bq/kg]	14.1		< 0.1		0.5	0.004	0.2	0.04	0.2	0.01	2.0	0.03	2.3	0.02	9
Ra [Bq/kg]	12.3		< 1.3		0.4	0.5	2.5	0.3	< 0.8		< 5.0		< 1.1		9

* standard deviation (SD) < 5 %; ** standard deviation (SD) < 10 %; *** standard deviation (SD) < 20 %
NA¹: element was not analysed; NA²: no calibration curve was obtained; ND = not detectable

The activities of uranium, radium and thorium in the quartzite are similar to each other (Table 31). In the quartz vein, Th and U activities are somewhat higher, at about 20 Bq/kg, while Ra is depleted (9 Bq/kg). While concentrations of trace elements are negligible in the quartz vein sample, about 3% of Al and Fe occur in the quartzite. They are likely to be bound to oxides/hydroxides, as the highest concentrations of Fe and Al occur in the fraction of the Fe oxides.

Uranium and thorium distribution in the quartzite 133a is similar to the distribution of both radionuclides in the Gedinnian sandstones (Figure 50), except for much lower activities in each fraction. The highest activities occur in the extraction residual, followed by the proportions in the Fe oxide fractions. The activities in all other fractions are negligible for both radionuclides.

The distribution of radium in the quartzite only differs from those of the Gedinnian sandstones at first sight. Apart from the most important proportion of radium in the extraction residual, the highest activities were found in the exchangeable fraction and the fraction of the Mn oxides. No radium was detectable in the other fractions (Figure 50). For samples with such low activities as are observed in this case (12 Bq/kg) a general problem for the association of radium with any fraction occurs, because the detection limits (0.8 – 1.5 Bq/kg) for most fractions are higher than the expected radium activities. The Gedinnian samples discussed so far, rarely showed more than 7% of total radium activity in one fraction, which

would result in 0.8 Bq/kg in this case. The lack of any detectable radium in the crystalline fraction might nevertheless be caused by the high density of the rock, which lacks any transecting fractures and consists mainly of quartz (Figure 49), as was the case for the quartzitic sandstone 124.
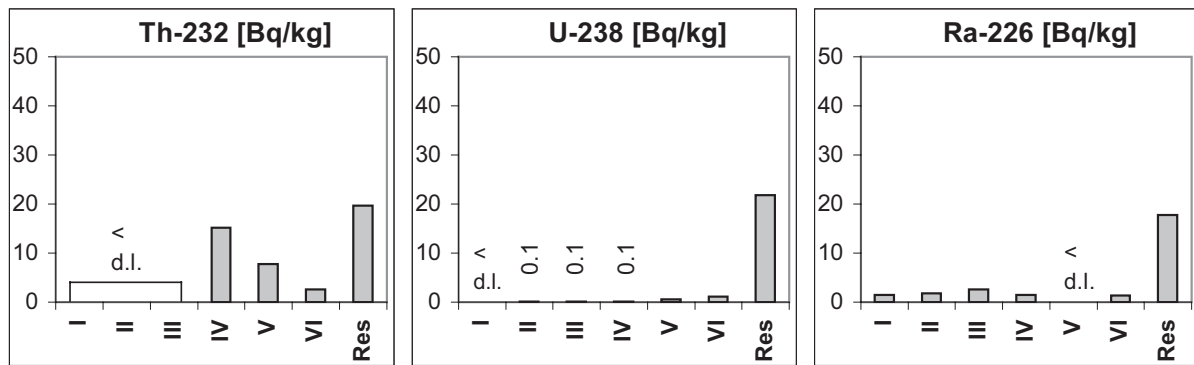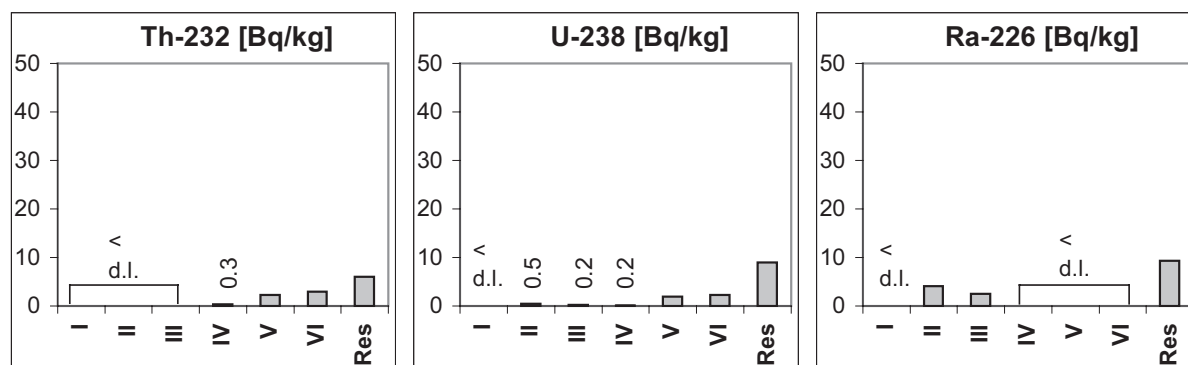

Figure 50: Radionuclide activities among extraction phases of sample 133a, a Gedinnian quartzite. (I = *mobile exchangeable*, **II =** *exchangeable*, **III =** *Mn oxides*, **IV =** *organic matter*, **V =** *amorphous Fe oxides*, **VI =** *crystalline Fe oxides, Res = extraction residual*)

The activity of radium in the fraction of the Mn oxides is similar to those in the other sandstones. Only the percentage is higher, which corresponds to relatively high concentrations of Mn in this fraction. The activity in the exchangeable fraction is nevertheless enhanced compared to the other Gedinnian samples, pointing to a stronger specific adsorption of radium to clay minerals in this sample.

The distribution of uranium and thorium in the quartz vein **sample 126**, which consists only of quartz with thin coatings of hematite and ferrihydrite, is about equal (Figure 51). The radionuclides are most abundant in the extraction residual. A higher mobility of uranium is nevertheless documented by a much lower activity in the extraction residual, though the total activities were about the same. The crystalline fraction is of secondary importance and in contrast to all other Gedinnian samples, the bonding to ferrihydrite is of no significance.

Table 32: Analytical results of the quartz vein sample126. For analytical methods see Table 18.

126	original sample	SD	I mobile exchangeable	SD	II exchangeable	SD	III Mn-Oxides	SD	IV organic matter	SD	V amorphous Fe oxides	SD	VI crystalline Fe oxides	SD	residual***
Al [ppm]	3452	*	NA²		6	0.3	8	1	47	2	113	4	229	4	< 3050
Mg [ppm]	< 600	*	53	3	31	3	27	2	25	0.4	43	1	104	2	< 600
Fe [ppm]	3659	*	2	0.1	43	16	73	6	653	36	629	4	1484	18	775
Zn [ppm]	19	**	1.3	0.1	0.9	0.2	2.0	0.5	NA²		1.8	0.3	7.9	0.4	< 5
Ba [ppm]	< 30	**	3.2	0.1	0.7	0.01	1.2	0.3	0.3	0.03	0.5	0.03	< 0.1		< 30
Mn [ppm]	< 230	*	96.1	5.6	30.4	9.8	33.3	7.9	27.9	6.6	39.7	0.2	10.9	0.5	< 300
Pb [ppm]	5	**	< 0.1		0.5	0.1	0.5	0.02	1.2	0.04	0.4	0.1	1.6	0.05	< 4
As [ppm]	12	*	< 0.1		< 0.1		< 0.1		0.7	0.1	1.2	0.1	7.5	0.1	< 4
Ti [ppm]	264	**	0.1	0.01	0.1	0.004	0.2	0.1	0.5	0.02	0.7	0.1	0.9	0.02	262
Ni [ppm]	17	**	2.1	0.1	0.7	0.1	1.1	0.1	1.9	0.2	1.9	0.3	4.7	0.1	4
V [ppm]	< 5	**	< 0.1		NA²		< 0.1		0.2	0.03	0.2	0.03	0.4	0.01	< 5
Cu [ppm]	4	**	0.6	0.01	1.0	0.01	0.7	0.2	1.5	0.2	1.4	0.2	NA²		< 4
Rb [ppm]	< 15	**	0.1	0.001	< 0.1		< 0.1		< 0.1		< 0.1		0.1	0.003	< 15
Sr [ppm]	< 10	**	2.0	0.1	1.1	0.1	1.0	0.05	1.1	0.02	0.4	0.02	0.5	0.02	< 10
Y [ppm]	< 10	**	0.1	0.01	0.1	0.01	0.0	0.05	0.2	0.01	0.3	0.01	0.4	0.01	< 10
Zr [ppm]	16	**	< 0.1		NA²		0.1	0.05	NA²		0.5	0.01	NA²		< 15
Cs [ppm]	< 3	**	0.02	0.001	< 0.01		< 0.01		< 0.01		< 0.01		0.04	0.001	< 3
La [ppm]	78	**	0.57	0.03	0.36	0.03	0.15	0.01	0.28	0.01	2.07	0.05	3.07	0.13	72
Ce [ppm]	> 150		0.86	0.07	1.05	0.08	0.39	0.03	0.77	0.01	4.74	0.11	6.97	0.30	ND
Dy [ppm]	NA¹		< 0.01		0.04	0.002	0.01	0.001	0.05	0.002	0.10	0.002	0.14	0.004	ND
Er [ppm]	NA¹		< 0.01		0.01	0.001	< 0.01		0.02	0.002	0.04	0.001	0.04	0.002	ND
Yb [ppm]	NA¹		< 0.01		0.01	0.001	< 0.01		0.01	0.001	0.02	0.001	0.03	0.001	ND
Hf [ppm]	NA¹		< 0.01		NA²		NA²		< 0.01		< 0.01		< 0.01		ND
Th [Bq/kg]	20.4		< 0.1		0.3	0.02	0.1	0.02	0.8	0.02	< 0.1		2.1	0.04	17
U [Bq/kg]	18.9		< 0.1		1.2	0.1	0.4	0.04	0.4	0.04	0.9	0.03	5.6	0.03	10
Ra [Bq/kg]	9.1		< 1.3		< 1.5		< 1.5		< 0.8		< 5.0	0.6	3.7	0.4	< 1

* standard deviation (SD) < 5 %; ** standard deviation (SD) < 10 %; *** standard deviation (SD) < 20 %
NA¹: element was not analysed; NA²: no calibration curve was obtained; ND = not detectable
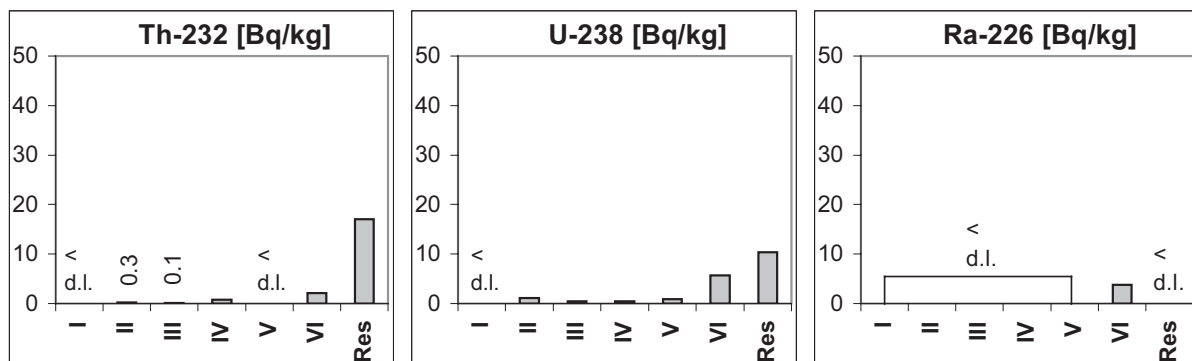
Figure 51: Radionuclide activities among extraction phases of a Quartz vein sample from Gedinnian host rock (126). (I = *mobile exchangeable*, II = *exchangeable*, III = *Mn oxides*, IV = *organic matter*, V = *amorphous Fe oxides*, VI = *crystalline Fe oxides, Res = extraction residual*)

Radium occurs with only half the activity of uranium in the total sample. It is detectable only in the fraction of the crystalline Fe oxides (Figure 51). As discussed for the quartzite 133a, the low overall activity of radium leads to a high percentage of undetectable radium in the single extraction phases. This result is therefore not discussed.

7.3.1.5 Gedinnian schist

Sample 131 was also taken from the outcrop in Hatrival. Only one rock sample was selected because schists are of minor importance in this geological unit.

Sample 131 shows much higher concentrations of Al, Mn, K, Na, Ti, Ba, Cr, Ga, Rb and Sr, as well as much lower concentrations of Si, Fe, As and Zn, reflecting higher concentrations of mica, clay minerals, chlorites and feldspars and lower concentrations of quartz and Fe oxides. The content of oxides and hydroxides of Al and Mn is increased, because not only higher total concentrations, but also higher concentrations in the oxide fractions occur (Table 33).

Table 33: Analytical results of the Gedinnian schist 131. For analytical methods see Table 18.

131	original sample	SD*	I mobile exchangeable	SD	II exchangeable	SD	III Mn-Oxides	SD	IV organic matter	SD	V amorphous Fe oxides	SD	VI crystalline Fe oxides	SD	residual***
Al [ppm]	202520	*	2	0.2	30	2	129	1	172	1	1052	8	710	4	200430
Mg [ppm]	2941	*	71	0.6	25	0.3	30	0.2	26	0.1	42	0.3	53	0.4	2693
Fe [ppm]	6330	*	< 1		< 1		114	1	22	0.3	141	1	588	3	5465
Zn [ppm]	35	**	0.7	0.01	1.0	0.1	17.3	0.06	2.4	0.08	4.0	0.1	3.6	0.2	< 8
Ba [ppm]	1489	**	9.9	0.05	2.5	0.3	37.5	0.02	1.0	0.01	4.8	0.04	2.9	0.03	1431
Mn [ppm]	1413	*	25.8	0.1	9.2	0.1	1196	2	19.0	0.2	79.1	0.1	84.4	0.2	< 233
Pb [ppm]	54	**	< 0.1		0.1	0.001	39.0	0.2	1.2	0.02	1.8	0.02	1.7	0.02	10
As [ppm]	7	**	< 0.1		< 0.1		0.3	0.01	0.2	0.01	1.6	0.01	2.6	0.02	< 4
Ti [ppm]	11850	*	0.2	0.01	< 0.1		1.1	0.02	0.6	0.01	< 0.1		2.2	0.05	11846
Ni [ppm]	45	**	0.3	0.01	0.2	0.01	17.3	0.03	1.2	0.01	9.6	0.01	11.3	0.2	5
V [ppm]	241	**	< 0.1		< 0.1		0.7	0.02	0.1	0.002	1.2	0.01	0.9	0.01	238
Cu [ppm]	12	**	0.1	0.004	0.6	0.01	11.8	0.05	1.3	0.02	2.2	0.003	NA[2]		< 4
Rb [ppm]	316	**	2.1	0.01	0.2	0.001	0.3	0.005	0.2	0.001	0.5	0.01	0.7	0.00	312
Sr [ppm]	610	**	5.7	0.02	1.4	0.01	2.4	0.01	1.3	0.01	2.6	0.01	1.5	0.01	595
Y [ppm]	63	**	0.3	0.001	0.5	0.01	0.5	0.003	0.2	0.002	1.3	0.004	1.6	0.01	59
Zr [ppm]	548	**	< 0.1		< 0.1		2.4	0.03	3.8	0.02	15.5	0.002	NA[2]		< 527
Cs [ppm]	22	**	0.88	0.004	0.07	0.001	0.07	0.001	0.03	0.001	0.06	0.001	0.13	0.003	21
La [ppm]	76	**	0.11	0.001	0.13	0.001	0.20	0.003	0.07	0.001	1.18	0.003	1.35	0.005	73
Ce [ppm]	87	**	0.14	0.003	0.34	0.003	2.00	0.01	0.20	0.002	3.29	0.005	3.50	0.02	78
Dy [ppm]	NA[1]		0.03	0.001	0.12	0.002	0.16	0.002	0.04	0.002	0.47	0.001	0.41	0.01	ND
Er [ppm]	NA[1]		0.02	0.001	0.06	0.002	0.08	0.001	0.02	0.001	0.19	0.003	0.21	0.01	ND
Yb [ppm]	NA[1]		< 0.01		0.04	0.001	0.07	0.005	0.02	0.001	0.17	0.001	0.20	0.003	ND
Hf [ppm]	NA[1]		< 0.01		< 0.01		0.08	0.01	0.18	0.001	0.87	0.01	0.76	0.003	ND
Th [Bq/kg]	143		< 0.1		0.8	0.003	1.6	0.1	2.6	0.03	39.8	1.0	13.3	0.6	85
U [Bq/kg]	74.2		< 0.1		2.0	0.02	1.2	0.002	0.6	0.01	6.7	0.02	6.9	0.04	57
Ra [Bq/kg]	76.5		5.2	0.7	2.7	0.4	11.5	1.1	1.6	0.2	< 5.0	0.6	1.9	0.3	54

* standard deviation (SD) < 5 %; ** standard deviation (SD) < 10 %; *** standard deviation (SD) < 20 %
NA[1]: element was not analysed; NA[2]: no calibration curve was obtained; ND = not detectable

Uranium and radium activities in the schist are a little higher (75 Bq/kg) relative to the Gedinnian sandstones. While uranium and radium are in equilibrium, thorium is twice as high (Table 33).

Thorium distribution in the schist does not differ significantly from that in the Gedinnian sand- and siltstones. Only negligible activities occur in the first four fractions, while the extraction residual is of most importance. The activities in the Fe oxide fractions are nevertheless higher, especially for the fraction of the amorphous Fe oxides. Only low Fe concentrations, but high Al concentrations, occur in this extraction step, so it can be deduced that Th is bound to amorphous Al hydroxides rather than to Al substituted ferrihydrite (Table 33). It is unlikely that Th and Al are associated with clay minerals in this step, as only

negligible proportions of silicates are dissolved in this extraction step (LANDA & GAST 1973; MCKEAGUE & SCHUPPLI 1985).
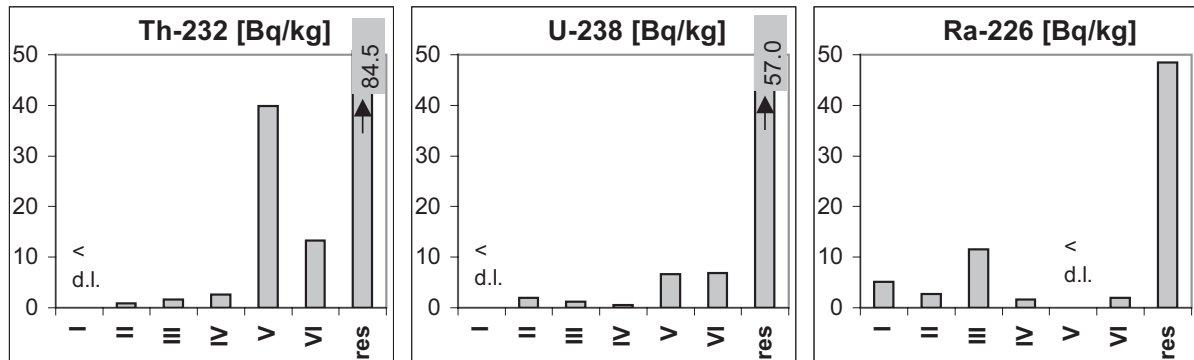
Figure 52: Radionuclide activities among extraction phases of Gedinnian schist 131. (I = *mobile exchangeable*, II = *exchangeable*, III = *Mn oxides*, IV = *organic matter*, V = *amorphous Fe oxides*, VI = *crystalline Fe oxides, Res = extraction residual*)

The distribution of uranium in sample 131 is different. By far the highest proportion of the uranium occurs in the extraction residual and only low proportions are dissolved during sequential extraction (Figure 52). Due to the at least five times lower content of Fe oxides, activities of uranium occurring in the Fe oxide fractions are much lower than for the Gedinnian sand- and siltstones.

As for the Gedinnian sandstones, radium distribution in the rock is obviously different from uranium distribution. Besides highest activities in the extraction residual, radium is most abundant in the Mn oxide fraction, followed by the mobile exchangeable phase. A high content of Mn oxides in this sample is confirmed by a Mn concentration more than eight times higher in fraction III than in the other Gedinnian samples. Mn oxides primarily occur on the rock fragment surfaces together with Fe oxides/hydroxides as dark brown to nearly black encrustations.

7.3.2 Siegenian schist and weathering product

A silty schist of Siegenian age (*Sg2*) (**sample 77c**) and its weathering product (**sample 77a**) were sampled from the northwestern part of Luxembourg, because relatively high indoor radon activities occur above the *Sg2* (median *Sg2*: 218 Bq/m^3 - median Eisléck: 128 Bq/m^3; unpublished data, Radiation Protection Department of Luxembourg).

Compared to the Gedinnian schist, concentrations of Al, K, Mn, Na, Ti, Ba, Sr and Rb are lower, but concentrations of Si, Fe and Mg are much higher.

The Siegenian schist shows about five times lower activities of all three radionuclides than the Gedinnian schist. Uranium and radium are in equilibrium and thorium activity is more than twice as high (Table 34).

By far the most thorium is found in the extraction residual (Figure 53). Compared to the Gedinnian schist, about 20% less thorium is dissolved. Thorium can be attributed to a higher percentage to clay minerals and silicates, which remain in the extraction residual. Accordingly, lower proportions of thorium occur in the extraction phases. In agreement with the Gedinnian schist, most thorium was determined in the fraction of the amorphous Fe oxides, matching with the highest Fe concentrations.

Uranium in the Siegenian schist is, in contrast to thorium, about 15% more soluble than in the Gedinnian schist. The distribution of uranium among the extraction phases is nevertheless not significantly different to the Gedinnian schist, apart from the lower activities (Figure 53).

Radium activities in all of the extraction phases are below the detection limits. All of the radium can be attributed to the extraction residual. As for the Gedinnian quartzite and the quartz vein, the detection limits of most fractions are higher than the expected radium activities. This result is therefore not discussed further.

In the weathered silty schist (77a) all radionuclide activities are higher. Uranium and radium are in equilibrium, whereas the thorium activity is higher. The enrichment factors are nonetheless drastically lower than for the Gedinnian weathering products, and about the same for U, Ra and Th (1.3 – 1.4).

The distribution of uranium and thorium in the weathering product is nearly equal to that of the parent rock (Figure 53). Compared to the rock sample, about the same activities were determined in the various extraction steps, leading to higher activities in the extraction residual (Table 34).

Table 34: Analytical results of the Siegenian silty schist (77c) and its weathering product (77a). For analytical methods see Table 18.

77c	original sample	SD	I mobile exchangeable	SD	II exchangeable	SD	III Mn-Oxides	SD	IV organic matter	SD	V amorphous Fe oxides	SD	VI crystalline Fe oxides	SD	residual***
Al [ppm]	65230	*	3	0.2	116	1	32	0.3	844	4	NA²		3488	8	< 60740
Mg [ppm]	18130	*	116	1	54	1	38	0.1	144	0.3	1464	13	1475	4	14830
Fe [ppm]	52830	*	NA²		NA²		89	0.4	809	1	7188	83	4825	4	< 39920
Zn [ppm]	146	**	< 0.1		< 0.1		1.6	0.1	6.3	0.1	22.4	0.3	20.0	0.2	96
Ba [ppm]	182	**	4.0	0.1	0.8	0.01	0.7	0.01	0.7	0.001	1.7	0.1	0.6	0.004	173
Mn [ppm]	748	*	7.5	0.03	4.2	0.05	7.8	0.02	13.5	0.1	58.4	0.6	57.5	0.1	600
Pb [ppm]	48	**	< 0.1		0.4	0.005	0.5	0.01	1.0	0.01	3.6	0.1	4.8	0.1	38
As [ppm]	7	*	< 0.1		< 0.1		< 0.1		0.3	0.001	4.8	0.1	0.6	0.02	< 4
Ti [ppm]	3616	**	< 0.1		< 0.1		0.2	0.01	1.3	0.01	NA²		4.7	0.1	< 3610
Ni [ppm]	73	**	0.2	0.01	0.3	0.02	0.1	0.01	1.8	0.02	10.2	0.01	8.8	0.04	51
V [ppm]	61	**	< 0.1		< 0.1		< 0.1		0.8	0.01	3.7	0.1	2.2	0.03	54
Cu [ppm]	22	**	0.1	0.01	0.3	0.01	0.4	0.01	1.1	0.01	7.8	0.01	NA²		< 13
Rb [ppm]	46	**	0.7	0.003	0.1	0.002	0.1	0.001	0.1	0.001	0.3	0.00	0.2	0.002	45
Sr [ppm]	19	**	1.3	0.001	0.9	0.01	0.8	0.001	0.8	0.01	0.5	0.01	0.8	0.02	14
Y [ppm]	25	**	< 0.1		0.1	0.004	< 0.1		0.1	0.002	0.4	0.004	0.3	0.003	25
Zr [ppm]	273	**	< 0.1		< 0.1		< 0.1		NA²		NA²		NA²		< 273
Cs [ppm]	7	**	0.04	0.001	< 0.01		0.01	0.001	< 0.01		0.02	0.001	0.07	0.002	7
La [ppm]	36	**	0.02	0.001	0.07	0.001	0.03	0.001	0.11	0.001	0.38	0.01	0.29	0.004	35
Ce [ppm]	50		0.02	0.002	0.12	0.001	0.06	0.002	0.22	0.002	0.73	0.01	0.48	0.003	49
Dy [ppm]	NA¹		< 0.01		0.02	0.001	< 0.01		0.03	0.001	0.10	0.003	0.06	0.002	ND
Er [ppm]	NA¹		< 0.01		< 0.01		< 0.01		0.02	0.001	0.05	0.001	0.03	0.001	ND
Yb [ppm]	NA¹		< 0.01		< 0.01		< 0.01		0.01	0.001	0.05	0.001	0.03	0.002	ND
Hf [ppm]	NA¹		< 0.01		< 0.01		< 0.01		< 0.01		0.10	0.003	< 0.01		ND
Th [Bq/kg]	34.7		< 0.1		0.1	0.002	0.1	0.01	1.0	0.1	4.3	0.2	1.2	0.1	28
U [Bq/kg]	15.7		< 0.1		0.3	0.001	0.1	0.005	0.2	0.003	1.7	0.004	3.1	0.002	10
Ra [Bq/kg]	14.1		< 1.3		< 1.5		< 1.5		< 0.8		< 5.0		< 1.1		14

* standard deviation (SD) < 5 %; ** standard deviation (SD) < 10 %; *** standard deviation (SD) < 20 %
NA¹: element was not analysed; NA²: no calibration curve was obtained; ND = not detectable

77a	original sample	SD	I mobile exchangeable	SD	II exchangeable	SD	III Mn-Oxides	SD	IV organic matter	SD	V amorphous Fe oxides	SD	VI crystalline Fe oxides	SD	residual***
Al [ppm]	99820	*	6	0.1	< 1		39	0.4	522	3	2985	7	3592	48	92680
Mg [ppm]	15990	*	101	1	< 1		32	0.3	68	1	756	5	1664	24	13370
Fe [ppm]	55970	*	< 1		NA²		81	1	340	2	5675	41	5188	14	< 44690
Zn [ppm]	166	**	< 0.1		< 0.1		2.8	0.1	6.0	1.8	16.3	0.3	27.5	0.2	113
Ba [ppm]	538	**	6.5	0.002	1.2	0.01	1.1	0.02	0.7	0.01	3.0	0.02	0.7	0.02	525
Mn [ppm]	743	*	8.3	0.04	4.5	0.01	13.0	0.02	10.4	0.02	38.8	0.2	64.3	0.2	604
Pb [ppm]	67	**	< 0.1		0.5	0.005	0.6	0.05	0.9	0.01	15.4	0.1	16.8	0.3	33
As [ppm]	11	*	< 0.1		< 0.1		< 0.1		0.2	0.01	8.1	0.01	1.2	0.01	< 4
Ti [ppm]	5258	**	< 0.1		0.1	0.02	0.2	0.01	1.1	0.02	8.5	0.1	4.6	0.01	5243
Ni [ppm]	91	**	0.2	0.001	0.3	0.01	0.2	0.004	1.2	0.03	9.8	0.1	12.8	0.1	67
V [ppm]	122	**	< 0.1		< 0.1		0.1	0.01	0.6	0.01	3.9	0.02	2.0	0.02	115
Cu [ppm]	35	**	0.1	0.001	0.3	0.01	0.4	0.005	1.0	0.01	10.4	0.02	NA²		< 22
Rb [ppm]	157	**	1.4	0.01	0.1	0.001	0.2	0.003	0.1	0.002	0.6	0.01	0.3	0.01	154
Sr [ppm]	32	**	1.6	0.01	1.1	0.003	0.7	0.01	0.9	0.004	0.6	0.01	0.6	0.02	27
Y [ppm]	33	**	< 0.1		< 0.1		< 0.1		0.1	0.002	0.4	0.001	0.3	0.004	32
Zr [ppm]	186	**	< 0.1		0.1	0.002	< 0.1		NA²		NA²		< 0.1		< 186
Cs [ppm]	8	**	0.07	0.001	< 0.01		0.02	0.001	< 0.01		0.03	0.001	0.05	0.001	8
La [ppm]	42	**	0.01	0.001	0.05	0.001	0.04	0.01	0.07	0.001	0.36	0.003	0.35	0.01	41
Ce [ppm]	59		0.01	0.001	0.09	0.001	0.07	0.01	0.15	0.001	0.73	0.004	0.59	0.01	57
Dy [ppm]	NA¹		< 0.01		0.01	0.001	< 0.01		0.02	0.001	0.11	0.002	0.07	0.002	ND
Er [ppm]	NA¹		< 0.01		< 0.01		< 0.01		< 0.01		0.06	0.001	0.03	0.001	ND
Yb [ppm]	NA¹		< 0.01		< 0.01		< 0.01		< 0.01		0.06	0.001	0.03	0.001	ND
Hf [ppm]	NA¹		< 0.01		< 0.01		< 0.01		< 0.01		NA²		< 0.01		ND
Th [Bq/kg]	49.0		< 0.1		0.2	0.01	0.1	0.01	1.0	0.1	4.9	0.1	2.3	0.2	40
U [Bq/kg]	21.5		< 0.1		0.4	0.01	0.2	0.004	0.1	0.0	2.1	0.0	3.3	0.0	15
Ra [Bq/kg]	18.2		< 1.3		< 1.5		2.6	0.3	< 0.8		< 8.4		3.6	0.4	12

* standard deviation (SD) < 5 %; ** standard deviation (SD) < 10 %; *** standard deviation (SD) < 20 %
NA¹: element was not analysed; NA²: no calibration curve was obtained; ND = not detectable

Apart from having the highest activities in the extraction residual, radium was found in the Mn oxide phase and the crystalline Fe fraction. Activities in all other fractions were below the detection limit. The affinity of radium to oxides of Fe and Mn is as high as for the

Gedinnian weathering products, whereas the bonding in the mobile exchangeable fraction is of less importance (Figure 53).

silty schist (77c)
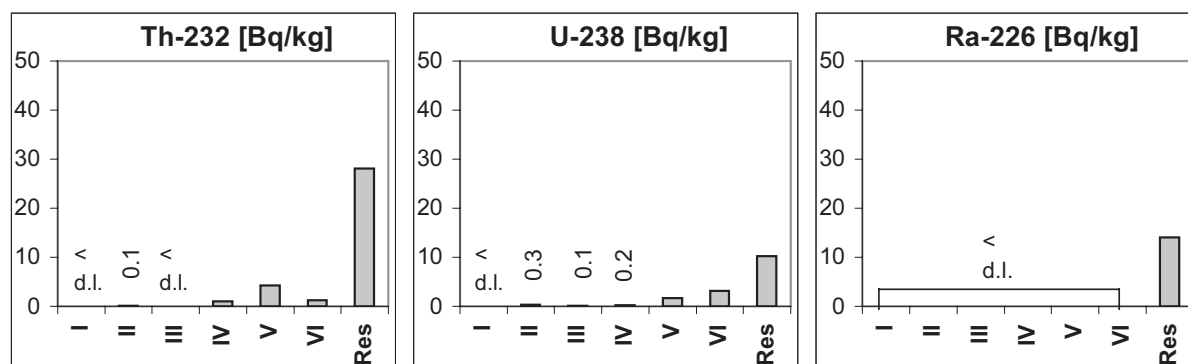
weathered silty schist (77a)
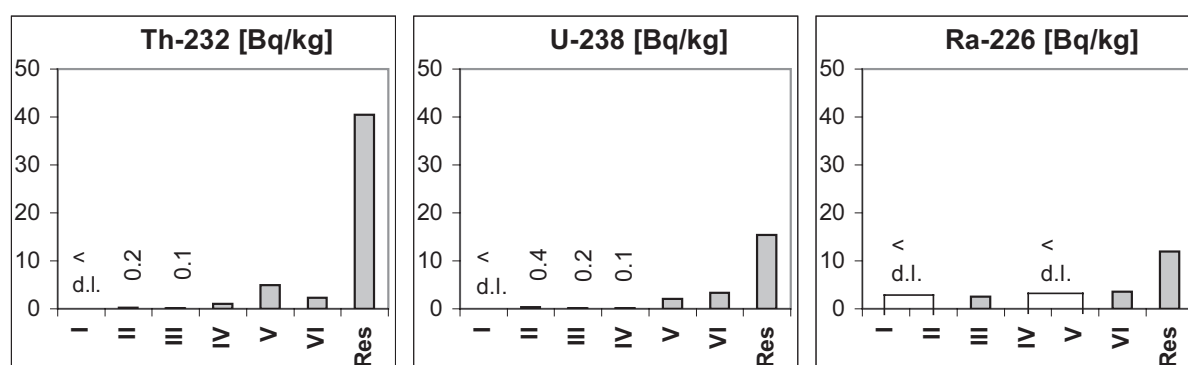
Figure 53: Radionuclide activities among extraction phases of Siegenian silty schist (77c) and its weathering product (77a). (I = *mobile exchangeable*, II = *exchangeable*, III = *Mn oxides*, IV = *organic matter*, V = *amorphous Fe oxides*, VI = *crystalline Fe oxides, Res = extraction residual*)

The results of the Siegenian samples show some strong distinctions to the Gedinnian samples. Apart from five times lower overall activities and the differences of the distribution of uranium and thorium in the rock sample, the enrichment factors for Th, U and Ra in the weathering product are drastically lower. The speciations of thorium are about the same for the Siegenian and the Gedinnian weathering products, but radium, and especially uranium, show inconsistent distributions. Whereas uranium in the Gedinnian weathering products occurred preferentially in the fractions of the Fe oxides and only low proportions - less than 10% - were determined in the extraction residual, the latter fraction is of the greatest significance (70%) for the Siegenian weathered silty schist.

The differences in distribution can be explained by the differences in mineral composition. Though Fe concentrations are as high as for sample 134 (weathered Gedinnian sandstone), only about 10% of the total iron was determined in each fraction of the Fe oxides. Not only is the amount of Fe oxides/hydroxides low in comparison to the Gedinnian weathered materials, but even more drastically, the amounts of Mn- and Ti oxides. The elements are instead attributed to silicate minerals remaining in the extraction residual.

7.3.3 Mesozoic sandstones

Many Mesozoic stratigraphic units contain mainly carbonatic rocks, which are not suitable for sequential extraction. Not only the extraction scheme developed by ZEIEN (1995), but also most other extraction schemes, require samples with less than 5% carbonate. A fairly widespread rock type in the Gutland is the Luxembourg sandstone (*li2*), which has been investigated in an earlier study by ROTH (1997). The sequential extraction scheme used in the previous survey was different from the one used in this thesis (see Chapter 7.1.1), but the results for the Luxembourg Sandstone were plausible and further investigations within the current thesis were not considered necessary.

ROTH (1997) investigated a soil profile above Luxembourg Sandstone located in Ernzen, Germany (r ^{25} 31 185/ h ^{55} 21 290), close to the border with Luxembourg. The soil type is pseudogley.

Table 35: Profile description of Luxembourg sandstone (li2). Horizon description after „Bodenkundliche Kartieranleitung" (AG BODENKUNDE 1982), soil type description after US-Soil Taxonomy.

horizon	soil type	comments
Ap (0-25 cm)	slightly loamy sand	Mn-Fe concretions
SBv (25-56 cm)	sandy loam	Mn/Fe concretions, Depletion of clay minerals
BtS (56-94 cm)	loamy sand	Mn/Fe concretions, coatings of clay on soil aggregates, accumulation of clay minerals
(S)Bv (94-126 cm)	sandy loam	Mn/Fe concretions up to 1 cm diameter
Cv (> 126 cm)	sandstone	

The **Luxembourg sandstone (*li2*)** is siliceous sandstone with calcitic cement. Unweathered sandstone contains up to 30% $CaCO_3$, but consists mainly of quartz. Up to 10% heavy minerals occur in the Luxembourg sandstone (*li2*), e.g. zircon, tourmaline, rutile, garnet, anatase, brookite and staurolite (ROTH 1997; JUNGERIUS 1958). The radionuclide concentrations are rather low (Th < 14 Bq/kg; U < 26 Bq/kg; Ra < 22 Bq/kg), except for the layer of the "surface taraudée" (Th: 26 Bq/kg; U: 118 Bq//kg; Ra: 121 Bq//kg).

Sequential extraction by ROTH (1997) shows that radium in the **rock sample** of the Luxembourg sandstone (*li2*) is mainly bound to Mn oxyhydroxides and partially adsorbed

onto clay minerals. About 71% of total radium remains in the extraction residual, which consists, for the extraction scheme used, primarily of detrital, primary and secondary minerals (e.g. crystalline Fe oxides, quartz, zircon, pedogenic clay minerals) and stable organic compounds.

Eighty seven percent of total uranium is left in the extraction residual. Dissolved uranium was found in the fraction of Mn oxyhydroxides (8%) and in the organic fraction (5%). In the latter silicatic minerals are also dissolved, which is most probably the reason for uranium being found in this fraction, as no correlation to carbon could be established.

A much lower percentage (30%) of thorium is left in the extraction residual. Sequential extraction does not provide sufficient information about the speciation of thorium, but significant positive correlation of thorium with potassium led to the conclusion that thorium was most probably adsorbed onto clay minerals (ROTH 1997).

About 84% of total iron was found in the extraction residual; it can therefore be assumed, that uranium, radium and thorium were partly bound in crystalline Fe oxides.
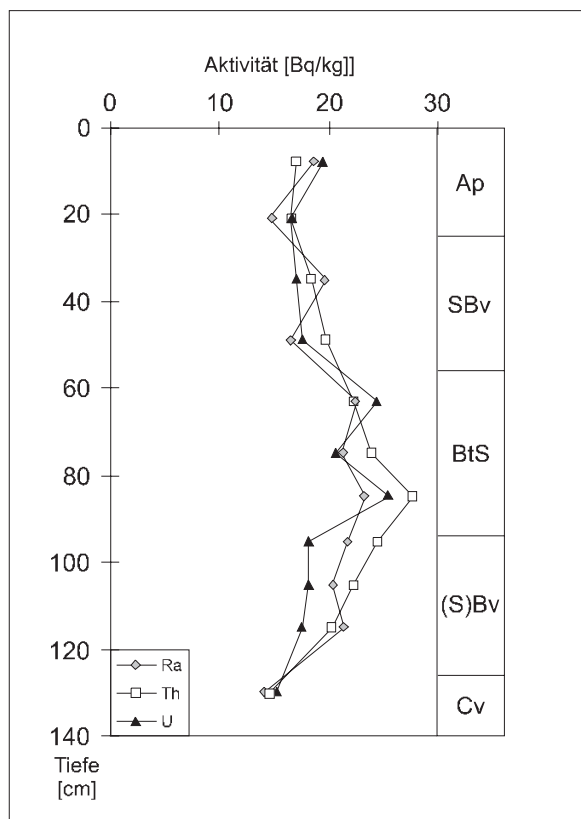
Figure 54: Activities of Ra, Th und U in the soil profile of the Luxembourg Sandstone (li2) (AP = disturbance by ploughing; SBv = weathering horizon with depletion of clay minerals, gleying; BtS = weathering horizon with accumulation of clay minerals, gleying; (S)Bv = accumulation of clay minerals, slight gleying; Cv = sligthly weathered rocks).

The dominant mineral in the **soil samples/weathering products** of the *li2* is quartz. Accompanying minerals are illite, feldspar, ore mineral grains of Fe-/Mn oxides and some kaolinite and chlorite. Carbonate concentrations are very low (Ca oxide 0.2 - 0.4 [weight%]). Carbonate is dissolved during weathering and often precipitated in clefts in the sandstone.

The survey by ROTH (1997) revealed that in the course of weathering, pedogenic clay minerals are accumulated in the BtS horizon. Fe and Mn oxyhydroxides are precipitated as coatings on mineral grains, in voids, and along fractures if the permeability of soils is low, or as concretions in the soils if the permeability is high. All radionuclides are up to twice as high, which is also the case for the samples investigated in this thesis.

Radium in the weathering products is bound to Mn oxyhydroxides, to clay minerals and most probably to crystalline Fe oxides.

Uranium is found mainly in the extraction residual, as is thorium. Uranium is also found in the oxidic phase.

Sequential extraction together with analysis of correlation shows that the radionuclides are significantly positively correlated with typical terrigenous elements such as Al, K, Ti, Ce, Ga, Rb, Y. Precipitation with Fe and Mn oxyhydroxides appears to be only of second importance.

For the investigations in this thesis, samples of Buntsandstein age have been selected. **Upper Buntsandstein** outcrops are relatively widespread in river valleys and along the border to the Devonian basement in the north of Luxembourg.
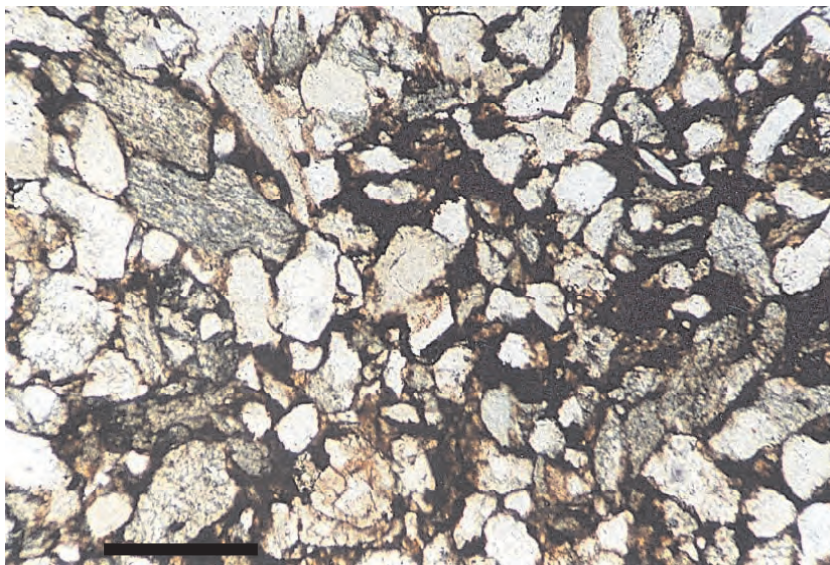
Figure 55: Fine-grained sandstone of Buntsandstein (Lower Triassic) age (98). Badly sorted quartz crystals and detritus of Palaeozoic rocks coated with hematite. The detritus consists partly of fragments of sandstones and partly of foliated rock fragments, as shown by the internal grain fabric. Length of scale bar is 200 µm.

The sandstone **sample 98** consists of badly sorted quartz crystals and detritus of Palaeozoic rocks, which are coated with hematite (Figure 55). Besides quartz, other dominant minerals are chlorites, illite and kaolinite. Heavy minerals are less abundant than in the Luxembourg Sandstone and the Devonian samples, with anatase, rutile and titanite as major representatives.

Uranium and radium in the rock and in the weathering product (**sample 102**) are in equilibrium, while thorium activities are about twice as high (Table 36).

Although thorium activities are elevated in the weathering product, the speciations do not differ from those in the parent sandstone. Activities in the first three fractions are negligible and thorium is most abundant in the extraction residual. As was the case for the Siegenian samples, about 15% more thorium is left in the extraction residual than in the Gedinnian samples and the excess thorium in the weathering product is found in the extraction residual.

The highest activities among the extraction phases were determined in the crystalline Fe oxide fraction and in the organic fraction, even for the rock sample, though C_{org} is < 1% for both. One Gedinnian sandstone (127a) showed high proportions of thorium in the organic fraction, too (Table 25). Hardly any relationship can be established between these two sandstones and no specific elements occur with unusual concentrations in the organic fraction of either sandstone.

Uranium activity in the weathering product is 1.6 times higher than in the sandstone, but bound in similar fractions (Figure 56). Speciations resemble those of the Siegenian silty schist and the excess uranium activity occurs in the extraction residual.

Table 36: Analytical results of sandstone 98 of Buntsandstein age (*so*) and its weathering product (102). For analytical methods see Table 18.

98	original sample	SD	I mobile exchangeable	SD	II exchangeable	SD	III Mn-Oxides	SD	IV organic matter	SD	V amorphous Fe oxides	SD	VI crystalline Fe oxides	SD	residual***
Al [ppm]	58620	*	9	1	37	0.4	8	0.3	317	0.1	NA[2]		1282	8	< 56970
Mg [ppm]	11770	*	362	1	93	0.0	51	0.3	64	0.1	254	1	686	3	10260
Fe [ppm]	30660	*	28	10	NA[2]		33	0.3	166	1	971	7	12074	22	< 17390
Zn [ppm]	49	**	0.4	0.05	< 0.1		0.4	0.03	1.0	0.1	2.1	0.2	2.6	0.1	43
Ba [ppm]	267	**	8.7	0.03	1.4	0.01	1.0	0.03	0.6	0.02	1.1	0.01	0.6	0.01	254
Mn [ppm]	262	*	11.7	0.04	10.4	0.01	2.0	0.01	2.5	0.01	5.9	0.02	23.2	0.1	206
Pb [ppm]	7	**	< 0.1		< 0.1		< 0.1		0.4	0.004	0.3	0.01	1.6	0.04	5
As [ppm]	5	*	< 0.1		< 0.1		< 0.1		0.4	0.005	1.0	0.02	0.8	0.01	< 4
Ti [ppm]	4168	**	< 0.1		NA[2]		0.3	0.02	1.5	0.04	NA[2]		121	0.23	< 4045
Ni [ppm]	43	**	0.6	0.03	0.6	0.002	0.2	0.004	0.6	0.02	1.9	0.03	4.6	0.01	34
V [ppm]	65	**	< 0.1		< 0.1		< 0.1		0.3	0.01	1.3	0.004	8.1	0.03	56
Cu [ppm]	4	**	0.1	0.01	0.3	0.01	0.3	0.01	0.3	0.01	0.8	0.004	NA[2]		< 4
Rb [ppm]	77	**	1.3	0.01	0.2	0.003	0.4	0.003	0.1	0.003	0.3	0.003	0.5	0.005	74
Sr [ppm]	99	**	2.4	0.02	1.1	0.27	0.9	0.005	1.8	0.01	0.4	0.03	1.1	0.001	92
Y [ppm]	27	**	< 0.1		0.2	0.002	0.1	0.001	0.8	0.005	0.3	0.001	0.4	0.001	25
Zr [ppm]	295	**	< 0.1		< 0.1		< 0.1		NA[2]		NA[2]		NA[2]		< 295
Cs [ppm]	14	**	0.84	0.01	0.08	0.001	0.22	0.003	0.06	0.001	0.10	0.001	0.22	0.002	12
La [ppm]	42	**	NA[2]		0.13	0.01	0.04	0.001	0.30	0.002	0.16	0.001	0.26	0.001	< 41
Ce [ppm]	92		NA[2]		0.28	0.001	0.10	0.004	0.91	0.003	0.39	0.01	0.56	0.002	< 90
Dy [ppm]	NA[1]		< 0.01		0.05	0.001	0.02	0.001	0.25	0.001	0.06	0.001	0.08	0.002	ND
Er [ppm]	NA[1]		< 0.01		0.02	0.001	< 0.01		0.07	0.001	0.04	0.001	0.06	0.003	ND
Yb [ppm]	NA[1]		< 0.01		0.02	0.002	< 0.01		0.04	0.001	0.04	0.001	0.07	0.003	ND
Hf [ppm]	NA[1]		< 0.01		< 0.01		< 0.01		0.01	0.002	0.13	0.001	< 0.01		ND
Th [Bq/kg]	41.0		< 0.1		0.2	0.01	0.1	0.005	3.1	0.1	1.3	0.04	3.2	0.3	33
U [Bq/kg]	20.2		< 0.1		0.4	0.001	0.1	0.01	0.2	0.002	0.6	0.003	6.9	0.0	12
Ra [Bq/kg]	23.0		< 1.3		2.0	0.3	2.4	0.4	2.5	0.4	< 5.0		3.3	0.5	13

* standard deviation (SD) < 5 %; ** standard deviation (SD) < 10 %; *** standard deviation (SD) < 20 %
NA[1]: element was not analysed; NA[2]: no calibration curve was obtained; ND = not detectable

102	original sample	SD	I mobile exchangeable	SD	II exchangeable	SD	III Mn-Oxides	SD	IV organic matter	SD	V amorphous Fe oxides	SD	VI crystalline Fe oxides	SD	residual***
Al [ppm]	80453	*	11	1	29	0.2	21	1	591	1	1717	11	1620	6	76465
Mg [ppm]	15250	*	518	4	705	3	78	1	109	0.3	489	1	759	4	12592
Fe [ppm]	45624	*	34	1	< 1		56	0.3	377	2	2590	11	15980	611	26586
Zn [ppm]	71	**	1.0	0.1	0.3	0.01	0.9	0.02	2.2	0.1	3.8	0.6	5.1	0.1	57
Ba [ppm]	404	**	24.3	0.1	3.7	0.05	1.7	0.01	0.8	0.01	3.3	0.004	1.4	0.03	369
Mn [ppm]	383	*	5.1	0.02	31.8	0.8	6.4	0.02	15.8	0.1	18.6	0.1	46.1	1.1	259
Pb [ppm]	12	**	< 0.1		0.1	0.003	0.1	0.005	1.0	0.02	1.0	0.001	2.6	0.02	8
As [ppm]	15	*	0.1	0.01	0.1	0.001	0.1	0.02	1.5	0.02	6.8	0.03	2.3	0.02	4
Ti [ppm]	5521	**	< 0.1		< 0.1		0.7	0.1	2.3	0.04	15.4	0.1	154	3	5348
Ni [ppm]	56	**	0.4	0.01	1.0	0.001	0.2	0.01	1.2	0.01	3.9	0.02	5.1	0.04	44
V [ppm]	98	**	< 0.1		< 0.1		0.3	0.04	0.6	0.003	3.5	0.003	12.8	0.05	80
Cu [ppm]	12	**	0.1	0.003	0.2	0.01	0.3	0.01	0.8	0.01	1.3	0.02	< 0.1		9
Rb [ppm]	127	**	3.4	0.01	0.4	0.001	0.7	0.01	0.2	0.003	1.0	0.01	0.9	0.01	120
Sr [ppm]	211	**	4.0	0.03	1.7	0.02	1.1	0.02	1.9	0.01	0.8	0.01	1.5	0.02	200
Y [ppm]	37	**	< 0.1		0.3	0.003	0.1	0.002	1.2	0.005	0.5	0.002	0.4	0.00	35
Zr [ppm]	482	**	< 0.1		< 0.1		< 0.1		< 0.1		< 0.1		< 0.1		482
Cs [ppm]	19	**	2.14	0.01	0.27	0.002	0.41	0.004	0.10	0.001	0.33	0.002	0.35	0.001	16
La [ppm]	67	**	< 0.01		0.16	0.003	0.05	0.001	0.49	0.001	0.32	0.001	0.27	0.002	65
Ce [ppm]	118		NA[2]		0.31	0.004	0.10	0.001	1.35	0.01	0.75	0.003	0.59	0.01	114
Dy [ppm]	NA[1]		< 0.01		0.05	0.001	0.02	0.001	0.33	0.001	0.12	0.003	0.09	0.001	ND
Er [ppm]	NA[1]		< 0.01		0.02	0.001	< 0.01		0.11	0.001	0.07	0.001	0.07	0.001	ND
Yb [ppm]	NA[1]		< 0.01		0.02	0.001	< 0.01		0.07	0.001	0.07	0.001	0.07	0.001	ND
Hf [ppm]	NA[1]		< 0.01		< 0.01		< 0.01		0.07	0.003	< 0.01		0.06	0.01	ND
Th [Bq/kg]	58.7		< 0.1		0.1	0.01	0.1	0.003	4.0	0.1	2.4	0.1	4.2	0.05	48
U [Bq/kg]	32.8		0.2	0.02	0.4	0.04	0.2	0.004	0.2	0.001	1.0	0.01	6.9	0.04	24
Ra [Bq/kg]	32.7		1.8	0.3	< 1.5		2.5	0.4	1.8	0.3	< 8.4		2.8	0.3	24

* standard deviation (SD) < 5 %; ** standard deviation (SD) < 10 %; *** standard deviation (SD) < 20 %
NA[1]: element was not analysed; NA[2]: no calibration curve was obtained; ND = not detectable

sandstone (98)
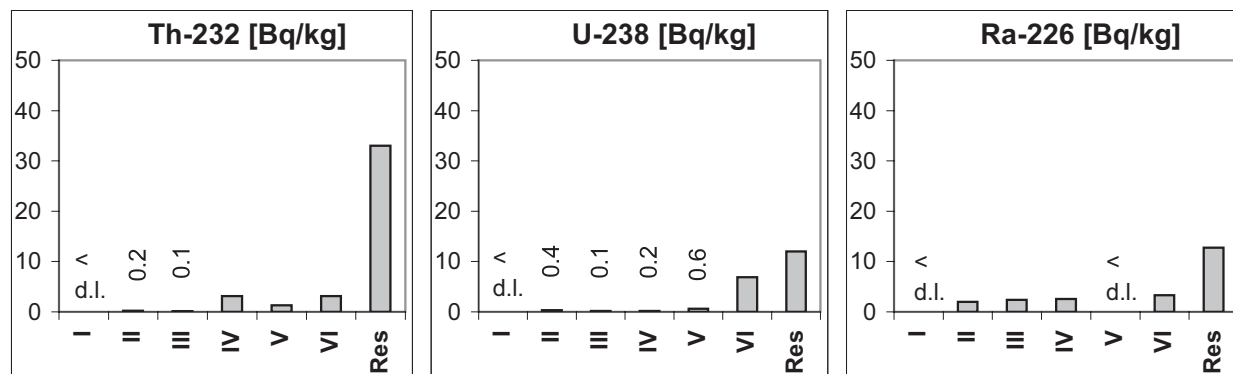
weathering product (102)
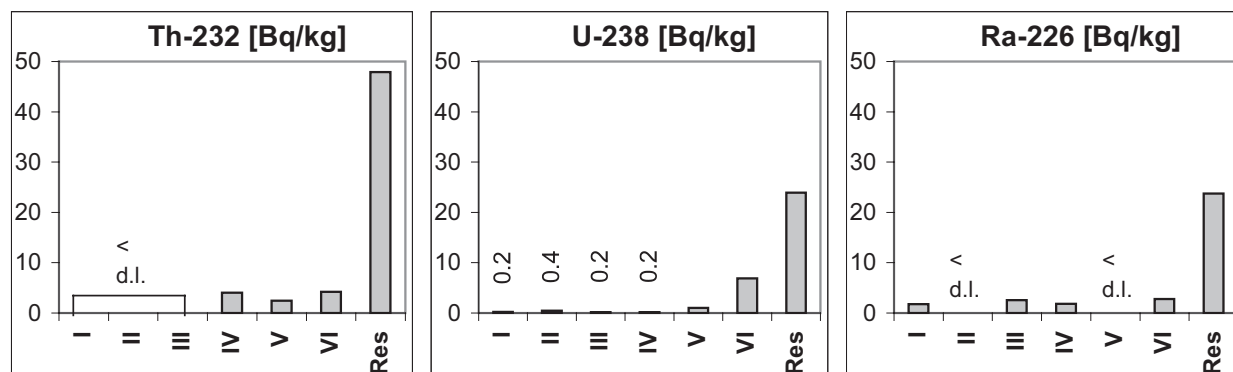
Figure 56: Radionuclide activities among extraction phases of a sandstone of Buntsandstein age (98) and its weathering product (102). (I = *mobile exchangeable***, II =** *exchangeable***, III =** *Mn oxides***, IV =** *organic matter***, V =** *amorphous Fe oxides***, VI =** *crystalline Fe oxides, Res = extraction residual***)**

The similarity of bondings in the rock and in the weathering sample also applies for radium (Figure 56). Only the activities in the exchangeable phases diverge (Table 36). While radium activities in the exchangeable fraction exceed those of the mobile exchangeable fraction in the rock sample, the situation is reversed for the weathering product. However, the measured activities are very low and close to the detection limits. In contrast to the Siegenian schist, radium distribution is equal to the distribution in the Gedinnian rocks and weathering products, though the activities are lower. Most radium is found in the extraction residual. Radium, dissolved during weathering, is mainly bound to Mn oxides and crystalline Fe oxides. Adsorption onto the surface of clay minerals, bonding to organic matter, or precipitation with various oxides/hydroxides of Fe, Mn, Al, and Ti is of less importance.

7.4 Radium speciation and emanation

The results of sequential extraction show a clear difference in the geochemistry of Gedinnian rocks and their accompanying weathering products. Much more radon is released from weathering products than from their parent rocks, because of radium enrichment and high emanation coefficients. Besides this, it is likely that the speciation of radium influences radon emanation (Table 37).

Table 37: Radon activity concentrations[1], emanation coefficients and radium activities of sequentially extracted Gedinnian samples.

	Radon [Bq/kg*][1]	Radium [Bq/kg]	Emanation [%]
Mesozoic samples			
Sandstone 98	1.2	23.0	5
Weathered sandstone 102	0.8	32.7	2
Siegenian samples			
Silty schist 77c	1.1	14.1	8
Weathered silty schist 77a	2.6	18.2	14
Gedinnian sand- and siltstones			
124	1.4	64.6	2
127a	1.5	26.4	6
132a	4.2	53.1	8
135	1.5	34.8	4
136a	1.3	58.9	2
137	1.5	48.1	3
Sandy Gedinnian weathering products			
127b	1.6	69.5	2
134	58.3	339.3	17
136b	127.7	769.0	17
Gedinnian schist			
131	2.1	76.5	3
Gedinnian quartzite			
133a	0.3	12.3	3
Quartz vein in Gedinnian host rock			
126	1.3	9.1	15

[1] *Radon activity concentration referring to the released radon in sample pore gas related to weight of emanating material at secular equilibrium – see Equation 4*

Table 37 shows the radium activities of the samples together with the radon activity concentrations and the emanation coefficients.

Regarding **Gedinnian** sandy rock samples, it is remarkable that the radon activity concentration of the siltstone is about three times higher than that of the sandstones. The sequential extraction of the siltstone showed that radium was distributed either as mobile

exchangeable cations or in the extraction residual. As the proportion of radium in the mobile exchangeable fraction is not higher than for the sandstones, the reason for the higher radon emanation is most probably the smaller grain size of the siltstone, which results in a greater internal surface area.

Radon release of the Gedinnian schist is in between the values for sandstones and siltstone (Table 37). Nevertheless, the emanation coefficient is as low as for the sandstones.

The quartzite releases only small quantities of radon, because of its smooth grain surfaces and low content of iron hydroxides and clay minerals, resulting in an emanation coefficient similar to the sandstones and the schist (Table 37).

The amount of radon that is released from the quartz vein sample is low, but the emanation coefficient is higher than for the sandy weathering products (Table 37). The results of the sequential extraction had shown that radium in this sample is associated with crystalline Fe oxides to a high degree (Figure 51). Iron oxides are located on the quartzite as coatings, from where radon is easily released into the pore space. The emanation coefficient is therefore high, even though the radium activity of the bulk sample is low.

Much higher radon activity concentrations were determined for the Gedinnian weathering products than for the parent rocks. The emanation coefficients of the weathered materials are at least twice as high, except for sample 127b. Sequential extraction of sample 127b showed that the distribution of radium in the weathering product is similar to the distribution of radium in the rock samples (Figure 48), leading to equally low radon release. This sample represents a weathering residue, consisting mainly of quartz and an assemblage of weathering-resistant minerals such as muscovite/illite, kaolinite, chlorites and stable heavy minerals (see Chapter 7.3.1.2).

All other weathered samples derive from enrichment zones with high amounts of various oxides and hydroxides of Fe, Mn, Ti and Al, as well as clay minerals and chlorites. Sequential extraction has proven that radium is preferentially bound to pedogenic clay minerals, adsorbed onto the surface of various oxides/hydroxides or clay minerals and occluded in Mn- and crystalline Fe oxides. A great deal of radium is therefore bound on the internal surfaces of weathering materials, from where radon can escape easily.

High emanation coefficients of the Gedinnian weathering products are not so much conditional on the total activity of radium, but on the distribution of radium. Typically, high internal surface areas of weathering materials, usually due to small grain size and corrosion of the grains, together with the enrichment of radium with clay minerals and Fe/Mn oxide coatings on grains surfaces, lead to high emanation coefficients of weathering products.

Though radium activities of the **Siegenian** rock and its weathering product are similar, the radon release and the emanation of the latter are about twice as high.

In contrast to the Gedinnian and the Siegenian samples, radon release from the weathering product of the **Mesozoic** sample is not elevated. Regarding the Buntsandstein samples, the emanation is not very different for the weathering product than it is for the parent rock. The sandstone even releases slightly more radon (1.2 Bq/kg) than the weathering product (0.8 Bq/kg) and has a slightly higher emanation coefficient, too.

Emanation of the Luxembourg Sandstone was investigated in the current study. The measurements showed the same results as for the Buntsandstein samples. Emanation coefficients and radon release are about equal (Appendix 4,Tables A4-1 to A4-4).

In order to verify the most important speciation of radium for radon emanation, the correlation of radium activity, radon activity concentration and emanation coefficient with radium activity in the extraction steps was determined. The calculations were carried out separately for rocks and weathering products. Calculation of correlation coefficients for rock samples showed no significant correlation. The emanation of radon from the rock samples is independent of the distribution and speciation of radium.

The results for the weathering products, as detailed in Table 38, show significant correlations, though the statistical information on the basis of only a few samples (n=5) is not very reliable. The statistically significant correlation coefficients show evidence of a correlation between radon emanation and the speciation of radium. Total radium correlates with total Fe and with Fe in the fraction of the crystalline Fe oxides. Radon activity concentrations and emanation coefficients correlate with Fe in the crystalline Fe oxide fraction as well, as well as with radium in the same fraction.

Mn in the Mn oxide fraction correlates with radium, radon activity concentration and the emanation coefficient.

Table 38: Correlation coefficients for radon and emanation of weathering products with Ra, Fe and Mn in selected extraction phases. Values are significant on the 0.05 confidence level; n = 5 (I = *mobile exchangeable*, II = *exchangeable*, III = *Mn oxides*, IV = *organic matter*, V = *amorphous Fe oxides*, VI = *crystalline Fe oxides, Res = extraction residual*)

	Fe (Total)	Fe (V)	Fe (VI)	Ra (I)	Ra (II)	Ra (III)	Ra (IV)	Ra (V)	Ra (VI)	Ra (Res)	Mn (III)
Ra (total)	0.95		0.96	0.99	0.99	1.00					0.96
Rn [Bq/kg*][1]			0.97	0.99	0.99	1.00			0.95		0.97
E [%]			0.95						0.98		0.97

[1] *radon activity concentration referring to the released radon in sample pore gas related to weight of emanating material at secular equilibrium*

EDSFELDT (2001) found emanation and radon in soil samples best correlated with the oxide fractions. It was not differentiated between the three oxidic phases (Mn oxides, amorphous Fe oxides, and crystalline Fe oxides), so it cannot be determined, whether each of the oxide fractions correlates significantly positively, or only the total amount of oxide-bound radium. The correlation with exchangeable-bound radium was only weak for radon and not significant for emanation. In contrast to the results of the present study, EDSFELDT (2001) found radon significantly positively correlated with residual radium.

The assumption that the speciation of radium influences radon emanation only holds for weathering products. In the course of weathering rocks are mechanically disintegrated, pedogenic clay minerals with high specific surface areas are formed and mineral grains are corroded and coated with Fe-/Mn oxides. Radium enriches during weathering, preferentially bound to pedogenic clay minerals and various oxides, which also provide high specific surface areas. Bonding to Fe-/Mn oxides is especially important, as oxides tend to build extensive coatings on weathered and corroded rocks, providing high internal surfaces in addition. The general difference in emanation of Palaeozoic and Mesozoic weathering products compared to their parent rocks is most probably due to the abundance of precipitation of Fe-/Mn oxides in the Palaeozoic weathering products, which indicates an intense weathering grade. The higher the weathering grade, the higher the resultant radon activity concentration.

In rocks, the speciation of radium does not influence radon emanation. The release of radon from rocks is governed exclusively by the distribution of the radium atoms, the internal structure of the rock and the particle size distribution.

8   Conclusion

The current study shows that the activities of thorium, uranium, and radium are generally higher for Palaeozoic rocks of the Eisléck than for Mesozoic rocks of the Gutland. This is in contrast to earlier studies by KIES et al. (1996). The difference is even more distinct for the weathering products of the rocks.

Weathering products are generally enriched in radionuclide activities, but enrichment factors are not equal for uranium, radium, and thorium. While radium enrichment is generally highest, thorium enrichment is lowest. Due to the higher mobility of uranium, clear departures from equilibrium occur in the ^{238}U series for about one third of the weathering products. It is assumed that enrichment of ^{226}Ra in weathering products is initially caused by an enrichment of ^{230}Th during weathering. The highest radium activity concentrations occur in samples with ^{230}Th activities above 120 Bq/kg.

The differences in enrichment of natural radionuclides (Th, U, and Ra) in weathering products are governed by their geochemical affinities, analysed by **sequential extraction**:

Thorium distribution is relatively uniform for rocks and weathering products. Most thorium occurs in the extraction residual, followed by variable proportions in the two iron oxide fractions. Activities in all other fractions are generally lower than 5% of total thorium. Clay-rich samples appear to have about 15 – 20% higher proportions of thorium left in the extraction residuals.

Radium in rocks and weathering products is most abundant in the extraction residual, followed by second highest activities in the mobile exchangeable fraction - reflecting unspecific adsorption - or in the fraction of the crystalline iron oxides (hematite and goethite). In weathering products radium is also abundant in the Mn oxide fraction, and the proportion of radium in the extraction residual is enhanced due to the precipitation together with pedogenic clay minerals.

Uranium bonding differs considerably from that of radium. Uranium in rocks is most abundant in the extraction residual. Compared to radium, the activities in the extraction residual were generally lower for uranium. The second most important fraction for uranium is always the fraction of the crystalline iron oxides, with activities usually exceeding those of radium in this fraction. In contrast to radium, the fraction of amorphous iron oxides (ferrihydrite) is the third most significant fraction, while uranium activities in the mobile exchangeable fraction are negligible.

A significant change of preferentially bonding is evident between rocks and weathering products. Most uranium in weathering products is dissolved during sequential extraction, leaving less than 10% of total uranium in the extraction residual. The higher mobility of uranium during weathering is furthermore underlined by much lower overall

uranium activities in all weathering products, in comparison to radium. While radium is enriched up to 14 times, uranium activities are elevated only 9 times. Uranium is most abundant in the fractions of crystalline iron oxides, followed by high proportions in the amorphous iron oxide phase. Less than half of the total activities are distributed among the remaining fractions. Again, activities in the mobile exchangeable fraction are less than 0.1% of total uranium. Unspecific adsorption to negatively charged soil particles is evidently of no significance for uranium, which rather forms stable and mobile complexes.

The enhanced radium activities of the Palaeozoic weathering products are reflected by higher **emanation coefficients** and higher **radon activity concentrations**. The availability of radon in the ground and the transfer into houses depends primarily on the release of radon from weathering products, and much less on the radon release of rocks. While rock samples of different stratigraphic units do not show considerably different radon activity concentrations, the weathering products of rocks of Palaeozoic age have about twice the radon activity concentrations of weathering products of Mesozoic rocks. By far the highest radon activity concentrations were measured for weathered materials with more than 10% Fe_2O_3. Although radium in the weathering products is mainly bound to pedogenic clay minerals, it is rather the amount of radium bound in crystalline iron oxides/hydroxides (goethite, hematite) and in Mn oxides that is the cause for enhanced radon emanation, as can be seen from Table 38.

The high indoor radon activities occurring in the Eisléck arise for a variety of reasons. The Devonian bedrock was strongly faulted and folded by the variscian orogeny, which provides pathways for advective transport of radon. The folding and faulting of the Palaeozoic bedrock is of importance, because it provides more pathways for advective transport of radon than in the mainly undisturbed, relatively flat-lying Mesozoic strata, which are generally cut by few fault systems, causing only local structural radon anomalies. The interrelation of strong foliation and radiometric anomalies was also shown by DEHANDSCHUTTER et al. (2004). Intense weathering phases during Permotriassic times under arid climate conditions and during Late Cenozoic to Early Tertiary times under tropical to subtropical conditions (MEYER 1998) led to precipitation of Fe-/Mn oxides in fissures and fractures in deep weathering zones of several hundred metres in depth (MÜCKENHAUSEN 1958, KNAPP 1980, FELIX-HENNINGSEN 1990 cum lit, MEYER 1998). Enrichment of radium along faults, shear zones, caverns and fractures of the deeply weathered Palaeozoic bedrock together with Fe/Mn oxides, which provide high specific surface areas, leads to high radon activity concentrations.

Soils above the Palaeozoic bedrock are generally poorly developed and show high permeability (Figure 3), while the less permeable soils above the flat-lying Mesozoic bedrocks with clayey interlayers, characteristic for most Mesozoic stratigraphic units, build up natural barriers for the vertical migration of radon. High radium and radon activities of Mesozoic calcitic precipitations or veins (Jurassic and Middle Keuper) do not lead to generally higher indoor radon activities, because they are usually covered by interlayers of low permeability. The only enhanced indoor radon activities above Upper Muschelkalk (*mo*) have the same causes as those of the Palaeozoic of the Eisléck. Radium is adsorbed on dissolution residuals with high specific surface areas (clay minerals and Fe-/Mn oxides) at fractures and joints in the dolomites. In addition, the partial karstification of the *mo* provides pathways for advective transport of radon.

9   References

AD-HOC ARBEITSGRUPPE BODEN (1996): Anleitung zur Entnahme von Bodenproben.- Geol. Jb., G1, Hannover

AMES, L. L., MCGARRAH, J. E. & WALKER, B. A. (1983a): Sorption of trace constituents from aqueous solutions onto secondary minerals. I. Uranium.- Clays and Clay Minerals, 31: 321 - 334

AMES, L. L., MCGARRAH, J. E. & WALKER, B. A. (1983c): Sorption of trace constituents from aqueous solutions onto secondary minerals. II. Radium.- Clays and Clay Minerals, 31: 335 - 342

AMES, L. L., MCGARRAH, J. E., WALKER, B. A. & SALTER, P. F. (1983b): Uranium and radium sorption on amorphous ferric oxyhydroxides.- Chem. Geol., 40: 135 – 148

AMES, L.L & RAI, D. (1978): Radionuclide interactions with soil and rock media.- Final Report for Contract 68-03-2514, Vol 1, Las Vegas

ANDERSON, B.J., JENNE, E.A. & CHAO, T.T. (1973): The sorption of silver by poorly crystallized manganese oxides.- Geochim. Cosmochim. Acta, 37: 611-622

APPLETON, J.D. & BALL, T.K. (1995): Radon and background radioactivity from natural sources: characteristics, extent and relevance to planning and development in Great Britain.- Brit. Geol. Surv. Techn. Rep. WP/95/2, Geochemistry Series, Keyworth, Nottingham

ARCHER, V.E. (1987): Association of lung cancer mortality with Precambrian granite.- Archives of Environ. Health, 42: 87-91

ASSELBERGHS, E. (1926): Siegenien, Siegenerschichten, Hunsrèckschiefer et Taunusquarzit.- Bull. Soc. Belg. de Geol., de Paléont. et d'Hydrol., 36, Bruxelles

BARRETTO, P.M.C., CLARK, B.R. & ADAMS, J.A.S (1975): Physical characteristics of radon-222 from rocks, soils and minerals: Its relation to temperature and alpha dose.- in: Adams, J.A.S., Lowder, W.M. & Gesell, T.F. (eds.): The natural radiation environment II: 731-740, Washington, D.C.

BARTON, T.P. & ZIEMER, P.L. (1986): The effect of particle size and moisture content on the emanation of Rn from coal ash.- Health Phys., 50, 5: 581-588

BENEŠ, P. (1990): Speciation procedure.- in: IAEA: The Environmental Behaviour of Radium.- Technical Report Series No. 310, Vol 1: 11-56, Vienna

BERG (1965): Die Klüfte im Paläozoikum und Mesozoikum von Luxembourg und der westlichen Eifel. Ihre Beziehungen zur allgemeinen Tektonik und ihr Einfluß auf das Gewässernetz.- Publ. Serv. Géol. Lux., XVI, Luxembourg

BERNERS, H.-P. (1983): A lower liassic offshore bar environment, contribution to the sedimentology of the Luxemburg sandstone.- Ann. Soc. Géol. Belg., 106: 87-102

BERNERS, H.-P. & MULLER, A. (1984): Einführung zu den Exkursionen.- Jber. Mitt. Oberrhein. Geol. Ver., N.F., 66: 25-34

BINTZ, J. (1984): Morphologie und Geologie von Süd-Luxemburg.- in: Trierer geographische Studien / Sonderheft, 6, pp. 297-304, Trier

BINTZ, J., HARY, A. & MULLER, A. (1973): Luxembourg.- in: Guides géologiques régionaux: Ardenne/Luxembourg.: 135-202, Paris

BÖHM, C. (2003): Einfluss des Untergrundes auf die Radonkonzentration in Gebäuden - dargestellt anhand einiger Beispielen.- Available at: , accessed October 2003

BOENIGK, W. (1983): Schwermineralanalyse.- Stuttgart, Enke

BOSSUS, D.A.W. (1984): Emanating power and specific surface area.- Rad. Prot. Dosim. 7, 1-4: 73-76

BOYLE, D. (1982): Geochemical prospecting for thorium and uranium deposits.- Amsterdam, Elsevier

BROOKINS, D.G. (1991): Correlation of soil radon and uranium with indoor radon in the Albuquerque, New Mexico area.- Environm. Geol. Water Sci., 17, 3: 209-217

CALMANO, W. & FÖRSTNER, U (1985): Schwermetall-Bindungsformen in Küstensedimenten - Standardisierung von Extraktionsverfahren.- BMFT-FB-M 85-004, Hamburg.

CHARLET, J.M., DOREMUS, P. & QUINIF, Y. (1995): Radon methods used to discover uranium mineralizations in the Lower Devonian of the Ardenne Massif (Belgium).- in: DUBOIS, C. (ed.): Gas Geochemistry, Science Reviews: 1-18, Northwood

CHARLET, J.M., DEJONGHE, L., DE WITTE, S.M., DRUMEL, B., HENRY, J., HERBOSCH, A., LEFIN, J.P. & MARTIN, H. (1983): Reconnaissance survey for uranium in the Belgian Paleozoic.- Serv. Geol. Belg. Prof. Paper 1983/1, 196

CHARLET, J.M., DOREMUS, P. & QUINIF, Y. (1987): Concentration mechanisms of uranium in mineralized fractuires of the Lower Devonian of the Belgian Ardenne. The case of the Oizy area.- Uranium, 3: 387-405

CHARLET, J.M., ZHU, H.C. & POFFIJN, A. (1999): The radon anomaly of Porcheresse (Ardennes, Belgium). A case study.- Il Nuovo Cimento, 22C (3-4): 491-496

CIOLKOSZ, E.J., CRONCE, R.C. & DOBOS, R.R. (1988): Pennsylvania State University soil characterization laboratory manual.- Agronomy Series, 101, Pennsylvania

COHEN, B.L. (1993): Relationship between exposure to radon and various types of cancer.- Health Phys., 65, 5: 529-532

CREMER, S. (1986): Entwicklung von Methoden zur differenzierten Extraktion reduzierter Elemente.- Diploma thesis, Ruhr-Universität Bochum, Bochum (unpubl.).

DAMKJÆR, A. & KORSBECH, U. (1985): Measurement of the emanation of Radon-222 from Danish soils.- Sci. Total Environm., 45: 343-350

DEARLOVE, J.P.L., GREEN, D.C & IVANOVICH, M. (1988): Uranium transport and the partitioning of U, Th, and Ra isotopes between solid and aqueous phases.- Sci. Basis Nucl. Waste Manag. XII: 927-932

DEARLOVE, J.P.L., IVANOVICH, M. & GREEN, D.C. (1989): Partition coefficients (Rd) for the U-series radionuclides in ion exchange sites and amorphous Fe phase in illite and granite samples.- in: Proceedings of the 6th Water/Rock Interaction Conference, Malvern, U.K.; Balkema: Rotterdam: 191-195

DIN Deutsches Institut für Normung e. V. (1994): DIN 32 645.- Berlin, Beuth Verlag

DITTRICH, D. (1993): Erläuterungen zur geol. Karte von Luxemburg. 1:25 000 - Blatt Grevenmacher u. Blatt Remich.- Publ. Serv. Géol., Bull. 16, Luxembourg

DITTRICH, D. (1984): Erläuterungen zur Geologischen Karte von Luxemburg 1: 25 000. Blatt Nr. 8 Mersch.- Publ. Serv. Géol. Lux., XXV, Luxembourg.

DITTRICH, D. (1989): Beckenanalyse der Oberen Trias der Trier-Luxemburger Bucht. Revision der stratigraphischen Gliederung und Rekonstruktion der Paläogeographie.- Publ. Serv. Géol. Lux., XXVI, Luxembourg.

DITTRICH, D (1999): Triassic and Liassic of the Trier Embayment.- Meuse-Rhine Euregio Geologists Meeting at Trier, May 7-8, 1999, Excursion Guide, Mainz (unpubl.)

DOREMUS, P., DEJONGHE, L. & CHARLET, J.-M. (1992): Radon et gaz rares dans les sciences de la terre et de l'environnement.- Mem. Expl. Cartes Geologique et Minieres de la Belgique, 32, Brussels

DUVAL, J.S. & OTTON, J.K. (1990): Radium distribution and indoor radon in the Pacific Northwest.- Geophys. Res. Lett., 17, 6: 801-804

DYCK, W. (1978): The mobility and concentration of uranium and its decay products in temperate surficial environments.- in: Kimberley, M.M. (ed.): Uranium deposits: their mineralogy and origin: 57-100, Toronto

EDSFELDT, C. & FERNLUND, J. M. R. (1998): Radium distribution in Swedish soils analysed with chemical sequential extraction - Implications on radon emanation.- in: BARNET, I., NEZNAL, M. (eds.): Radon Investigations in the Czech Repubic VII and the 4th International Workshop on the Geological Aspects of Radon Risk Mapping: 76-84, Prague

EDSFELDT, C. (2001): The radium distribution in some Swedish soils and its effect on radon emanation.- Dissertation, Royal Institute of Technology, Stockholm

FEIDER, M. & KIES, A. (1996): The radon policy in the Grand-Duchy of Luxembourg.- Annales Association Belge de Radioprotection, 21, 1:101-106

FELIX-HENNINGSEN, P. (1990): Die mesozoisch-tertiäre Verwitterungsdecke (MTV) im Rheinischen Schiefergebirge – Aufbau, Genese und quartäre Überprägung.- Relief Boden Paläoklima 6, Berlin - Stuttgart, Gebr. Bornträger

FIELD, R.W., STECK, D.J., SMITH, B.J., BRUS, C.P., FISHER, E.F., NEUBERGER, J.S., PLATZ. C.E., ROBINSON, R.A., WOOLSON, R.F. & LYNCH, C.F. (2000): Residential radon gas exposure and lung cancer: The Iowa Radon Lung Cancer Study.- Am. J. Epidemiol. 151: 1091-1102

FLEISCHER, R.L. (1981): A possible association between lung cancer and phosphate mining and processing.- Health Phys. 41, 1: 171-175

FLEISCHER, R.L. (1982): Alpha-recoil damage and solution effects in minerals: uranium isotopic disequilibrium and radon release.- Geochim. Cosmochim. Acta 46, 11: 2191-2202

FLEISCHER, R.L. (1986): A possible association between lung cancer and a geological outcrop.- Health Phys. 50, 6: 823-827

FLEISCHER, R.L. (1988): Radon in the environment - Opportunities and hazards.- Int. J. Radiat. Appl. Instrum., Part D, Nucl. Tracks Radiat. Meas. 14, 4: 421-435

FLEISCHER, R. L. & RAABE, O. G. (1978): Recoiling alpha-emitting nuclei. Mechanism for uranium-series disequilibrium.- Geochim. Cosmochim. Acta 42: 973-977

FLEXSER, S., WOLLENBERG, H.A. & SMITH, A.R. (1993): Distribution of radon sources and effects on radon emanation in granitic soil at Ben Lomond, California.- Environm. Geol. 22: 162-177

FLÜGGE, S. & ZIMEN, K.E. (1939): Die Bestimmung von Korngrößen und Diffusionskonstanten aus dem Emaniervermögen. Die Theorie der Emaniermethode.- Z. phys. Chem. B 42: 179-220

FORASTIERE, F., VALESINI, S., ARCA, M., MAGLIOLA, M.E., MICHELOZZI, P. & TASCO, C. (1985): Lung cancer and natural radiation in an italian province.- Sci. Total Environm. 45: 519-526

GASCOYNE, M. & CRAMER, J. (1987): History of actinide and minor element mobility in an Archean batholith in Manitoba, Canada.- Appl. Geochem. 2: 37-53

GERKEN, M., KREIENBROCK, L., WELLMANN, J., KREUZER, M. & WICHMANN, H.E. (2000): Models for retrospective quantification of indoor radon exposure in case-control studies.- Health Phys. 78-3: 268-278

GREEMAN, D. J. & ROSE, A. W. (1996): Factors controlling the emanation of radon and thoron in soils of the eastern USA.- Chem. Geol. 129: 1 – 14

GREEMAN, D.J. (1992): The geochemistry of uranium, thorium and radium in soils of the Eastern United States.- Dissertation, Pennsylvania State University, Ann Arbor/Michigan.

GREINER, N.R. (1985): Radon emanation from coals: Effects of moisture and particle size.- Health Phys. 48, 3: 283-288

GUNBY, J.A., DARBY, S.C., MILES, J.C.H., GREEN, B.M.R. & COX, D.R. (1993): Factors affecting indoor radon concentration in the United Kingdom.- Health Phys. 64: 2-12

HAHN, O. (1921): Über eine neue radioaktive Substanz im Uran.- Berichte der Deutschen Chemischen Gesellschaft, 54: 1131-1142

HAKL, J., HUNYADI, I., CSIGE, I., GÉCZY, G., LÉNÁRT, L. & TÖRÖCSIK, I. (1992): Outline of natural radon occurences on karstic terrains of Hungary.- Rad. Prot. Dosim. 45, 1/4: 183-186

HAYNES, R.M. (1988): The distribution of domestic radon concentrations and lung cancer mortality in England and Wales.- Rad. Prot. Dosim. 25: 93-96

HEINRICH, M. (1994): Radon-Emanationskoeffizienten verschiedener Gesteine in Abhängigkeit von Feuchte und Korngröße.- Diploma thesis, Rheinische Friedrich-Wilhelms-Universtät, Bonn (unpubl.)

HESS, C.T., WEIFFENBACH, C.V. & NORTON, S.A. (1983): Environmental radon and cancer correlations in Maine.- Health Phys. 45, 2: 339-348

HOFMANN, W., KATZ, R. & ZHANG, C.X. (1985): Lung cancer in a Chinese high background area - epidemiological results and theoretical interpretation.- Sci. Total Environm. 45: 527-534

HOWARD, A.J., SIMSARIAN, J.E. & STRANGE, W.P. (1995): Measurements of ^{220}Rn emanation from rocks.- Health Phys. 69, 6: 936-943

IARC (International Agency for Research on Cancer) (1988): Man-made mineral fibers and radon.- Monographs on the evaluation of carcinogenic risks to humans, 43, Lyon, IARC

ICRP (1993): Protection against radon-222 at home and at work.- IRCP-Publ. 65, Annals of ICRP 23, 2, Amsterdam, Elsevier

INGLES, J. C., SUTARNO, R., BOWMAN, W. S. & FAYE, G. H. (1977): Radioactive Ores DH-1, DL-1, BL-2, BL-3 and BL-4 - Certified Reference Materials.- CANMET Rpt. 77-64, Canada Centre for Mineral and Energy Technology, Ottawa

IVANOVICH, M., LATHAM, A. G., LONGWORTH, G. & GASCOYNE, M. (1992): Applications to radioactive waste disposal studies.- in: Ivanovich, M. & Harmon, R.S. (eds.): Uranium-series disequilibrium: Applications to earth, marine, and environmental sciences: 583-630, Oxford, Clarendon Press

IVANOVICH, M. & HARMON, R.S. (eds.) (1992): Uranium-series disequilibrium: Applications to earth, marine, and environmental sciences.- Oxford, Clarendon Press

KEIL, R. (1979): Hochselektive spektralphotometrische Spurenbestimmung von Uran(VI) mit Arsenazo III nach Extraktionstrennung.- Fresenius Z. Anal. Chem. 297: 384-387

KELLER, G. & SCHÜTZ, M. (1988): Radon exhalation from the soil.- Rad. Prot. Dosim. 24, 1-4: 43-46

KEMSKI, J., KLINGEL, R., SCHNEIDERS, H., SIEHL, A., WIEGAND, J. (1992): Geological structure and geochemistry controlling radon in soil gas.- Rad. Prot. Dosim. 45, 1/2: 235-239

KEMSKI, J., KLINGEL, R., SIEHL, A. (1996 a): Die terrestrische Strahlung durch natürlich radioaktive Elemente in Gesteinen und Böden.- in: SIEHL, A. (ed.): Umweltradioaktivität: 69-96, Berlin, Ernst & Sohn.

KEMSKI, J., KLINGEL, R., SIEHL, A. (1996 b): Das geogene Radon-Potential.- in: SIEHL, A. (ed.): Umweltradioaktivität: 179-222, Berlin, Ernst & Sohn.

KEMSKI, J., KLINGEL, R., SIEHL, A. (1996 c): Classification and mapping of radon affected areas in Germany.- Environm. Int., Vol. 22, Suppl. 1: S789-S798.

References

KEMSKI, J., SIEHL, A., STEGEMANN, R., VALDIVIA-MANCHEGO, M. (1999): Geogene Faktoren der Strahlenexposition unter besonderer Berücksichtigung des Radon-Potentials (Abbschlußbericht zum Forschungsvorhaben St. Sch. 4106).- Schriftenreihe Reaktorsicherheit und Strahlenschutz, BMU-1999-534, Bonn

KEMSKI, J., SIEHL, A., VALDIVIA-MANCHEGO, M., LEHMANN, R. (1998): Comparison of radon concentrations in buildings in Oberfranken (Bavaria) with the geogenic radon potential.- in: BARNET, I. & NEZNAL, M. (eds.): Radon Investigations in the Czech Repubic VII and the 4th International Workshop on the Geological Aspects of Radon Risk Mapping: 53-62, Prague

KEMSKI, J., SIEHL, A., STEGEMANN, R., VALDIVIA-MANCHEGO, M. (2001): Mapping the geogenic radon potential in Germany.- Sci. Tot. Environm., 272: 217-230

KEMSKI, J., KLINGEL, R., SIEHL, A., STEGEMANN, R., VALDIVIA-MANCHEGO, M. (2002): Transferfunktion für die Radonkonzentration in der Bodenluft und der Wohnraumluft (Abschlussbericht zu den Forschungsvorhaben St. Sch. 4186 und St. Sch. 4187: Ermittlung einer Transferfunktion für die Radonkonzentration in der Bodenluft und in der Wohnraumluft incl. Radonmessungen in Häusern zur Validierung des geologisch induzierten Radonpotentials. Teil A: Bodenuntersuchungen zum geogenen Radonpotential. Teil B: Validierung der geologischen Prognose durch Messungen der Radonkonzentration in Gebäuden).- Schriftenreihe Reaktorsicherheit und Strahlenschutz, BMU-2002-598, Bonn

KEMSKI, J., KLINGEL, R., SIEHL, A., STEGEMANN, R. (2003): Die Deutschlandkarte zum Radon im Boden – Abschlußbericht.- in: Forschung zum Problemkreis "Radon", 16. Statusgespräch, Bundesministerium für Umwelt, Naturschutz und Reaktorsicherheit, Bonn

KIES, A., FEIDER, M., BIELL, A. & ROWLINSON, L. (1994): Radon mapping in the Grand-Duchy of Luxembourg.- in: Barnet, I. & Neznal, M. (eds.): Radon Investigations in Czech Republic V and the 2nd International Workshop on the Geological Aspects of Radon Risk Mapping: 142-152, Prague

KIES, A. & FEIDER, M. (1996): Radon-Messungen im Grossherzogtum Luxembourg. - in: SIEHL, A. (ed.): Umweltradioaktivität: 233-243, Berlin, Ernst&Sohn

KIES, A., BIELL, A., ROWLINSON, L. & FEIDER, M. (1996a): Radon survey in Luxembourg - Indoor measurements related to house features, soil, geology and environment.- Environm. Int., Vol. 22, Suppl. 1: 805-808

KIES, A., ROBINET, A., FEIDER, M. & MAQUIL, R. (1996b): Study of the radon potential for a traverse of the Grand-Duchy of Luxembourg.- in: Barnet, I. & Neznal, M. (eds.): Radon

investigations in the Czech Republic VI and the third international workshop on the geological aspects of radon risk mapping: 46-50, Prague

KLINGEL, R. (1991): Geochemische Untersuchungen zur Verwitterung von Bergematerialien im Lysimeterversuch.- Dissertation, Universität des Saarlandes, Saarbrücken.

KLINGEL, R., KLINGER, C. & THEIN, J. (1995): Zur Mobilität von Uran und Radium.- in: MERKEL, A., HURST, S., LÖHNERT, E.P. & STRUCKMEIER, W. (eds.): Uranium Mining and Hy-drogeology.- Proc. Intern. Conf. Freiberg, Oct. 1995: 315-324, Köln, S. von Loga

KLINGER, C. (1993): Mobilisationsverhalten von anorganischen Schadstoffen in der Umgebung von untertägigen Versatzbereichen am Beispiel von Reststoffen aus Müllverbren-nungsanlagen im Steinkohlengebirge des Ruhrkarbons.- Dissertation, Rheinische Friedrich-Wilhelms-Universtät, Bonn

KLOSEN, M. (1998): Analyse par scintillation liquide et spectrometrie gamma des radioelements dans les milieux aquatiques.- Centre Universitaire de Luxembourg, Luxembourg

KNAPP, G. (1980): Erläuterungen zur Geologischen Karte der nördlichen Eifel 1:100 000 .- Krefeld, GLA NRW

KONRAD, H.J & WACHSMUT, W. (1973): Zur Lithologie und Tektonik des Unterdevons im südlichen Ösling Luxemburgs.- Publ. Serv. Géol., Bull. 5, Luxembourg

KREIENBROCK, L., KREUZER, M., GERKEN, M., DINGERKUS, G., WELLMANN, J., KELLER, G., WICHMANN, H. E. (2001): Case-control study on lung cancer and residential radon in West Germany.- American Journal of Epidemiology, 153/1: 42-52

KREIENBROCK, L., POFFIJN, A., TIRMARCHE, M., KAYSER, P., DARBY, S. & WICHMANN, H.E. (1993): Radon and lung cancer in the Ardennes and Eifel region - concepts and experiences of an international study.- in: Michaelis et al. (eds.): Medizinische Informatik, Biometrie und Epidemiologie, 76: 19-23, München, MMV Medizin Verlag

KREIENBROCK, L. & SIEHL, A. (1996): Multiple statistische Analyse von Radon-Erhebungsmessungen in der Bundesrepublik Deutschland.- in: SIEHL, A. (ed.): Umweltradioaktivität: 299-310, Berlin, Ernst & Sohn.

LANDA, D.R. & GAST, R.G. (1973): Evaluation of crystallinity in hydrated ferric oxides.- Clays Clay Miner., 21: 121-130

LANGMUIR, D. (1978): Uranium solution-mineral equilibria at low temperatures with applications to sedimentary ore deposits.- Geochem. Cosmochim. Acta, 42: 547 - 569

LATHAM, A.G. & SCHWARCZ, H.P. (1987): The relative mobility of U, Th and Ra isotopes in the weathered zones of the Eye-Dashwa Lakes granite pluton, northwestern Ontario, Canada.- Geochim. Cosmochim. Acta, 51: 2787-2793

LIENERT, C., SHORT, S.A. & VON GUNTEN, H.R. (1994): Uranium infiltration from a river to shallow groundwater.- Geochim Cosmochim. Acta, 58: 5455-5463

LINDMARK, A. & ROSEN, B. (1985): Radon in soil gas - exhalation tests and in situ measurements.- Sci. Tot. Environm., 45: 397-404

LOGANATHAN, P. & BURAU, R.G. (1973): Sorption of heavy metal ions by hydrous manganese oxides.- Geochim. Cosmochim. Acta, 37: 1277-1293

LONGWORTH, G., IVANOVICH, M. & HASLER, S.A. (1989): Measurements of the partition of long-lived uranium and thorium isotopes in mineral phases of Eden Shale (Lounthwaite) and granite (Strath Halladale).- Nirex Report NSS/R181

LUBIN, J.H., BOICE, J.D. & SAMET, J.M. (1995): Errors in exposure assessment, statistical power and the interpretation of residential radon studies.- Radiat. Res., 144: 329-341

LUCIUS, M. (1937): Die Geologie Luxemburgs in ihren Beziehungen zu den benachbarten Gebieten.- Publ. Serv. Géol., I, Luxembourg

LUCIUS, M. (1945): Die Luxemburger Minetteformation und die jüngeren Eisenerzbildungen unseres Landes.- Publ. Serv. Géol., IV, Luxembourg

LUCIUS, M. (1948): Das Gutland. Erläuterungen zu der geologischen Specialkarte Luxemburgs.- Publ. Serv. Geol. Lux., V, Luxembourg

LUCIUS, M. (1950): Das Oesling. Erläuterungen zu der geologischen Specialkarte Luxemburgs.- Publ. Serv. Geol. Lux., VI, Luxembourg

MAGNUS, K., ENGELAND, A., GREAM, B.M.R, HALDORSEN, T., MUIRHEAD, C.R. & STRAND, T. (1993): Residential radon exposure and lung cancer - An epidemiological study of Norwegian municipalities.- Rep. KM/THO, The Cancer Registry Norway, Institute for Epidemiological Cancer Research, Norway

MAQUIL, R., MOSAR, J. & THEIN, J. (1984): Unterdevon-Stratigraphie und variskischer Gebirgsbau im Eislek / Nord - Luxemburg.- Jber. Mitt. oberrhein. geol. Ver. N.F., 66: 57-75.

MAQUIL, R. & LÖHNERTZ, W. (1984): Das Pumpspeicherwerk Vianden und die Geologie seiner Umgebung (Exkursion B am 24. April 1984).- Jber. Mitt. oberrhein. geol. Ver., N.F., 66: 41-50

MARKKANEN, M. & ARVELA, H. (1992): Radon emanation from soils.- Rad. Prot. Dosim., 45, 1/4: 269-272

MARTÍNEZ-AGUIRRE, A. & PERIÁÑEZ, R. (2001): Sedimentary speciation of U and Th isotopes in a marsh area at the southwest of Spain.- Journal of Radioanalytical and Nuclear Chemistry, 247: 45-52

MAXE, L. (2000): Bestämning av markmaterialets specifika yta. - Slutrapport Projekt SGU.- Royal Institute of Technology, Stockholm

MCDOWELL, W.J. & MCDOWELL, B.L. (1994): Liquid Scintillation Alpha Spectrometry.- CRC Press, Boca Raton, U.S.

MCKEAGUE, J.A. & SCHUPPLI, P.A. (1985): An assessment of EDTA as an extractant of organic-comlpexed and amorphous forms of Fe and Al in soils.- Geoderma, 35: 109-118

MEGUMI, K. & MAMURO, T. (1974): Emanation and exhalation of radon and thoron gases from soil particles.- J. Geophys. Res., 79, 23: 3357-3360

MEYER, W. (1998): Geologie der Eifel.- Stuttgart, Schweizerbart

MINISTRY OF HEALTH AND SOCIAL AFFAIRS (1996): Miljörelaterade hälsorisker. Bilga 1 till Miljöhälsoutredningen.- Ministry of Health and Social Affairs, Statens offentliga utredningar 1996, 124, Stockholm

MITTMEYER, H.-G. (1974): Zur Neufassung der Rheinischen Unterdevon-Stufen.- Mainzer geowiss. Mitt., 3: 69-79

MOLINARI & SNODGRASS (1990): The chemistry and radiochemistry of radium and the other elements of the uranium and thorium natural decay series.- in: IAEA: The Environmental Behaviour of Radium.- Technical Report Series No. 310, Vol 1: 11-56, Vienna

MOORE, W. S. (1972): Radium: element and geochemistry.- in: FAIRBRIDGE, R.W. (ed.): The Encyclopedia of Geochemistry and Environmental Sciences, Encyclopedia of Earth Sciences Series, Vol. IVA: 1006-1007, Van Nostrand Reinhold, Princeton, NJ and New York

MORAWSKA, L. & JEFFRIES, C. (1994): Distribution of radium in mineral sand grains and its potential effect on radon emanation.- Rad. Prot. Dosim., 56, 1-4: 199-200

MORAWSKA, L. & PHILLIPS, C.R. (1993): Dependence of the radon emanation coefficient on radium distribution and internal structure of the material.- Geochim. Cosmochim. Acta, 57: 1783-1797

MUECKENHAUSEN, (1958): Bildungsbedingungen und Umlagerung der fossilen Böden der Eifel.- Fortschr. Geol. Rheinld. Westf., 2: 495-502

MUIRHEAD, C.R. (2002): Uncertainties in assessing health risks from natural radiation, including radon.- in: BURKART, W., SOHRABI, M. & BAYER, A. (eds.): High levels of natural radiation and radon areas: Radiation dose and health effects - International Congress Series 1225: 231–237, Amsterdam, Excerpta Medica

NATIONAL BOARD OF HEALTH AND WELFARE (1997): Cancer incidence in Sweden 1994.- Centre for Epidemiology, National Board of Health and Welfare, Statistik/Hälsa och sjukdomar, 2, Stockholm

NAZAROFF, W.W. & SEXTRO, R.G. (1989): Technique for measuring the indoor ^{222}Rn source potential of soil.- Environm. Sci. Technol., 23: 451-458

NEZNAL, M., NEZNAL, M. & SMARDA, J. (1991): Radon infiltration risk from the ground in Chaby, Prague.- in: Barnet, I. (ed.): Radon investigations in Czechoslovakia II: 34-39, Prague

NITON ELECTRONICS (1992): RAD 7 Radon detector - Owners´s manual, Version 2.1., Bedford (USA.)

NORRISH, K. & TAYLOR, R.M. (1961): The isomorphous replacement of iron by aluminium in soil goethite.- J. Soil Sci., 12: 294-306

PELLEGRINI, D. (1997): Étude de l'émanation du radon a partir de résidus de traitement de minerais d'uranium. Mise en évidence de relations entre le facteur d'émanation et les caractéristiques du matériau. – Dissertation, L'Universite de Franche-Comte, Besançon

PERSHAGEN, G., ÅKERBLOM, G., AXELSON, O., CLAVENSJÖ, B., DAMBER, L., DESAI, G., ENFLO, A., LAGARDE, F., MELLANDER, H., SVARTENGREN, M. & SWEDJEMARK, A. (1994): Residential radon exposure and lung cancer in Sweden.- New England Journal of Medicine, 330: 159-164

PICKERING, W.F. (1981): Selective chemical extractions of soil components and bound metal species.- CRC, Critical Rev. Anal. Chem., 12: 233-266

PRICHARD, H.M., VENSO, E.A. & DODSON, C.L: (1992): Liquid scintillation analysis of ^{222}Rn in water by alpha/beta discrimination.- Radioactivity and Radiochemistry, 3, 10: 28-36

PRUTKINA, M.I. & SHASKIN, V.L. (1967): Radon emanation from uraniferous ores and minerals immersed in liquids.- Sov. At. Energy, 22, 2: 153-154

ROBINET, A. (1996): Etude de la radioactivité gamma effectuée sur une tranche transversale du Grand-Duché de Luxembourg.- Centre Universitaire de Luxembourg, Luxembourg

ROSE, A.W., SCHMIERMUND, R.L. & MAHAR, D.L. (1977): Geochemical dispersion of uranium near prospects in Pennsylvania.- U.S. Departement of Energy Report GJBX-59(77),

ROTH, S. (1997): Teil I: Geologische Kartierung in der Trier-Bitburger Bucht zwischen Irrel und Ralingen (Blatt 5104 Bollendorf u. Blatt 6105) und Teil II: Geochemische Untersuchungen zur Mobilität von natürlichen Radionukliden an drei Verwitterungsprofilen.- Diploma thesis, Rheinische Friedrich-Wilhelms-Universtät, Bonn (unpubl.)

ROTH, S. (1998): Zwischenbericht zur Studie zur Untersuchung der geochemischen Signatur natürlicher Radionuklide in Gesteinen und Böden Luxembourgs.- Progress Report for project BFR96/009, Luxembourg

ROTH, S. & FEIGE, S. (1998): Emanation measurements with a solid state alpha detector.-in: BARNET, I., NEZNAL, M. (eds.): Radon Investigations in the Czech Repubic VII and the 4th International Workshop on the Geological Aspects of Radon Risk Mapping: 85-92, Prague

ROTH, S. (2001): Abschlussbericht zur Studie zur Untersuchung der geochemischen Signatur natürlicher Radionuklide in Gesteinen und Böden Luxembourgs.- Final Report for project BFR96/009, Luxembourg

ROWLINSON, L. (1998): Radon research in Luxembourg relating to geology.- Final report for project BFR93/041, Luxembourg

RUTHERFORD, P.M., DUDAS, M.J. & AROCENA, J.M. (1995): Radon emanation coefficients for phosphogypsum.- Health Phys., 69, 4: 513-520

SACHS, L. (1999): Angewandte Statistik - Anwendung statistischer Methoden.- Berlin, Springer

SCHEFFER, F. & SCHACHTSCHABEL, P. (2002): Lehrbuch der Bodenkunde.- München, Elsevier

SCHMITZ, C. (1997): Etude sur le radium et ses produits de filiation dans le milieux aquatiques au Grand-Duché de Luxembourg.- Centre Universitaire de Luxembourg, Luxembourg

SCHRADER, E. (1983): Ein Sedimentationsmodell der Trias in der Eifeler Nord-Süd-Zone unter besonderer Berücksichtigung der Nord-Eifel (Mechernich-Maubacher Triasdreieck).- Dissertation, R.W.T.H. Aachen, Aachen.

SCHUMANN, R.R. & GUNDERSEN, L.S.C. (1996): Geologic radon potential of EPA region 5.- U.S. Geol. Surv., Open-file rep. 93-292-E

SCHWERTMANN, U. (1984): Aluminiumsubstitution in pedogenen Eisenoxiden – eine Übersicht.- Z. Pflanzenernähr. Bodenk., 147: 385-399

SCHWERTMANN, U., FITZPATRICK, R.W., TAYLOR, R:M: & LEWIS, D.G. (1979): The influence of aluminium on iron oxides. Part II. Preparation and properties of Al substituted hematites.- Clays Clay Miner., 27: 105-112

SEMKOW, T.M. & PAREKH, P.P. (1990): The role of radium distribution and porosity in radon emanation from soils.- Geophys. Res. Lett., 17, 6: 837-840

SHUMAN, L.M. (1985): Fractionation method for soil microelements.- Soil Science, 140: 11-22

SIEHL, A. & THEIN, J. (1978): Geochemische Trends in der Minette (Jura, Luxemburg/Lothringen).- Geol. Rdsch., 67: 1052-1077

SIEHL, A. & THEIN, J. (1989): Minette-type ironstones.- in: YOUNG, T.P. & TAYLOR, W.E.G. (eds.) (1989): Phanerozoic ironstones.- Geol. Soc. Special Publ., 46: 175-193,

SIMS, J.L. & PATRICK, W.H. (1978): The distribution of micronutrient cations under conditions of varying redox potential and pH.- Soil Sci. Soc. Am., 42: 258-262

STEGEMANN, R., KLINGEL, R. & SIEHL, A. (1999): Measuring methods for determination of gas transport parameters in soils.- Il Nuovo Cimento, 22 C, 3-4: 537-543

STEINDORF, K., LUBIN, J. H., WICHMANN, H. E. & BECHER, H. (1995): Lung cancer deaths attributable to indoor radon exposure in West Germany.- Int. J. Epidemiol. 24: 485-492

STRANDEN, E. (1987): Radon-222 in Norwegian Dwellings.- in: HOPKE, P.K. (ed.)(1987): Radon and its decay products: occurence, properties and health effects.- American Chemical Society: 70-83, Washington D.C.

STRANDEN, E., KOLSTAD, A.K. & LIND, B. (1984a): Radon exhalation: Moisture and temperature dependence.- Health Phys., 47, 3: 480-484

STRANDEN, E., KOLSTAD, A.K. & LIND, B. (1984b): The influence of moisture and temperature on radon exhalation.- Rad. Prot. Dosim., 7, 1-4: 55-58

STRONG, K.P. & LEVINS, D.M. (1982): Effect of moisture content on radon emanation from uranium ore and tailings.- Health Physics, 42, 1: 27-32

SUOMELA, J. (1993): Method for determination of radium-226 in water by liquid scintillation counting.- Swedish Radiation Protection Institute, SSI-report 93-12

SURBECK (1991): Radium und Radon im Boden: Meßtechnische und geologische Aspekte.- in: Völkle, H., Borchardt, D. (eds.): Messung von Radon und Radon-Folgeprodukten. Fortschritte im Strahlenschutz. Fachverband für Strahlenschutz: 132-141, Köln

SZTANYIK, B.L. & NIKI, I. (1993): A short summary of the programmes performed in Hungary on the measurement of the indoor radon activity-concentration.- Manuscript presented at the WHO-Meeting in Eilat, Israel, March 1993

TANNER, A. (1980): Radon migration in the ground: A supplementary review.- in: Gesell, T.F. & Lowder, W.M. (eds.): The natural radiation environment III, U. S. Department of Energy Report CONF-780422 Vol. 1: 5-56, Springfield

TANNER, A. (1988): A tentative protocol for measurement of radon availability from the ground.- Rad. Prot. Dosim., 24, 1-4: 79-83

TANNER, A. (1991): The role of diffusion in radon entry into houses.- in: The 1990 International Symposium on Radon and Radon Reduction Technology, Atlanta, Ga., 19-23 February 1990: Research Triangle Park, N.C., U.S. Environmental Protection Agency Rept. EPA600/9-91-026b, Proceedings, Vol. 2: Symposium Oral Papers, Paper No. V-2: 5-21--5-32, Atlanta

TAYLOR, R.M. (1987): Non-silicate oxides and hydroxides.- in: NEWMAN, A.C.D. (ed.): Chemistry of Clays and Clay Minerals.- Mineralogical Society Monograph No. 6: 129-209, London, Longman

TESSIER, A., CAMPBELL, P.G.C. & BISSON, M. (1979): Sequential extraction procedure for the speciation of particulate trace metals.- Anal. Chem. 51, 844-851

TEYSSEN, T.A.L. (1984): Sedimentology of the Minette oolitic ironstones of Luxembourg and Lorraine: a Jurrasic subtidal sandware complex.- Sedimentology, 31: 195-211

THEIN, J. (1975): Sedimentologisch-stratigraphische Untersuchungen in der Minette des Differdinger Beckens (Luxemburg).- Publ. Serv. Géol., XXIV, Luxembourg

TITAYEVA, N. A. & VEKSELER, T. L. (1977): The state of radioactive equilibrium in the uranium and thorium series as an indicator of migration of radioactive elements and active interaction between phases under natural conditions.- Geochem. Intl., 14: 99-107

TONDEUR, F., ZHU, H.C., CHARLET, J.M., GERARDY, I. & PERRAUX, R. (1996): Radon from the subsoil to the dwelling in southern Belgium.- Environm. Int., Vol. 22, Suppl. 1: S535 - S543

VANDENBYGAART, A. J., PROTZ, R. & MCCABE, D. C. (1999): Distribution of natural radionuclides and 137Cs in soils of southwestern Ontario.- Canadian Journal of Soil Science, 79 (1): 161 – 171

VON GUNTEN, H.R., SURBECK, H. & RÖSSLER, E. (1996): Uranium series disequilibrium and high thorium and radium enrichments in karst formations.- Environ. Sci. & Technol., 30/4: 1268-1274

VONSTILLE, W.T. & SACARELLO, H.L.A. (1990): Radon and cancer: Florida study finds no evidence of increased risk.- J. Environ. Health: 53: 25-28

WALTER, R. (1995): Geologie von Mitteleuropa.- Stuttgart, Schweizerbart

WAMPLER, J. M. (1972): Actinide Series.- in: FAIRBRIDGE, R.W. (ed.): The Encyclopedia of Geochemistry and Environmental Sciences, Encyclopedia of Earth Sciences Series, Vol. IVA: 5-9; Van Nostrand Reinhold, Princeton, NJ and New York

WHO (1987): Air quality guidelines for Europe.- WHO Regional Office for Europe, Copenhagen

WICHMANN, H.E. (1996): Radonrisiko aus epidemiologischer Sicht.- in: SIEHL, A. (ed.): Umweltradioaktivität: 311-330, Berlin, Ernst & Sohn

WICHMANN, H.E., GERKEN, M., WELLMANN, J., KREUZER, M., KREIENBROCK, L., KELLER, G., WÖLKE, G. & HEINRICH, J. (1999): Lungenkrebsrisiko durch Radon in der Bundesrepublik Deutschland (Ost) - Thüringen und Sachsen. Landsberg/Lech, ecomed

WICHMANN, H.E., KREIENBROCK, L., KREUZER, M., GERKEN, M., DINGERKUS, G., WELLMANN, J., KELLER, G. & KAPPEL, R. (1998): Lungenkrebsrisiko durch Radon in der Bundesrepublik Deutschland (West).- Landsberg/Lech, ecomed

WICHMANN, H.E., HEINRICH, J., GERKEN, M., KREUZER, M., WELLMANN, J., KELLER, G. & KREIENBROCK, L. (2002): Domestic radon and lung cancer – current status including new evidence from Germany.- in: BURKART, W., SOHRABI, M. & BAYER, A. (eds.): High levels of natural radiation and radon areas: Radiation dose and health effects - International Congress Series 1225: 247–252, Amsterdam, Excerpta Medica

WIEGAND, J. & KUSCHKOWITZ, T. (1998): Die Radium-Mobilisierung in Tiefenwässern.- Terra Nostra 98/3: 204-205

ZEIEN, H. & BRÜMMER, G.W. (1991): Chemische Extraktion zur Bestimmung der Bindungsformen von Schwermetallen in Böden.- in: BMFT (ed.): Auswirkungen von Siedlungsabfällen auf Böden, Bodenorganismen und Pflanzen: 62-91, Jülich.

ZEIEN, H. (1995): Chemische Extraktionen zur Bestimmung der Bindungsformen von Schwermetallen in Böden.- Bonner Bodenkundl. Abh., 17, Bonn

ZIEGLER, P.A. (1988): Evolution of the Arctic-North Atlantic and the Western Tethys.- Am. Assoc. Petrol. Geol., Mem. 43, Tulsa, Oklahoma

ZHU, H.C., CHARLET, J.M., DOREMUS, P., FLEMAL, J.M. & HALLEZ, S. (1995): Some geological factors relative to concentration of radon in underground water in Wallonia.- in: Dubois, C. (ed.): Gas Geochemistry.- Science Reviews:119-134

ZHU, H.C., CHARLET, J.M. & TONDEUR, F. (1998): Geological controls to the indoor radon distribution in Southern Belgium.- Sci. Tot. Environm., 220, 2-3: 195-214

10   Acknowledgements

11 Appendix

Table A1:   Sample sites.

Table A2:   Analyse of radionuclides of all samples, grouped by stratigraphic units.

Table A3:   Chemical analyse of all samples, grouped by stratigraphic units.

Table A4-1: Radium activities, radon activity concentrations and emanation coefficients (E) of rocks and weathering products.

Table A4-2: Emanation coefficients (E) of rocks.

Table A4-3: Emanation coefficients (E) of weathering products.

Table A4-4: Radon activity concentrations (referring to the released radon in sample pore gas, related to the weight of the emanating material under equilibrium conditions) of rocks and weathering products.

Table A5:   Analytical results for two samples, which were extracted in 3 parallel sessions and measured at least 9 times for each fraction. Results are given with standard deviation (SD) and coefficient of variation (RSD).

Map A6:   General geological map of Luxembourg, Sampling sites.

Table A1: Sample sites.

sample number	classification	rock type	x (R)	y (H)
Middle Dogger "*Limestone of Haut-Pont*" (*dom3*)				
188	rock	limestone	58 320	66 600
189	rock	limestone	58 320	66 600
191a	wp < 2 mm	limestone	58 320	66 600
191b	rock	limestone	58 320	66 600
Lower Dogger "*Minette*" (*dou*)				
192a	wp < 2 mm	limestone	57 740	66 790
192b	rock	limestone	57 740	66 790
192mA	wp < 2 mm	limestone	57 740	66 790
193a	wp < 2 mm	calcite vein	57 740	66 790
193b	wp > 2 mm	calcite vein	57 740	66 790
194a	wp < 2 mm	limestone	57 740	66 790
194b	rock	limestone	57 740	66 790
Middle Lias "*Upper Spianatus*" (*lm3b*)				
183	rock	sandstone	61 910	72 300
184	rock	Fe ore	61 940	72 405
185a	wp < 2 mm	sandstone	61 940	72 405
185b	rock	sandstone	61 940	72 405
186a	wp < 2 mm	sandstone	61 930	72 450
186b	rock	sandstone	61 930	72 450
187	rock	sandstone	61 930	72 450
Middle Lias "*Lower Spianatus*" (*lm3a*)				
180a	wp < 2 mm	marl	61 930	72 340
180b	rock	marl	61 930	72 340
181	rock	limestone	61 930	72 340
182a	wp < 2 mm	marl	61 925	72 340
182b	rock	marl	61 925	72 340
Lower Lias "*Marl and Limestone of Strassen*" (*li3*)				
123a	wp < 2 mm	calcite vein	85 100	64 440
123b	wp > 2 mm	calcite vein	85 100	64 440
138a	rock	sandstone	85 100	64 440
138b	wp < 2 mm	sandstone	85 100	64 440
139b	rock	marl	85 100	64 440
176	rock	marl	73 850	75 370
177	f	marl	73 850	75 370
178a	wp < 2 mm	marl	73 850	75 400
178b	rock	marl	73 850	75 400
179a	wp < 2 mm	marl	73 850	75 400
179b	rock	marl	73 850	75 400
179c	rock	marl	73 850	75 400
195	rock	marl	88 710	64 490
Lower Lias "*Luxemburger Sandstein*" (*li2*)				
20	rock	sandstone	78 900	91 510
81	wp < 2 mm	sandstone	81 460	76 860
82	rock	sandstone	81 460	76 860
83	wp < 2 mm	sandstone	81 460	76 860
103	rock	sandstone	88 700	89 710
104a	wp < 2 mm	sandstone	88 700	89 710
104b	rock	sandstone	88 700	89 710
106	wp > 2 mm	sandstone	88 650	89 700
107	wp < 2 mm	sandstone	88 650	89 700
115a	rock	sandstone	85 100	64 440
115b	rock	sandstone	85 100	64 440
116	wp > 2 mm	calcite vein	85 100	64 440
117	wp > 2 mm	sandstone	85 100	64 440
118	rock	sandstone	85 100	64 440
119a	wp < 2 mm	sandstone	85 100	64 440
119b	rock	sandstone	85 100	64 440
120	rock	sandstone	85 100	64 440
140	rock	sandstone	85 100	64 440

Table A1 (continued): Sample sites.

sample number	classification	rock type	x (R)	y (H)
Upper Keuper "*Rhät*" (*ko1*)				
175	rock	sandstone	79 105	85 395
Middle Keuper "*Steinmergelkeuper*" (*km3*)				
108a	rock	marl	88 680	89 550
108b	wp < 2 mm	marl	88 680	89 550
109a	wp > 2 mm	calcite vein	88 680	89 550
109b	wp < 2 mm	calcite vein	88 680	89 550
110	rock	marl	88 680	89 550
111	wp > 2 mm	calcite vein	88 680	89 550
112a	rock	dolomite	88 680	89 550
112b	wp < 2 mm	dolomite	88 680	89 550
113	wp > 2 mm	calcite vein	88 680	89 550
114	rock	dolomite	88 680	89 550
169a	wp < 2 mm	marl	73 850	84 680
169b	rock	marl	73 850	84 680
171a	wp < 2 mm	marl	79 215	85 240
171b	rock	marl	79 215	85 240
172a	wp < 2 mm	marl	79 210	85 275
172b	rock	marl	79 210	85 275
173	wp < 2 mm	marl	79 190	85 320
174	wp < 2 mm	marl	79 160	85 360
Middle Keuper "*Schilfsandstein*" (*km2s*)				
85	rock	sandstone	93 105	80 840
86	rock	sandstone	93 105	80 840
87a	rock	sandstone	93 105	80 840
88a	rock	sandstone	93 105	80 840
88b	wp < 2 mm	sandstone	93 105	80 840
Middle Keuper "*Pseudomorphosenkeuper*" (*km1*)				
141a	rock	sandstone	71 410	95 360
141b	wp < 2 mm	sandstone	71 410	95 360
142	rock	sandstone	71 410	95 360
143a	rock	marl	74 220	92 670
143b	wp < 2 mm	marl	74 220	92 670
143d	wp < 2 mm	marl	74 220	92 670
144b	wp < 2 mm	marl	74 220	92 670
145a	wp < 2 mm	marl	74 220	92 670
145b	rock	marl	74 220	92 670
146a	wp < 2 mm	marl	74 220	92 670
146b	rock	marl	74 220	92 670
147b	wp < 2 mm	marl	74 220	92 670
148a	rock	dolomite	74 220	92 670
148b	wp < 2 mm	dolomite	74 220	92 670
Upper Muschelkalk (*mo2*)				
16	rock	sandstone	76 650	94 940
17	wp < 2 mm	sandstone	76 650	94 940
21	wp < 2 mm	dolomite	76 020	96 860
22	rock	dolomite	76 020	96 860
54	wp > 2 mm	dolomite	91 650	83 530
89	rock	dolomite	91 650	83 530
90a	rock	marl	91 650	83 530
90b	wp < 2 mm	marl	91 650	83 530
91	wp > 2 mm	calcite vein	91 650	83 530
92	wp < 2 mm	marl	91 650	83 530
163a	wp < 2 mm	dolomite	98 200	95 260
163b	rock	dolomite	98 200	95 260
164	rock	marl	98 200	95 260
165a	wp < 2 mm	marl	98 200	95 260
165b	rock	marl	98 200	95 260
166	rock	dolomite	99 150	96 050
167a	wp < 2 mm	dolomite	99 150	96 050
167b	wp > 2 mm	dolomite	99 150	96 050
168a	wp < 2 mm	dolomite	99 150	96 050
168b	rock	dolomite	99 150	96 050

Table A1 (continued): Sample sites.

sample number	classification	rock type	x (R)	y (H)
Upper Muschelkalk (*mo1*)				
33	wp > 2 mm	calcite vein	86 360	105 000
34a	wp < 2 mm	dolomite	86 360	105 000
34b	wp > 2 mm	dolomite	86 360	105 000
35	rock	dolomite	86 360	105 000
39	rock	dolomite	91 770	100 195
84	rock	dolomite	95 840	74 780
93	rock	dolomite	97 650	85 820
95	wp > 2 mm	dolomite	97 650	85 820
96	wp > 2 mm	calcite vein	97 650	85 820
97a	wp < 2 mm	dolomite	97 650	85 820
97b	wp > 2 mm	dolomite	97 650	85 820
Middle Muschelkalk (*mm*)				
32	rock	dolomite	86 180	105 630
Lower Muschelkalk (*mu*)				
19	rock	sandstone	83 100	107 570
157a	wp < 2 mm	sandstone	104 500	96 180
158a	wp > 2 mm	sandstone	104 500	96 180
158b	wp > 2 mm	sandstone	104 500	96 180
159a	wp < 2 mm	sandstone	104 500	96 180
160	rock	sandstone	104 500	96 180
161	rock	marl	104 500	96 180
162	rock	sandstone	104 500	96 180
Buntsandstein (*so*)				
15	rock	sandstone	84 760	107 150
53	rock	sandstone	83 420	108 125
98	rock	sandstone	104 550	93 750
99	wp > 2 mm	sandstone	104 550	93 750
100	rock	sandstone	104 550	93 750
101	rock	sandstone	104 550	93 750
102	wp < 2 mm	sandstone	104 550	93 750
Upper Emsian (*E3*)				
6	rock	schist	55 280	114 375
28	wp > 2 mm	schist	62 780	114 350
29	rock	schist	62 780	114 350
42	rock	schist	75 880	122 150
50	rock	siltstone	61 490	113 670
56a	wp < 2 mm	schist	76 100	123 570
56b	rock	schist	76 100	123 570
66	wp < 2 mm	schist	72 225	120 545
70a	rock	schist	68 070	120 805
70b	rock	schist	68 070	120 805
71a	rock	schist	68 070	120 805
71b	rock	quartz vein	68 070	120 805
73	rock	schist	76 250	132 505
Middle Emsian "*Quarzit von Berlé*" (*E2q*)				
43	rock	quartzite	61 460	113 665
48	rock	quartzite	61 655	113 440
67a	rock	quartzite	71 650	120 690
67b	rock	quartzite	71 650	120 690
Middle Emsian "*Bunte Schiefer von Clerf*" (*E2*)				
8	rock	schist	55 670	114 710
55a	wp < 2 mm	schist	76 670	124 155
55b	rock	schist	76 670	124 155
68	wp > 2 mm	sandstone	71 275	120 915
69	rock	sandstone	72 275	121 915

Table A1 (continued): Sample sites.

sample number	classification	rock type	x (R)	y (H)
Lower Emsian (*E1b*)				
13	rock	sandstone	71 335	124 585
45	wp	sandstone	63 265	113 205
72	rock	siltstone	68 380	122 340
149	rock	schist	70 650	129 980
150	rock	quartzite	70 650	129 980
Lower Emsian (*E1a*)				
1	wp < 2 mm	schist	54 200	105 400
7	rock	schist	54 200	105 400
18	wp	schist	84 270	108 240
23	rock	siltstone	57 620	116 895
46	rock	sandstone	63 400	111 620
49	rock	schist	57 225	118 080
Upper Siegenian (*Sg 3*)				
2a	rock	schist	53 060	101 720
2b	rock	schist	53 060	101 720
2c	wp > 2 mm	schist	53 060	101 720
3	wp < 2 mm	schist	52 870	101 220
4	rock	schist	52 870	101 220
5	rock	schist	52 870	101 220
9	rock	schist	58 630	119 240
10	rock	schist	60 680	123 560
11	rock	schist	60 680	123 560
12	rock	schist	60 680	123 560
24	wp < 2 mm	schist	68 850	103 100
25a	wp > 2 mm	schist	68 720	103 200
25b	wp < 2 mm	schist	68 720	103 200
26	wp < 2 mm	schist	68 720	103 200
27	rock	schist	68 720	103 200
30	wp < 2 mm	schist	65 030	105 920
31	rock	schist	65 030	105 920
36	rock	siltstone	63 620	110 820
37	rock	siltstone	63 620	110 820
47	rock	schist	57 660	117 690
74	rock	siltstone	74 200	131 575
75	rock	quartz vein	74 200	131 575
76	rock	schist	68 480	132 890
78	rock	siltstone	68 985	134 470
79	rock	schist	69 935	134 395
Middle Siegenian (*Sg 2*)				
38	rock	siltstone	57 350	120 200
44	rock	schist	56 670	118 690
51	rock	schist	56 790	120 040
77a	wp < 2 mm	schist	65 495	135 315
77b	rock	siltstone	65 495	135 315
77c	rock	schist	65 495	135 315
154a	wp < 2 mm	schist	57 060	120 150
154b	wp > 2 mm	schist	57 060	120 150
155a	wp < 2 mm	schist	57 060	120 150
155b	rock	schist	57 060	120 150
156	rock	schist	57 060	120 150
Lower Siegenian (*Sg 1*)				
40	rock	schist	55 365	118 485
41	rock	schist	55 495	118 620

Table A1 (continued): Sample sites.

sample number	classification	rock type	x (R)	y (H)	
Gedinnian (*Ged*)					
124	rock	sandstone	^{6}66 020	^{55}42 050	Hatrival, Belgium
125a	wp > 2 mm	sandstone	^{6}66 020	^{55}42 050	Hatrival, Belgium
125b	wp < 2 mm	sandstone	^{6}66 020	^{55}42 050	Hatrival, Belgium
126	rock	quartz vein	^{6}66 020	^{55}42 050	Hatrival, Belgium
127a	wp > 2 mm	sandstone	^{6}66 020	^{55}42 050	Hatrival, Belgium
127b	wp < 2 mm	sandstone	^{6}66 020	^{55}42 050	Hatrival, Belgium
128a	rock	sandstone	^{6}66 020	^{55}42 050	Hatrival, Belgium
128b	wp < 2 mm	sandstone	^{6}66 020	^{55}42 050	Hatrival, Belgium
129	rock	sandstone	^{6}66 020	^{55}42 050	Hatrival, Belgium
130	rock	sandstone	^{6}66 020	^{55}42 050	Hatrival, Belgium
131	rock	schist	^{6}66 020	^{55}42 050	Hatrival, Belgium
132a	rock	siltstone	^{6}66 020	^{55}42 050	Hatrival, Belgium
132b	wp < 2 mm	siltstone	^{6}66 020	^{55}42 050	Hatrival, Belgium
133a	rock	quartzite	^{6}66 020	^{55}42 050	Hatrival, Belgium
134	wp < 2 mm	sandstone	^{6}66 020	^{55}42 050	Hatrival, Belgium
135	rock	sandstone	^{6}66 020	^{55}42 050	Hatrival, Belgium
136a	rock	sandstone	^{6}66 020	^{55}42 050	Hatrival, Belgium
136b	wp < 2 mm	sandstone	^{6}66 020	^{55}42 050	Hatrival, Belgium
137	rock	sandstone	^{6}66 020	^{55}42 050	Hatrival, Belgium

N.B.: Coordinate systems are LUREF for Luxembourg and LAMBERT for Hatrival, Belgium

Table A2: Analyse of radionuclides of all samples, grouped by stratigraphic units.

sample number	classification	rock type	232Th [Bq/kg]	SD [Bq/kg]	238U [Bq/kg]	SD [Bq/kg]	230Th [Bq/kg]	SD [Bq/kg]	226Ra [Bq/kg]	SD [Bq/kg]	210Pb [Bq/kg]	SD [Bq/kg]	40K [Bq/kg]	SD [Bq/kg]	137Cs [Bq/kg]	SD [Bq/kg]
Middle Dogger "Limestone of Haut-Pont" (dom3)																
188	rock	limestone	15.2	0.4	7.5	3.2	<		7.5	0.4	9.4	3.8	32	4	<	
189	rock	limestone	30.1	0.6	13.5	4.4	<		12.8	0.5	14.7	4.0	37	4	1.2	0.3
191a	wp < 2 mm	limestone	51.5	2.1	23.9	6.3	<		21.4	1.8	26.4	4.8	352	14	4.4	0.8
191b	rock	limestone	41.2	0.6	12.9	4.4	<		13.6	0.5	12.7	4.0	109	5	<	
Lower Dogger "Minette" (dou)																
192a	wp < 2 mm	limestone	64.6	2.1	17.0	5.4	<		18.4	1.8	23.4	4.6	47	1	<	
192b	rock	limestone	56.2	0.7	14.4	4.4	<		17.9	0.5	14.8	3.8	18	4	<	
192mA	wp < 2 mm	limestone	68.2	2.3	32.1	7.4	<		29.1	1.9	31.9	4.9	51	2	<	
193a	wp < 2 mm	calcite	67.6	0.7	18.8	5.1	<		17.9	0.5	18.0	4.2	51	5	1.3	0.3
193b	wp > 2 mm	calcite	19.9	0.5	9.8	3.9	<		6.6	0.4	7.7	3.8	10	4	<	
194a	wp < 2 mm	limestone	76.1	0.8	12.6	4.4	<		13.4	0.5	13.5	4.0	34	4	<	
194b	rock	limestone	48.9	0.6	16.9	4.7	<		15.9	0.5	13.8	4.0	26	4	<	
Middle Lias "Upper Spianatus" (lm3b)																
183	rock	sandstone	36.0	0.5	11.3	3.7	118	31	9.0	0.4	8.6	3.9	257	7	<	
184	rock	Fe ore	45.5	0.6	25.5	5.6	<		39.7	0.6	25.4	4.0	10	4	<	
187	rock	sandstone	40.5	0.6	21.7	5.5	<		19.6	0.5	21.1	4.7	289	7	<	
185a	wp < 2 mm	sandstone	66.3	0.8	24.4	6.1	<		24.1	0.6	25.1	4.9	515	10	<	
185b	rock	sandstone	51.9	0.7	20.3	5.4	<		21.3	0.5	21.6	4.6	343	8	<	
186a	wp < 2 mm	sandstone	70.8	0.9	17.9	5.6	<		30.2	0.6	33.3	5.2	566	11	<	
186b	rock	sandstone	58.2	2.3	39.9	8.7	<		37.2	2.1	38.6	5.2	721	14	<	
Middle Lias "Lower Spianatus" (lm3a)																
181	rock	limestone	19.8	0.5	14.7	4.4	<		13.7	0.5	14.4	3.9	218	7	<	
180a	wp < 2 mm	marl	45.3	0.8	22.5	6.2	<		28.7	0.7	50.8	5.5	537	11	4.1	0.4
180b	rock	marl	38.4	0.5	24.9	5.3	<		25.2	0.4	23.0	3.4	506	7	<	
182a	wp < 2 mm	marl	45.6	2.1	37.1	8.2	<		37.0	2.1	39.5	5.4	824	7	<	
182b	rock	marl	45.0	2.1	32.1	7.5	<		30.3	2.0	30.7	5.3	804	9	<	
Lower Lias "Marl and Limestone of Strassen" (li3)																
176	rock	marl	11.0	0.5	52.3	9.8	<		53.1	0.6	48.1	4.3	115	5	1.3	0.2
177	f	marl	5.4	0.4	21.8	5.2	<		28.0	0.6	24.0	4.2	36	4	<	
195	rock	marl	44.3	0.7	44.5	8.9	<		45.2	1.0	31.9	4.9	497	10	<	
123a	wp < 2 mm	calcite	11.1	0.8	11.6	6.0	<		11.8	0.7	60.4	6.9	86	8	<	
123b	wp > 2 mm	calcite	8.4	1.3	15.0	4.7	<		27.7	1.9	26.2	4.4	129	4	<	
138a	rock	sandstone	16.5	0.6	14.6	4.9	<		13.7	0.6	11.5	4.8	234	1	<	
138b	wp < 2 mm	sandstone	40.3	0.7	24.0	6.1	<		41.5	0.7	34.5	5.0	320	9	<	
139b	rock	marl	36.2	0.7	19.0	5.6	<		21.4	0.7	22.6	5.2	492	2	<	
178a	wp < 2 mm	marl	20.2	0.6	34.6	7.2	<		42.3	0.6	35.5	4.4	255	7	2.3	0.3
178b	rock	marl	14.0	0.4	25.4	5.3	<		19.1	0.4	28.1	4.0	196	6	<	
179a	wp < 2 mm	marl	36.2	0.6	44.8	8.9	<		44.8	0.7	44.7	4.9	508	10	<	
179b	rock	marl	18.7	1.6	33.5	7.2	<		31.6	1.9	36.1	4.7	430	10	<	
179c	rock	marl	36.1	0.6	37.2	7.6	<		40.9	0.6	42.5	4.6	492	9	<	

Table A2 (continued): Analyse of radionuclides of all samples, grouped by stratigraphic units.

sample number	classification	rock type	232Th [Bq/kg]	SD [Bq/kg]	238U [Bq/kg]	SD [Bq/kg]	230Th [Bq/kg]	SD [Bq/kg]	226Ra [Bq/kg]	SD [Bq/kg]	210Pb [Bq/kg]	SD [Bq/kg]	40K [Bq/kg]	SD [Bq/kg]	137Cs [Bq/kg]	SD [Bq/kg]
Lower Lias "Luxemburger Sandstein" (li2)																
20	rock	sandstone	7.1	0.3	3.2	0.9	<		5.1	0.4	4.1	0.9	145	1	<	
81	wp < 2 mm	sandstone	12.5	0.8	< 13.7		<		6.9	0.8	NA		76	1	8.4	0.5
82	rock	sandstone	9.5	0.0	13.2	0.0	<		11.2	0.0	21.4	4.1	151	5	<	
83	wp < 2 mm	sandstone	7.2	0.6	7.8	4.3	<		4.9	0.6	5.6	4.8	71	1	<	
103	rock	sandstone	6.9	0.4	4.1	2.9	<		2.2	0.3	4.9	3.8	122	6	<	
106	wp > 2 mm	sandstone	19.5	0.7	6.2	4.5	<		19.1	0.7	15.8	5.0	367	1	<	
107	wp < 2 mm	sandstone	22.2	0.7	11.4	4.6	<		13.4	0.7	12.4	4.8	361	3	<	
116	wp > 2 mm	calcite	1.1	0.1	6.5	1.3	<		<2.5		24.6	0.0	34	1	<	
117	wp > 2 mm	sandstone	7.3	0.5	37.1	7.5	<		42.9	0.6	38.2	4.4	68	4	<	
118	rock	sandstone	26.0	0.5	117.8	20.6	121	45	120.7	1.4	118.6	5.4	68	5	<	
120	rock	sandstone	6.5	0.4	16.4	4.5	<		21.3	0.5	72.4	3.4	40	4	<	
140	rock	sandstone	7.6	0.4	10.2	3.5	<		3.9	0.4	9.9	4.1	57	5	<	
104a	wp < 2 mm	sandstone	20.5	0.5	13.4	4.4	<		13.8	0.5	14.6	4.1	222	7	<	
104b	rock	sandstone	14.3	0.6	8.6	4.2	<		8.4	0.6	8.7	4.6	350	6	<	
115a	rock	sandstone	4.6	0.4	25.5	5.7	<		21.5	0.5	24.5	4.2	53	5	<	
115b	rock	sandstone	5.6	0.4	19.7	5.0	<		22.4	0.5	20.0	4.1	49	4	<	
119a	wp < 2 mm	sandstone	13.6	0.5	23.0	5.4	<		20.8	0.5	22.6	4.1	208	7	<	
119b	rock	sandstone	11.8	0.5	20.0	5.0	<		18.5	0.5	20.9	4.1	164	6	<	
Upper Keuper "Rhät" (ko1)																
175	rock	sandstone	13.6	0.5	23.8	5.5	<		18.1	0.5	21.3	4.1	241	7	<	
Middle Keuper "Steinmergelkeuper" (km3)																
110	wp > 2 mm	marl	7.4	0.0	71.6	0.1	<		319.8	0.1	314.8	9.9	309	3	<	
111	wp > 2 mm	calcite	33.0	0.8	82.5	15.1	<		87.6	0.9	69.8	6.1	1 279	9	<	
113	wp > 2 mm	calcite	5.1	0.7	48.3	9.6	334	61	262.6	1.3	234.9	6.9	301	6	<	
114	rock	dolomite	11.9	0.7	78.5	14.3	<		78.0	0.9	71.2	5.7	625	1	<	
108a	rock	marl	34.6	0.6	74.9	13.5	<		75.8	1.1	152.3	9.5	1 074	15	<	
108b	wp < 2 mm	marl	36.2	0.6	72.4	13.0	<		67.7	0.6	71.2	5.0	1 200	15	<	
109a	wp > 2 mm	calcite	8.1	0.7	67.1	12.9	261	70	264.0	1.4	243.9	7.2	330	6	<	
109b	wp < 2 mm	calcite	32.3	0.9	64.7	12.7	<		87.4	1.6	85.7	7.1	1 067	17	1.6	0.4
112a	rock	dolomite	7.5	0.4	32.2	6.3	<		33.7	0.5	51.5	4.3	291	8	<	
112b	wp < 2 mm	dolomite	11.3	0.0	53.0	0.1	<		80.8	0.0	89.0	5.8	618	11	<	
173	wp < 2 mm	marl	38.0	0.6	34.6	7.3	<		33.0	0.6	36.6	4.7	823	12	2.3	0.3
174	wp < 2 mm	marl	52.2	0.6	22.0	5.2	<		27.4	0.5	25.1	4.5	744	12	2.2	0.3
169a	wp < 2 mm	marl	28.0	0.6	26.9	6.1	<		24.4	0.5	27.0	4.4	634	11	<	
169b	rock	marl	24.4	0.5	27.6	5.9	<		18.2	0.5	19.4	4.4	662	12	<	
171a	wp < 2 mm	marl	30.1	0.6	39.0	0.8	<		38.5	0.6	38.3	4.7	743	12	6.6	0.4
171b	rock	marl	24.8	0.5	36.4	7.1	<		33.4	0.5	32.5	4.4	835	13	<	
172a	wp < 2 mm	marl	31.4	0.6	32.7	7.3	<		49.0	1.0	46.1	5.2	689	12	5.0	0.4
172b	rock	marl	24.8	0.6	34.7	7.3	<		41.0	0.7	42.8	4.8	786	12	<	

Table A2 (continued): Analyse of radionuclides of all samples, grouped by stratigraphic units.

sample number	classification	rock type	232Th [Bq/kg]	SD [Bq/kg]	238U [Bq/kg]	SD [Bq/kg]	230Th [Bq/kg]	SD [Bq/kg]	226Ra [Bq/kg]	SD [Bq/kg]	210Pb [Bq/kg]	SD [Bq/kg]	40K [Bq/kg]	SD [Bq/kg]	137Cs [Bq/kg]	SD [Bq/kg]
Middle Keuper "Schilfsandstein" (km2s)																
85	rock	sandstone	32.5	0.7	20.5	5.9	<		19.9	0.7	18.2	5.6	1 891	11	<	
86	rock	sandstone	49.4	0.7	33.7	7.5	<		34.2	0.6	33.5	5.0	1 710	19	<	
87a	rock	sandstone	49.5	0.7	31.9	7.2	<		30.7	0.6	48.5	5.2	1 760	19	<	
88a	rock	sandstone	49.2	0.8	34.5	7.7	<		41.3	0.8	30.8	5.5	1 986	16	<	
88b	wp < 2 mm	sandstone	56.6	0.8	55.3	10.7	<		46.1	0.8	41.4	5.5	2 207	14	<	
Middle Keuper " Rote Gipsmergel" (km2)																
143a	rock	marl	10.2	0.6	25.0	6.0	124	31	23.6	0.7	22.0	4.7	170	1	<	
143b	wp < 2 mm	marl	26.4	0.6	38.6	7.7	<		40.0	0.6	79.5	8.4	340	9	<	
143d	wp < 2 mm	marl	21.7	0.5	30.8	6.3	<		39.5	0.6	84.9	8.0	190	7	<	
144b	wp < 2 mm	marl	50.2	0.8	41.0	8.6	<		40.3	0.8	41.4	5.6	1 136	8	<	
145a	wp < 2 mm	marl	45.0	0.6	48.0	9.0	<		40.0	0.6	78.8	8.2	840	13	<	
145b	rock	marl	44.1	0.7	48.4	9.2	<		38.9	0.6	69.2	8.2	912	14	<	
146a	wp < 2 mm	marl	43.4	2.0	35.6	8.0	<		33.1	2.0	36.1	5.4	884	13	<	
146b	rock	marl	40.0	0.6	35.4	7.0	<		24.7	0.5	28.2	4.4	761	12	<	
147b	wp < 2 mm	marl	44.2	0.7	46.1	9.1	<		42.1	0.6	43.3	4.9	879	13	<	
148a	rock	dolomite	11.7	0.6	60.4	11.4	<		70.3	0.8	59.7	5.2	324	2	<	
148b	wp < 2 mm	dolomite	18.2	0.6	49.4	9.5	<		46.4	0.8	52.5	5.0	381	9	<	
Middle Keuper "Pseudomorphosenkeuper" (km1)																
142	rock	sandstone	26.5	0.6	19.6	5.1	<		18.3	0.5	19.6	4.5	429	9	<	
141a	rock	sandstone	30.6	0.7	18.5	5.7	<		19.0	0.7	20.5	5.1	862	2	<	
141b	wp < 2 mm	sandstone	39.8	0.8	21.4	5.9	<		21.1	0.7	24.3	5.2	1 103	3	1.5	0.3
Upper Muschelkalk (mo2)																
16	rock	sandstone	12.6	0.4	27.6	1.7	<		22.0	0.6	26.4	1.1	384	48	<	
17	wp < 2 mm	sandstone	33.6	0.8	42.7	7.5	<		57.1	1.1	44.0	2.0	1 087	26	5.0	0.3
21	wp < 2 mm	dolomite	37.5	0.8	49.6	8.7	<		97.0	1.6	67.0	2.4	894	22	14.1	0.5
22	rock	dolomite	8.5	0.4	28.5	5.0	<		33.6	0.8	27.2	4.8	105	2	<	
54	wp > 2 mm	dolomite	9.8	0.6	6.6	4.3	<		9.8	0.6	11.9	4.8	375	8	0.8	0.3
89	rock	dolomite	10.9	0.5	10.9	4.4	<		12.5	0.6	11.8	4.5	247	1	<	
91	wp > 2 mm	calcite	<2.4		13.5	0.0	<		12.0	0.0	13.1	3.9	36	1	<	
92	wp < 2 mm	marl	35.2	0.7	42.8	8.8	<		42.8	0.7	45.9	5.6	1 485	25	60.5	0.8
164	rock	marl	14.9	0.5	24.6	5.8	<		21.7	0.5	23.1	4.3	571	10	<	
166	rock	dolomite	11.4	1.3	24.3	6.0	<		24.3	1.8	35.6	4.6	236	5	<	
163a	wp < 2 mm	dolomite	25.0	0.6	15.1	4.8	<		24.2	0.5	23.8	4.5	822	12	2.0	0.3
163b	rock	dolomite	15.9	0.5	12.3	4.6	<		13.7	0.5	12.2	5.3	577	10	<	
165a	wp < 2 mm	marl	40.9	0.7	34.8	7.4	<		45.7	0.6	38.7	4.9	1 488	17	<	
165b	rock	marl	43.1	0.7	42.7	8.9	<		39.5	0.7	39.3	5.6	1 557	18	<	
167a	wp < 2 mm	dolomite	14.0	0.5	23.7	5.4	<		21.9	0.5	24.0	4.0	186	6	1.2	0.2
167b	wp > 2 mm	dolomite	6.4	0.5	16.6	4.5	<		13.0	0.5	13.5	3.9	112	5	<	
168a	wp < 2 mm	dolomite	19.0	0.5	15.7	4.8	<		35.8	0.6	26.7	4.4	285	8	<	
168b	rock	marl	11.8	0.5	16.3	4.7	<		11.9	0.5	18.1	4.1	197	7	<	
90a	rock	marl	37.5	0.7	35.0	7.5	<		38.5	0.8	32.2	5.1	NA		<	
90b	wp < 2 mm	marl	51.9	0.9	79.2	14.6	<		80.9	0.9	42.0	6.0	2 202	19	1.6	0.3

Table A2 (continued): Analyse of radionuclides of all samples, grouped by stratigraphic units.

sample number	classification	rock type	232Th [Bq/ kg]	SD [Bq/ kg]	238U [Bq/ kg]	SD [Bq/ kg]	230Th [Bq/ kg]	SD [Bq/ kg]	226Ra [Bq/ kg]	SD [Bq/ kg]	210Pb [Bq/ kg]	SD [Bq/ kg]	40K [Bq/ kg]	SD [Bq/ kg]	137Cs [Bq/ kg]	SD [Bq/ kg]
Upper Muschelkalk (*mo1*)																
33	wp > 2 mm	calcite	25.9	0.4	57.8	6.3	<		59.5	1.3	67.3	3.2	691	16	3.2	0.0
35	rock	dolomite	6.3	0.3	14.2	2.6	<		18.7	0.6	18.2	1.2	69	4	<	
39	rock	dolomite	6.6	0.8	9.3	5.1	<		9.9	0.7	8.4	5.5	NA		<	
84	rock	dolomite	7.6	0.6	8.9	4.3	<		12.0	0.6	12.1	4.8	105	1	<	
93	rock	dolomite	8.8	0.6	10.0	4.5	<		5.0	0.6	<8.6		129	0	<	
95	wp > 2 mm	dolomite	7.8	0.6	13.5	4.8	<		15.4	0.6	14.6	4.9	NA		<	
96	wp > 2 mm	calcite	5.0	0.4	14.0	3.7	<		9.6	0.4	12.9	3.8	72	5	1.1	0.2
34a	wp < 2 mm	dolomite	25.2	0.4	38.8	3.0	<		36.5	0.7	36.9	1.5	401	9	<	
34b	wp > 2 mm	dolomite	10.2	0.1	28.7	1.7	<		18.5	0.3	22.8	0.8	129	2	<	
97a	wp < 2 mm	dolomite	39.7	0.9	40.0	9.0	<		42.7	1.0	54.1	6.8	1 183	24	43.5	0.8
97b	wp > 2 mm	dolomite	31.8	3.8	<36.3		<		8.9	2.6	74.1	27.7	NA		6.9	1.7
Middle Muschelkalk (*mm*)																
32	rock	dolomite	18.2	0.5	17.6	3.3	<		18.4	0.6	16.5	1.3	190	9	<	
Lower Muschelkalk (*mu*)																
19	rock	sandstone	51.5	0.8	41.9	8.5	<		31.2	0.7	22.9	5.1	1 613	28	<	
160	rock	sandstone	49.5	0.7	34.5	7.2	<		33.9	0.6	35.6	4.6	1 143	14	<	
161	rock	marl	61.8	0.8	41.9	8.8	<		42.0	0.7	43.0	5.5	1 676	19	<	
162	rock	sandstone	25.4	0.5	23.5	5.2	<		24.2	1.9	28.2	5.1	1 111	15	<	
157a	wp < 2 mm	sandstone	51.9	0.8	45.8	9.5	<		49.2	0.7	44.4	5.6	920	15	<	
158a	wp < 2 mm	sandstone	48.2	0.6	35.0	7.0	<		31.3	0.5	34.9	4.7	1 092	14	6.4	0.3
158b	wp > 2 mm	sandstone	50.5	0.7	37.0	7.7	<		31.8	0.6	42.6	4.8	1 017	14	3.0	0.3
159a	wp < 2 mm	sandstone	40.4	0.6	29.8	6.8	<		33.4	0.6	30.1	4.8	800	12	<	
Buntsandstein (so)																
15	rock	sandstone	14.8	0.5	11.0	2.3	<		14.0	0.5	12.2	1.4	1 323	18	<	
53	rock	sandstone	32.5	1.0	26.0	7.2	<		24.3	0.9	23.8	6.6	462	14	2.4	0.5
98	rock	sandstone	41.0	0.7	20.2	5.5	<		23.0	0.7	20.1	0.5	836	3	<	
99	wp > 2 mm	sandstone	61.8	0.9	36.4	8.0	<		31.2	0.8	33.5	5.6	1 115	3	<	
100	rock	sandstone	60.7	0.8	31.5	7.3	<		29.4	0.7	31.7	5.5	1 067	21	<	
101	rock	sandstone	56.0	0.8	34.0	7.6	<		34.2	0.7	34.2	5.5	1 007	6	<	
102	wp < 2 mm	sandstone	58.7	0.9	32.8	7.6	<		32.7	0.8	33.3	5.9	1 181	7	<	

Table A2 (continued): Analyse of radionuclides of all samples, grouped by stratigraphic units.

sample number	classification	rock type	232Th [Bq/kg]	SD [Bq/kg]	238U [Bq/kg]	SD [Bq/kg]	230Th [Bq/kg]	SD [Bq/kg]	226Ra [Bq/kg]	SD [Bq/kg]	210Pb [Bq/kg]	SD [Bq/kg]	40K [Bq/kg]	SD [Bq/kg]	137Cs [Bq/kg]	SD [Bq/kg]
Upper Emsian (E3)																
6	rock	schist	65.2	0.9	35.6	8.1	<		43.3	0.9	37.4	6.0	1 324	26	<	
28	wp > 2 mm	schist	50.6	0.8	44.0	8.8	<		40.6	0.8	27.6	5.1	728	117	11.8	0.5
29		schist	61.2	1.1	41.9	9.3	<		42.9	0.9	26.3	6.4	979	18	<	
42	rock	schist	65.1	0.8	32.8	7.1	<		35.3	0.7	35.2	5.5	1 301	3	<	
50	rock	siltstone	51.4	1.0	31.9	5.7	<		31.7	0.8	29.9	1.8	1 141	2	<	
66	wp < 2 mm	schist	67.2	1.2	45.0	9.9	<		44.9	1.0	44.2	6.8	942	19	<	
73	rock	schist	55.1	0.6	38.7	7.5	<		31.7	0.5	40.0	4.3	1 060	14	<	
56a	wp < 2 mm	schist	93.7	2.7	47.2	18.5	<		101.2	2.7	121.4	19.5	1 208	72	7.1	1.3
56b	rock	schist	66.6	0.9	32.0	7.6	<		33.4	0.8	28.3	6.0	1 369	11	<	
70a	rock	schist	60.2	0.9	26.9	6.8	<		38.1	0.7	26.7	5.5	1 237	11	<	
70b	rock	schist	55.8	0.8	34.1	7.4	<		38.6	0.8	35.4	5.1	1 048	22	<	
71a	rock	schist	69.3	0.9	37.1	8.2	<		35.5	0.7	33.2	5.8	1 555	45	<	
71b	rock	quartz vein	3.6	0.4	8.5	3.3	<		<2.9		7.2	0.0	28	1	<	
Middle Emsian "Quarzit von Berlé" (E2q)																
43	rock	quartzite	7.2	0.3	6.4	1.4	<		5.6	0.4	5.7	5.2	129	7	<	
48	rock	quartzite	6.9	0.8	7.8	4.7	<		6.9	0.6	<8.1		58	7	<	
67a	rock	quartzite	6.8	0.6	<14.1		<		4.9	0.8	<16.0		103	1	1.2	0.3
67b	rock	quartzite	6.1	0.6	<13.5		<		<3.1		<15.8		89	1	0.6	0.0
Middle Emsian "Bunte Schiefer von Clerf" (E2)																
8	rock	schist	52.8	1.0	36.9	6.5	<		35.7	0.9	39.5	5.6	852	13	<	
68	wp > 2 mm	sandstone	55.2	0.8	40.8	8.4	<		38.1	0.7	47.8	5.9	839	14	1.0	0.3
69	rock	sandstone	54.9	1.0	30.5	8.0	<		33.9	0.9	31.8	6.2	786	16	<	
55a	wp < 2 mm	schist	89.5	4.1	59.0	28.9	<		70.0	4.1	158.2	32.7	1 286	23	<	
55b	rock	schist	56.7	0.8	28.2	6.8	<		32.0	0.7	31.7	5.4	1 177	8	<	
Lower Emsian (E1b)																
13	rock	sandstone	47.5	0.9	35.0	6.2	<		36.4	0.8	35.2	1.8	927	20	1.0	0.2
45	wp	sandstone	47.6	0.9	37.1	6.6	<		37.4	0.9	36.0	1.8	812	3	<	
72	rock	siltstone	62.0	0.9	34.8	7.7	<		35.2	0.7	34.5	5.6	629	3	<	
149	rock	schist	56.8	0.9	34.8	7.9	<		33.2	0.7	28.2	5.6	1 234	3	<	
150	rock	quartzite	<1.3		<14.1		<		<3.4		<4.8		7	0	<	

Table A2 (continued): Analyse of radionuclides of all samples, grouped by stratigraphic units.

sample number	classification	rock type	232Th [Bq/kg]	SD [Bq/kg]	238U [Bq/kg]	SD [Bq/kg]	230Th [Bq/kg]	SD [Bq/kg]	226Ra [Bq/kg]	SD [Bq/kg]	210Pb [Bq/kg]	SD [Bq/kg]	40K [Bq/kg]	SD [Bq/kg]	137Cs [Bq/kg]	SD [Bq/kg]
Lower Emsian (*E1a*)																
1	wp < 2 mm	schist	55.3	1.0	42.5	7.5	<		43.6	1.0	40.2	2.0	1 231	26	<	
7	rock	schist	52.1	1.0	49.5	8.7	<		48.1	1.0	48.7	2.1	1 264	24	<	
18	wp	schist	55.1	1.1	33.0	7.7	<		33.5	0.8	28.2	5.9	1 053	19	<	
23	rock	siltstone	29.8	0.5	19.4	4.8	<		24.6	0.5	19.2	3.9	572	8	<	
46	rock	sandstone	43.0	0.9	26.4	4.7	<		24.4	0.7	22.8	1.6	842	2	2.1	0.2
49	rock	schist	57.5	0.8	36.7	8.0	<		39.6	0.7	40.5	5.5	1 372	1	<	
Upper Siegenian (*Sg 3*)																
3	wp < 2 mm	schist	55.2	1.0	35.2	6.3	<		35.2	0.9	41.0	2.0	1 254	27	<	
4	rock	schist	43.6	0.9	25.1	4.5	<		22.7	0.5	21.6	1.6	1 379	31	<	
5	rock	schist	45.8	0.9	31.9	5.7	<		30.5	0.8	25.4	1.6	782	18	0.7	0.2
9	rock	schist	57.8	1.1	41.0	7.2	<		40.7	0.9	30.3	1.9	933	219	<	
10	rock	schist	26.7	0.5	20.5	3.7	<		19.2	0.6	21.2	1.4	451	12	<	
11	rock	schist	29.0	0.7	24.6	4.4	<		23.3	0.7	21.8	5.9	268	5	<	
12	rock	schist	47.4	0.9	36.7	6.5	<		27.4	0.7	33.4	1.8	865	39	<	
24	wp < 2 mm	schist	48.6	0.7	34.1	7.0	<		33.6	0.6	34.0	8.0	844	12	<	
26	wp < 2 mm	schist	49.4	1.0	29.1	5.2	<		28.1	0.7	27.0	1.8	1 384	30	<	
27	rock	schist	55.4	1.0	31.5	5.6	<		27.8	0.8	23.6	1.8	1 363	31	<	
30	wp < 2 mm	schist	59.5	1.2	61.2	12.5	<		62.8	1.2	59.6	7.3	916	19	25.8	0.9
31	rock	schist	57.9	1.1	33.3	6.0	<		32.5	0.8	27.8	1.8	975	220	<	
36	rock	siltstone	49.7	1.0	32.8	7.9	<		45.9	1.0	35.0	6.0	830	17	<	
37	rock	siltstone	40.9	1.0	40.2	8.8	<		31.8	0.8	34.1	6.3	647	15	<	
47	rock	schist	53.2	1.0	30.7	5.5	<		32.7	0.8	31.3	1.8	1 101	2	<	
74	rock	siltstone	29.9	0.7	18.9	5.2	<		17.4	0.6	41.1	8.9	269	9	<	
75	rock	quartz vein	1.1	0.2	<17.5		<		3.9	0.5	9.6	5.1	11	6	<	
76	rock	schist	51.9	0.7	34.7	6.9	<		25.5	0.5	29.7	4.4	1 097	15	1.3	0.2
78	rock	siltstone	45.5	0.8	20.9	5.8	<		22.6	0.7	23.1	5.2	860	6	2.4	0.3
79	rock	schist	50.8	0.5	31.9	6.1	<		31.8	0.4	26.7	3.2	836	9	0.9	0.2
25a	wp > 2 mm	schist	52.4	0.7	32.8	7.2	<		28.3	0.6	31.3	4.7	1 418	19	<	
25b	wp < 2 mm	schist	58.3	0.8	41.6	8.7	<		44.0	0.7	42.7	5.6	1 311	8	<	
2a	rock	schist	47.8	0.4	46.1	0.7	<		26.1	0.2	28.3	0.5	1 188	27	<	
2b	rock	schist	41.9	0.3	25.8	1.2	<		25.3	0.2	22.8	0.4	1 173	25	<	
2c	wp > 2 mm	schist	56.9	0.6	31.6	1.8	<		36.2	0.3	32.7	0.6	1 254	25	<	

Table A2 (continued): Analyse of radionuclides of all samples, grouped by stratigraphic units.

sample number	classification	rock type	232Th [Bq/kg]	SD [Bq/kg]	238U [Bq/kg]	SD [Bq/kg]	230Th [Bq/kg]	SD [Bq/kg]	226Ra [Bq/kg]	SD [Bq/kg]	210Pb [Bq/kg]	SD [Bq/kg]	40K [Bq/kg]	SD [Bq/kg]	137Cs [Bq/kg]	SD [Bq/kg]
Middle Siegenian (Sg 2)																
38	rock	siltstone	38.4	0.9	29.5	7.2	<		26.5	0.8	24.8	5.6	488	13	2.4	0.4
44	rock	schist	56.3	1.1	37.1	8.6	<		36.5	0.9	36.4	6.3	814	18	10.9	0.4
51	rock	schist	41.2	0.6	19.8	4.6	<		19.8	0.5	20.5	3.8	559	12	<	
156	rock	schist	41.1	0.7	24.9	6.0	<		25.1	0.6	28.9	4.6	642	11	<	
154a	wp < 2 mm	schist	53.2	0.7	48.3	9.5	<		51.8	0.7	50.0	5.0	811	12	<	
154b	wp > 2 mm	schist	41.9	0.7	35.4	7.9	<		32.3	0.6	35.5	6.1	784	11	<	
155a	wp < 2 mm	schist	88.0	0.9	100.4	18.1	120	48	139.5	1.1	130.0	6.1	826	13	<	
155b	rock	schist	45.1	0.7	89.3	15.8	<		44.2	0.6	95.3	4.4	808	12	<	
77a	wp < 2 mm	siltstone	49.0	0.8	21.5	6.0	<		18.2	0.7	18.0	5.3	1 117	10	<	
77b	rock	siltstone	45.3	0.8	22.6	6.2	<		22.5	0.7	20.2	5.4	775	15	<	
77c	rock	schist	34.7	0.7	15.7	5.1	<		14.1	0.6	17.9	5.0	451	5	<	
Lower Siegenian (Sg 1)																
40	rock	schist	48.7	0.9	26.4	6.9	<		22.6	0.8	21.8	1.7	853	18	<	
41	rock	schist	55.0	0.9	32.6	7.7	<		27.0	0.8	24.6	1.7	948	18	3.2	0.5
Gedinnian (Ged)																
124	rock	sandstone	34.5	0.6	67.1	12.1	<		64.6	0.6	82.7	5.1	267	8	<	
126	rock	quartz vein	20.3	0.4	18.9	4.3	<		9.1	0.4	11.3	3.7	<		<	
129	rock	sandstone	34.5	0.7	32.1	7.1	<		34.3	0.7	36.0	5.1	303	1	<	
130	rock	sandstone	72.5	0.9	43.1	9.0	<		48.2	0.8	43.1	5.8	1 124	8	<	
131	rock	schist	142.7	1.4	74.2	14.1	<		76.5	0.9	65.3	6.5	2 095	12	<	
134	wp < 2 mm	sandstone	95.5	1.0	198.4	34.7	343	82	339.3	1.4	323.0	9.0	964	14	<	
135	rock	sandstone	35.3	0.8	32.2	7.3	<		34.8	0.7	27.5	5.2	371	2	<	
137	rock	sandstone	42.4	0.8	47.7	9.5	<		48.1	1.2	44.1	5.3	792	5	<	
125a	wp > 2 mm	sandstone	9.2	0.9	65.8	13.0	129	44	115.8	1.9	103.1	7.8	222	4	<	
125b	wp < 2 mm	sandstone	70.8	1.9	451.2	78.9	1 315	232	1 249.0	14.7	660.0	19.3	663	13	<	
127a	wp > 2 mm	sandstone	45.2	0.7	23.8	6.0	<		26.4	0.6	27.9	4.9	616	11	<	
127b	wp < 2 mm	sandstone	54.7	2.3	92.8	17.0	<		69.5	2.5	82.5	6.0	367	7	<	
128a	rock	sandstone	58.0	0.9	64.9	12.4	<		113.8	1.0	88.0	6.2	1 129	4	<	
128b	wp < 2 mm	sandstone	117.4	1.4	248.3	43.4	484	97	511.5	2.1	444.5	11.6	995	3	<	
132a	rock	siltstone	42.5	0.6	52.4	9.6	<		53.1	0.6	61.3	4.5	595	10	<	
132b	wp < 2 mm	siltstone	109.8	1.6	361.5	62.9	709	147	718.1	5.6	402.8	13.4	778	16	<	
133a	rock	quartzite	11.7	0.4	14.1	3.5	<		12.3	1.2	12.0	3.5	70	4	<	
136a	rock	sandstone	42.1	0.7	54.0	10.3	<		58.9	0.8	64.0	5.8	838	16	<	
136b	wp < 2 mm	sandstone	142.9	1.9	467.4	81.3	780	158	769.0	3.1	643.2	18.3	640	18	<	

Table A3: Chemical analyse of all samples, grouped by stratigraphic units.

sample number	classification	rock type	SiO₂ [%]	Al₂O₃ [%]	MnO [%]	MgO [%]	Na₂O [%]	CaO [%]	K₂O [%]	TiO₂ [%]	P₂O₅ [%]	Fe₂O₃ [%]	As [ppm]	Ba [ppm]	Ce [ppm]	Cr [ppm]	Cs [ppm]	Cu [ppm]	Ga [ppm]	La [ppm]	Nb [ppm]	Ni [ppm]	Pb [ppm]	Rb [ppm]	Sr [ppm]	V [ppm]	Y [ppm]	Zn [ppm]	Zr [ppm]	Corg [%]
Middle Dogger "Limestone of Haut-Pont" (dom3)																														
188	rock	limestone	8.1	1.6	0.18	0.4	<0.05	45.0	0.2	0.09	0.10	4.9	49.1	37	<20	<20	13	50	<2	25	<4	24	7	<15	424	178	16	33	28	NA
189	rock	limestone	8.0	2.2	0.27	0.4	<0.05	43.7	0.2	0.11	0.24	10.2	48.2	<30	21	100	<3	61	<2	49	<4	33	11	<15	421	294	27	51	32	NA
191a	wp < 2 mm	limestone	40.8	8.6	0.30	0.8	0.1	5.1	1.1	0.44	0.31	14.5	92.8	187	123	178	4	48	4	68	9	64	27	27	60	327	42	215	201	NA
191b	rock	limestone	19.0	4.8	0.16	0.7	0.1	32.6	0.6	0.27	0.17	8.3	41.3	83	56	77	3	55	<2	50	4	46	14	<15	250	223	29	164	99	NA
Lower Dogger "Minette" (dou)																														
192a	wp < 2 mm	limestone	10.9	6.4	0.53	0.9	0.3	7.3	0.2	0.43	1.12	>50.0	>330.0	145	47	>300	18	202	16	24	5	208	84	16	112	>1000	68	492	199	NA
192b	wp > 2 mm	limestone	12.8	5.4	0.49	0.7	0.3	8.1	0.2	0.37	0.95	>50.0	>330.0	194	41	>300	10	178	19	21	6	194	72	<15	110	939	59	418	155	NA
192mA	wp < 2 mm	limestone	11.9	4.7	0.44	0.7	0.1	20.6	0.1	0.28	0.87	>50.0	>330.0	121	27	221	19	152	13	18	<4	143	52	<15	148	747	56	323	133	NA
193a	wp < 2 mm	calcite vein	15.5	6.7	0.47	1.1	0.3	10.3	0.3	0.47	0.95	>50.0	>330.0	250	36	>300	23	186	15	40	6	194	91	20	96	>1000	64	460	197	NA
193b	wp > 2 mm	calcite vein	<8	1.6	0.09	0.3	<0.05	47.4	0.1	0.10	0.25	17.3	126.6	53	<20	51	13	76	<2	6	<4	40	21	<15	47	240	14	93	35	NA
194a	wp < 2 mm	limestone	13.1	7.3	0.51	1.1	0.2	5.2	0.2	0.48	1.17	>50.0	>330.0	862	49	>300	23	207	21	51	7	207	116	20	129	>1000	71	507	228	NA
194b	rock	limestone	10.0	4.8	0.41	0.9	0.1	26.9	0.2	0.29	0.81	>50.0	271.1	3760	35	183	7	127	10	28	<4	123	60	<15	274	609	62	281	111	NA
Middle Lias "Upper Spianatus" (lm3b)																														
183	rock	sandstone	44.3	6.6	0.29	1.2	0.3	6.8	1.1	0.40	0.17	11.4	33.7	196	43	74	<3	41	3	22	6	33	24	21	81	197	17	110	146	NA
184	rock	Fe ore	10.8	7.2	0.44	0.5	0.4	0.5	0.1	0.41	1.50	>50.0	>330.0	246	83	>300	46	367	50	75	<4	338	96	31	73	>1000	151	726	198	<1
185a	wp < 2 mm	sandstone	48.6	16.8	0.51	1.3	0.3	0.7	2.2	0.79	0.18	15.0	85.7	345	84	152	8	64	12	40	12	86	33	67	52	276	32	124	174	NA
185b	rock	sandstone	40.0	13.3	0.79	1.0	0.3	0.7	1.7	0.67	0.41	27.9	77.4	339	113	123	7	76	12	64	8	90	31	46	34	288	43	110	161	NA
186a	wp < 2 mm	sandstone	52.0	19.0	0.17	1.7	0.3	0.9	2.6	0.98	0.17	9.0	93.4	389	83	144	8	57	11	46	15	88	29	78	69	271	35	123	288	NA
186b	rock	sandstone	50.9	16.0	0.18	1.4	0.5	0.9	2.3	0.84	0.23	7.3	60.4	351	88	112	6	46	8	51	13	68	23	59	57	208	32	95	312	NA
187	rock	sandstone	28.7	10.9	0.71	1.1	0.2	14.3	1.5	0.63	0.36	31.9	54.7	218	114	109	12	97	9	63	8	66	30	45	194	267	40	82	174	NA
Middle Lias "Lower Spianatus" (lm3a)																														
180a	wp < 2 mm	marl	53.0	15.6	0.21	1.6	0.4	1.9	2.4	0.89	0.22	8.9	33.2	428	83	105	4	54	8	39	14	59	26	66	76	172	28	113	250	NA
180b	rock	marl	49.3	13.4	0.17	1.5	0.5	9.1	2.2	0.83	0.17	6.2	16.6	361	67	94	6	49	8	40	13	46	18	59	147	133	29	81	223	NA
181	rock	limestone	23.4	7.6	>0.80	2.6	0.4	14.9	1.1	0.49	0.31	42.8	12.6	187	37	80	<3	114	9	33	5	47	24	41	207	245	22	54	134	NA
182a	wp < 2 mm	marl	55.8	17.2	0.08	1.8	0.5	0.8	2.6	1.01	0.16	7.6	21.3	423	74	110	5	56	12	39	16	62	30	81	75	143	31	110	234	NA
182b	rock	marl	57.9	16.9	0.07	1.8	0.5	0.8	2.6	0.98	0.17	6.6	17.2	415	75	105	12	50	11	45	16	53	19	73	72	145	30	95	261	NA
Lower Lias "Marl and Limestone of Strassen" (li3)																														
123a	wp < 2 mm	calcite vein	10.4	2.5	0.06	0.3	<0.05	44.2	0.5	0.17	0.08	2.2	9.4	49	<20	25	6	49	<2	19	<4	21	7	<15	64	143	<10	24	69	NA
123b	wp > 2 mm	calcite vein	8.8	2.0	0.05	0.3	0.1	47.5	0.4	0.14	0.08	1.4	<4.0	31	<20	11	<3	47	<2	11	<4	11	7	<15	116	124	<10	17	50	NA
138a	rock	sandstone	36.7	3.4	0.05	0.6	0.1	28.5	0.7	0.22	0.06	2.0	7.1	53	46	40	<3	8	<2	19	5	11	8	24	192	33	18	18	215	NA
138b	wp < 2 mm	sandstone	46.3	11.2	0.07	1.0	0.2	9.7	1.6	0.48	0.10	6.7	33.1	194	47	90	12	47	6	33	9	37	16	64	63	193	30	41	249	NA
139b	rock	marl	61.1	8.7	<0.03	0.8	0.2	8.4	1.6	0.47	0.08	2.9	11.7	155	73	71	9	6	7	27	9	20	13	55	57	78	20	32	307	NA
176	rock	marl	11.2	3.2	0.07	0.9	0.1	44.1	0.6	0.19	0.72	1.8	16.4	39	<20	37	8	47	<2	21	<4	15	9	15	343	202	31	45	57	NA
177	f	marl	<8	1.5	<0.03	0.3	0.1	49.2	0.3	0.08	0.39	0.5	4.8	<30	<20	13	5	44	<2	18	<4	8	6	<15	388	128	12	22	10	NA
178a	wp < 2 mm	marl	29.1	9.4	0.08	1.6	0.2	23.9	1.5	0.48	0.70	9.7	42.8	160	41	80	10	60	4	29	7	52	16	36	184	199	25	44	101	NA
178b	rock	marl	16.6	5.0	0.08	1.3	0.1	37.7	0.9	0.27	0.15	5.3	36.2	73	<20	49	6	54	<2	18	4	26	10	21	288	157	13	33	73	NA
179a	wp < 2 mm	marl	49.2	14.3	0.06	1.9	0.1	11.9	2.5	0.83	0.17	5.3	90.0	243	59	100	11	54	9	37	14	54	17	81	144	211	23	70	222	NA
179b	rock	marl	27.3	8.1	0.08	1.7	0.2	29.7	1.4	0.45	0.10	5.5	75.7	119	26	61	5	55	3	31	6	32	11	33	251	189	16	42	129	NA
179c	rock	marl	47.5	13.9	0.06	2.0	0.1	13.0	2.4	0.80	0.22	5.2	80.5	239	57	93	11	53	8	33	13	50	15	78	149	191	25	68	218	NA
195	rock	marl	47.7	15.4	0.04	1.3	0.2	12.0	2.1	0.79	0.05	4.0	11.6	227	63	100	10	21	16	40	15	53	17	110	293	138	26	56	181	NA

The SDs of the trace elements < 1%, exceptionally up to 5%. The SDs of the other elements < 10%

Table A3 (continued): Chemical analyse of all samples, grouped by stratigraphic units.

sample number	classification	rock type	SiO₂ [%]	Al₂O₃ [%]	MnO [%]	MgO [%]	Na₂O [%]	CaO [%]	K₂O [%]	TiO₂ [%]	P₂O₅ [%]	Fe₂O₃ [%]	As [ppm]	Ba [ppm]	Ce [ppm]	Cr [ppm]	Cs [ppm]	Cu [ppm]	Ga [ppm]	La [ppm]	Nb [ppm]	Ni [ppm]	Pb [ppm]	Rb [ppm]	Sr [ppm]	V [ppm]	Y [ppm]	Zn [ppm]	Zr [ppm]	Corg [%]
Lower Lias "Luxemburger Sandstein" (li2)																														
20	rock	sandstone	>90	1.4	<0.03	0.1	<0.05	8.0	0.5	0.07	0.03	0.8	<4.0	79	35	24	<3	<4	<2	<4	<4	9	6	<15	30	12	<10	<8	37	NA
81	wp < 2 mm	sandstone	>90	1.0	<0.03	<0.10	<0.05	0.2	0.2	0.07	0.04	0.3	<4.0	<30	28	17	<3	<4	<2	17	<4	<5	7	<15	<10	11	<10	<8	37	NA
82	rock	sandstone	86.1	2.2	<0.03	0.2	0.1	0.6	0.5	0.09	0.05	1.0	5.9	59	22	37	<3	22	<2	11	<4	9	6	<15	<10	71	<10	13	24	NA
83	wp < 2 mm	sandstone	>90	0.9	<0.03	<0.10	<0.05	0.2	0.2	0.06	0.03	0.3	<4.0	<30	23	15	<3	<4	<2	13	<4	<5	6	<15	<10	7	<10	<8	29	NA
103	rock	sandstone	>90	1.9	<0.03	<0.10	<0.05	<0.1	0.5	0.09	0.04	0.6	<4.0	<30	30	14	<3	<4	<2	9	<4	7	5	<15	<10	11	<10	<8	75	NA
104a	wp < 2 mm	sandstone	85.8	6.5	<0.03	0.5	0.1	0.1	1.3	0.39	0.08	2.2	6.3	137	46	53	<3	4	5	25	8	13	12	34	18	53	13	15	189	NA
104b	rock	sandstone	71.1	6.2	<0.03	0.3	0.2	0.1	1.1	0.27	0.07	1.7	5.3	115	28	33	<3	22	<2	12	5	12	7	<15	<10	80	13	12	133	NA
106	wp > 2 mm	sandstone	88.5	5.2	0.06	0.6	0.1	0.1	1.2	0.20	0.08	1.8	6.6	141	72	35	4	<4	4	26	4	16	11	31	14	37	13	33	122	NA
107	wp < 2 mm	sandstone	83.2	7.0	<0.03	0.7	0.1	0.1	1.2	0.23	0.07	3.2	12.1	128	57	55	4	6	6	24	5	26	11	42	15	62	11	34	115	NA
115a	rock	sandstone	23.1	0.8	<0.03	0.5	0.1	34.2	0.2	0.05	0.08	0.6	5.4	<30	<20	16	4	<4	<2	17	<4	<5	5	<15	221	8	<10	11	57	NA
115b	rock	sandstone	30.1	0.8	0.07	0.3	0.1	34.9	0.2	0.06	0.08	0.7	7.1	32	<20	36	8	41	<2	5	<4	9	7	<15	196	87	11	13	54	NA
116	wp > 2 mm	calcite vein	<8	0.3	<0.03	<0.10	0.1	50.0	0.0	0.02	0.03	<0.05	<4.0	<30	<20	<5	6	38	<2	<4	<4	5	<4	<15	23	108	<10	<8	<10	NA
117	wp > 2 mm	sandstone	20.6	3.6	0.05	0.2	<0.05	2.1	0.4	0.18	0.25	45.8	148.4	135	53	269	5	52	3	28	6	26	33	<15	15	237	20	116	66	NA
118	rock	sandstone	64.2	2.2	<0.03	0.2	<0.05	2.3	0.4	0.12	>2.00	15.1	126.0	113	35	128	5	49	<2	22	<4	22	35	<15	85	212	17	25	57	NA
119a	wp < 2 mm	sandstone	49.9	6.7	<0.03	0.6	0.2	5.0	1.3	0.40	0.11	10.9	28.7	126	36	57	5	43	3	9	7	16	15	27	18	127	14	137	202	NA
119b	rock	sandstone	43.8	4.5	<0.03	0.5	0.1	12.8	0.9	0.28	0.10	12.4	20.6	75	24	54	10	10	5	9	5	13	13	26	12	69	<10	166	171	NA
120	rock	sandstone	62.7	1.5	<0.03	0.1	0.1	2.2	0.3	0.09	0.14	24.7	29.4	37	<20	29	<3	71	3	13	<4	25	14	<15	<10	75	<10	99	83	NA
140	rock	sandstone	84.0	1.3	<0.03	<0.10	<0.05	10.1	0.3	0.08	0.05	0.7	<4.0	<30	24	19	<3	<4	<2	21	<4	<5	5	<15	20	8	<10	<8	100	NA
Upper Keuper "Rhät" (ko1)																														
175	rock	sandstone	21.6	4.9	0.09	1.2	0.1	36.7	1.2	0.24	0.09	1.7	8.0	74	28	26	7	12	6	24	4	13	8	36	216	38	18	57	78	NA
Middle Keuper "Steinmergelkeuper" (km3)																														
108a	rock	marl	34.1	9.6	0.09	8.0	0.2	11.1	3.7	0.56	0.14	5.7	<4.0	224	47	58	<3	48	9	29	11	43	11	86	276	131	23	35	94	NA
108b	wp < 2 mm	marl	39.8	11.1	0.07	6.5	0.2	8.0	4.2	0.64	0.14	6.5	5.1	263	55	64	11	51	9	33	13	50	14	101	199	139	25	40	109	NA
109a	wp > 2 mm	calcite vein	10.3	3.2	0.11	2.4	0.2	42.5	1.1	0.19	0.07	1.8	<4.0	57	<20	11	8	45	<2	27	<4	22	5	<15	125	138	26	14	19	NA
109b	wp < 2 mm	calcite vein	33.2	9.2	0.09	7.1	0.2	15.1	3.4	0.56	0.13	5.7	7.2	268	37	59	5	55	8	30	10	48	14	84	190	150	22	36	87	NA
110	rock	marl	9.6	3.0	0.11	2.0	0.1	45.5	1.0	0.17	0.07	1.4	<4.0	44	<20	14	15	57	<2	31	<4	20	5	<15	125	142	26	13	20	NA
111	wp > 2 mm	calcite vein	40.2	11.2	0.09	9.9	0.2	11.4	4.2	0.56	0.18	4.7	<4.0	207	49	69	6	35	17	36	12	45	13	117	318	102	24	45	104	NA
112a	rock	dolomite	11.9	3.1	0.17	18.3	0.1	25.4	1.2	0.13	0.06	1.3	<4.0	843	22	16	5	15	3	7	<4	15	9	24	435	42	<10	22	27	NA
112b	wp < 2 mm	dolomite	19.1	5.5	0.18	11.1	0.2	21.9	2.0	0.27	0.07	2.6	4.0	2061	<20	35	10	63	3	9	4	38	11	36	307	156	12	27	38	NA
113	wp < 2 mm	calcite vein	9.7	2.8	0.14	3.5	0.1	45.1	1.0	0.15	0.08	1.3	<4.0	65	<20	12	9	86	<2	12	<4	26	8	<15	108	128	20	15	17	NA
114	rock	dolomite	17.9	5.0	0.16	16.5	0.1	22.3	2.0	0.22	0.21	2.3	<4.0	278	29	27	3	33	6	15	5	23	11	49	229	52	13	30	37	NA
169a	wp < 2 mm	marl	27.2	8.5	0.15	11.0	0.1	19.1	2.9	0.49	0.06	4.6	13.1	136	38	53	<3	61	5	21	9	35	18	67	367	112	18	38	83	NA
169b	rock	dolomite	24.6	7.9	0.13	10.8	0.1	22.5	2.7	0.46	0.05	4.2	11.0	110	25	46	5	57	6	31	8	32	14	59	328	123	18	32	71	NA
171a	wp < 2 mm	marl	27.0	8.3	0.08	11.3	0.2	16.6	3.2	0.46	0.06	5.1	7.9	207	28	52	5	50	7	27	8	37	18	80	353	122	17	47	74	NA
171b	rock	marl	25.7	8.2	0.07	12.3	0.1	17.7	3.3	0.43	0.04	5.3	6.4	161	39	49	8	47	6	22	7	35	12	79	385	106	15	34	61	NA
172a	wp < 2 mm	marl	23.8	10.7	0.12	9.7	0.2	13.7	3.9	0.59	0.07	5.5	6.9	1270	49	69	13	52	8	34	13	33	18	93	503	128	18	40	96	NA
172b	rock	marl	29.7	7.9	0.07	11.7	0.2	15.0	3.2	0.41	0.04	3.4	<4.0	1028	35	47	12	5	10	27	9	28	11	83	481	71	16	35	86	NA
173	wp < 2 mm	marl	36.2	11.1	0.12	8.1	0.1	13.2	3.7	0.68	0.08	5.7	12.5	210	61	70	6	59	9	36	12	44	18	90	268	137	25	39	116	NA
174	wp < 2 mm	marl	48.5	19.0	0.04	2.0	0.1	7.6	3.3	1.02	0.08	6.5	11.3	292	72	101	15	66	14	70	18	57	19	102	62	160	42	46	196	NA

The SDs of the trace elements < 1%, exceptionally up to 5%. The SDs of the other elements < 10%

Table A3 (continued): Chemical analyse of all samples, grouped by stratigraphic units.

sample number	classification	rock type	SiO₂ [%]	Al₂O₃ [%]	MnO [%]	MgO [%]	Na₂O [%]	CaO [%]	K₂O [%]	TiO₂ [%]	P₂O₅ [%]	Fe₂O₃ [%]	As [ppm]	Ba [ppm]	Ce [ppm]	Cr [ppm]	Cs [ppm]	Cu [ppm]	Ga [ppm]	La [ppm]	Nb [ppm]	Ni [ppm]	Pb [ppm]	Rb [ppm]	Sr [ppm]	V [ppm]	Y [ppm]	Zn [ppm]	Zr [ppm]	C_org [%]
Middle Keuper "Schilfsandstein" (km2s)																														
85	rock	sandstone	68.0	12.0	0.20	1.3	1.3	0.3	>5.0	0.47	0.13	4.0	10.6	561	62	60	<3	8	11	37	10	32	13	86	116	58	23	38	140	NA
86	rock	sandstone	60.1	16.2	0.03	2.8	0.7	0.5	>5.0	0.80	0.13	4.1	7.0	457	70	84	6	24	18	43	15	43	14	118	164	96	38	68	217	NA
87a	rock	sandstone	59.2	16.5	0.03	2.9	0.6	0.5	>5.0	0.82	0.14	4.3	10.0	474	78	72	<3	29	20	42	11	48	14	122	168	102	37	82	219	NA
88a	rock	sandstone	51.1	12.6	<0.03	1.8	0.7	0.3	>5.0	0.59	0.13	8.2	79.9	404	59	72	<3	67	14	38	12	47	176	88	124	72	37	189	207	NA
88b	wp < 2 mm	sandstone	58.8	14.4	<0.03	1.8	0.7	0.3	>5.0	0.67	0.12	6.1	43.9	429	78	87	<3	52	14	47	14	42	139	100	141	72	43	159	234	NA
Middle Keuper "Pseudomorphosenkeuper"(km1)																														
141a	rock	sandstone	73.9	8.4	0.05	2.8	0.1	1.9	2.8	0.86	0.06	4.2	9.2	193	63	85	<3	<4	9	30	15	34	13	69	23	64	24	50	315	NA
141b	wp < 2 mm	sandstone	68.1	11.3	0.05	2.4	0.2	0.8	3.5	0.78	0.07	5.3	9.9	276	60	99	8	5	11	30	15	40	17	91	26	80	24	62	280	NA
142	rock	sandstone	75.5	7.5	0.05	2.8	0.1	1.9	2.3	1.08	0.06	3.1	4.3	159	65	85	<3	<4	8	30	15	29	9	52	17	50	22	43	381	NA
143a	rock	marl	13.1	2.3	0.18	5.2	0.1	36.7	0.5	0.11	0.06	1.9	5.4	89	34	13	<3	6	<2	17	<4	9	6	<15	>1400	31	<10	25	48	NA
143b	wp < 2 mm	marl	19.5	5.2	0.31	4.0	0.1	32.3	1.3	0.32	0.09	6.1	23.8	208	<20	34	9	61	3	21	6	33	9	44	>1400	168	<10	52	35	NA
143d	wp < 2 mm	marl	13.7	3.4	0.44	3.0	<0.05	37.8	0.8	0.19	0.09	7.3	31.4	178	<20	23	3	65	2	11	5	33	8	28	>1400	186	<10	55	<10	NA
144a	wp < 2 mm	marl	45.1	13.8	0.05	8.5	0.2	7.1	3.6	0.65	0.08	5.9	6.2	381	55	81	14	9	18	37	15	45	8	147	>1400	105	26	86	153	NA
145a	wp < 2 mm	marl	39.5	13.0	0.06	7.1	0.2	12.3	3.3	0.74	0.07	6.1	9.0	479	52	82	14	56	9	40	13	52	10	113	>1400	166	23	74	135	NA
145b	rock	marl	45.8	14.0	0.05	7.6	0.2	7.1	3.6	0.78	0.07	5.9	9.0	477	52	85	5	51	10	35	14	53	9	113	1363	166	26	71	171	NA
146a	wp < 2 mm	marl	50.7	14.3	0.06	7.9	0.2	4.0	3.6	0.78	0.07	6.5	7.6	531	62	87	13	48	10	40	14	57	7	125	817	142	26	80	161	NA
146b	rock	marl	57.1	12.3	0.04	6.1	0.3	3.0	3.0	0.73	0.07	5.0	4.8	405	39	76	6	40	7	36	13	46	6	89	567	138	27	58	209	NA
147b	wp < 2 mm	marl	42.2	16.2	0.07	10.8	0.3	5.8	3.9	0.76	0.15	7.4	8.7	1344	70	95	16	20	20	42	15	51	9	156	362	120	29	92	174	NA
148a	rock	dolomite	11.4	3.5	0.18	17.7	0.1	24.8	1.0	0.17	0.11	1.6	<4.0	89	<20	20	8	<4	4	4	4	14	6	32	130	30	11	28	45	NA
148b	wp < 2 mm	dolomite	20.5	6.9	0.20	16.2	0.2	21.0	1.8	0.32	0.16	3.4	5.7	205	27	39	10	13	9	15	7	22	6	68	143	58	16	45	63	NA
Upper Muschelkalk (mo2)																														
16	rock	sandstone	56.5	20.1	0.05	2.5	0.2	0.3	4.3	0.91	0.14	9.4	19.8	482	114	119	16	<4	24	60	18	78	17	172	89	139	35	90	181	NA
17	wp < 2 mm	sandstone	38.5	9.4	0.06	7.7	0.2	12.7	3.4	0.52	0.41	5.2	18.7	269	67	59	5	11	9	27	10	41	14	101	122	79	23	48	201	NA
21	wp < 2 mm	dolomite	35.8	11.9	0.10	7.0	0.2	13.0	2.8	0.52	0.18	6.2	59.5	403	77	76	6	31	12	32	10	65	43	104	75	101	22	670	141	NA
22	rock		<8	1.1	0.10	19.5	<0.05	27.7	0.3	0.03	0.06	1.2	13.0	77	<20	5	<3	<4	<2	6	<4	11	21	<15	74	20	<10	151	25	NA
54	wp > 2 mm	dolomite	13.4	3.8	0.11	12.2	0.2	26.0	1.2	0.17	0.12	2.3	14.9	89	<20	24	<3	45	<2	5	<4	29	16	<15	25	129	<10	23	28	NA
89	rock	dolomite	9.5	2.3	0.10	19.0	0.1	27.1	0.8	0.13	0.07	1.6	11.6	89	42	17	<3	14	2	9	5	17	19	<15	29	20	<10	17	27	NA
90a	rock	marl	31.6	10.9	0.13	7.6	0.2	11.0	4.0	0.59	0.28	3.9	14.6	250	<20	79	13	45	9	18	7	56	16	74	41	74	11	33	45	NA
90b	wp < 2 mm	marl	54.7	16.1	0.13	3.6	0.2	3.6	>5.0	0.68	0.37	5.9	49.1	465	49	124	17	60	20	32	13	109	50	165	145	131	24	107	187	NA
91	calcite vein		<8	0.6	<0.03	1.0	0.2	48.0	0.1	0.03	0.03	0.1	<4.0	31	40	<5	<3	38	<2	<4	<4	7	3	<15	114	136	<10	10	<10	NA
92	wp > 2 mm	marl	40.6	11.9	0.14	5.0	0.2	11.1	4.8	0.62	0.27	5.4	32.6	363	40	90	16	81	9	22	10	79	46	99	63	157	20	89	141	NA
163a	wp < 2 mm	dolomite	31.5	10.2	0.14	8.2	0.2	17.6	4.0	0.50	0.14	4.5	9.8	299	28	72	10	64	6	19	7	57	16	85	29	140	15	42	75	NA
163b	rock	dolomite	23.8	7.3	0.15	11.6	0.1	22.7	2.9	0.34	0.12	3.4	6.7	135	<20	46	11	54	3	16	5	35	12	52	25	118	13	29	56	NA
164	rock	marl	23.6	7.3	0.15	12.8	0.2	21.7	2.7	0.29	0.20	3.3	5.8	131	44	45	14	14	7	15	5	32	12	66	33	56	12	35	46	NA
165a	wp < 2 mm	marl	46.8	15.7	0.08	6.4	0.2	2.7	>5.0	0.74	0.14	8.1	21.2	394	40	134	17	76	22	30	14	109	28	202	36	128	19	102	114	NA
165b	rock	marl	47.6	15.6	0.05	6.4	0.2	2.4	>5.0	0.74	0.13	7.4	13.8	376	38	131	19	56	22	27	14	97	23	199	36	121	18	93	114	NA
166	rock	dolomite	9.3	1.9	0.06	17.5	0.1	28.3	0.8	0.17	0.07	1.3	12.3	90	<20	12	9	42	<2	6	<4	13	14	<15	24	94	<10	14	40	NA
167a	wp < 2 mm	dolomite	9.4	2.5	0.07	16.6	0.1	28.3	1.0	0.21	0.09	1.8	11.1	128	15	15	9	45	<2	13	<4	18	25	18	33	87	<10	32	32	NA
167b	wp > 2 mm	dolomite	<8	1.3	0.06	20.1	0.1	27.6	0.5	0.11	0.07	1.2	6.5	75	24	7	<3	<4	<2	7	<4	17	17	<15	26	11	<10	12	19	NA
168a	wp < 2 mm	dolomite	16.1	4.8	0.06	11.8	0.2	24.1	1.6	0.34	0.13	1.8	11.9	465	<20	24	5	42	<2	12	5	20	24	24	39	105	12	32	44	NA
168b	rock	dolomite	8.9	2.1	0.06	18.7	0.1	26.2	0.9	0.18	0.10	1.2	5.6	122	40	14	8	<4	2	13	4	9	13	16	31	19	<10	18	34	NA

The SDs of the trace elements < 1%, exceptionally up to 5%. The SDs of the other elements < 10%

Table A3 (continued): Chemical analyse of all samples, grouped by stratigraphic units.

sample number	classification	rock type	SiO₂ [%]	Al₂O₃ [%]	MnO [%]	MgO [%]	Na₂O [%]	CaO [%]	K₂O [%]	TiO₂ [%]	P₂O₅ [%]	Fe₂O₃ [%]	As [ppm]	Ba [ppm]	Ce [ppm]	Cr [ppm]	Cs [ppm]	Cu [ppm]	Ga [ppm]	La [ppm]	Nb [ppm]	Ni [ppm]	Pb [ppm]	Rb [ppm]	Sr [ppm]	V [ppm]	Y [ppm]	Zn [ppm]	Zr [ppm]	C$_{org}$ [%]
Upper Muschelkalk (mo1)																														
33	wp > 2 mm	calcite vein	22.8	6.4	0.04	5.1	0.2	25.0	2.1	0.38	0.17	2.4	29.4	422	42	36	<3	19	6	13	8	32	44	49	51	55	13	28	82	NA
34a	wp < 2 mm	dolomite	18.4	4.8	0.08	10.8	0.2	22.7	1.2	0.38	0.17	3.1	22.4	121	41	30	4	12	3	14	7	28	27	29	38	43	13	49	66	NA
34b	wp > 2 mm	dolomite	<8	1.7	0.07	15.8	0.2	25.8	0.4	0.17	0.11	1.6	9.1	36	<20	9	4	<4	<2	7	4	11	12	<15	32	18	<10	26	35	NA
35	rock	dolomite	<8	1.0	0.08	16.2	0.1	27.5	0.3	0.12	0.09	1.2	10.3	<30	<20	8	<3	33	<2	10	<4	9	11	<15	18	87	<10	12	23	NA
39	rock	dolomite	<8	1.1	0.07	17.1	<0.05	28.2	0.4	0.10	0.08	1.1	4.6	<30	<20	6	<3	<4	<2	5	<4	6	9	<15	21	8	<10	13	15	NA
84	rock	dolomite	<8	1.1	0.08	20.2	0.1	28.5	0.3	0.09	0.07	1.1	5.0	<30	<20	5	<3	<4	<2	5	<4	6	12	<15	51	8	<10	12	14	NA
93	rock	dolomite	<8	1.1	0.06	20.8	<0.05	28.6	0.4	0.11	0.08	1.1	<4.0	<30	<20	7	<3	<4	<2	<4	<4	<5	7	<15	26	8	<10	13	16	NA
95	wp > 2 mm	calcite vein	28.7	14.0	0.06	4.3	0.1	6.2	0.3	0.62	0.18	8.7	32.5	223	58	113	5	55	15	26	6	65	16	150	53	102	16	59	116	NA
96	wp > 2 mm	dolomite	<8	1.2	0.03	5.1	0.1	42.5	0.4	0.09	0.08	2.2	26.6	90	<20	6	12	46	<2	<4	<4	13	13	<15	113	119	<10	38	<10	NA
97a	wp < 2 mm	dolomite	38.3	10.6	0.11	4.2	0.2	12.0	3.8	0.70	0.27	5.0	29.7	297	44	67	23	81	6	26	12	51	59	84	69	146	22	140	166	NA
97b	wp > 2 mm	dolomite	<8	1.3	0.06	5.5	0.1	10.9	0.5	0.19	0.10	1.9	26.9	195	42	61	<3	43	4	23	5	17	17	<15	47	117	<10	51	106	NA
Middle Muschelkalk (mm)																														
32	rock	dolomite	15.5	2.3	0.10	17.7	0.1	23.5	0.8	0.25	0.08	1.5	5.6	40	51	32	<3	5	<2	12	5	12	24	<15	46	26	15	26	294	NA
Lower Muschelkalk (mu)																														
19	rock	sandstone	76.2	10.0	0.06	1.2	0.1	0.1	>5.0	0.72	0.10	2.8	<4.0	315	84	52	6	<4	9	39	13	26	11	86	44	50	29	46	341	NA
157a	wp < 2 mm	sandstone	50.9	13.3	0.13	3.0	0.3	4.9	4.0	0.77	0.14	4.9	17.9	381	71	70	12	46	7	34	14	44	17	104	80	132	30	63	342	NA
158a	wp > 2 mm	sandstone	40.9	10.3	0.13	3.6	0.2	9.9	4.0	0.65	0.13	3.3	11.3	295	54	46	9	34	5	30	11	29	9	76	64	124	28	38	330	NA
158b	wp > 2 mm	sandstone	42.6	8.9	0.15	4.8	0.2	9.3	3.9	0.63	0.13	2.9	15.8	264	62	44	11	38	4	35	11	24	12	73	63	107	29	32	362	NA
159a	wp < 2 mm	sandstone	54.2	13.8	0.19	2.4	0.3	1.9	3.7	0.68	0.18	6.3	22.5	414	87	80	14	52	8	38	12	54	20	96	61	127	29	72	221	NA
160	wp < 2 mm	sandstone	59.1	11.4	0.06	2.6	0.2	2.0	4.7	0.78	0.11	3.5	9.0	374	67	57	9	36	5	32	13	31	7	89	57	101	31	43	330	NA
161	rock	marl	49.1	19.1	0.05	3.1	0.2	2.1	>5.0	0.97	0.13	5.8	25.3	636	79	84	29	48	15	59	18	54	13	191	156	163	33	74	226	NA
162	rock	sandstone	57.4	7.5	0.15	4.7	0.1	7.5	4.3	0.48	0.11	2.8	8.2	345	37	34	<3	38	4	22	8	23	8	68	45	90	22	34	164	NA
Buntsandstein (so)																														
15	rock	sandstone	>90	5.8	<0.03	0.4	0.2	0.2	4.2	0.18	0.11	1.2	14.6	406	36	30	<3	<4	6	12	5	13	17	96	59	16	12	15	82	NA
53	rock	sandstone	76.9	8.3	0.05	1.6	0.1	0.1	2.1	0.99	0.08	4.2	7.3	213	90	86	4	<4	9	38	14	38	9	56	18	63	20	52	282	NA
98	rock	sandstone	72.5	11.1	0.03	2.0	0.2	0.4	2.7	0.70	0.09	4.4	4.7	267	92	93	14	4	11	42	13	43	7	77	99	65	27	49	295	<1
99	wp > 2 mm	sandstone	64.1	14.0	0.05	2.6	0.2	1.1	3.6	0.86	0.11	5.8	13.6	355	104	117	16	8	16	59	17	52	12	109	175	88	38	61	520	NA
100	rock	sandstone	50.8	13.8	0.04	2.0	0.3	0.2	3.4	0.90	0.09	5.5	13.5	361	71	106	18	32	7	49	17	50	8	75	121	132	33	47	444	NA
101	rock	sandstone	68.4	13.0	0.04	2.1	0.2	0.2	3.3	0.88	0.09	5.1	10.7	312	109	111	14	5	15	52	18	48	10	93	123	78	38	57	516	NA
102	wp < 2 mm	sandstone	63.1	15.2	0.05	2.5	0.2	1.1	3.8	0.92	0.11	6.5	15.2	404	118	119	19	12	19	67	18	56	12	127	211	98	37	71	482	<1

The SDs of the trace elements < 1%, exceptionally up to 5%. The SDs of the other elements < 10%

Table A3 (continued): Chemical analyse of all samples, grouped by stratigraphic units.

sample number	classification	rock type	SiO₂ [%]	Al₂O₃ [%]	MnO [%]	MgO [%]	Na₂O [%]	CaO [%]	K₂O [%]	TiO₂ [%]	P₂O₅ [%]	Fe₂O₃ [%]	As [ppm]	Ba [ppm]	Ce [ppm]	Cr [ppm]	Cs [ppm]	Cu [ppm]	Ga [ppm]	La [ppm]	Nb [ppm]	Ni [ppm]	Pb [ppm]	Rb [ppm]	Sr [ppm]	V [ppm]	Y [ppm]	Zn [ppm]	Zr [ppm]	C_org [%]
Upper Emsian (E3)																														
6	rock	schist	57.9	21.3	0.18	2.0	0.7	<0.1	4.2	0.97	0.12	8.8	19.9	577	99	116	10	39	27	55	18	83	22	186	68	169	35	110	186	NA
28	wp > 2 mm	schist	53.7	14.2	0.24	1.5	0.6	0.3	2.8	0.72	0.15	5.3	16.4	424	78	92	15	19	14	43	15	44	47	111	49	96	33	97	261	NA
29	rock	schist	57.2	20.2	0.12	2.2	0.7	0.2	4.0	0.91	0.11	7.4	16.4	493	103	113	9	31	23	62	18	72	24	163	70	149	37	97	205	NA
42	rock	schist	55.3	20.8	0.10	2.3	0.8	0.2	4.1	0.95	0.11	8.1	19.9	551	96	115	14	33	26	53	19	72	25	187	76	153	34	89	195	NA
50	rock	siltstone	56.4	18.6	0.31	1.7	0.5	0.1	3.6	0.87	0.11	7.2	9.9	679	76	109	8	33	21	58	17	79	35	145	60	115	33	123	188	NA
56a	wp < 2 mm	schist	50.0	20.0	0.76	1.8	0.5	0.4	3.9	0.99	0.17	10.2	39.5	759	109	111	29	101	15	61	19	111	75	150	68	198	38	171	214	NA
56b	rock	schist	54.7	22.7	0.10	2.1	0.7	0.3	4.5	1.03	0.11	8.3	20.5	623	88	128	8	39	28	60	20	75	26	209	79	169	36	138	194	NA
66	wp < 2 mm	schist	56.5	19.6	0.45	2.0	0.5	0.2	3.8	0.98	0.14	9.1	26.6	683	117	114	22	46	23	57	20	77	63	179	78	145	42	245	203	NA
70a	rock	schist	60.0	20.2	0.14	2.2	1.0	0.2	4.0	0.99	0.12	8.0	18.8	586	99	129	<3	40	25	60	20	78	20	179	62	156	41	108	235	NA
70b	rock	schist	64.3	16.9	0.17	1.4	0.9	0.1	3.3	0.74	0.12	7.2	28.4	404	77	116	5	41	21	45	17	72	43	142	55	135	34	126	221	NA
71a	rock	schist	50.6	23.3	0.09	2.6	0.7	0.5	4.9	0.94	0.10	8.0	15.4	601	91	134	7	35	29	53	21	77	15	226	61	178	38	83	207	NA
71b	rock	quartz vein	>90	0.5	0.19	1.4	<0.05	2.5	0.0	0.03	0.05	0.8	<4.0	<30	<20	30	5	6	<2	<4	<4	6	65	<15	<10	<5	<10	32	<10	NA
73	rock	schist	50.6	18.8	0.03	1.6	0.3	0.2	3.7	0.94	0.11	7.4	19.3	642	66	103	7	60	13	50	18	75	23	130	53	183	35	86	197	NA
Middle Emsian "Quarzit von Berlé" (E2q)																														
43	rock	quartzite	>90	3.2	<0.03	0.1	<0.05	<0.1	0.6	0.17	0.05	0.7	<4.0	94	36	72	<3	<4	2	15	<4	11	5	<15	17	18	<10	10	133	NA
48	rock	quartzite	>90	2.1	<0.03	<0.10	<0.05	<0.1	0.4	0.10	0.04	0.6	<4.0	55	21	47	<3	<4	<2	6	<4	11	<4	<15	14	7	<10	9	70	NA
67a	rock	quartzite	>90	1.7	<0.03	<0.10	<0.05	<0.1	0.3	0.12	0.04	0.4	<4.0	<30	39	56	<3	<4	<2	8	<4	6	4	<15	<10	8	<10	<8	97	NA
67b	rock	quartzite	>90	1.8	<0.03	<0.10	<0.05	<0.1	0.3	0.11	0.04	0.7	<4.0	<30	34	67	<3	<4	<2	8	<4	7	<4	<15	<10	8	<10	<8	82	NA
Middle Emsian "Bunte Schiefer von Clerf" (E2)																														
8	rock	schist	64.7	18.1	0.14	1.5	0.9	0.2	3.6	0.90	0.14	7.4	15.1	468	96	121	4	37	22	53	17	76	25	153	74	146	39	110	283	NA
55a	wp < 2 mm	schist	51.4	19.7	0.66	1.8	0.5	0.3	4.1	1.25	0.20	8.8	17.0	923	146	120	33	82	14	>80	23	73	27	146	94	190	45	85	278	NA
55b	rock	schist	55.6	18.8	0.12	2.1	0.7	0.2	3.8	0.86	0.09	7.6	<4.0	603	91	106	11	5	21	51	18	63	17	160	69	113	31	86	204	NA
68	wp > 2 mm	sandstone	69.8	20.4	0.06	1.5	0.9	0.1	3.5	0.89	0.12	7.6	14.0	539	95	123	5	7	20	65	18	63	20	141	80	113	36	82	279	NA
69	rock	sandstone	61.6	19.4	0.05	1.4	0.9	0.1	3.5	0.88	0.08	7.2	5.0	500	91	110	4	7	22	58	17	61	15	139	76	110	34	77	252	NA
Lower Emsian (E1b)																														
13	rock	sandstone	60.0	16.8	0.13	1.8	0.6	0.3	2.9	0.72	0.17	7.5	<4.0	473	112	92	3	3	15	44	14	51	6	103	58	99	32	84	216	NA
45	wp	sandstone	68.8	12.4	0.07	0.9	0.7	0.1	2.5	0.75	0.17	5.6	19.0	338	82	173	<3	7	10	47	15	68	34	71	47	71	35	93	506	NA
72	rock	siltstone	>90	0.5	<0.03	<0.10	<0.05	<0.1	0.0	0.03	0.03	1.4	<4.0	<30	<20	27	<3	<4	<2	<4	<4	10	<4	<15	<10	<5	<10	16	10	NA
149	rock	schist	58.0	19.2	0.13	2.6	0.7	0.2	3.9	0.83	0.11	8.0	15.6	583	72	122	13	28	24	38	17	72	19	165	55	121	34	105	169	NA
150	rock	quartzite	>90	0.4	0.38	<0.10	<0.05	0.1	0.0	0.03	0.05	1.7	8.6	<30	22	18	<3	<4	<2	<4	<4	<5	35	<15	<10	<5	<10	<8	<10	NA

The SDs of the trace elements < 1%, exceptionally up to 5%. The SDs of the other elements < 10%

Table A3 (continued): Chemical analyse of all samples, grouped by stratigraphic units.

sample number	classification	rock type	SiO2 [%]	Al2O3 [%]	MnO [%]	MgO [%]	Na2O [%]	CaO [%]	K2O [%]	TiO2 [%]	P2O5 [%]	Fe2O3 [%]	As [ppm]	Ba [ppm]	Ce [ppm]	Cr [ppm]	Cs [ppm]	Cu [ppm]	Ga [ppm]	La [ppm]	Nb [ppm]	Ni [ppm]	Pb [ppm]	Rb [ppm]	Sr [ppm]	V [ppm]	Y [ppm]	Zn [ppm]	Zr [ppm]	Corg [%]
Lower Emsian (E1a)																														
1	wp < 2 mm	schist	58.8	19.3	0.25	2.2	0.1	0.1	3.9	0.93	0.12	10.9	7.2	535	97	127	12	41	23	46	17	92	16	165	43	132	35	104	195	NA
7	rock	schist	60.8	19.5	0.06	2.4	0.1	<0.1	4.0	0.92	0.10	7.5	<4.0	525	93	128	9	14	25	51	17	80	13	173	43	134	33	96	177	NA
18	wp	schist	17.6	4.2	0.09	14.7	0.1	22.7	1.6	0.21	0.15	3.5	9.8	91	40	24	<3	<4	4	12	5	25	9	44	101	41	<10	24	67	NA
23	rock	siltstone	>90	9.1	0.05	0.3	0.6	0.3	1.8	0.45	0.10	2.5	6.8	237	67	87	8	9	10	32	9	30	15	59	56	45	21	53	245	NA
46	rock	sandstone	60.5	15.9	0.13	2.6	0.9	0.2	2.6	0.71	0.16	8.3	10.5	375	62	108	6	24	16	36	14	76	26	101	47	89	28	102	209	NA
49	rock	schist	61.1	20.1	0.19	1.0	1.2	0.1	4.3	0.97	0.14	7.8	11.2	672	93	135	6	37	24	62	18	82	22	180	102	131	39	98	216	NA
Upper Siegenian (Sg 3)																														
2a	rock	schist	60.4	19.4	0.06	2.5	0.1	<0.1	3.7	0.91	0.11	9.2	22.3	450	109	28	9	42	25	46	16	96	35	162	35	150	36	121	169	NA
2b	rock	schist	60.1	19.5	0.07	2.5	0.1	<0.1	3.6	0.91	0.10	9.4	27.8	454	73	32	<3	51	25	34	17	100	32	162	35	147	36	134	177	NA
2c	wp > 2 mm	schist	60.2	20.2	0.05	2.3	0.1	0.1	4.0	0.96	0.09	8.2	11.8	507	82	136	8	40	27	40	18	89	28	182	39	153	37	117	186	NA
3	wp > 2 mm	schist	61.6	20.2	0.05	2.0	0.1	<0.1	3.9	0.95	0.09	7.6	9.6	472	70	130	8	31	25	42	18	73	18	175	38	153	34	100	202	NA
4	rock	schist	61.4	21.2	0.04	1.8	0.1	<0.1	4.4	1.03	0.12	7.6	17.5	550	70	139	13	34	28	45	19	66	20	203	43	172	32	95	199	NA
5	rock	schist	59.1	17.0	0.27	3.5	0.1	0.5	2.5	0.84	0.34	14.2	17.9	330	56	125	6	45	23	36	15	115	27	110	58	130	39	233	152	NA
9	rock	schist	58.3	20.5	0.10	2.8	0.3	0.1	4.2	0.96	0.10	8.3	14.6	610	73	136	9	38	26	40	18	92	18	180	60	143	41	118	188	NA
10	rock	schist	70.4	13.1	0.08	2.7	0.5	0.2	1.8	0.54	0.12	5.9	6.6	240	72	97	4	17	13	37	12	64	14	60	47	71	26	84	200	NA
11	rock	schist	74.3	11.5	0.07	2.6	0.4	0.1	1.3	0.50	0.10	5.4	5.8	166	75	100	4	14	10	30	11	55	20	39	34	57	25	79	244	NA
12	rock	schist	62.9	17.7	0.10	2.9	0.2	0.1	3.2	0.69	0.10	7.1	9.9	442	109	127	8	23	20	53	16	73	22	126	51	115	34	100	216	NA
24	wp < 2 mm	schist	60.4	19.0	0.04	2.4	0.1	0.1	4.0	0.89	0.11	7.6	<4.0	488	106	128	15	<4	22	49	17	81	5	156	72	126	33	98	198	NA
25a	wp > 2 mm	schist	55.4	18.5	0.03	1.9	0.1	0.1	4.5	0.99	0.12	10.1	28.1	588	73	138	18	71	15	54	17	81	18	157	83	172	35	90	184	NA
25b	wp < 2 mm	schist	61.4	19.4	<0.03	1.4	0.1	0.1	4.3	0.93	0.14	7.7	34.4	570	105	129	38	28	25	65	18	49	39	181	244	129	39	74	221	NA
26	wp < 2 mm	schist	58.5	19.7	0.04	2.4	0.1	<0.1	4.4	0.92	0.10	9.1	12.9	513	98	137	18	28	24	51	17	83	17	179	95	139	33	108	177	NA
27	rock	schist	57.8	20.0	0.04	2.6	0.1	<0.1	4.3	0.91	0.08	8.2	7.1	485	97	132	15	19	23	53	17	87	14	171	88	136	32	108	172	NA
30	wp < 2 mm	schist	53.4	21.0	0.33	1.9	0.1	0.4	3.8	0.89	0.16	8.5	27.7	445	97	120	20	51	20	50	16	70	38	147	92	123	32	83	218	NA
31	rock	schist	56.2	19.1	0.09	2.9	0.3	0.8	3.9	0.86	0.13	7.4	<4.0	443	109	132	9	4	20	52	16	72	12	141	75	125	33	87	256	NA
36	rock	siltstone	58.7	17.8	0.15	2.7	0.8	0.2	3.4	0.84	0.15	7.7	6.9	465	90	119	10	30	19	46	16	82	35	125	66	111	32	111	217	NA
37	rock	siltstone	60.6	15.8	0.15	2.7	0.9	0.2	2.7	0.73	0.16	8.3	5.5	372	60	99	<3	23	16	39	14	86	26	95	57	92	31	120	198	NA
47	rock	schist	60.0	18.4	0.06	2.7	0.8	0.2	3.5	0.90	0.12	7.3	5.1	506	67	132	11	32	21	39	17	76	19	141	62	119	35	99	229	NA
74	rock	siltstone	75.1	9.3	0.30	0.7	0.1	0.1	1.3	0.47	0.23	6.7	13.6	233	74	92	<3	6	7	29	9	42	15	36	24	47	23	69	321	NA
75		quartz vein	72.1	12.1	0.17	0.5	1.7	0.1	2.0	0.59	0.14	5.3	7.9	302	83	117	4	10	10	35	11	50	14	66	62	61	26	61	277	NA
76	rock	schist	59.5	20.0	0.07	2.7	0.4	0.2	4.1	0.94	0.11	8.2	15.2	607	57	133	8	36	28	31	18	86	18	182	47	133	34	145	178	NA
78	rock	siltstone	65.4	15.8	0.05	2.1	0.4	0.2	2.8	0.73	0.09	5.8	8.2	401	67	149	13	17	16	37	14	63	20	98	28	86	28	91	300	NA
79	rock	schist	56.8	19.6	0.05	2.5	0.5	0.2	3.6	0.93	0.13	7.4	16.8	529	65	140	12	27	22	39	18	80	14	143	36	113	35	146	247	NA
Middle Siegenian (Sg 2)																														
38	rock	siltstone	68.9	12.8	0.06	2.3	1.3	0.2	2.3	0.62	0.14	5.8	4.6	332	91	141	6	8	13	42	13	38	20	74	91	83	28	70	279	NA
44	rock	schist	58.3	17.2	0.10	2.7	0.9	0.3	3.4	0.83	0.12	6.6	12.2	541	67	152	11	20	20	34	16	67	25	132	64	107	33	133	256	NA
51	rock	schist	68.4	14.2	0.08	2.8	1.0	0.2	2.9	0.66	0.12	5.5	11.5	394	70	158	5	10	16	30	13	59	8	106	62	85	30	73	333	NA
77a	wp < 2 mm	schist	61.4	18.9	0.10	2.7	0.2	<0.1	3.6	0.88	0.06	8.0	11.0	538	59	128	8	35	24	42	17	91	67	157	32	122	33	166	186	NA
77b	rock	siltstone	66.9	14.6	0.08	2.5	1.1	0.2	2.5	0.69	0.14	6.7	8.7	312	60	130	7	17	18	31	16	67	12	98	64	93	30	94	240	<1
77c	rock	schist	68.0	12.3	0.10	3.0	0.4	<0.1	1.5	0.60	0.07	7.6	7.0	182	50	121	7	22	13	36	12	73	48	46	19	61	25	146	273	<1
154a	wp > 2 mm	schist	57.5	16.4	0.10	2.7	0.9	0.3	3.6	0.78	0.13	8.4	21.4	584	89	135	10	65	12	54	16	101	26	111	68	137	35	80	236	NA
154b	wp > 2 mm	schist	62.6	15.5	0.30	2.6	0.7	0.3	3.6	0.77	0.12	7.5	18.0	545	84	139	14	59	11	46	15	76	27	106	60	137	35	74	246	NA
155a	wp > 2 mm	schist	50.1	15.8	0.72	2.2	0.4	0.4	3.4	0.85	0.29	13.2	79.7	534	>150	138	20	133	10	>80	16	221	149	106	60	155	49	110	290	NA
155b	rock	schist	61.6	15.7	0.24	2.6	0.6	0.3	3.7	0.77	0.13	7.5	24.1	555	97	140	9	62	11	66	15	95	47	105	55	147	36	79	253	NA
156	rock	schist	63.7	12.9	0.08	2.5	1.0	0.2	2.8	0.62	0.11	4.9	9.3	384	48	132	6	9	14	31	13	39	15	91	65	79	28	64	250	NA

The SDs of the trace elements < 1%, exceptionally up to 5%. The SDs of the other elements < 10%

Table A3 (continued): Chemical analyse of all samples, grouped by stratigraphic units.

sample number	classification	rock type	SiO$_2$ [%]	Al$_2$O$_3$ [%]	MnO [%]	MgO [%]	Na$_2$O [%]	CaO [%]	K$_2$O [%]	TiO$_2$ [%]	P$_2$O$_5$ [%]	Fe$_2$O$_3$ [%]	As [ppm]	Ba [ppm]	Ce [ppm]	Cr [ppm]	Cs [ppm]	Cu [ppm]	Ga [ppm]	La [ppm]	Nb [ppm]	Ni [ppm]	Pb [ppm]	Rb [ppm]	Sr [ppm]	V [ppm]	Y [ppm]	Zn [ppm]	Zr [ppm]	C$_{org}$ [%]
Lower Siegenian (Sg 1)																														
40	rock	schist	58.9	19.3	0.14	2.7	0.9	0.2	3.5	0.82	0.10	7.3	10.2	708	60	140	5	27	23	41	19	82	11	148	96	124	33	95	210	NA
41	rock	schist	55.8	20.8	0.15	2.9	0.7	0.3	4.0	0.95	0.14	8.5	<4.0	758	51	133	11	18	26	39	19	57	10	175	86	138	37	101	188	NA
Gedimnian (Ged)																														
124	rock	sandstone	82.9	7.3	0.05	1.5	0.2	<0.1	1.2	0.56	0.13	4.9	70.8	180	93	252	4	81	8	40	11	100	49	36	32	50	24	166	407	<1
125a	wp > 2 mm	sandstone	74.9	5.4	0.17	0.2	0.2	0.2	0.7	0.34	0.22	5.2	181.3	146	56	153	4	99	<2	28	6	125	24	<15	<10	107	29	158	124	NA
125b	wp < 2 mm	sandstone	38.0	26.0	>0.80	0.8	0.3	0.3	2.1	0.76	0.60	34.1	>330	994	119	188	33	>450	22	73	13	915	168	112	73	298	88	851	219	NA
126	rock	quartz vein	>90	0.7	<0.03	<0.10	<0.05	<0.1	0.1	0.04	0.07	0.5	11.6	<30	>150	30	<3	4	<2	78	<4	17	5	<15	<10	<5	<10	19	16	<1
127a	wp > 2 mm	sandstone	56.9	15.4	0.05	1.5	0.2	<0.1	1.2	1.05	0.13	5.2	35.6	230	90	175	3	41	6	50	19	80	17	28	24	137	42	96	805	<1
127b	wp < 2 mm	sandstone	57.8	16.0	0.09	1.3	0.2	0.1	1.2	0.89	0.21	6.6	80.8	285	73	140	5	64	6	39	16	102	49	27	25	132	35	124	504	<1
128a	rock	sandstone	38.3	26.7	>0.80	0.9	0.6	0.2	3.2	0.97	0.33	11.1	177.9	1261	101	192	40	371	25	60	19	796	204	136	144	176	51	597	327	NA
128b	wp < 2 mm	sandstone	55.3	21.8	0.56	1.5	1.0	<0.1	3.6	0.92	0.12	8.0	59.8	769	67	209	13	90	22	41	18	211	67	138	177	142	41	210	370	NA
129	rock	sandstone	78.1	9.0	0.21	1.9	0.2	0.1	1.0	0.58	0.06	5.8	11.5	196	67	300	<3	19	10	32	11	65	47	30	27	59	20	116	556	NA
130	rock	sandstone	56.8	23.3	0.13	2.2	0.9	0.1	3.7	1.09	0.07	9.3	64.2	712	59	147	8	32	28	37	21	72	50	162	202	142	45	135	236	NA
131	rock	schist	41.5	38.3	0.18	0.5	2.1	<0.1	>5.0	1.98	0.04	0.9	6.6	1489	87	>300	22	12	37	76	36	45	54	316	610	241	63	35	548	<1
132a	rock	siltstone	68.8	16.6	0.04	1.2	0.9	<0.1	2.6	0.74	0.08	4.5	32.6	445	79	157	9	23	17	45	14	51	28	97	151	92	36	87	312	<1
132b	wp < 2 mm	siltstone	37.3	25.0	>0.80	0.9	0.5	0.3	2.5	1.03	0.57	25.7	>330	526	106	201	35	>450	21	>80	18	391	>240	119	131	230	69	508	360	<1
133a	rock	quartzite	89.6	5.1	0.07	1.6	0.1	<0.1	0.4	0.23	0.04	4.6	10.0	64	44	64	<3	13	5	22	5	31	18	<15	<10	21	11	74	102	<1
134	wp < 2 mm	sandstone	44.3	29.6	0.40	0.6	1.5	0.1	4.2	1.20	0.26	8.5	164.1	977	133	297	36	283	28	80	22	160	240	178	295	174	72	212	463	<1
135	rock	sandstone	80.9	8.7	0.07	1.6	0.4	<0.1	1.2	0.49	0.05	4.3	18.1	181	69	276	7	9	8	36	10	60	11	37	55	47	25	83	357	<1
136a	rock	sandstone	62.9	19.4	0.04	1.3	1.2	<0.1	3.1	0.70	0.07	4.3	24.8	524	71	280	13	24	18	41	13	70	29	114	202	114	42	84	322	<1
136b	wp < 2 mm	sandstone	35.7	27.8	>0.80	1.0	0.5	0.2	2.4	0.99	0.46	22.2	>330	592	>150	256	41	>450	30	75	22	403	>240	149	152	204	65	503	340	<1
137	rock	sandstone	67.7	16.6	0.05	1.4	0.9	<0.1	2.6	0.72	0.06	4.6	17.7	442	71	171	16	14	17	39	14	50	17	92	135	88	34	82	300	<1

The SDs of the trace elements < 1%, exceptionally up to 5%. The SDs of the other elements < 10%

Table A4-1: Radium activities, radon activity concentrations and emanation coefficients (E) of rocks and weathering products.

sample number	classification	rock type	226Ra [Bq/ kg]	SD [Bq/ kg]	222Rn [Bq/ kg]	SD [Bq/ kg]	E [%]	SD [%]
Middle Dogger "*Limestone of Haut-Pont*" (*dom3*)								
189	rock	limestone	12.8	0.5	1.4	0.11	11	9
191a	wp < 2 mm	limestone	21.4	1.8	3.4	0.32	16	13
191b	rock	limestone	13.6	0.5	1.1	0.12	8	12
Lower Dogger "*Minette*" (*dou*)								
192a	wp < 2 mm	limestone	18.4	1.8	0.9	0.08	5	13
192b	rock	limestone	17.9	0.5	2.2	0.15	12	7
193b	wp > 2 mm	calcite	6.6	0.4	0.5	0.09	7	21
194a	wp < 2 mm	limestone	13.4	0.5	1.8	0.20	13	12
194b	rock	limestone	15.9	0.5	1.5	0.19	9	13
Middle Lias "*Upper Spianatus*" (*lm3b*)								
183	rock	sandstone	9.0	0.8	0.9	0.11	10	13
184	rock	Fe ore	39.7	0.7	2.2	0.06	5	3
187	rock	sandstone	19.6	0.5	1.7	0.43	9	26
185a	wp < 2 mm	sandstone	24.1	1.0	2.1	0.20	9	10
185b	rock	sandstone	21.3	0.7	2.0	0.24	9	12
Middle Lias "*Lower Spianatus*" (*lm3a*)								
180a	wp < 2 mm	marl	28.7	0.7	1.3	0.18	4	14
180b	rock	marl	25.2	0.8	1.5	0.22	6	15
182a	wp < 2 mm	marl	37.0	0.9	2.5	0.25	7	12
182b	rock	marl	30.3	0.7	2.0	0.25	7	14
Lower Lias "*Marl and Limestone of Strassen*" (*li3*)								
176	rock	marl	53.1	0.9	2.9	0.15	5	5
138a	rock	sandstone	13.7	0.9	0.5	0.05	4	10
179a	wp < 2 mm	marl	44.8	0.7	1.3	0.08	3	6
179c	rock	marl	40.9	0.7	3.1	0.48	8	16
Lower Lias "*Luxemburger Sandstein*" (*li2*)								
20	rock	sandstone	5.1	0.8	0.8	0.18	16	23
83	wp < 2 mm	sandstone	4.9	0.7	0.4	0.07	8	22
103	rock	sandstone	2.2	0.3	0.3	0.07	15	28
106	wp > 2 mm	sandstone	19.1	0.7	0.8	0.15	4	18
120	rock	sandstone	21.3	0.6	1.2	0.23	5	20
140	rock	sandstone	3.9	0.8	0.3	0.15	8	48
Upper Keuper "*Rhät*" (*ko1*)								
175	rock	sandstone	18.1	0.7	1.1	0.13	6	12

Table A4-1 (continued): Radium activities, radon activity concentrations and emanation coefficients (E) of rocks and weathering products.

sample number	classification	rock type	226Ra [Bq/ kg]	SD [Bq/ kg]	222Rn [Bq/ kg]	SD [Bq/ kg]	E [%]	SD [%]
Middle Keuper "*Steinmergelkeuper*" (*km3*)								
111	wp > 2 mm	calcite	87.6	0.4	3.1	0.44	4	7
114	rock	dolomite	78.0	1.0	6.1	0.34	8	6
169a	wp < 2 mm	marl	24.4	0.7	1.7	0.19	7	11
171a	wp < 2 mm	marl	38.5	0.8	2.8	0.17	7	6
171b	rock	marl	33.4	1.0	2.0	0.06	6	3
Middle Keuper "*Schilfsandstein*" (*km2s*)								
85	rock	sandstone	19.9	1.2	1.8	0.20	9	12
87a	rock	sandstone	30.7	0.7	3.8	0.31	12	9
88a	rock	sandstone	41.3	0.8	7.6	0.91	18	12
88b	wp < 2 mm	sandstone	46.1	0.6	8.5	0.18	18	3
Upper Muschelkalk (*mo2*)								
17	wp < 2 mm	sandstone	57.1	0.6	5.8	0.35	10	6
21	wp < 2 mm	dolomite	97.0	3.1	19.7	0.59	20	3
22	rock	dolomite	33.6	1.2	2.2	0.73	6	34
92	wp < 2 mm	marl	31.7	1.4	11.7	0.47	37	4
166	rock	dolomite	24.3	0.9	2.1	0.50	9	25
163b	rock	dolomite	13.7	0.7	1.8	0.20	13	12
90b	wp < 2 mm	marl	80.9	2.1	7.6	0.51	9	7
Upper Muschelkalk (*mo1*)								
84	rock	dolomite	12.0	0.8	1.0	0.13	9	13
93	rock	dolomite	5.0	0.6	0.5	0.08	11	18
Middle Muschelkalk (*mm*)								
32	rock	dolomite	18.4	0.8	1.1	0.29	6	26
Lower Muschelkalk (*mu*)								
160	rock	sandstone	33.9	0.9	1.2	0.12	4	10
161	rock	marl	42.0	0.9	1.1	0.23	3	20
157a	wp < 2 mm	sandstone	49.2	0.5	2.6	0.23	5	9
158a	wp < 2 mm	sandstone	31.3	0.6	0.2	0.06	1	25
159a	wp < 2 mm	sandstone	33.4	0.5	1.2	0.18	4	15
Buntsandstein (*so*)								
53	rock	sandstone	24.3	0.5	1.4	0.27	6	20
98	rock	sandstone	23.0	0.5	1.2	0.19	5	16
101	rock	sandstone	34.2	0.3	1.1	0.14	3	13
102	wp < 2 mm	sandstone	32.7	0.4	0.8	0.14	2	18

Table A4-1 (continued): Radium activities, radon activity concentrations and emanation coefficients (E) of rocks and weathering products.

sample number	classification	rock type	226Ra [Bq/ kg]	SD [Bq/ kg]	222Rn [Bq/ kg]	SD [Bq/ kg]	E [%]	SD [%]
Upper Emsian (*E3*)								
42	rock	schist	35.3	0.6	2.0	0.40	6	20
50	rock	siltstone	31.7	0.7	2.7	0.42	9	16
66	wp < 2 mm	schist	44.9	0.6	5.2	0.62	12	12
56b	rock	schist	33.4	0.4	2.4	0.25	7	11
70a	rock	schist	38.1	0.6	2.7	0.18	7	7
71a	rock	schist	35.5	0.6	1.5	0.16	4	11
71b	rock	quartz vein	<2.87		<		<	
Middle Emsian *"Quarzit von Berlé"* (*E2q*)								
48	rock	quartzite	6.9	0.4	0.6	0.11	9	21
67a	rock	quartzite	4.9	2.0	0.3	0.06	6	26
67b	rock	quartzite	<3.05		0.4	0.06	>12	
Middle Emsian "*Bunte Schiefer von Clerf*" (*E2*)								
8	rock	schist	35.7	0.6	2.5	0.30	7	12
68	wp > 2 mm	sandstone	38.1	0.5	3.0	0.21	8	7
69	rock	sandstone	33.9	2.1	2.5	0.23	7	10
55b	rock	schist	32.0	0.4	2.3	0.16	7	7
Lower Emsian (*E1b*)								
13	rock	sandstone	36.4	0.5	0.7	0.16	2	25
45	wp	sandstone	37.4	0.6	3.9	0.20	11	6
72	rock	siltstone	35.2	0.6	1.7	0.17	5	10
149	rock	schist	33.2	0.6	0.9	0.17	3	18
Lower Emsian (*E1a*)								
1	wp < 2 mm	schist	43.6	1.6	5.1	0.30	12	6
18	wp	schist	33.5	0.8	6.4	0.25	19	5
23	rock	siltstone	24.6	1.1	1.5	0.33	6	21
46	rock	sandstone	24.4	0.6	3.1	0.42	13	14
49	rock	schist	39.6	1.8	1.9	0.32	5	17
Upper Siegenian (*Sg 3*)								
3	wp < 2 mm	schist	35.2	0.5	3.2	0.48	9	15
4	rock	schist	22.7	0.8	1.9	0.23	8	12
11	rock	schist	23.3	0.6	2.0	0.20	9	10
12	rock	schist	27.4	0.9	2.6	0.18	10	7
24	wp < 2 mm	schist	33.6	0.6	4.7	0.23	14	5
26	wp < 2 mm	schist	28.1	0.5	4.4	0.35	16	8
27	rock	schist	27.8	0.8	2.1	0.23	7	11
30	wp < 2 mm	schist	62.8	0.9	5.8	0.35	9	6
74	rock	siltstone	17.4	0.7	1.7	0.20	10	12
78	rock	siltstone	22.6	0.7	1.0	0.17	4	18
25b	wp < 2 mm	schist	44.0	0.6	4.7	0.23	11	5
2	rock and wp	schist	29.2	0.6	2.9	0.19	10	18
2c	wp > 2 mm	schist	36.2	0.7	1.9	0.27	5	14

Table A4-1 (continued): Radium activities, radon activity concentrations and emanation coefficients (E) of rocks and weathering products.

sample number	classification	rock type	226Ra [Bq/ kg]	SD [Bq/ kg]	222Rn [Bq/ kg]	SD [Bq/ kg]	E [%]	SD [%]
Middle Siegenian (*Sg 2*)								
38	rock	siltstone	26.5	1.1	1.2	0.15	5	12
44	rock	schist	36.5	0.7	2.6	0.39	7	15
156	rock	schist	25.1	0.7	1.4	0.12	5	9
154a	wp < 2 mm	schist	51.8	0.6	9.0	0.63	17	7
155a	wp < 2 mm	schist	139.5	0.7	17.5	0.70	13	4
77a	wp < 2 mm	siltstone	18.2	0.6	2.6	0.21	14	9
Lower Siegenian (*Sg 1*)								
41	rock	schist	27.0	0.7	2.2	0.42	8	20
Gedinnian (*Ged*)								
124	rock	sandstone	64.6	0.5	1.4	0.16	2	11
126	rock	quartz vein	9.1	0.9	1.3	0.15	15	12
131	rock	schist	76.5	0.7	2.1	0.29	3	14
134	wp < 2 mm	sandstone	339.3	0.7	58.2	1.89	17	3
135	rock	sandstone	34.8	0.8	1.5	0.18	4	12
137	rock	sandstone	48.1	5.0	1.5	0.07	3	6
128a	rock	sandstone	113.8	0.3	3.4	0.21	3	6
128b	wp < 2 mm	sandstone	511.5	0.8	16.6	0.33	3	2
132a	rock	siltstone	53.1	0.9	4.1	0.25	8	6
133a	rock	quartzite	12.3	0.7	0.3	0.05	3	19
136a	rock	sandstone	58.9	1.2	1.3	0.14	2	11
136b	wp < 2 mm	sandstone	769.0	0.7	127.7	11.05	17	9

Table A4-2: Emanation coefficients (E) of rocks.

rocks			^{226}Ra [Bq/kg]		E [%]	
			median	range	median	range
Mesozoic	Jurassic	dom3	12.8	7.5 - 13.6	9	8 - 11
		dou	16.9	15.9 - 17.9	11	9 - 12
		lm3b	21.3	9.0 - 39.7	9	5 - 10
		lm3a	25.2	13.7 - 30.3	6	6 - 7
		Li3	29.8	13.7 - 53.1	5	4 - 8
		Li2	14.9	2.2 -120.7	11	5 - 16
	Triassic	ko1	18.1	—	6	—
		km3	41.0	18.2 - 319.8	7	6 - 8
		km2s	32.5	19.9 - 41.3	12	9 - 18
		mo	18.7	5.0 - 39.5	9	6 - 13
		mm/mu	31.2	18.4 - 42.0	4	3 - 6
		so	24.3	14.0 - 34.2	5	3 - 6
Paleozoic	Devonian	E3	35.4	25.3 - 43.3	7	4 - 9
		E2q	5.6	4.9 - 6.9	7	6 - 9
		E2	33.9	32.0 - 35.7	7	7
		E1b	35.2	33.2 - 36.4	3	2 - 5
		E1a	32.1	24.4 - 48.1	6	5 - 13
		Sg3	27.4	3.9 - 45.9	9	4 - 10
		Sg1/Sg2	25.1	14.1 - 44.2	6	5 - 8
		Ged	48.2	9.1 - 113.8	3	2 - 15

Table A4-3: Emanation coefficients (E) of weathering products.

weathering products			^{226}Ra [Bq/kg]		E [%]	
			median	range	median	range
Mesozoic	Jurassic	dom3	21.4	—	16	—
		dou	17.9	6.6 - 29.1	7	5 - 13
		lm3b	27.1	24.1 - 30.2	9	—
		lm 3a	32.9	28.7 - 37.0	6	4 - 7
		Li3	41.5	11.8 - 44.8	3	—
		Li2	13.8	4.9 - 42.9	6	4 - 8
	Triassic	ko1	NA		NA	
		km3	67.7	24.4 - 264.0	7	4 - 7
		km2s	46.1	—	18	—
		mo	33.7	8.9 - 97.0	15	9 - 37
		mm/mu	32.6	31.3 - 49.2	4	1 - 5
		so	31.9	31.2 - 32.7	2	—
Paleozoic	Devonian	E3	44.9	40.6 - 101.2	12	—
		E2q	NA		NA	
		E2	54.0	38.1 - 70.0	8	—
		E1b	37.4	—	11	—
		E1a	38.6	33.5 - 43.6	15	12 - 19
		Sg3	34.4	28.1 - 62.8	10	5 - 16
		Sg1/Sg2	42.0	18.2 - 139.5	14	13 - 17
		Ged	425.4	26.4 - 1249.0	17	3 - 17

Table A4-4: Radon activity concentrations (referring to the released radon in sample pore gas, related to the weight of the emanating material under equilibrium conditions) of rocks and weathering products.

			^{222}Rn [Bq/kg *]			
			rocks		weathering products	
			median	range	median	range
Mesozoic	Jurassic	dom3	1.2	1.1 - 1.4	3.4	—
		dou	1.8	1.5 - 2.2	0.9	0.5 - 1.8
		lm3b	1.8	0.9 - 2.2	2.1	—
		lm3a	1.7	1.5 - 2.0	1.9	1.3 - 2.5
		li3	2.9	0.5 - 3.1	1.3	—
		li2	0.6	0.3 - 1.2	0.6	0.4 - 0.8
	Triassic	ko	1.1	—	NA	
		km3	4.1	2.0 - 6.1	2.8	1.7 - 3.1
		km2s	3.8	1.8 - 7.6	8.5	—
		mo	1.8	0.5 - 2.2	9.6	5.8 - 19.7
		mu/mm	1.1	1.1 - 1.2	1.2	0.2 - 2.6
		so	1.2	1.1 - 1.4	0.8	—
Paleozoic	Devonian	Ems3	2.4	1.5 - 2.7	5.2	—
		Ems2q	0.4	0.3 - 0.6	NA	
		Ems2	2.5	2.3 - 2.5	3.0	—
		Ems1b	0.9	0.7 - 1.7	3.9	—
		Ems1a	1.9	1.5 - 3.1	5.7	5.1 - 6.4
		Sg3	2.0	1.0 - 2.9	4.5	1.9 - 5.8
		Sg1/Sg2	1.8	1.2 - 2.6	9.0	2.6 - 17.5
		Ged	1.5	0.3 - 4.1	58.2	16.6 - 127.7

Table A5: Analytical results for two samples, which were extracted in 3 parallel sessions and measured at least 9 times for each fraction. Results are given with standard deviation (SD) and coefficient of variation (RSD)

136a	mobile exchangeable fraction (I)			echangeable fraction (II)			Mn oxides (III)			Organic matter (IV)			amorphous Fe oxides (V)			crystalline Fe oxides (VI)		
	Mean [mg/kg]	SD [mg/kg]	RSD	Mean [mg/kg]	SD [mg/kg]	RSD	Mean [mg/kg]	SD [mg/kg]	RSD	Mean [mg/kg]	SD [mg/kg]	RSD	Mean [mg/kg]	SD [mg/kg]	RSD	Mean [mg/kg]	SD [mg/kg]	RSD
Zn	0.3	0.1	0.23	1.6	0.5	0.31	1.1	0.3	0.31	0.4	0.1	0.13	8.5	0.7	0.08	30.3	6.7	0.22
Al	8	2	0.19	91	16	0.18	44	6	0.14	147	49	0.33	1056	54	0.05	2236	357	0.16
Ba	7.3	0.1	0.01	1.6	0.2	0.14	2.2	0.1	0.06	0.3	0.1	0.22	3.2	0.6	0.20	2.7	0.5	0.17
Mg	65	5	0.08	40	6	0.14	19	3	0.14	20	2	0.11	226	24	0.11	448	39	0.09
Mn	33.3	1.4	0.04	19.6	2.8	0.15	28.3	2.4	0.08	8.3	1.2	0.14	32.8	1.8	0.06	51.8	12.5	0.24
Fe	4	1	0.28	47	10	0.21	58	8	0.13	145	11	0.08	2535	191	0.08	7808	1389	0.18
Pb	0.0	0.0	0.10	3.2	0.4	0.14	2.4	0.2	0.08	1.0	0.2	0.22	3.1	0.2	0.06	7.5	0.3	0.04
As	0.1	0.0	0.13	0.2	0.0	0.13	0.1	0.0	0.13	0.3	0.0	0.14	5.9	0.4	0.06	17.7	4.3	0.25
Ti	0.3	0.1	0.31	< 0.1			0.4	0.1	0.24	0.5	0.1	0.27	4.7	0.3	0.06	5.0	0.8	0.17
Ni	0.8	0.0	0.04	0.8	0.1	0.14	0.4	0.1	0.19	0.5	0.1	0.20	5.6	0.3	0.06	17.1	3.1	0.18
V	< 0.1	0.0	0.22	0.1	0.0	0.11	0.3	0.0	0.11	0.1	0.0	0.09	1.8	0.1	0.05	4.4	0.8	0.18
Cu	0.6	0.2	0.38	1.0	0.0	0.01	0.7	0.0	0.08	0.7	0.2	0.27	4.9	0.5	0.10	16.1	1.6	0.10
Rb	1.2	0.0	0.01	0.2	0.0	0.14	0.3	0.0	0.04	0.0	0.0	0.17	0.4	0.1	0.18	0.5	0.1	0.28
Sr	3.4	0.2	0.05	0.9	0.2	0.17	1.3	0.0	0.03	0.5	0.1	0.12	1.3	0.1	0.08	1.1	0.2	0.16
Y	0.2	0.0	0.09	0.5	0.1	0.14	0.3	0.0	0.02	0.1	0.0	0.10	0.7	0.1	0.10	1.3	0.2	0.19
Zr	< 0.1	0.0	0.20	0.1	0.0	0.13	0.2	0.0	0.14	0.5	0.0	0.06	< 0.1			NA		
Cs	0.4	0.0	0.01	0.0	0.0	0.13	0.1	0.0	0.03	NA			0.0	0.0	0.26	0.1	0.0	0.32
La	0.16	0.01	0.05	0.16	0.04	0.24	0.10	0.00	0.04	0.03	0.00	0.08	0.45	0.01	0.03	0.69	0.10	0.15
Ce	0.21	0.01	0.05	0.36	0.05	0.14	0.23	0.00	0.02	0.08	0.01	0.11	1.34	0.04	0.03	1.54	0.20	0.13
Dy	0.02	0.00	0.10	0.12	0.02	0.14	0.05	0.00	0.03	0.02	0.00	0.16	0.18	0.01	0.07	0.31	0.05	0.17
Er	0.01	0.00	0.08	0.06	0.01	0.12	0.03	0.00	0.03	0.01	0.00	0.10	0.09	0.01	0.09	0.16	0.03	0.18
Yb	0.01	0.00	0.14	0.05	0.01	0.12	0.02	0.00	0.02	0.01	0.00	0.23	0.08	0.01	0.09	0.15	0.02	0.17
Hf	< 0.1			0.03	0.01	0.19	0.02	0.00	0.11	< 0.1			< 0.1			0.32	0.04	0.12
Th	< 0.01			0.09	0.02	0.18	0.04	0.00	0.09	0.16	0.04	0.27	1.49	0.09	0.06	1.73	0.33	0.19
U	0.01	0.00	0.27	0.21	0.04	0.17	0.10	0.00	0.03	0.02	0.00	0.15	0.41	0.05	0.12	0.73	0.04	0.05

136b	mobile exchangeable fraction (I)			echangeable fraction (II)			Mn oxides (III)			Organic matter (IV)			amorphous Fe oxides (V)			crystalline Fe oxides (VI)		
	Mean [ppm]	SD [ppm]	RSD	Mean [ppm]	SD [ppm]	RSD	Mean [ppm]	SD [ppm]	RSD	Mean [ppm]	SD [ppm]	RSD	Mean [ppm]	SD [ppm]	RSD	Mean [ppm]	SD [ppm]	RSD
Zn	5.5	0.2	0.04	0.6	0.1	0.22	35.8	1.6	0.04	21.4	1.4	0.07	49.2	1.4	0.03	61.8	5.1	0.08
Al	52	2	0.04	27	4	0.16	52	7	0.14	795	106	0.13	4940	88	0.02	6332	393	0.06
Ba	46.4	1.1	0.02	4.7	0.3	0.06	69.8	2.8	0.04	0.7	0.1	0.09	1.7	0.4	0.23	3.0	0.7	0.22
Mg	NA			56	2	0.04	86	4	0.05	25	2	0.09	94	11	0.12	67	10	0.15
Mn	129	2	0.01	15.8	0.3	0.02	3619	38	0.01	200	8	0.04	1280	36	0.03	208	9	0.04
Fe	7	2	0.22	24	4	0.18	189	25	0.14	870	42	0.05	12882	369	0.03	44012	2921	0.07
Pb	0.5	0.0	0.08	1.4	0.2	0.12	219	3	0.01	151	5	0.03	60.5	1.9	0.03	54.1	7.2	0.13
As	0.1	0.0	0.13	0.1	0.0	0.08	0.2	0.0	0.17	1.2	0.1	0.07	81	2	0.03	153	3	0.02
Ti	1.2	0.1	0.07	1.0	0.1	0.15	1.4	0.0	0.03	6.3	0.3	0.04	NA			212.9	1.8	0.01
Ni	3.5	0.1	0.02	< 0.1			34.9	0.4	0.01	10.0	0.5	0.04	111	3	0.03	42.9	1.9	0.05
V	< 0.1			< 0.1			2.5	0.3	0.11996	1.4	0.1	0.089	12.3	0.3	0.024	35.7	0.8	0.023
Cu	0.6	0.1	0.13	1.0	0.1	0.13	18.8	0.1	0.01	24.0	0.7	0.03	37.5	1.0	0.03	0.8	0.0	0.06
Rb	5.1	0.1	0.01	0.5	0.0	0.02	1.0	0.0	0.04	0.0	0.0	0.15	0.5	0.1	0.27	0.6	0.0	0.05
Sr	7.9	0.1	0.01	1.2	0.1	0.06	1.6	0.2	0.11	0.8	0.1	0.07	0.8	0.1	0.09	0.7	0.1	0.11
Y	6.4	0.1	0.02	1.4	0.0	0.03	3.5	0.3	0.10	2.5	0.1	0.06	6.2	0.1	0.02	3.5	0.1	0.03
Zr	0.2	0.0	0.28	NA			0.2	0.0	0.21	NA			< 0.1			21.3	0.4	0.02
Cs	4.7	0.1	0.02	0.9	0.0	0.03	0.8	0.0	0.05	0.0	0.0	0.24	0.2	0.1	0.33	0.2	0.0	0.15
La	2.03	0.03	0.01	0.22	0.01	0.03	0.90	0.10	0.11	0.47	0.04	0.09	1.12	0.09	0.08	0.72	0.22	0.31
Ce	4.89	0.08	0.02	0.67	0.03	0.04	9.99	0.14	0.01	7.73	0.42	0.05	34.09	0.64	0.02	14.65	2.63	0.18
Dy	0.74	0.02	0.03	0.29	0.01	0.03	0.83	0.07	0.09	0.60	0.03	0.06	1.67	0.03	0.02	0.95	0.07	0.07
Er	0.39	0.01	0.03	0.13	0.00	0.03	0.39	0.03	0.08	0.36	0.01	0.04	0.87	0.02	0.02	0.54	0.03	0.05
Yb	0.24	0.01	0.03	0.08	0.00	0.03	0.28	0.02	0.06	0.40	0.01	0.03	0.84	0.02	0.02	0.54	0.02	0.04
Hf	< 0.1			NA			0.06	0.01	0.12	< 0.1			< 0.1			0.61	0.08	0.13
Th	< 0.01	0.01	0.32	0.02	0.00	0.18	0.16	0.02	0.10	1.40	0.19	0.13	NA			5.20	0.42	0.08
U	0.02	0.00	0.06	4.87	0.05	0.01	5.67	0.95	0.17	1.22	0.15	0.12	11.04	0.20	0.02	8.21	0.46	0.06

Map A6

General geological map of Luxembourg

Sampling sites

Tectonics
- Faults
- Thrusts

Surficial deposits
- Alluvium

Mesozoic Cover
- Middle Dogger (dom)
- Lo. Dogger & Up.Liassic, 'Minette' (dou,lo7,lo6)
- Upper Liassic (lo1-5)
- Middle Liassic (lm)
- Lower Liassic, marls & limestones (li3-4)
- Lower Liassic, sandstone (li2)
- Lower Liassic, marls & limestones (li1)
- Upper Keuper (Rhaetian) (ko)
- Middle Keuper, sandstone (km2s)
- Middle Keuper (km)
- Lower Keuper (ku)
- Upper Muschelkalk (mo)
- Middle Muschelkalk (mm)
- Lower Muschelkalk (mu)
- Upper Buntsandstein (so)

Devonian Basement
- Upper Emsian (E3)
- Upper Emsian, quartzites (q)
- Middle Emsian (E2)
- Lower Emsian (E1b)
- Lower Emsian (E1a)
- Upper Siegenian, sandy (Sg3s)
- Upper Siegenian, slaty (Sg3a)
- Upper Siegenian (Sg3)
- Middle Siegenian (Sg2)
- Lower Siegenian (Sg1)

Sampling site, sample number

N

0   10 km

SGL 2007

MINISTÈRE DES TRAVAUX PUBLICS
Administration des ponts et chaussées

Service géologique du Luxembourg